IMPROVING THE CYTOCOMPATIBILITY AND INFECTION, WEAR AND CORROSION RESISTANCES OF COMMERCIALLY PURE TITANIUM BY LASER MICROPATTERNING AND CERAMIC CONVERSION TREATMENT

by

IKRA KHAN

A thesis submitted to the University of Birmingham for the degree of DOCTOR OF PHILOSOPHY

School of Metallurgy and Materials

College of Engineering and Physical Sciences

The University of Birmingham

December 2020

ABSTRACT

Commercially pure titanium (cp-Ti) is a popular material choice for biomedical implants due to its good cytocompatibility, high corrosion resistance and mechanical properties. Nevertheless, titanium surfaces are susceptible to infection and wear which has led to implant failure and removal. Ceramic conversion treatment (CCT) has displayed improved wear resistances and surface hardness's of titanium whereas, laser induced periodic surface structures (LIPSS) have displayed good antibacterial capabilities. Nonetheless, LIPSS have poor durability. There is limited research in combining these surface engineering techniques to create a duplex treated surface on titanium. It is hoped that by combining LIPSS with CCT, the durability of the LIPSS will improve whilst also maintaining the antibacterial, cytocompatible and wear resistances. Hence, the aim of this study was to investigate the antibacterial efficacy, cytocompatibility, wear resistance and corrosion resistance of a duplex surface treatment that involved CCT and LIPSS undertaken on commercially pure titanium (grade II).

In this study femtosecond pulsed laser micro-patterning was applied to polished cp-Ti and CCT treated cp-Ti to form LIPSS with a depth of about 1 µm and a spacing of approximately 300 nm. CCT was undertaken at 600˚C for 85 hours to produce an approximately 2 µm thick rutile-based TiO_2 layer that had good bonding to the substrate and was supported by the formation of oxygen diffusion zones. The LIPSS and CCT were tested for their antibacterial efficacy against *S. aureus* and *E. coli* and also, the cytocompatibility of these surface treatments was measured using osteoblast like SaOS-2 cells. The wear resistance was also assessed in dry (air) and lubricated (Ringer's solution) conditions. Using Ringer's solution, the corrosion resistance was measured of the surface treatments.

The LIPSS had the greatest effect on the antibacterial resistance due to the small size and the limited contact area for the bacteria to attach to. The highest percentage reduction for both bacteria was seen for the duplex treated sample (oxide first then pattern) which indicated that when combining the two surface treatments, the antibacterial properties are the most optimum. The TiO_2 led to high SaOS-2 cell viabilities whereas LIPSS reduced the SaOS-2 cell number. However, when LIPSS was combined with CCT the SaOS-2 cell numbers increased which suggested when the surface treatments are combined they are cytocompatible, non-toxic and also antibacterial.

Untreated cp-Ti underwent severe adhesive and abrasive wear in both air and Ringer's solution. The wear resistance of untreated and laser micro-patterned cp-Ti was improved by CCT however, LIPSS treated cp-Ti revealed very poor wear resistances causing the LIPSS to be fully destroyed. This demonstrates that the durability of the LIPSS formed on cp-Ti is very low. The durability of LIPSS on cp-Ti was however, effectively improved by the novel duplex treatment combining LIPSS with pre-CCT under both dry and lubricated conditions. Nearly all of the surface treated samples had lower corrosion rates and higher corrosion potentials when compared with untreated cp-Ti. The novel duplex surface system developed from the research by combining CCT treatment with laser micro-patterning provided the best antibacterial results, good cytocompatibility, high corrosion and wear resistances and thus, long durability. This study has demonstrated that when combined, CCT and LIPSS have the potential to be applied in medical implants in order to improve the infection and wear resistance whilst also maintaining the good corrosion resistance of cp-Ti and causing no toxicity issues.

ACKNOWLEDGEMENTS

Firstly, I would like to thank God for giving me this ability to complete my research.

I am incredibly grateful for the financial support from the Centre for Doctoral Training in Innovative Metal Processing (IMPaCT) funded by the UK Engineering and Physical Sciences Research Council (EPSRC). Without this funding I would not be able to complete this PhD.

I would also like to express my sincere gratitude to my supervisors Professor Hanshan Dong and Dr Rachel Sammons and to Dr Xiaoying Li and Dr Zhenxue Zhang for their invaluable advice, guidance and supervision throughout my PhD at the University of Birmingham.

I would like to thank all of my colleagues in the Surface Engineering Group at the School of Metallurgy, especially to Xiao Tao and Shaojun Qi for their time and effort in helping and assisting me. I am also grateful towards Professor Stefan Dimov and his group especially to Pavel Penchev and Tahseen Jwad for assisting me with the laser micro-patterning and to Dr Baogui Shi for the XPS assistance and Dr Alejandro Avila-Sierra for assistance with the wettability measurements.

I would also like to thank all of the faculty and staff in the School of Metallurgy and Materials and the Birmingham Dental Hospital for their help and support.

Finally, I would like to thank my family for their constant support throughout my PhD.

TABLE OF CONTENTS

Page

LIST OF ABBREVIATIONS

˚ Degrees

Λ Periodicity

ƛ Wavelength

α Alpha

β Beta

Ar Argon

ASTM American institute for testing and materials

bcc Body-centred cubic

BSD Back-scattered diffraction

C Carbon

CA Contact angle

CCT Ceramic conversion treatment

Co-Cr Cobalt chromium alloy

Co-Cr-Mo Cobalt chromium molybdenum alloy

CoF Coefficient of friction

cp-Ti Commercially pure titanium

DNA Deoxyribonucleic acid

E. coli *Escherichia coli*

EDX Energy-dispersive X-ray spectroscopy

FCS Foetal calf serum

FIB Focused ion beam

fs Femtosecond

HDMS Hexadimethysilizane

HEPES (4-(2-hydroxyethyl)-1-piperazineethanesulfonic acid) buffer

HS Hardened steel

HSFL High spatial frequency LIPSS

HV Vickers's hardness

LIPSS Laser induced periodic surface structures

LSFL Low spatial frequency LIPSS

MP Polished sample treated with LIPSS

MP48 Polished sample treated with LIPSS at 48% power

MP58 Polished sample treated with LIPSS at 58% power

MPTO duplex treated sample, LIPSS first then CCT

N Nitrogen

nm Nanometre

O Oxygen

ODZ Oxygen diffusion zone

P mirror polished untreated sample

PBS Phosphate-buffered saline

PD Potentiodynamic

ps Picosecond

PTO Polished sample treated with CCT

Ra Average surface roughness

Rt Average peak to valley height (roughness)

S epidermidis *Staphylococcus epidermidis*

S. aureus *Staphylococcus aureus*

SaOS-2 Osteosarcoma cell with osteoblast like behaviour

SCC Stress corrosion cracking

SCE Saturated calomel reference electrode

SD Standard deviation

SEM Scanning electron microscope

SFE Surface free energy

Ti Titanium

Ti-6Al-4V Titanium alloy alloyed with aluminium and vanadium

TiN Titanium nitride

TiO_2 Titanium oxide

TO Thermal oxidation

TOMP duplex treated sample, CCT first then LIPSS

TOMP48 duplex treated sample, CCT first then 48% power LIPSS

TOMP58 duplex treated sample, CCT first then 58% power LIPSS

TSA Tryptone soya agar

µm Micrometre

WC Tungsten carbide

WCA Water contact angle

wt% Weight percentage

XPS X-ray photoelectron spectroscopy

XRD X-ray-diffraction

Chapter 1

INTRODUCTION

The purpose of this chapter is for the reader to gain an insight into the motivation behind this project, the aims and objectives and the structure of the thesis.

1.1 Motivation

Titanium and its alloys are a popular choice for biomaterials due to their excellent cytocompatibility, outstanding corrosion resistance, high mechanical properties and low modulus as well as low density. Titanium and its alloys (especially commercially pure titanium) have been widely considered to be the most cytocompatible in all metals which makes them an optimum choice for medical implants. The presence of the native, passive oxide layer that forms spontaneously is responsible for titanium's corrosion resistance and cytocompatibility. Due to its high reactivity, when titanium is exposed to air it reacts with oxygen to form an oxide layer within micro-seconds that has a thickness in the nanometre range. This oxide layer prevents corrosion from occurring. Nonetheless, although this oxide layer is cytocompatible and resistant to corrosion it is susceptible to damage and removal when exposed to higher loads (1).

Titanium and its alloys possess poor resistances to wear and are prone to wear damage. Due to this, the application of titanium is limited in high load-bearing applications and in applications that involve high contact forces (such as hip or knee implants). In medical implants, if a material is susceptible to abrasive wear the formation of wear debris and particles is likely. Wear debris can lead to implant loosening, bone loss and negative

inflammatory responses such as allergic reactions. Degradation of implants is one of the major reasons of implant failure and is accountable for almost 80 % of revision surgeries. Abrasive wear by-products have also been recorded in the livers and spleens of patients which can lead to toxic effects. In order to combat this issue, the use of surface engineering techniques have widely shown improvements in lowering friction coefficients and wear resistances of titanium implants (1).

Titanium implants are also susceptible to infection. Infection along with wear is also one of the major causes of implant failure. The issue of increased antibiotic resistance and highly expensive revision surgeries have led to increased research in technologies that can help increase infection resistance. When bacterial colonisation occurs on an implant, bone formation and the consequent integration of the implant is severely limited. The most important stage of bacterial colonisation is the initial contact to the surface of an implant. The initial attachment of bacteria to the surface is reversible and can be limited by surface engineering techniques undertaken on an implant (2).

In order to improve infection resistance, the use of surfaces that have been impregnated with antibacterial substances like silver and copper have been investigated. These techniques have displayed good antibacterial results. However, the release of these antibacterial agents cannot be controlled and hence, the antibacterial effect may be limited over time. Also, silver and copper have caused allergic reactions and toxicity issues in patients and therefore, other techniques need to be found. Bacteria are sensitive to surface topographies, chemistry and wettability and thus, these factors can be altered in order to limit bacterial colonisation (2).

Surface texturing via the use of ultra-fast laser pulses has displayed promising antibacterial results. This method referred to as laser induced periodic surface textures (LIPSS) uses a laser in the femtosecond range to produce reproducible, uniform and controllable surface features or patterns. Also, as LIPSS does not involve the use of toxic substances, this technique does not pose any risk of toxicity (2). Nevertheless, some researchers have reported how LIPSS have caused no effect on wear resistances. The presence of LIPSS led to no change in friction coefficients and wear resistances when compared to untreated titanium samples mainly due to the low durability of the micro-scale patterns on relatively soft titanium surfaces (3). This suggests, another surface treatment that can combine improved wear resistance and mechanical properties with improved infection resistance and cytocompatibility is required.

Surface coatings and surface diffusional technologies have displayed positive results in combating the issue of poor wear resistance. These processes have shown improved strength and wear resistance of the material's surface nonetheless, they are also known to alter the corrosion resistance of pure titanium. However, with surface coatings there can be issues between the bonding of the substrate to the treated surface which can pose a risk of displacement and degradation of the surface treated layer (4). The process of ceramic conversion treatment, CCT (a type of controlled thermal oxidation) has shown to improve wear resistances and surface hardness's of titanium without the associated issue of poor bonding or affecting the corrosion resistance due to its in-situ conversion nature (4).

Ceramic conversion treatment is able to improve the wear resistances and mechanical properties of titanium surfaces and although LIPSS are able to improve the

infection resistance and long-term cytocompatibility of a sample, LIPSS alone do not improve wear resistances. Also, CCT has limited research on the antibacterial efficacy without the use of photoactivation. Thus, combining these two surface treatments to create a novel duplex surface system would be the most ideal solution with high infection and wear resistances and good cytocompatibilities.

1.2 Aim & Objectives

The overall aim of this PhD project was to investigate the antibacterial efficacy, cytocompatibility, wear resistance and corrosion resistance of a duplex surface treatment that involves CCT and LIPSS undertaken on commercially pure titanium (grade II). The technical objectives are as follows:

1. To study the microstructure and mechanical properties of CCT treated (600 °C for 85 hours) and femtosecond laser textured (LIPSS) commercially pure titanium (grade II). The two surface treatments were combined to investigate their synergetic effect.
2. To investigate the antibacterial efficacy via bacterial anti-adhesion and percentage reduction tests of CCT and LIPSS on Gram positive and negative bacteria. The bacteria used were a cocci-shaped *S. aureus* and rod-shaped *E. coli* to assess the effect bacteria size and shape have on the antibacterial efficacy of the CCT, LIPSS and duplex surface treatment.
3. To investigate the cytocompatibility of the CCT, LIPSS and duplex surface treatment via measurements in the cell viability of SaOS-2 cells (osteoblast-like cells).
4. To evaluate the tribological (friction coefficients, and wear resistance) and corrosion behaviour (corrosion potential and corrosion rate) of the surface treated cp-Ti.

1.3 Thesis structure

This thesis follows a classic structure and it starts with a comprehensive literature review in Chapter 2, covering medical devices and implants, infection and immune responses, current approaches, surface texturing and thermal oxidation followed by Materials and Methods (Chapter 3). The experimental results and their interpretation and discussion are given in Chapters 4 and Chapter 5, respectively. The thesis completes with the conclusions and future work (Chapter 6).

Chapter 2

LITERATURE REVIEW

This purpose of this review chapter is for the reader to gain an understanding in the requirement of a medical device related to bone and teeth, how and why titanium is used as a material in medical devices, the current implications (infection and poor wear resistance) related to titanium medical devices and how these implications are currently combated. Current research regarding the topics of thermal oxidation, laser-patterning and their capabilities in infection resistance on titanium surfaces are reviewed. Based on the literature review, the gaps and hence the drive for this research are identified.

2.1 Medical Implants & Biomaterials

Medical implants can be defined as artificial devices that possess a particular function that improves, supports or replaces the processes in the human body. These implantable devices can also be used to replace human tissues. Medical implants possess the capability to be introduced and applied in the human body without causing any issues in the body. The most common implants in current use are orthopaedic or cardiovascular implants (5,6). Orthopaedic implants are mainly used in joint arthroplasties, reconstruction of the spine or for bone fracture repair. The main purpose of orthopaedic implants is to support the alignment and function of bone tissue as well as structural and mechanical stabilisation (7).

2.1.1 Requirements of a medical implant

The requirement of a medical implant and the material chosen for an implant is dependent on the application of the implant. The longevity of an implant is taken into consideration as well as treatment length and disease prevention. These all help determine the appropriate

medical implant for an application (8). On the whole, medical implants need to meet certain criteria in order to be suitable for application in the human body such as: cytocompatibility, biofunctionality, bioadhesion and corrosion resistance. These properties determine whether a material can be suitable for medical applications (9).

There are a wide range of applications for medical implants for instance; artificial arteries, limb replacements and joint replacements. The reasoning behind these implants may be due to increasing life expectancies, replacement of damaged tissue due to disease, old age or could simply be for aesthetic purposes. Below Table 2.1.1 lists some examples of medical implant requirements in relation to their applications (10). Due to higher life-expectancies and medical science breakthroughs there is a greater demand for medical implants and research into medical materials (11).

Table 2.1.1. Properties important for some medical implants and applications (adapted from 4).

Material property	Prevention	Application example
Biological/chemistry • Cytocompatibility	Negative immuno-response	Dental root
Bulk properties • Adequate stiffness	Stress shielding and bone resorption	Load-bearing bone implant
Surface properties • Hydrophilicity	Adequate wettability and lubrication	Contact lenses
• Surface corrosion and wear resistance	Degradation of implant leading to wear debris and wear particle release	Hip and knee implants
• Hard surface with low friction coefficients	Allergic response or toxicity Wear	Orthopaedic and dental implants

2.1.2 Different materials used in medical implants

There are typically three classes of materials used in medical implants; polymers, metals and ceramics. Each material group has certain advantages and disadvantages and thus, are used in specific applications according to their properties (10). A different approach to class biomaterials is via the tissue response they evoke upon application. On this basis, biomaterials can be grouped into three types. Bioinert (all materials elicit an immune response however, bioinert materials evoke a very minimal response), bioactive materials (these materials encourage bonding to the site of implantation and thus, help integrate the implant via stimulation of new tissue growth) and finally, biodegradable/bioresorbable materials (these materials initially integrate into the host tissue and then completely degrade over time once their function is complete). Ceramics can be bioactive, bioinert or resorbable whereas metals tend to be inert. Polymers may also be inert or bioresorbable (11).

2.1.2.1 Polymers and ceramics

A wide range of polymers are used in medical implants and devices and are commonly referred to as biopolymers. They can either be used in the form of a coating to protect the implant, as an adhesive to seal the interface between two materials or as a substrate for the implant (12–14). Polymers are ductile and corrosion-resistant but their mechanical properties are much lower than metals/alloys and ceramics (12).

On the other hand, ceramics are hard and brittle and possess elastic moduli that are higher than that of bone. In orthopaedics, ceramics tend to be used in artificial femoral heads and dental crowns and bridges due to their highly suitable properties such as, high mechanical strengths, low friction coefficients and lastly, high durability (11).

On the whole, ceramics are challenging to manufacture, brittle and hard to work with due to their high stiffness's. As a result, the most common type of material used in surgery are metals and alloys especially for orthopaedic and orthodontic load-bearing implants (10).

2.1.2.2 Metals and alloys

Current metallic implants are mainly formed of austenitic stainless steel, cobalt-chromium-molybdenum (Co-Cr-Mo) or titanium alloys (8). Orthopaedic and dental implants consisting of hip, knee and spinal implants are the most desired implants across the world and all of these implants consist of some form of metal (11). Stainless steel based implants include fracture plates, orthopaedic nails and screws used in joint arthroplasty. Similarly titanium is also used in fracture plates, screws and nails but, titanium is also used in pacemaker cases and artificial heart valves due to its low stiffness, low density, high cytocompatibility, high strength and corrosion resistance. Additionally, Co-Cr alloys are primarily used in dental implants and Co-Cr-Mo are used in hip implants because of their high corrosion and fatigue resistances and also their high strengths (8).

Nonetheless, the use of these metal alloys all come with some sort of limitation(s). One of the most pivotal requirements of any medical implant is to remain stable in body fluids and tissues. This stability must be in the form of chemical and mechanical stability as well as cytocompatibility (15).

Corrosion is one of the leading processes that causes the failure of a metallic implant. It can affect the ability and longevity of an implant. Metal-based implants possess electron currents and localised tissues possess ionic currents. Both of these currents should maintain a balance to prevent the possibility of corrosion. If the electric current of the

implant is higher than the ionic current of the tissue, negative effects can occur on the nervous system. This imbalance of currents can also lead to corrosion and release of metallic ions into the surrounding tissues and bodily fluids which again can cause toxicity issues. Thus, the corrosion potential of the metallic alloy must be higher than that of bodily fluids (approximately 400 mV). This can prevent penetration of metallic ions in the passivation layer of bodily tissues (10).

With stainless steel based implants there have been reports of localised pitting and crevice corrosion occurring on an implant. This led to damage of the implant and reduced its functionality (15). Additionally, with austenitic stainless alloys (although the use of this metal can be permanent in implants) there have been reports of nickel-ion release which can lead to nickel hypersensitivity (8,16). Corrosion has also affected the functionality of Co-Cr alloy based implants. For instance, there have been reports of carcinogenic nickel, cobalt and chromium ion release from Co-Cr alloys which has led to allergic responses such as dermatitis (skin condition) and a higher risk of cancer (15).

Problems such as physical incompatibility and stress shielding have also been encountered with Co-Cr and stainless steel based implants. Metallic implants used in orthopaedics must have high tensile strengths and fatigue resistances for load-bearing applications (hip and knee implants). Co-Cr and stainless steel alloys possess these qualities which make them a suitable choice, however they do not have a Young's modulus similar to that of bone (15).

The elastic modulus of an alloy must be taken into consideration for dental and orthopaedic implants. If the elastic modulus of the implant material is similar to that bone, the implant has better load-bearing capabilities and integrates better into the implantation

site as bone formation can be initiated more promptly (10). Therefore, the large differences between the Young's modulus of bone and alloys such as Co-Cr and stainless steel has led to the occurrence of stress shielding. In this phenomenon, bone is resorbed and hence, the implant detaches from the site of implantation which leads to failure of the implant (15). Nonetheless, due to the high stiffness's of stainless steel and Co-Cr alloys the occurrence of implant deformation can be reduced but, there is still a risk of stress shielding and poor integration of an implant using these alloys in load-bearing orthopaedic and dental applications (10).

Titanium alloys possess an elastic modulus similar to that of bone (approximately 60 GPa (17). This makes titanium an excellent choice for orthopaedic and dental implants as it also possesses a high corrosion resistance, cytocompatibility and high strengths. The use of titanium can limit the occurrence of stress shielding and can thereby initiate bone formation and reduce bone resorption. Nonetheless, the primary concern with titanium alloys is their low wear resistance and the release of wear particles. Although titanium forms a stable, hard and corrosion resistant titanium oxide film (TiO_2) it still is however, susceptible to wear and can cause wear particle release (11).

2.2 Titanium and Its Alloys

Titanium possesses a self-forming and highly stable TiO_2 film which provides high corrosion resistance and cytocompatibility making it an optimal choice in cardiovascular, dental and orthopaedic applications (11). Titanium is considered to be cytocompatible due to its low electrical conductivity. This low electrical conductivity aids the formation of the stable passive oxide film due to the electrochemical oxidation titanium undergoes. This TiO_2 layer is resistant to corrosion and can remain stable in the human body due to possessing an

oxide isoelectric point of 5-6 (9). The isoelectric point is defined as the pH at which a molecule, solute or surface carries a neutral charge or no net electrical charge (18).

Titanium and its alloys also possess low reactivity with macromolecules and have a low affinity to form ions in aqueous environments. This is ideal for its application in the human body where implants come into contact with bodily fluids. Titanium and its alloys are mainly used in the application where hard tissues need to be replaced for instance in: dental and orthopaedic implant such as knee joints, bone fixation plates and screws and also in pacemakers and cornea back plates. The most preferred alloys are commercially pure titanium (cp-Ti) and Ti-6Al-4V. Commercially pure titanium is more corrosion resistant and cytocompatible due to its highly inert and stable self-forming oxide layer. This oxide layer spontaneously forms when exposed to oxidising media (9).

Nevertheless, most if not all medical implants comprising of titanium alloys do not consist of any contacting surfaces when in motion. This is due to the issue of titanium seizing when in sliding contact. Moreover, this issue prevents the use of titanium alloys in contacting surfaces or implants with sliding motion for example hip or knee implants (19). The high wear rates of titanium can lead to the release of wear particles in the surrounding tissues and fluids which can cause negative immune and allergic responses as well as tissue necrosis (19). There have also been some documented issues regarding the release of vanadium or aluminium from alloys such as Ti–6Al–4V which again have caused toxicity issues and allergic responses (11). Ti–6Al–4V is susceptible to failure due to corrosion fatigue in bodily fluids. The release of aluminium is likely if a Ti–6Al–4V has been placed in the body over a long period of time. These aluminium ions are severely neurotoxic and have the capability to accumulate in the cells of the nervous system such as astrocytes and

neurons thereby, hindering the function of the nervous system and the whole body. Thus, research is currently being undertaken to alter the surface of Ti–6Al–4V alloys to make them more corrosion resistant (20).

Using pure titanium in orthopaedic and dental applications can prevent this issue as there is no presence of potentially toxic vanadium or aluminium ions. Nonetheless, the problem with using pure titanium is its low hardness and low load-bearing capacity. This has been recognised to lower the wear resistance and hence, increase the probability of wear particle release (21).

2.2.1 Microstructure and classification of Ti alloys

Titanium exists in two allotropic forms, α and β phases. The alpha phase has a hexagonal close-packed (hcp) structure and the β phase has a body-centred cubic (bcc) structure (22). The α phase is stable up to temperatures of 882°C whereas, the β phase is stable at higher temperatures up to the melting point (23). Therefore, pure titanium consists of two elementary crystal structures α and β, and titanium alloys can be classified into four microstructural groups; α (alpha) alloys, near-α alloys, α-β alloys and β (beta) alloys.

2.2.2 Commercially pure titanium

Commercially pure titanium (cp-Ti) is widely used for applications in the medical industry. As mentioned above, cp-Ti consists of the α phase and thus, cp-Ti displays tensile strengths between 240-550 MPa. This range of tensile strength is suitable for bone related applications and cp-Ti also has a Young's modulus of about 103 GPa which is not too dissimilar when compared to bone (~60 GPa). This helps prevent stress shielding from

occurring between the implant and bone (24). The properties of the cp-Ti grades can be seen below in Table 2.2.2.

Table 2.2.2. Table displaying The American Society for Testing and Materials (ASTM) classification of unalloyed cp-Ti into grades 1-4 (25).

Maximum impurity (wt%)						Elongation	Tensile strength (MPa)	Young's Modulus (GPa)
ASTM Grade	**O**	**C**	**N**	**H**	**Fe**			
I	0.18	0.10	0.03	0.015	0.20	25	240	103
II	0.25	0.10	0.03	0.015	0.30	20	340	103
III	0.35	0.10	0.05	0.015	0.30	18	450	103
IV	0.40	0.10	0.05	0.015	0.50	15	550	103

Grade II cp-Ti is the key unalloyed titanium used in dental applications. The yield strength of grade II cp-Ti is 275 MPa which is similar to that of heat treated austenitic stainless steels (26). Previous studies have reported how the use of cp-Ti is preferred when compared to Ti-6Al-4V alloy in regard to its stability. It was found that the cp-Ti implant was more stable in the bone bed of a rabbit and had better contact between the bone and the implant surface when compared to the Ti-6Al-4V screws (27–29). On the other hand, it has also been shown that although cp-Ti is electrochemically stable (at a pH of 2.0), it is still susceptible to corrosion fatigue and thus degrades under sliding conditions at a near neutral pH. The reasoning behind this is that when exposed to a neutral pH, the TiO_2 layer is destroyed and cannot reform with a strong bond between the oxide and substrate (unlike

previously). The pH in the oral cavity is 6.3 (near neutral) and hence, these findings suggest that cp-Ti cannot be used for dental implants due to its susceptibility to corrosion (20).

The presence of titanium's naturally occurring oxide film due to its high affinity to oxygen, provides cp-Ti with excellent corrosion resistance and good antibacterial resistances which aids the cytocompatibility of titanium and its alloys (30). Another reason behind titanium's excellent cytocompatibility for orthopaedic implants is due to its ability to osseointegrate and due to the osteoconductive response (ability to initiate bone growth on the implants surface) of titanium oxide (27,31,32). Osseointegration can be defined as the direct structural and functional interaction between ordered, living bone and the surface of a load-bearing implant. It is an essential process in providing implant stability and success (33).

2.3 Infection and Immune Responses

Although titanium and its alloys possess good cytocompatibilities, corrosion resistance and high strengths, titanium implants are still susceptible to infection and wear. Infections related to orthopaedic implants can be fatal and often lead to implant failure and the need for revision surgeries. These surgeries are expensive and complicated and thus, the need for techniques that aid the reduction in the risk of infections is highly desirable (31).

The risk of bacterial contamination is everywhere from food handling to surgery and even at home. In clinical settings the risk of bacterial presence is highly dangerous as it can lead to an infection in people with low immune systems. The risk of infection is however, the most critical during surgery and the likelihood of infection occurring during surgery is most high during artificial implant surgery (34). Infection occurs in 1% of total joint

arthroplasties due to bacteria adhering on the implant surface but this value increases considerably for revision surgery where the failed implant must be removed. For instance, in the case of dental implants, peri-implantitis has been recorded for nearly 14% of all cases which has in some cases led to sepsis. In order to combat or prevent this occurrence, antibiotics need to be administered over a long period of time to patients which is costly and also undesired due to increasing antibiotic resistances by bacterial strains. There is currently a lack of effective treatments for infection other than antibiotics hence, new research techniques are being undertaken to alter the implant surface to make it more infection resistant (34).

2.3.1 Bacteria

Infection is one of the main causes of implant failure. The risk of infection is high for all medical implants. Within seconds of device implantation, proteins adsorb onto the surface and produce a film onto which osseointegration occurs. However, the presence of bacteria can hinder this process because bacterial cells compete for adhesion with the native cells (35).

The process of bacterial adhesion on a solid synthetic surface is dependent on the characteristics of the bacterial microbes involved and the surfaces. Bacteria possess protein based attachments in the form of flagella or pili which help anchor the microbes to the solid surfaces. These features are usually in the nanoscale region with a diameter of 10 nm and a length of 100 nm. In terms of the synthetic surfaces, some novel techniques have led to the formation of certain patterns or coatings that can also be in the nanoscale region. These surface structures can aid the formation of bone making cells (osteoblasts) but may also

enable bacterial adhesion thus, all of this needs to be taken into consideration when testing novel surface engineering techniques (34).

Bacteria are also able to form films on implant surfaces via the release of exopolymeric substances (can be in the form of polysaccharides or macromolecules). This film is responsible for the permanent contamination of a surface and is referred to as a biofilm. Biofilms irreversibly adhere to a surface and are defined as a polysaccharide matrix which encapsulates a community of different micro-organisms. This polysaccharide matrix protects the bacterial organisms from fluid shear stresses and antibiotics and also provides nutrients to the micro-organisms allowing them to multiply. This makes biofilms almost impossible to treat or remove from an implant. Once biofilm formation occurs on an implant it almost always leads to the failure of an implant and thus, expensive revision surgery is required to prevent the spread of infection in the body (34).

The formation of biofilms can be separated into four sequential stages. In the initial stage, surface features and chemistry such as roughness's, topography and hydrophobicity greatly affect the ability of bacteria to adhere to the surface. The attachment of bacteria at this stage is reversible and is mainly due to surface-microbe interactions, Van der Waals forces and cellular Brownian motion. In the second stage, the bacteria (if successful) grow and proliferate and eventually adhere to the surface. This stage is irreversible and is facilitated by the presence of adhesion proteins, bacterial features such as flagella and extracellular polymeric substance production. In the third stage, the biofilm matures and aids the formation of bacterial micro-colonies. Lastly, in the final and fourth stage bacteria is

released or detached from the biofilm to repeat the process on a new surface to achieve bacterial colonisation (34,36,37).

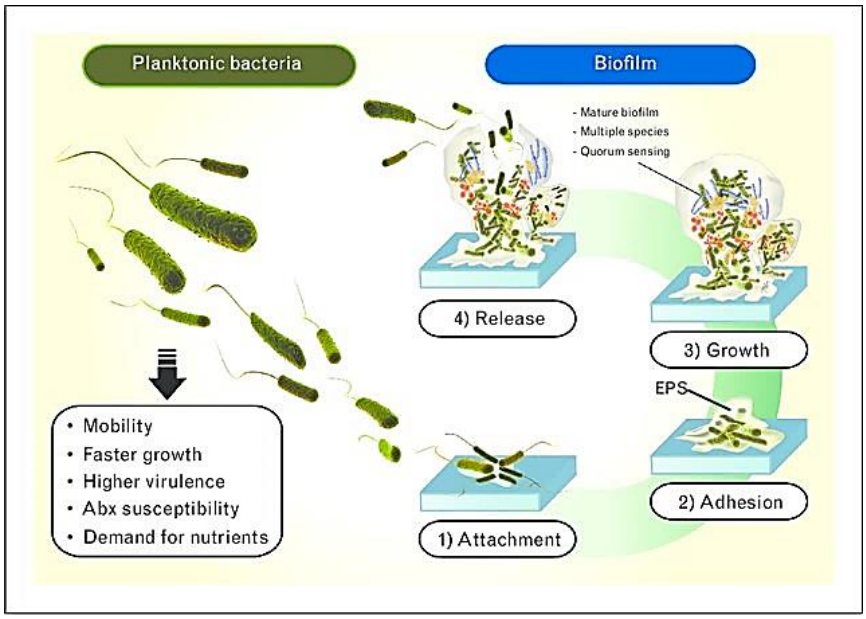

Figure 2.3.1a. Image depicting the biofilm formation stages (38).

The main bacteria involved in orthopaedic implant infections are *Staphylococcus aureus (S. aureus)* and *Staphylococcus epidermidis (S. epidermidis). S. aureus* is the main bacterial organism involved in metal-based implants whereas, *S. epidermidis* is mainly prevalent in polymeric implants. Bacteria tend to be in the size range of 0.5-2 µm and thus, surface roughness's of implants in the micron range can affect the process of bacterial adhesion. It has been reported that a surface roughness in the range of 10 µm can increase bacterial adhesion due to a larger surface area present for bacteria to adhere to. On the other hand, surface roughness values below 0.2 µm or in the nanoscale range have shown to prevent bacterial adhesion and hence, limit or prevent the formation of a biofilm. It has also been reported that if a surface is hydrophobic there is a higher risk of bacterial colonisation. Therefore, surface roughness, topography, the degree of hydrophobicity and

surface chemistry can all greatly affect the probability of an infection occurring in an implant (34,39).

It has been reported previously that metallic surfaces tend to have a higher risk of infection especially if they are inert like stainless steels when compared to reactive metal alloys such as titanium. The reasoning behind this may be due to inert metals possessing lower capabilities to allow tissue integration. For instance, as discussed previously titanium is osteoconductive and if bone was to form on the surface there would be a smaller surface area remaining for bacteria to adhere to. This phenomenon is referred to as the "race for the surface" which is between cells and bacteria. In orthopaedic implants this race would tend to be between osteoblasts and bacteria and if the osteoblasts are successful in their adherence to the implant surface, there would be less colonisation of bacteria. Thus, a possible solution for infection resistance would be to use a technique that can alter the surface of an implant to make it more osteoconductive (34).

Escherichia coli (E. coli) is another bacteria that is prevalent in implant infections. *E. coli* has been found in infections related to Ti-6Al-4V and cp-Ti implants with a greater infection rate occurring in the former. Pure metals such as gold, titanium, cobalt, chromium and aluminium have been shown to possess antibacterial capabilities. Nonetheless, the reasoning or technique behind the antibacterial behaviours of these metals has not been discovered. For instance, it is not known whether the techniques these metals use are in the form of anti-adhesion (preventing the adhesion of bacteria to the surface), bactericidal (preventing the growth of bacteria) or cytotoxic ion release (ions that can affect the genetic makeup or function of bacteria) (34).

Bacteria can be classified as Gram negative or Gram positive which is dependent on the physical features of the bacteria. Majority of Gram negative bacteria (90-95%) are pathogenic whereas, most Gram positive bacteria tend to be non-pathogenic. Gram negative bacteria have a higher resistance to antibiotics due to their thick peptidoglycan layer, teichoic acids, release of toxins and also their high resistance to physical disruption. Bacteria in general are classified according to their cell shape: bacilli are the rod shaped bacteria and cocci are the spherical shaped bacteria. *E coli* is a Gram negative rod shaped bacteria and *S. aureus* is a Gram positive cocci bacteria (40).

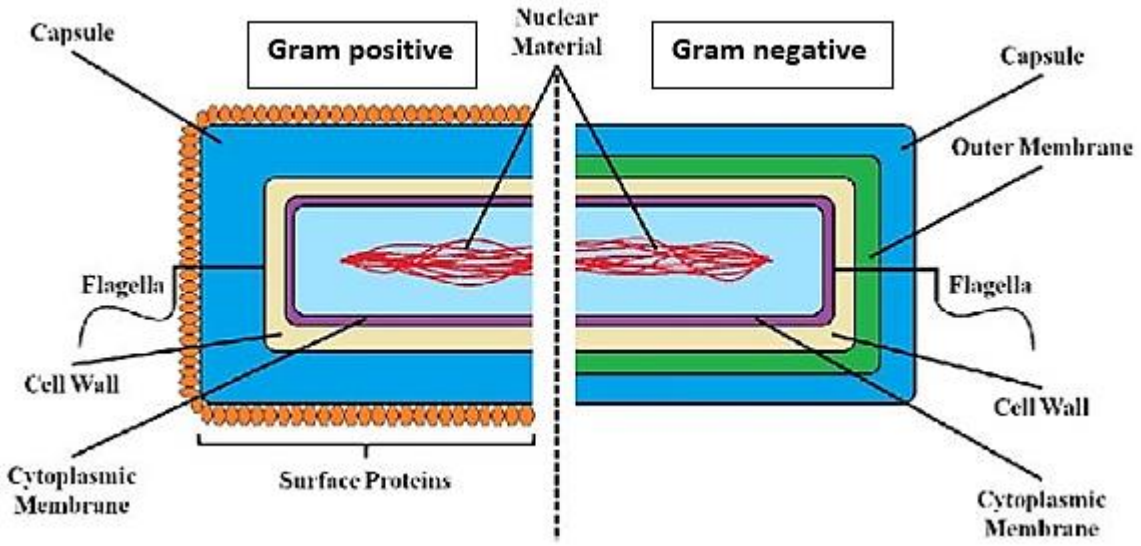

Figure 2.3.1b. Diagram depicting the differences between Gram positive and negative bacteria (41)**.**

2.3.2 Causes of infection in medical devices

When implants are implanted into the body a number of different interactions transpire between the host environment and the surface of the implant. These interactions can take place in the form of protein adsorption onto the materials surface to begin integration of the implant into the surrounding tissue. Thus, as mentioned previously the surface of an implant is extremely important in the integration and success of a biomedical implant. The

surface characteristics that are highly important consist of surface morphology, composition, surface properties and microstructure. Most if not all of these properties affect the adsorption of proteins, host cells and foreign micro-organisms (such as bacteria) onto a surface. Therefore, the surface of a biomaterial is one of the most important research topics in the field of bio-engineering and biomaterials (34,42).

As mentioned previously, orthopaedic and dental implants are successful but are also susceptible to infection due to them mostly consisting of metallic surfaces. These infections can lead to apoptosis (cell death) of the host cells and can lead to necrosis of the surrounding tissues (43). Titanium and its alloys are an excellent choice for orthopaedic implants due to their cytoompatibility, strength and corrosion resistance. Nonetheless, titanium is vulnerable to infection. Hence, there is a need for an antibacterial titanium surface that can help combat the issue of costly revision surgery (44).

Pre-surgical contamination is the major cause of prosthetic implant infections and can cause infections to occur within three months of implantation. There are a few techniques in current use that can help reduce the risk of infection in orthopaedic and dental implants. One such technique involves the application of antimicrobial agents onto the implant surface. These agents can either be bactericidal or antistatic and can thus, affect and limit the interaction between the surface of the material and the bacterial micro-organisms. Another technique that is adopted is to incorporate silver onto the implant surface. The issue with these techniques is the release of these agents or silver ions cannot be controlled and can thus, lose their potency over time or pose a risk of toxicity (45).

As discussed previously, the best approach to combat infection would be to limit the crucial stage of reversible bacterial adhesion. Hence, an anti-adherent approach to alter the surface topography of an implant would be more beneficial than surface coatings. Extensive research is required in this field as much less is known regarding the behaviour of bacteria with surface engineered implants when compared to human cells (45).

2.3.3 Silver as an antibacterial agent

As previously discussed, metallic implants are susceptible to infection and biofilm formation. Silver and silver-based compounds are known for their antibacterial potential and behaviour. Silver is also low risk in regards to its toxicity to humans. The use of silver as an antibacterial agent is a highly popular and current strategy to reduce infection in medical implants. The antibacterial mechanism of silver has been widely researched and is thought to be due to the release of silver ions which are particularly effective when in the nanoscale range. Silver has been applied in the form of crystalline nano-rods which have displayed high antibacterial efficacies with a sustained release of silver ions over a long period of time. Some studies have also managed to combine silver with TiO_2 which provided pronounced antibacterial behaviours (43).

At the present time, the understanding behind the antimicrobial mechanism behind silver is not understood. It is proposed that there are potentially four mechanisms by which silver can kill bacteria. The initial step in all four mechanisms is the binding of silver to the cell membrane of the bacterial cells leading to absorption of silver into the cells. Once inside the cells, silver accumulates until the concentration increases and becomes fatal for the bacterial cells (46).

In the first mechanism it has been suggested how silver is able to inhibit the enzymes in bacterial cells thus, disrupting the electron transport system which leads to low functionality. Secondly, silver ions can disrupt the cell wall of the bacteria. When this occurs, the bacterial cell is unable to move or function and cannot access the essential nutrients for it to survive thus leading to cell death. In the third mechanism it is suggested how silver can interact with bacterial DNA leading to mutation and eventual cell death. Bacterial DNA is accessible to silver because bacterial cells do not possess a nucleus to protect DNA unlike eukaryotic cells. Thus, this mechanism cannot affect human cells. In the final mechanism, silver free radicals destroy the bacterial cells. Silver free radicals have unpaired electrons that are highly antibacterial due to their ability to disrupt the electron transport chain, impair bacterial DNA and rupture the bacterial cell membrane. If this occurs, bacterial cell death is inevitable (46).

Silver nanoparticles, salts and metallic ions have all been researched for their potential antibacterial effect. Although, they have shown strong antibacterial results there is still some concern regarding the cytotoxity of silver ions due to the limited understanding behind the antibacterial mechanism. Silver particles are able to diffuse into the native cells and release silver ions which can cause negative effects to the cellular function (41). An additional problem with the use of silver as an antibacterial agent is the resistance of bacteria towards its antibacterial effects (47). Clinical results have shown silver to possess low antibacterial efficacy due to some bacterial strains such as *S. aureus* developing a resistance to silver. Moreover, it has also been reported how silver can cause allergic reactions and staining of the skin and tissues therefore, the use of silver can be detrimental for some patients (46,47).

2.3.4 Implant integration

Research in the field of medical devices has increased greatly over the past decade to improve the cytocompatibility and integration of orthopaedic and dental implants into the host tissues (45). The cytocompatibility of a material is defined as the ability of a material to interact with living tissue without causing harmful immune reactions and to not be injurious to the tissue (9). Mechanical properties have also improved so that the elastic modulus matches that of bone to help prevent stress shielding. Steps have been taken to improve the bioinert nature of titanium in order to improve osseointegration and likewise corrosion and wear resistances have been explored to help prevent wear particle release that can cause aseptic loosening of the implant (45).

As mentioned previously, titanium and its alloys are used in dental applications for single or multiple tooth prostheses. The stable properties and presence of TiO_2 on titanium helps osseointegration to take place on the dental prostheses and in doing so also aids the prevention of bacterial colonisation. At present, most dental implant surfaces undergo physical modification that can be in the form of acid-etching or grit blasting. Both of these techniques increase the roughness of the surfaces (micrometre scale) and thereby, increase the interaction of bone with the implant surface via mechanical interlocking (48).

Using strong acids in the process of chemical etching, pits in the micrometre scale are formed on the surface of the implant. These pits increase the protein adsorption and cell adhesion via increases in surface energy which thereby collectively improves osseointegration. The optimum surface roughness for ossoeintegration to occur is in the range of 0.5-2 μm and chemical etching and grit blasting both create surface roughness's in this range. Hence, these processes are widely used at the present time. Nonetheless, there

are negatives to most approaches and with these techniques the disadvantage is the limited control over the microstructure or topography formed. For instance, the rough surfaces produced by these techniques are random and it has been documented how proteins and eukaryotic cells tend to have higher interaction with surfaces that have uniform nanometre surface features (48,49).

Nanostructures on titanium implants have been shown to affect the behaviour of osteoblast cells. These nanostructures can cause the osteoblasts to differentiate into mesenchymal stem cells (stem cells found in the bone marrow that are important for the formation and repair of hard tissues such as bone and cartilage) and can increase their adhesive capabilities to the implant surface. Osteoblast cells are also capable of undergoing elongation to align with certain surface structures (depressions) that are less than 100 nm in size. Nanostructured surfaces have also been incorporated with TiO_2 to form columnar TiO_2 nanotubes in an *in vitro* study via titanium implant anodization. With this technique it was found that osteoblast cells were able to differentiate and bone fixation was increased on the implant surface. The surface topographies produced in this study were regular and controlled and thus, offered a better solution to grit blasting or chemical itching. Nevertheless, more research is needed to assess whether this technique would produce similar results *in vivo* (49).

It is still not understood why bone is unable to fully form around an implant to achieve full implant integration. The contact between bone and titanium has been reported at most to be in the range of 45 %-65 % whereas, the ideal number should be 100 %. This figure indicates that the titanium surface of an implant is surrounded by connective tissue like cartilage rather than bone tissue. Improper implant fixation is related to implant failure

due to destruction of bone tissue at the implant and bone interface. Osteoblasts adhere to surfaces that are rough rather than smooth so it is proposed that controlling the roughness of an implant surface can affect the likelihood of osteoblasts adhering. However, this is difficult to achieve as a number of other factors need to be considered for instance, whether the surface will also promote bacterial adhesion due to its chemical properties or whether the implant surface is resistant to wear and corrosion. Wettability and surface topographies are also critical in the process of bone formation on an implant surface and hence, these factors must also be taken into account (50).

Previous studies have reported how the presence of carbon on titanium surfaces can hinder the integration of an implant. For instance, in a study it was found that when analysing the surface compositions of failed oral implants, most of the surfaces were contaminated with carbon at values between 17 %-76.5 %. Carbon deposition on titanium surfaces is inevitable and cannot be altered with surface topographical changes. Thus, other factors such as wettability and surface roughness should be of greater importance than chemical composition in regards to osseointegration (50).

Titanium and its alloys are an excellent choice for load-bearing applications due to their excellent strength-weight ratio, low elastic modulus, corrosion resistance and adequate fracture toughness. Although these properties are highly important for orthopaedic and dental applications, other properties such as bioactivity and cytocompatibility must also be considered. Bioactivity of an implant can be improved using bone inducing coatings such as hydroxyapatite but with cytocompatibility this is not the case as there have been very limited studies on the understanding behind the cytocompatibility of an implant (48).

The cytocompatibility of an implant is dependent on the interaction and adhesion of cells to the implants surface. Within seconds of the implantation of a prosthesis, proteins collect onto the surface of the implant. A few hours later (4-8 h) phagocytes produce a protein layer on the implants surface which adsorb and begin the process of cellular adhesion. This stage is highly dependent on the chemical and physical properties of the synthetic surface (when tested *in vitro*). This process is what enables osseointegration and implant fixation and thus, the success of an implant. Insufficient implant surfaces may lead to improper bone formation that is weak and can consequently cause poor implant fixation. Therefore, when developing new implants it is essential to consider the cytocompatibility of the material. It is difficult to test the cytocompatibility of a material as *in vitro* results can differ to *in vivo*. It is unethical to use living creatures for the testing of new implants and thus, the use of osteoblast like cells can be used for orthopaedic implant research (48).

These cells are referred to as SaOs-2 cells and are widely recognised cells that present similar phenotypic traits to human osteoblasts (51). SaOS-2 is the human osteosarcoma cell line, and the cells were initially isolated in 1975 from an 11 year old Caucasian female. The cell displays a mature osteoblast phenotype with similar ALP (alkaline phosphatase) activity to human osteoblast cells. SaOS-2 cells have shown to produce collagen and a bone-like calcified woven matrix indicating that their behaviour is very similar to human osteoblasts. They present no interspecies differences when compared to osteoblasts and also there are an unlimited number of cells henceforth, making SaOS-2 cells the chosen cell model to replicate the behaviour of human osteoblast like cells for *in vitro* testing (52).

2.4 Surface Degradation

2.4.1 Corrosion

As discussed previously, the cytocompatibility of a material is essential for biomedical applications and must be considered. Corrosion is also equally as important as both properties are related to one another. For instance, as the corrosion rate for an implant increases the likelihood for toxic ion release also increases which can thus lead to a higher risk of a negative immune response or rejection of the implant (53). This indicates that the higher the corrosion rate the likelihood of an implant being cytocompatible decreases. Implants must be compatible with water as the human body is comprised of many natural elements and water makes up approximately 65-75 % of the total composition. 96 % of these elements consist of oxygen, carbon, nitrogen and hydrogen which are present in all proteins. The remaining 4 % of the total elemental composition comprise of sodium, chlorine and potassium which are present in extracellular fluid and calcium, potassium and magnesium are present in bone and blood. In general, it is suggested that materials or implants are compatible in the body if they are formed of the above elements. Nonetheless, the elemental composition of the implant should be balanced as some of these elements can be toxic in larger doses which could be released as ions during wear or corrosion (53).

Additionally, implants should possess a specific load-bearing capacity in relation to their application to avoid fracture. Medical implants should also have high resistances to corrosion and wear as the environment (human body) they are placed in is corrosive due to its pH. At the present time, attaining an implant with all of the above properties is almost impossible as nearly all functioning implants fail within 12-15 years due to inappropriate

corrosion and wear resistances, mechanical properties as well as improper manufacturing or surgical techniques (53).

Corrosion is one of the more predominant issues in regard to implant failure. There are several different types and mechanisms of corrosion such as; galvanic, crevice, fretting, uniform, fatigue, stress cracking and pitting corrosion. These mechanisms are dependent on the material or implant environment and can have varying effects on the implant and human body. Corrosion can lead to ion release and can thus, limit an implant's function, lifespan and can induce allergic responses. Hence, it is essential for an implant to undergo a corrosion screening test to investigate its behaviour in various different environments and conditions (53). The corrosion behaviours of implants must be investigated in different conditions as the pH of the body can vary (3.5-9) according to the wound or infection (24). Some techniques regarding modification of implant surfaces via oxide production for example with titanium have shown to limit and delay the occurrence of corrosion (53).

2.4.1.1 Types of corrosion and their mechanisms

<u>Uniform corrosion</u>

During uniform corrosion, the complete surface is exposed to the cathodic reactants and the rate at which the corrosion occurs is the same across the whole surface. There are two stages for this corrosion type to transpire. Initially the metal surface is bombarded by the chemical solutions in the body which leads to the creation of a primary stage where the anodic and cathodic positions almost attach to each other. In the second stage, a corrosion nucleus forms on the surface of the metal. When this occurs, the passivation of the protective film will be blocked and hence, the metal surface will now be more reactive.

Therefore, it is essential for protective films (like oxides) to be resistant to corrosion to decrease oxidation from occurring. In order to be corrosion resistant, passive films must be non-porous, must have a structure that can prevent the electrons and ions to pass through the oxide boundary and lastly, the passive film must be resistant to abrasion. This phenomenon is referred to as uniform corrosion because the rate at which the corrosion occurs is the same across the whole surface (53).

Pitting corrosion

The second form of corrosion that can occur in biological implants is pitting corrosion which is also referred to as localised corrosion. Unlike uniform corrosion, corrosion in this phenomenon occurs as spots or pits on the surface. Pitting corrosion occurs via three stages; firstly, stable pit nucleation's form which cause a bare area on the metal surface that is no longer protected by the passive film. In the second stage, a metastable pit nucleation is formed which can re-passivate. This leads to the formation of a pit embryo which is a dissolved area on the metal surface formed due to local dissolution of the underlying metal. In the third and final stage, the surface is damaged as the pit stabilises and the re-passivation of the metastable pits begins (53).

Fretting corrosion

With fretting corrosion small, oscillatory movements (between 1-100 μm) transpire between the contacting surfaces when in the presence of corrosive medium (due to cyclic loading). Corrosion that occurs on orthopaedic implants such as artificial hip or knee joints usually undergo fretting corrosion due to exposure to the synovial fluid in the joints (53). Fretting corrosion is especially predominant in load-bearing orthopaedic implants. It tends to occur in the interfaces between the stem and cement or between the bone and stems

(24). Subsequently, when fretting corrosion occurs the release of ions and particles in the form of debris can enter crevices. Once they have entered the crevices, these particles behave in an abrasive fashion and can therefore, accelerate wear especially in sites of articulation. This can then lead to loosening and eventual failure of the implant (54).

Previous studies have reported how titanium implants (upon removal due to failure) have undergone discoloration. The neighbouring tissues of the implant also had a presence of metal ions which accumulated as the implant corrosion increased over time. With a Ti-6Al-4V implant it was found that the adjacent tissues had titanium, aluminium and vanadium particles. This suggests that the implant surface's passive layer may have undergone fretting wear which led to the release of wear debris. This debris may have dissolved in the corrosive fluids which again could have worsened the corrosion. Although titanium has its naturally occurring, corrosion resistant oxide layer it is still vulnerable to low shear stresses (even when rubbed against soft tissues) and can be disrupted by low stresses. Fretting conditions can also fracture the oxide layer and thus, the use of titanium can be limited in corrosive environments (54).

The corrosion behaviour of an implant is also dependent on the re-passivation of an implant once it has corroded in a solution. Titanium alloys are more likely to re-passivate than other metals such as stainless steel or Co-Cr alloys. The composition of the natural oxide changes once it has been re-passivated due to the incorporation of ions and again this affects the corrosion resistance of an implant. The re-passivated film comes into contact with electrolytes from the environment and is likely to undergo dissolution and re-precipitation. For instance with a titanium implant after implantation, the TiO_2 of a jaw

implant has been recorded to consist of calcium, sulphur and phosphorus which otherwise would not have been present before (24).

2.4.2 Wear

There are two major mechanisms of wear that occur in biological implants. Adhesive wear occurs when atomic bonding forces present between contacting materials are stronger than the strength of one of the materials. In this process, the removed material (in the form of wear debris or particles) remains attached to the surface of the other material. On the other hand, abrasive wear occurs when one material is stronger than the other material. When this stronger material slides on to the softer material, material is displaced or cut in the form of debris (55). The wear behaviour of a material depends on the displacement type, the contacting material and the load (24).

Implants fail due to wear because of the release of wear debris which corrode to form wear ions. As discussed previously, not only does the release of wear debris cause allergic responses or higher corrosion rates, the presence of wear ions can also lead to bone resorption. When bone is resorbed, the implant fixation decreases and hence, the implant loosens and detaches from the site of implantation. This phenomenon is common in orthopaedic implants and is referred to as aseptic loosening. Reports of post-mortems undertaken on patients who have received hip or knee implants have shown the accumulation of wear debris in the spleen, liver and also in the lymph nodes. This suggests that wear ions are able to travel across the body and can thus, cause unknown effects in other parts of the body (as shown in Figure 2.4.3) (24).

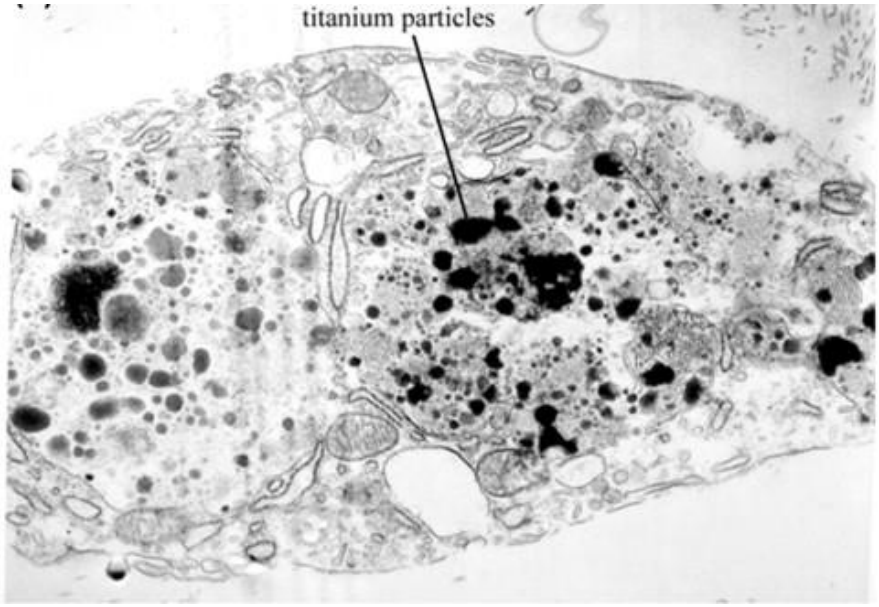

Figure 2.4.3. Transmission Electron Micrograph displaying a macrophage (found in lymph nodes) containing phagocytized titanium particles, obtained from (56).

The type of material used and the lubricant present in the site of implantation both affect the friction coefficient of implants. For instance, the friction coefficient for implant materials under *in vitro* dry conditions can be between 0.05-0.16 whereas, the average coefficient of friction for load-bearing synovial joints (lubricated with synovial fluid) such as hip or knee joints is approximately 0.02 with a wear rate of 106 mm^3/N (57). The use of titanium and its alloys for orthopaedic implants (particularly with articulating surfaces) is limited due to their poor wear resistances. This poor wear resistance is mainly due to the improper hardness of the oxide film and titanium's low resistance to plastic shearing (24).

The wear loss however, of titanium implants has been recorded to be less in lubricated environments (such as simulated body fluid or synovial fluid) than in dry conditions such as in air. This suggests that the wear mechanism that occurs for titanium implants is adhesive wear. The type of wear processes that occur can be further characterised as mild or severe wear. Mild wear causes small wear losses, is steady and

causes fine wear particles. Conversely, severe wear causes large wear particles to be released which cause a large wear loss. In order to combat poor wear resistances, several techniques such as oxidation, nitriding and thermal sprays have been introduced to harden the surface of materials and thereby, reduce wear. With oxidation and nitriding the additional advantage is that these processes are simple and there is no concern over interface debonding (17).

2.4.3 Complications of surface degradation of medical devices

The environment of the human body is highly corrosive due to the presence of chlorine and proteins in body fluids. When an implant is implanted into the body, several reactions take place on the surface. The metal surface of the implant is oxidised which leads to the formation of metal ions and the dissolution of the oxygen film leads to the formation of hydroxide ions. Nonetheless, although corrosion occurs for most metal implants, the rate at which it occurs can be decreased considerably due to the presence of the passive surface films (24).

Stainless steel implants are particularly susceptible to crevice corrosion and pitting corrosion. With the 316L stainless steel alloy, crevice corrosion has occurred at the interface between the fixation screw and bone plate due to the presence of chloride ions. When this has occurred in hip arthroplasties it has been documented to have led to the accumulation of cobalt in blood plasma and chromium release in urine. Pitting corrosion has often transpired in 304 stainless steel implants predominantly in the oral cavity due to the acidic presence of food and saliva. Pitting corrosion has also taken place in cobalt based alloys which has led to the release of carcinogens (cancer causing particles or substances).

Titanium is susceptible to corrosion when placed in an environment that has a high fluoride content. An example of this would be the oral cavity (24).

As discussed previously, when implants corrode or are worn they lead to the release of toxic metal ions such as iron, chromium, cobalt and titanium. It has been suggested that the initial release of metal ions would not be deemed to be toxic however, as the corrosion of an implant would increase, the probability of these ions to diffuse across the body would also increase. For instance, iron is required for all humans as it is involved in the transfer of oxygen from the lungs to the tissues via blood. Nonetheless, iron particle release due to wear has been found to damage proteins, DNA and cells which are all the building blocks of the human body. High iron concentrations can also lead to negative effects on the heart and liver and can thus cause liver failure, organ damage or even death if left untreated (53)

Similarly, chromium is present in the human body and can aid the control of blood sugar. When a chromium containing alloy undergoes wear and wear particle release in the body, the chromium ion is initially released as chromium IV. This is then reduced in the body to chromium III which is toxic. Chromium III can enter cells and lead to damage to DNA, kidneys, liver and blood. Furthermore, allergic reactions such as dermatitis and itching have been caused by nitrogen containing implants whereas, cobalt containing implants have led to negative neurological effects, cramping, muscular fatigue and dysfunction and memory difficulties (53). Thus, the occurrence of corrosion and wear must be avoided as much as possible for all medical implants.

2.5 Current Approaches

As previously mentioned, cp-Ti is used in orthopaedic and dental applications owing to its excellent cytocompatibility and inert passive oxide film. Nonetheless, cp-Ti possesses poor

tribological properties which can lead to the release of wear particles. Pure titanium has an inadequate strength for its use in orthopaedic implants and hence, due to all of the above issues related to cp-Ti, techniques that can modify the surface to reduce these complications are necessary. The type of current surface treatments that can be applied to titanium implants can either be surface coatings or diffusional surface treatments. The latter surface treatment is able to improve the tribological and hardness properties of the material, whereas the surface coating technique can be applied to improve the wear resistance, bioactivity and infection resistance of a material (4). Other more advanced forms of surface modification that have been potentially identified to improve the wear resistance, corrosion resistance, bioactivity and cytocompatibility can be in the form of surface oxidation or surface texturing (53), which will be discussed in Sections 2.6 & 2.7.

2.5.1 Surface coatings

In theory, a surface coating is the formation of an outer protective film or layer than can combat the issue of surface corrosion or wear. Additionally, it is anticipated that the addition of a surface coating can prevent the release of metal ions in the surrounding tissue or site of implantation (53).

Titanium nitriding has potential to improve the tribology of titanium and is commonly applied for this reason. When used as a hard coating, titanium nitride (TiN) has shown to be chemically inert and thus, improves corrosion resistance. In order to improve the interfacial bonds of surface coatings, the surface of a material must possess coupling agents, polar chemical groups (for the coating to bond to) or a high surface roughness so

that the surface bonding area is increased to improve the mechanical interlocking of the coating to the material's surface (21).

The issue with metallic biomaterials is their limited or no bio-function which can prevent the integration and fixation of an implant. Some surface coatings have demonstrated superlative bioactive properties in terms of improved osseointegration and blood compatibility for implants. For example, bioactive coatings in the form of hydroxyapatite have been used on cytocompatible metals due to its similar chemical composition, structure and biological properties to that of teeth and bone. Hydroxyapatite is a cytocompatible bio-ceramic material formed of calcium phosphate that can aid the regeneration of bone (58).

However, the concern with surface coatings is the insufficient adhesion strength between the coating and substrate. Fatigue stresses due to cyclic loading in orthopaedic implants can cause the spallation of the coating from the substrate which can lead to adverse effects in the surrounding tissue due to the release of detached particles (59). The durability of a coating is dependent on the cohesion and adhesion between the substrate material and the coating (Figure 2.5.1). Cohesion is referred to as the internal strength of a material which is related to the attraction of particles within the material and the coating. Whereas, adhesion is defined as the attraction between surfaces which is dependent on the force that resists the separation of the substrates and while holding the substrates together (59).

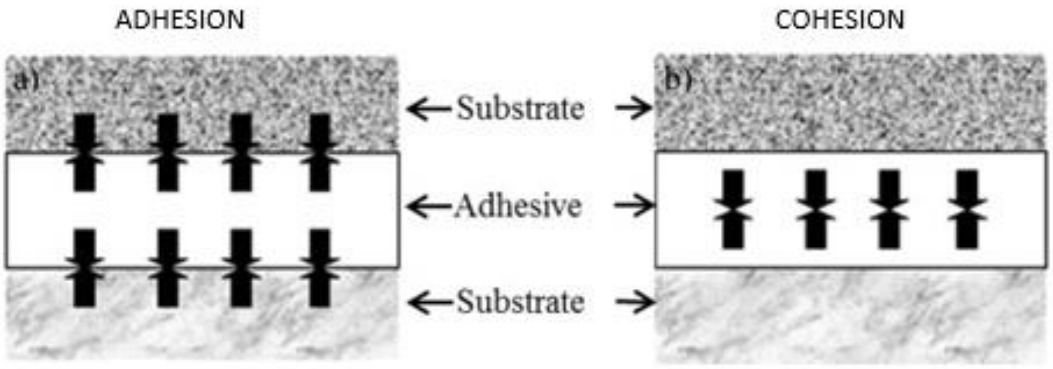

Figure 2.5.1. Illustration demonstrating the adhesive and cohesive forces present between the substrate and coating (59).

Plasma Nitriding

Plasma nitriding is a diffusion-based surface modification treatment that could be used for medical titanium and steel implants to improve their wear and corrosion resistances. Both surface coating and nitriding of Ti can produce a surface TiN layer with high hardness and wear resistance. However unlike TiN coating, the TiN layer formed during plasma nitriding has superior bonding to the substrate due to the metallurgical bonding nature; in addition, the load-bearing capacity is also much higher due to the formation of a nitrogen diffusion induced hard subsurface case (60).

However, plasma nitriding of Ti and its alloys is carried out at temperatures above 800 °C, which will cause distortion and loss of fatigue properties of the treated Ti implants. In addition, the phenomenon of an edging effect occurs because the electric field is distorted around the outer circumference or edges of the materials surface. The resulting features such as hardness and surface treatment thickness are non-uniform and hence, the corrosion and wear resistances will not be the same for the complete surface (61).

In the present time, the use of surface treatments and modifications have been widely used due to their ability to improve the mechanical, tribological and biological

properties. One surface treatment that has garnered interest is the use of TiO_2 to increase the osseointegration and antibacterial resistance of metallic medical implants. Anatase TiO_2 coatings have displayed antibacterial effects via the reduction of antibacterial attachment on the material's surface without negatively affecting the cytocompatibility. Thermal oxidation is a surface modification technique that has displayed promising results. With this modification technique, TiO_2 can be formed directly on the materials surface and in doing so the problem of poor bonding between treatment layer and material substrate is eliminated. This process is time and cost efficient and has good repeatability (62).

Furthermore, another surface modification technique that has an antibacterial potential is the process of creating structures or textures onto the materials surface. These structures can alter the wettability and surface roughness of the materials surface and thus, affect the adhesion of bacteria (2).

2.6 Surface Texturing & Micro-Patterning

2.6.1 Surface texturing

Surface texturing has been used in biomedical implants as a modification technique that can increase the cytocompatibbility of an implant, reduce the corrosion rate and initiate osseointegration. Techniques such as electropolishing, acid etching, sand blasting and anodic oxidation are all techniques that fall in the category of surface texturing. Surface texturing can increase the surface roughness of metal implants and in doing so, promote fixation of the implant by encouraging bone healing and regeneration (59). In dental implants, surface roughness's in the micrometre and sub-micrometre range have displayed improvements in protein sythesis and cell proliferation when compared to a flat surface.

Therefore, the longevity of the implant was increased as tissue healing improved leading to better implamnt integration (63).

Laser micro-patterning

With the use of a femtosecond (fs) laser, ultrafast pulse formation occurs that possesses an insignificant dispersion of energy due to conduction by the bulk material. Consequently, there is an insignificant heat zone and the thermal effects on the treated surface are reduced. Thus, the use of femtosecond irradiation is a successful technique for surface modification (64,65).

When irradiating linear polarised laser pulses on a solid material using a laser in the femtosecond range (fs), the phenomenon of laser induced periodic surface structure (LIPSS) formation occurs. This technique is a single step process that is able to produce micro or nano sized structures (66,67). With fs irradiation, two types of LIPSS can be formed; low spatial frequency LIPSS (LSFL) and high spatial frequency LIPSS (HSFL). With LSFL the periodicity (Λ) is equal to the irradiation wavelength (λ) whereas, HSFL is formed when the periodicity is significantly shorter than the irradiation wavelength ($\Lambda < \lambda$). HSFL produces fine surface ripples while LSFL leads to the formation of coarse ripples (66,68).

The polarisation of the incident laser beam greatly affects the orientation of LIPSS and varies according to the material type, whether it is a strongly absorbing (metals or semi-conductors) or a dielectric material. In general, LSFL ripples are formed on absorbing materials perpendicular to the laser beam polarisation conversely, when polarisation occurs on dielectric materials LSFL can be oriented parallel or perpendicular to the laser beam polarisation. Metals with rough surfaces possess surface electromagnetic waves which interact with the incident laser beam and leads to the formation of LSFL. On the other hand,

HSFL are predominantly formed on dielectric materials with a χ in the fs-ps (picosecond) range (66).

Furthermore, there are three properties that affect the type of LIPSS formed; depth, periodicity and orientation. The ability to control these characteristics can lead to better organised surface features that can possess specific surface properties. Nonetheless, it is difficult to effectively control these properties as the formation mechanism of LIPSS is not yet fully understood. Previous studies have reported how the depth of LIPSS is dependent non-linearly to laser fluence (optical energy per unit area). Increasing the incident angle of the laser beam can lead to increased periodicity of LSFL however, some studies have disputed the importance of incident angle beam. The orientation of LIPSS is dependent on the electric field vector of the laser polarisation and is usually perpendicular to the polarisation vector. Hence, it can be said that the polarisation of the laser is of high importance as it can affect the laser material interaction (of which the width of the scan lines depends on) and the orientation of the LIPSS produced. Controlling the polarisation state can lead to correct LIPSS or surface feature formation (65).

A variety of surface properties can be altered with LIPSS such as; colorization, control of surface wettability and friction coefficients. Due to changes in friction behaviour produced by LIPSS, there is a possibility of reduced wear occurrence on the surface of materials with LIPSS. Therefore, this has led to increased attention from researchers for the use of LIPSS on biomaterials. LIPSS were initially observed five decades ago and are considered to be the smallest surface feature that can be formed. LIPSS can be formed on all material types (metal, polymer, semi-conductor or glasses) and can be produced in all environments (air, gas, vacuum or liquids) (3).

Moreover, fluctuating the orientation of LIPSS ripples or gratings can cause differing colorization on a materials surface in addition to the modification of the wetting properties of a surface. With LIPSS, the possibility of creating super hydrophobic surfaces is made possible which can affect the behaviour of cells and bacteria (69). Surfaces with a water contact angle (Θ) of less than 90° are referred to as hydrophilic and those with angles higher than 90° are referred to as hydrophobic (70). In general, hydrophobic surfaces are preferred in biomaterials as they possess improved protein adsorption properties (71). The ability to create surface tracks or grooves is also likely with LIPSS. Bacteria have shown to be able to grow and move along tracks and thus, the orientation of the LIPSS tracks can be predefined with an antibacterial function to limit the movement of bacteria on certain surfaces. LIPSS is a cost effective technique which offers many surface functionalisation opportunities and thus, is of great interest for researchers (69).

Therefore, along with improved tribological features and effect on wettability, these surface ripples have shown to impede the attachment of bacteria and enable eukaryotic cell growth (72–74). Bacteria and eukaryotic cells are alike in their sensitivity to surface properties such as topography, chemistry, composition and wettability. However, their responses to surface properties differ. Bacteria are less motile, smaller in size and more rigid than eukaryotic cells and hence, behave differently to surface characteristics. Biomaterials can be coated with bactericidal films (silver) or impregnated with drugs such as antibiotics but these techniques all carry risks of toxicity or failure over time. Therefore, the use of surface treatments that can engineer non-toxic and cytocompatible antibacterial features directly onto a materials surface are highly desired (75).

Surface texturing such as LIPSS allow a vast degree of surface feature formation that can differ in size or shape. Due to its reproducibility, simplicity and ease of control it is potentially a worthy technique for biomaterials and implants. Also, LIPSS has no issue of toxicity due to almost non-existent surface contamination. Surface roughness is a property that can be altered by laser texturing and it greatly affects the behaviours of eukaryotic cells and bacteria. Previous studies have reported how polished surfaces with low surface roughness's cause higher bacterial attachment to the surface. Surfaces with cavities or features larger than the size of the bacteria can also cause increased bacterial adhesion. However, there is limited research on the effect of LIPSS treated surfaces on both bacteria and eukaryotic surfaces together (75).

Previous studies have documented the formation of LIPSS in the micrometre scale. It was reported how LIPSS can positively affect cellular behaviour such as growth and attachment. Additionally, LIPSS in the sub-micron range can lead to the alignment of osteoblasts and cause osteoblasts to grow along the LIPSS tracks or grooves (67).

Other studies have demonstrated the effects of nanostructures on mesenchymal stem cells. With the use of a laser in the fs range, nanostructures were formed on grade II titanium alloys. It was documented how the cells (when in contact with the LIPSS treated surface) displayed reduced adhesion behaviour and therefore, reduced cellular surface area. However, when these cells were cultured in an osteogenic medium over a four week period, enhanced bone matrix mineralisation occurred with the mesenchymal stem cells differentiating into osteoblasts. This suggested that the LIPSS surfaces may have instantaneously reduced the mesenchymal stem cell count but, these surfaces in the long term led to better bone formation (75).

The results are conflicting and thus, must be researched further. In addition, it has been reported that the durability of micro-patterns formed on such soft substrates as austenitic stainless steel was poor. Also, LIPSS on Co-Cr-Mb have shown to cause increases in friction coefficients and therefore, low wear resistances when compared to polished samples. Therefore, it is of paramount importance to investigate the durability of LIPSS formed on cp-Ti (76).

2.7 Ceramic Conversion Treatment

As discussed in Section 2.4, Ti and its alloys are characterised by poor tribological properties in terms of high friction, high tendency for adhesion and low wear resistance. Therefore, it is reasonable to deduce that the durability of such micro-patterns as LIPSS formed on soft cp-Ti substrates would be low and how to improve its durability is a major technical challenge. However, as evidenced from the discussion in Section 2.5, current surface engineering technologies used for Ti engineering components are not suitable for Ti implants mainly due to the concerns over interface debonding, spallation of coatings on Ti substrates, the concern over high treatment temperature induced distortion and loss of fatigue properties associated with plasma nitriding. Recently, an advanced ceramic conversion treatment has been developed specifically for enhancing the tribological properties of Ti and its alloys (77).

2.7.1 Thermal oxidation and titanium oxide

As discussed in Section 2.5, the spontaneous passive oxide formation on titanium is responsible for its improved biological properties. Although the native TiO_2 is only a few nanometres thick, the chemical stability and structure it provides positively impacts the cytocompatibility, chemical inertness and corrosion resistance. The passive oxide layer is

compact, uniform and possesses good adhesion to the substrate. Hence why titanium is considered to be a good biomedical material. This oxide layer that forms comprises of an internal portion of nonstoichiometric oxides and the external portion consists of an amorphous TiO_2 layer (78).

The chemical inertness of the TiO_2 makes it bioinert in the human body which enables it be cytocompatible but also limits its application capability. In order for the integration of an orthopaedic implant to occur, the implant surface must allow or initiate bone formation and if the surface of the implant is bioinert this bioactivity is limited (42). Some techniques have shown promising results to improve the bioactivity of titanium via the use of TiO_2 in powder form. However, the problem with these powders is the lack of control to their morphology and hence, their mechanical properties. Thus, at the moment these powders cannot be used clinically. Another potential technique is plasma spraying. TiO_2 deposition via plasma spraying is a quick and flexible process. It is able to produce thick TiO_2 coatings at a relatively low cost. However, as with other coatings, the interface bonding between the coating and the metallic implants is always a major concern and this is a particularly issue for thermal sprayed coatings due to their mechanical bonding nature. Furthermore, plasma spraying produces TiO_2 coatings that are bioinert so the integration and bonding between the implant surface and bone tissue is often poor (42).

Moreover although the passive oxide layer can improve the corrosion resistance of titanium, it cannot effectively improve the wear resistance due to its thin nanometre thickness (78). One possibility for increasing the thickness of surface oxide film is through thermal oxidation at elevated temperatures for a prolonged time period. Nonetheless, the adhesion bond between the expanded oxide and the substrate material weakens when the

thermal oxidation is not optimally designed and controlled. Spallation of a thick oxide layer occurs especially under sliding contact and thus, high loads cannot be applied (19). Hence, it is essential to understand the mechanism of thermal oxidation of Ti and the formation of surface oxide layers.

Thermal oxidation takes place due to the high chemical affinity of titanium towards oxygen and its high diffusion capability at high temperatures (78). Thermal oxidation has displayed results of improving wear and corrosion resistances. Thermal oxidation has the capability to produce uniform 1 μm thick oxide layers. The uniformity of the oxide leads to a constant surface roughness and increases the surface energy. During thermal oxidation, the formation of a rutile-based oxide ceramic layer takes place and in the meantime an oxygen diffusion zone (ODZ) underneath also forms which can effectively harden Ti via solid solution strengthening (79).

Titanium surfaces modified using thermal oxidation display favourable properties due to the formation of a crystalline rutile based oxide layer. Controlling the temperature and duration of the thermal oxidation process can produce an ODZ with controlled composition, morphology and suitable corrosion, mechanical and wear properties (78).
It has been reported that there are five steps in the formation of TiO_2 during thermal oxidation. The initial step involves the absorption of oxygen, secondly the dissolution of oxygen takes place. Thereafter, a thin oxide film is formed on the surface which then grows and thickens and lastly, a thick oxide layer is formed (79). The oxide formation formula is shown below.

Eq 1. $Ti + O_2 = TiO_2$

Previous studies have reported the effect of temperature on oxide formation. For instance, it was found that longer treatment times and higher temperatures led to higher oxygen concentrations. XRD analyses displayed how high temperatures and treatment durations led to lower angles for α-Ti which suggested the lattice parameters increased. This increase in lattice parameters caused higher surface hardness of Ti and thus, the wear resistances improved. Increases in treatment temperature (ranging between 600 °C- 850 °C) also produced thicker oxide layers. This thicker and harder oxide layer also improved the corrosion resistance of Ti and it was found that the optimal treatment temperature to produce a good oxide layer was between 600 °C- 700 °C (79).

Reports have also suggested, when thermal oxidation treatment temperatures are between 600 °C- 900 °C a rutile based TiO_2 forms on the surface of pure titanium. Lower oxidation times and temperatures lead to a strong bond between the formed oxide and substrate. Higher temperatures leads to weaker bonding forces and thus, there is a risk of oxide spallation and poor wear resistances (79).

Moreover, when thermal oxidation occurs an oxygen diffusion case is present between the oxide layer and substrate, which comprises of an α-phase TiO solid solution. Increasing the thermal oxidation treatment time and temperature leads to an increase in the oxygen concentration in the oxygen permeating layer and thereby, the thickness of this diffusion case increases. In the initial stage of oxidation, both the oxide layer and the oxygen diffusion layer grow in accordance to the parabolic law. As the oxidation time increases, the growth of the oxide layer increases whilst the growth of the permeable layer remains constant. However, when oxidation times are short, the growth of the oxygen diffusion layer occurs at a faster rate than the growth of the oxide layer. Nonetheless, the effect of

temperature on oxidation is greater than the effect of treatment time when producing a thick stable oxide layer (79).

Other studies have also displayed similar results for instance, it has been shown that temperature is the most affecting factor in the thermal oxidation process. At temperatures below 700 °C, oxides that form consist of finer and more uniform oxide particles when compared to the oxides produced at lower temperatures (below 600 °C). The rutile based oxide that forms significantly increases the surface hardness (five times higher than raw titanium) and resistance to abrasive wear (78,79).

Ceramic conversion treatment

As discussed in the preceding section, increasing the thickness of the passive oxide film has some potential in improving the wear characteristics of titanium. This can be undertaken via optimally designed and controlled thermal oxidation or so-called ceramic conversion treatment (CCT) specifically tailored for surface treatment of Ti and its alloys, which is a simple, environmentally friendly and cost effective method. CCT is a relatively new surface engineering technique that was developed in 1997 specifically for titanium based materials. CCT is based on thermal oxidation and is undertaken in a controlled oxygen containing environment. With CCT, the titanium's surface reacts with oxygen to form an in-situ ceramic like titanium oxide. Also, interstitial solid solution hardening occurs when oxygen diffuses into the titanium and forms an oxygen hardened case. The advantage of this process is the ability to harden the titanium without damaging the surface unlike other thermochemical processes. CCT is cost effective and environmentally friendly and thus, it is a highly suitable surface engineering technique. CCT is undertaken in air with a composition of 20 % oxygen and 80 % nitrogen (80,81).

During CCT, Ti is exposed to an oxygen rich environment at an optimally selected temperature. The oxygen diffuses into titanium creating an oxygen diffusion zone (ODZ). At an appropriately elevated temperature, more oxygen diffuses into the surface and an oxide layer will form at the surface when the surface oxygen content exceeds the solid solubility of oxygen in Ti. The newly formed oxide layer has a strong bond and adhesion to the substrate material due the in-situ conversion nature and therefore, reduces the likelihood of bonding issues or fractures between the surface oxide layer and the substrate. The thick TiO_2 layer has an improved resistance to corrosion and wear (80,82).

Previous research undertaken has suggested the use of CCT on titanium with promising wear results. During CCT, a diffusionally bonded ceramic layer (rutile-based TiO_2) forms with an ODZ that is strengthened via oxygen. CCT offers more control to the thermal oxidation process and is typically undertaken at 600 °C with long treatment times (50-100 h) (81). Using temperatures of 600 °C or above, a rutile based TiO_2 layer forms during CCT which is similar to traditional thermal oxidation. However, the difference is with CCT the oxide layer that forms behaves in a similar fashion to ceramics in terms of mechanical properties. The oxygen diffusion hardened case that forms below the ceramic oxide layer provides mechanical support to the oxide and thus, a high load-bearing capability. Also with CCT the bonding between the ceramic oxide layer and the oxygen hardened case is strong due to the in-situ conversion mechanism of the TiO_2 formation and hence, there is not an associated issue of surface oxide removal. CCT is an environmentally friendly technique as there are no toxic by-products unlike anodising. Therefore, CCT produces oxides with improved properties (83). Increasing temperature and treatment times leads to the formation of thicker surface oxide layers and ODZ's. However, with these treatment

parameters the oxide layer that forms is porous and possesses poor bonding to the substrate. This could lead to poor hardness's and wear resistances and hence, a balance must be found between the duration and temperature of the CCT process (80,83).

Due to the formation of the surface ceramic oxide layer and the oxygen diffusion hardened case, the surface hardness of titanium can be greatly improved via CCT. The highly unstable friction coefficient of titanium and its alloys due to their high adhesion can also be improved via CCT. The rutile based oxide layer that forms due to CCT has shown to improve the friction coefficient especially under lubricating conditions. For instance, friction coefficients have shown to reduce from 0.4–0.5 (untreated material) to 0.1–0.2 after CCT under lubrication and similar results have been found under dry conditions too. Rutile has a layered structure which causes it to possess low shear stresses and friction coefficients. The formation of a rutile TIO_2 during CCT has shown to improve the wettability of titanium when using oil. This suggests that rutile, due to its higher wettability amplifies the lubricating effect and thus, the friction coefficients decrease under wet conditions. Ti applications in the human body encounter bodily fluids and require good friction coefficients under lubricating conditions. The improvement of friction coefficients under lubrication suggests CCT is a good surface engineering technique that can be used for medical Ti implants (80). The use of CCT has also shown improved adhesive wear properties due to increases in hardness. CCT undertaken on Ti6Al4V at 600 ˚C for 60 h had improved surface hardness from 450 to 1300 HV0.01. This increase in hardness led to high wear resistances under sliding conditions. Studies using CCT have also shown no negative effects on the cytocompatibility and corrosion resistance of Ti-6Al-4V. In fact CCT was shown to improve the osteoblastic cell attachment and bioactivity of Ti-6Al-4V (54).

As discussed previously, medical implants are susceptible to bacterial contamination and infection is one of the leading causes of failure. The use of antibacterial coatings such as silver coatings, have shown improved antibacterial properties but there are also uncertainties regarding silver ion release, poor bonding and toxicity. TiO_2 has shown to possess some antibacterial efficacy via photoactivity nonetheless, studies into the antibacterial nature of TiO_2 without the use of UV irradiation are limited (83).

2.8 Summary

As discussed, cp-Ti and other Ti alloys possess good corrosion resistances and cytocompatibility due to their native oxide layer. It has also been reported, the naturally occurring oxide layer may cause an antibacterial effect for Ti alloys. However, the durability of the naturally formed oxide film in contact with other surfaces is low due to its extremely thin nature and the soft substrate.

One of the major issues related to Ti and its alloys for its use in medical implants is the low hardness and poor wear resistances, especially adhesive wear. The occurrence of adhesive wear leads to the release of wear ions which can cause toxic effects towards the host and thus, lead to failure. Infection is also prevalent in Ti related implants and is one of the major causes of failure. The use of coatings or silver ions had led to improved infection resistances; nonetheless these techniques are associated with toxicity or poor bonding issues.

The use of surface texturing has proven to cause antibacterial effects. However, there has been limited research on the effect of LIPSS formed on cp-Ti using a laser in the femtosecond range on both Gram positive and negative bacteria with different shapes (rod-shaped bacteria or cocci shaped bacteria) together. In addition, no previous research has

combined the effect of LIPSS on both antibacterial efficacy and osteoblast like cell viability. To date, there has been very limited research on combining micro-patterning and titanium oxide to create a duplex treated surface. One study investigated the direct nano-micro-patterning of titania layers using X-ray lithography. However, no wear, corrosion or antibacterial tests were undertaken using this nano-patterned titania surface (84).

CCT has been proved to effectively improve the tribological properties of Ti and its alloys through in-situ conversion of Ti surface into a relative thick rutile oxide layer with strong bonding to the underneath oxygen diffusion hardened subsurface case which also effectively supported the surface oxide layer.

Nevertheless, in the present time no research has been undertaken to combine CCT and laser surface texturing to produce a novel duplex surface system that can combine the antibacterial effect and corrosion and wear resistance of both surface engineering techniques. Also, no study has been conducted to investigate the cytotoxicity or the cytocompatibility of the new duplex system for potential medical application.

Hence, the aim of this investigation was to investigate the antibacterial efficacy, cytocompatibility, wear resistance and corrosion resistance of the duplex surface system consisting of LIPSS and CCT on cp-Ti.

Chapter 3

MATERIALS AND METHODS

3.1 Materials and Sample Preparation

3.1.1 Substrate material

Commercially pure titanium can be classified into 4 grades by ASTM and in general is used in applications where low tensile strengths are required for instance, in dental implants. The properties of the different grades for cp-TI can be seen below in table 3.1.1 (85).

Table 3.1.1. The properties for each cp-TI grade. Grade 2 has been highlighted as this was used in this study (85).

CPTI Grade	Yield Strength MPa)	Elongation (%)	Elastic Modulus (GPa)	Ultimate Tensile Strength (MPa)
1	170	24	103-107	240
2	275	20	103-107	345
3	380	18	103-107	450
4	483	15	103-107	550

Cp-Ti was chosen in this investigation as it is widely used in dental applications due to its excellent resistance to corrosion and mechanical properties. Comparing it to the other widely used Ti alloy in medical implants (Ti-6Al-4V), cp-Ti has greater stability in orthopaedic applications and better bone to implant surface contact (20). As a result, cp-Ti grade II was chosen in this study due to its good combination of elongation and strength.

3.1.2 Sample preparation

Commercially pure titanium rods grade II (William Gregor Ltd, UK) with a length of 1 m and diameter of 25 mm were cut into round discs with a thickness of 6 mm using the Accutom-50 (Struers, UK) cutting machine. A silicon carbide blade was used and the cutting was undertaken at a speed of 3000 rpm with an initial and final feed rate of 0.05 mm/s and 0.15 mm/s respectively. Post cutting, the samples were ground and polished using a grinding/polishing machine (Buehler, UK). The samples were ground using metallographic abrasive paper (METPREP, UK) with a grade number of 240 and 400. Thereafter, the samples were polished using a 200 mm (diameter) MD-Largo composite disc (Struers, UK) with a 9 micron diamond polishing solution. After this step the samples underwent final polishing with a colloidal silica solution using a Struers MC Chem velvet disc. All of these steps were undertaken at a speed of 250 rpm. After grinding and polishing, the resulting thickness of the samples was approximately 5 mm. Prior to all the surface treatments, the samples were cleaned with domestic detergent and water and then in an ultrasonic bath using acetone for a duration of 5 min.

3.2 Surface treatments

Initially in total five sample types were to be used in this investigation; untreated/as polished (P), laser micro-patterned (MP), thermally oxidised (PTO), laser patterned thermally oxidised samples (MPTO) and lastly, thermally oxidised laser micro-patterned samples (TOMP). The as polished samples were used as the control (untreated) samples.

3.2.1 Ceramic conversion treatment

As reported in section 2.7, the oxidation of titanium leads to the formation of a stable TiO_2 film (83). Rutile based oxides however are the most stable structure formed during oxidation (54). A surface engineering technique was developed that enabled the formation of an oxide that had improved tribology. This process was referred to as ceramic conversion treatment due to the formation of diffusionally bonded ceramic layer of TiO_2 on the titanium alloy surface. The beneath oxygen diffusion zone can provide support to the resultant TiO_2 layer that is formed (79).

During this study the patterned and the untreated samples were placed in a large laboratory furnace (Elite Thermal Systems Ltd, UK) in air at a temperature of 600 °C with a duration time of 85 hours and under normal atmospheric conditions. The parameters used were the optimal parameters (83) in regard to the mechanical bonding and friction properties of the surface oxide layer and the load-bearing capacity of the surface system. After the CCT treatment, the samples were left overnight in the furnace to cool down to room temperature.

3.2.2 Laser micro-patterning

Laser-induced periodic surface features (LIPSS) are of particular interest due to the many functional properties the surface textures can affect. In this research, the micro-patterning of the as-polished and CCT treated samples was conducted to produce LIPSS as part of a collaboration with the Laser Surface Treatment Group at the Mechanical Engineering Department using the parameters as summarised in Table 3.2.2. The process was

undertaken in the atmosphere. The resulting hatch distance between the two patterns was 12 micron and the distance between each consecutive ripple (peak to peak) was 1 micron.

Table 3.2.2. Laser Micro-patterning Parameters (the parameters used were previously optimised by the laser surface treatment group (86).

Pulse duration (fs)	310
Wavelength of the laser (nm)	1030
Pulse repetition rate (KHz)	500
Number of pulses	18
Maximum peak power (MW)	32

A micro processing laser platform was used (Figure 3.2.2); within this platform a Yb-doped femtoseconds laser was integrated that was sourced from Amplitude Systems. For the patterning, a 310 fs pulse duration was used and the rate of maximum repetitions was 500 kHz. The maximum pulse energy used was 19 µJ and lastly, a central wavelength of 1030 nm was used. The beam delivery sub-system (Newson Engineering) included a 3D scan head

(RhoThor RTA) with a 100 mm tele-centric focusing lens. The input beam diameter of 5 mm was focused to an irradiation spot size of 30 µm and maximum peak power of 32 MW.

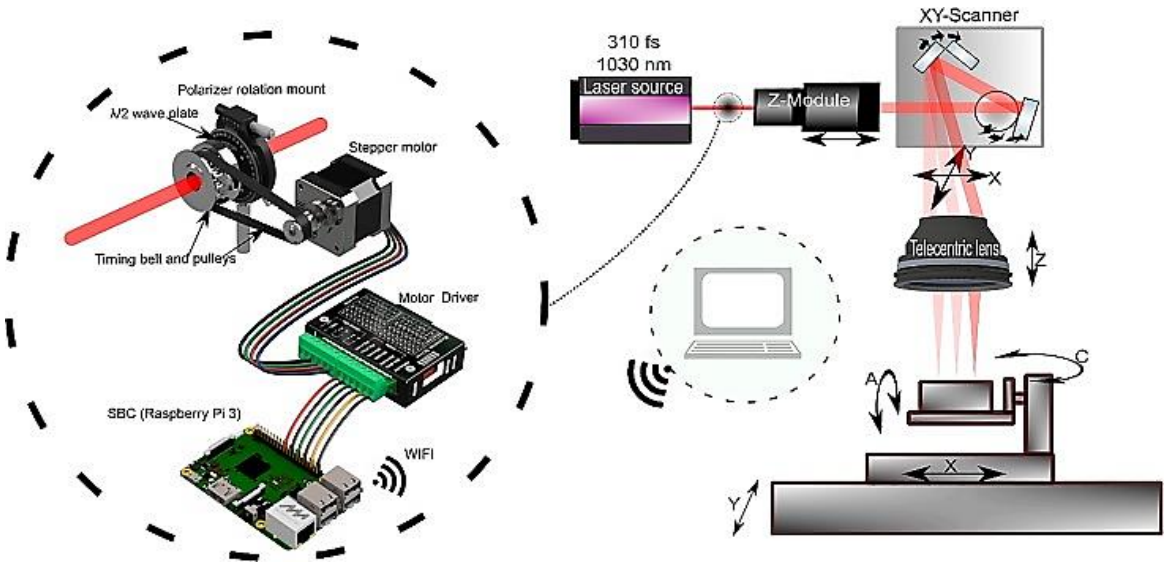

Figure 3.2.2. Illustration of the laser processing setup used in this research and a diagram showing the polarization control sub-system (65).

Mirror polished cp-Ti grade II substrates were used. The samples were ultrasonically cleaned in water and acetone and dried with hot air prior to laser processing. The quality of the processed LIPSS was analysed using a focus variation microscope (Bruker Alicona G5 Infinite Focus system, USA) and a scanning electron microscope.

However, towards the end of this study changes were made in the laser power used in order to reproduce the samples without removing or damaging the TiO_2 layer. Finally, powers of 48 % and 58 % were chosen where at a power of 48 % used on the TOMP samples there was less destruction of the oxide layer and as a result less LIPSS. On the other hand, at 5 8% power the TOMP samples had more ripples of the LIPSS and a greater destruction of the TiO_2. To produce comparable results the same was done to create the MP samples. As a result, there were now nine samples types (Table 3.2.3).

Table 3.2.3. Table displaying the 9 sample types used in this study.

Sample Types	
Sample Name	**Treatment Type**
P	Untreated, mirror polished
PTO	Polished sample that underwent CCT to form a rutile based oxide
MP	Polished sample with LIPSS. The pattern was in the form of 1 micron ripples.
MPTO	Polished, micro-patterned sample was placed in the furnace for CCT. As a result, this sample had combined LIPSS and CCT (LIPSS first, then CCT).
TOMP	LIPSS were formed on the polished samples that had undergone CCT. As a result this sample type had a combination of both treatment types (CCT first, then LIPSS).
MP48 – This sample was used in the bacterial attachment, tribology and corrosion tests only.	Polished sample with LIPSS. 48 % power was used of the laser which produced a surface that had greater spacing between each individual ripple (when compared with MP58).
MP58 – This sample was used in the bacterial attachment, tribology and corrosion tests only.	Polished sample with LIPSS. 58 % power was used of the laser which produced a surface that had lesser spacing between each

	individual ripple and hence, more ripples (when compared with MP48).
TOMP48 – This sample was used in the bacterial attachment, tribology and corrosion tests only.	LIPSS were formed on the polished samples that had undergone CCT. As a result this sample type had a combination of both treatment types (CCT first, then LIPSS). 48 % power was used of the laser which produced a surface that had greater spacing between each individual ripple (when compared with TOMP58).
TOMP58 – This sample was used in the bacterial attachment, tribology and corrosion tests only.	LIPSS were formed on the polished samples that had undergone CCT. As a result this sample type had a combination of both treatment types (CCT first, then LIPSS). 58 % power was used of the laser which produced a surface that had lesser spacing between each individual ripple and hence, more ripples (when compared with TOMP48).

3.3 Characterisation

3.3.1 Surface morphology and elemental analyses

The major characterisation technique used in this work is electron microscopy which involves scanning electron microscopy (SEM) and energy dispersive X-ray analysis (EDX). SEM is primarily used to study the surface textures, bacterial distribution, the morphology

of the bacteria and SaOS-2 cells. SEM is also used to observe any wear tracks produced from the dry and lubricated wear tests as well as any damage undertaken on the sample due to electro-chemical corrosion tests. EDX is a powerful tool in chemical analysis and was used to analyse the elemental distribution on the surfaces.

The surface morphologies of the different sample types were observed using a JEOL 5300LV SEM, Japan at 20 kV in high vacuum mode with a working distance of 9.5 mm. EDX was also undertaken using the same SEM to evaluate and compare the elemental distribution in the untreated and treated samples.

3.3.2 XRD analyses

The different phases and crystal types of each sample type was analysed using X-ray diffraction (XRD). The model used was the Inel X-ray Diffractometer Equinox 3000, France with Cu Kα radiation (λ= 0.154 nm). The diffraction angle (2θ) was between 20.01 and 70° and the scanning step was 0.02° for counting times of 1 s at each step. Subsequently, The X'pert High Score software with PCPDFWIN data-base was used to identify the presence of crystalline phases and to analyse the results gathered from the XRD.

3.3.3 XPS analyses

The X-ray Photoelectron Spectroscopy (XPS) analyses were conducted at The Midlands Surface Analysis Ltd at Aston University. The work was commissioned to analyse the MP, MPTO and TOMP samples in order to identify the different chemical bonding's and specifically identify the oxidational state of Ti. Under the conditions of these analyses, XPS also gives quantitative information on all elements, excluding H and He, at a detection limit of 0.1 %.

The XPS analysis was undertaken using a Thermofisher ESCALAB 250 electron spectrometer, USA equipped with a hemispherical sector energy analyser. Monochromatic Al Kα X-ray source was used for analysis to enhance the resolution. The area of analysis was selected to be 500 µm diameter. XPS survey scans were then recorded for each sample in order to identify all the elements present in the surface. Narrow region energy scan spectra were subsequently recorded for each element identified on each analysed area.

All the samples were first analysed in their "as received" state and great care was taken in these process not to introduce any further contamination. Further testing was conducted after Ar ion beam etching at an energy of 3 keV and current of 1 uA rastered over an area of 2 x 2 mm for a period of 150 s to remove 15 nm of the surface. The aim of this etching was to remove carbonaceous contamination from the surface of the samples.

3.3.4 Profilometer analyses

A XP Stylus Profiler (Ambios Technology Inc, USA) as seen in Figure 3.3.4 was used to measure the surface roughness (Ra) and to observe any topographical features of the untreated and treated samples. Ambios software was used to analyse the data. The samples were scanned at a driving frequency of 293.694 kHz using a standard tapping mode Si cantilever (Tap300-G) (Budget Sensors). The surface roughness measurements were taken along five different regions of each sample type and were then averaged to be used as the mean roughness measurements. The results were expressed as the mean ± standard deviation (SD) of the measurements.

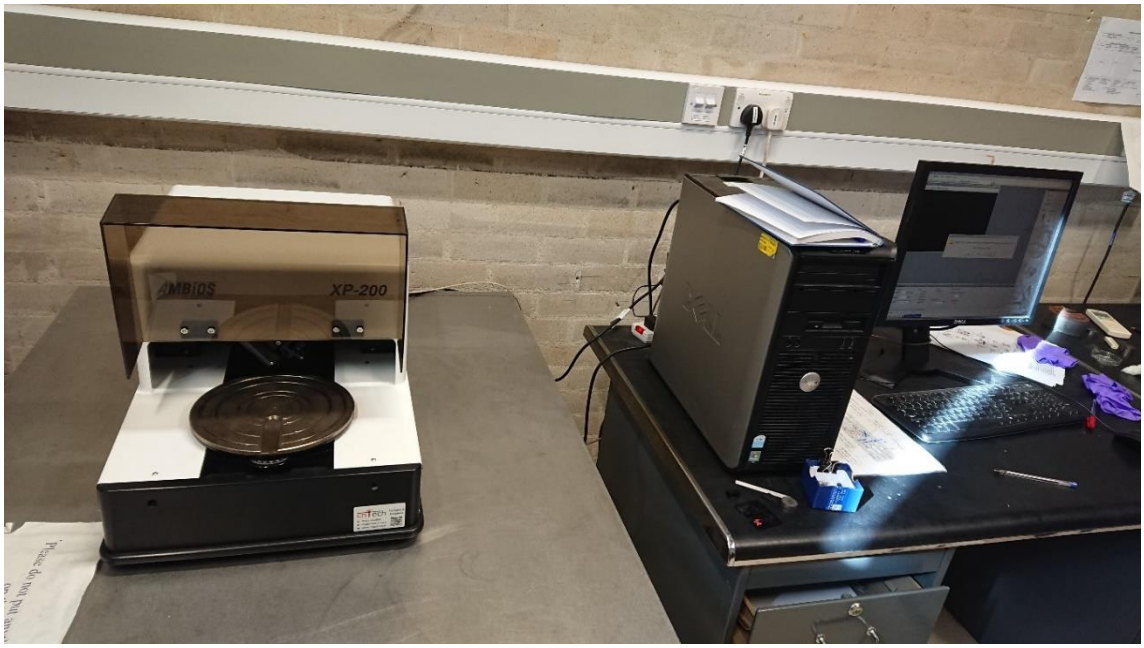

Figure 3.3.4. Image taken of the profilometer facilities at the School of Metallurgy at Birmingham.

3.3.5 Contact angle measurements

Water contact angle (CA) measurements were used to evaluate the surface wettability (hydrophobicity and hydrophilicity) of each sample type and to calculate the surface free energy (SFE). A sessile drop instrument GBX Digidrop (Aston University) was used for the P, PTO and MPTO samples with 2 µl droplets of distilled water. The water droplets were placed along three different regions of the three sample types at room temperature. The CA was then analysed using the GBX Visodrop software. The results were averaged and expressed as the mean ± SD of the measurements.

1 µl droplets of diiodomethane (CAS: 75-11-6) were also placed on the samples at room temperature to calculate the SFE (surface free energy) of the three sample types. Water acted as the polar solvent and diiodomethane acted as the non-polar solvent. Comparisons between the contact angles calculated with the different solvents were undertaken and the SFE was calculated using the Owens-Wendt-2 equation on the GBX

Visodrop software. The results of this experiment are also expressed as mean ± SD of the measurements. Using the software analyses, the wetting envelope of the three sample types were also acquired.

For the remaining samples (MP48, MP58, TOMP48 and TOMP58) the measurements were conducted at the School of Chemical Engineering in The University of Birmingham. The surfaces of the samples were not cleaned prior to the test and a sessile drop method was selected to measure the contact angle of deionised water (2µL) (18.2 MΩcm) upon the surfaces of interest. Equilibrium contact angle (ECA) was measured once the force balance at the interfaces was reached. The contact angle was recorded using an Ossila goniometer (Ossila Ltd, UK) in ambient conditions. ImageJ software (National Institutes of Health, USA) was used for image processing. 1 µl droplets of diiodomethane (CAS: 75-11-6) were also placed on the samples at room temperature to calculate the SFE (surface free energy) of the three sample types.

3.3.6 Cross section layer observation

The samples types were cut to expose the cross section using the Accutom-50 (Struers, UK) cutting machine. The blade used was a silicon carbide blade and the cutting was undertaken at a speed of 3000 rpm with an initial and final feed rate of 0.05 mm/s and 0.15 mm/s respectively. Once the samples had been cut they were then mounted using conductive Bakelite resin via hot mounting using an ATA Opal 460 mounting press.

Once the samples had been mounted, the mounts were then ground and polished using the same technique discussed in Section 3.1.2. The cross sections of the samples types were then etched for 5 s using Kroll's reagent (made up using hydrofluoric acid, nitric acid

and distilled water). The cross sections were then cleaned with acetone and imaged using a JEOL 7000F Benchtop SEM at 15 kV in high vacuum mode with a working distance of 8 mm to view the surface layers and EDX analyses to determine the elemental distribution in the surface layers. The samples were mounted in order to protect the surface coatings and to obtain perfect edges of the treated surfaces. It also helped with the handling of the samples.

3.3.6.1 Focused ion beam

Analysis of the surfaces using a focused ion beam microscope (FIB) was used on the duplex TOMP sample to determine whether the LIPSS continued under the TiO_2 layer or whether the TiO_2 disrupted the LIPSS formation. A Philips FEI Quants 200, UK instrument coupled with a Ga ion beam source was used. An approximate 2 µm thick platinum layer was initially deposited on the region of interest to prevent the destruction of the surface features. The Ga ion beam was used for trenching. The cross sections of region were then taken at a tilt angle of 52-54 °.

3.3.7 Micro-hardness measurement

The surface micro-hardness was measured to evaluate the hardness of the surface treatments. The surface micro-hardness of each sample type was found using the MVK-H1 Hardness Testing Machine (Mitutoyo Ltd, Japan) via the Vickers hardness test. The load used was 0.05kg (HV0.5) (higher loads damaged the surface and lower loads produced no results) and a diamond indenter was used to indent along five different regions from which the hardness was measured. The measurements were then averaged and expressed as the mean hardness ± standard deviation (SD) of each sample type.

3.4 Antibacterial Efficacy and Cell Viability Testing

3.4.1 Antibacterial test

The five different sample types, P, PTO, MP, MPTO and TOMP were tested to investigate the effect of the treatments on the survival and proliferation of bacteria. The standard Japanese JIS Z 2801:2000 spread plate method was used (87,88). Gram–positive *Staphylococcus aureus (S. aureus)* and Gram-negative *Escherichia Coli (E. coli)* were tested against the surface treatments. The bacteria were cultured in TSB (Tryptone soya broth) (Oxoid, UK) overnight at a temperature and mixing speed of 37 °C and 100 rpm respectively. The bacterial suspensions were then diluted; four BD falcon tubes labelled A, B C and D were filled with 900 µl of TSB. Into tube A 100 µl of the original bacterial suspension was added and into tube B 100 µl of the solution of tube A was added so that the concentration of cells reduced to 10^8 cells/ml. The original bacterial suspension had 10^9 cells/ml and the final solution was diluted so that the number of cells per ml was 10^5 (See Figure 3.4.1a for more detail).

Additionally, the samples, distilled water, glass slides, glass cover slips and filter paper were sterilised. This was undertaken by a medical autoclave at a temperature of 120 °C. Filter paper was placed inside sterile Petri dishes. The filter paper was then dampened with sterile water using a P200 pipette. This was undertaken to provide sufficient moisture to aid the growth of the bacteria. The sterile glass slides were placed onto the filter paper onto which a single sample was placed. Subsequently, 5 µl of the diluted bacterial suspension was placed onto each sample using a P200 pipette. A coverslip was then placed

onto the bacterial suspension to prevent the solution from drying. The petri dishes were then incubated for 6 h at 37 °C.

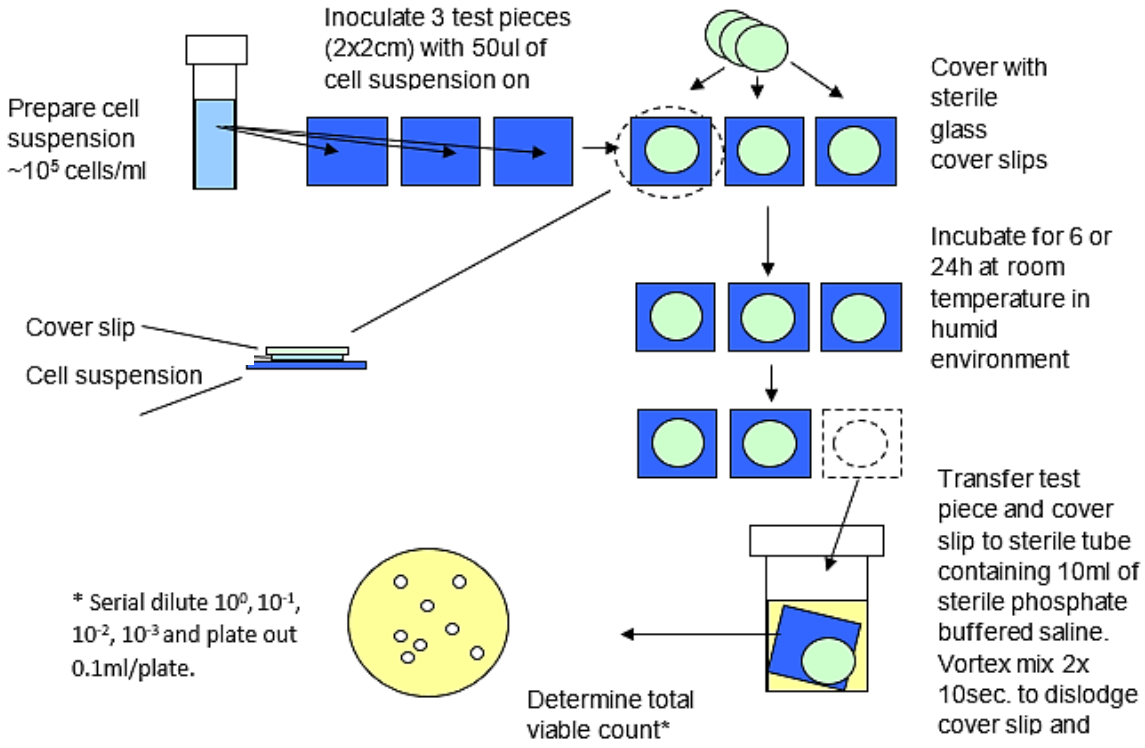

Figure 3.4.1a. Illustration detailing the bacterial suspension dilution steps. (Image provided by Rachel Sammons, 2016).

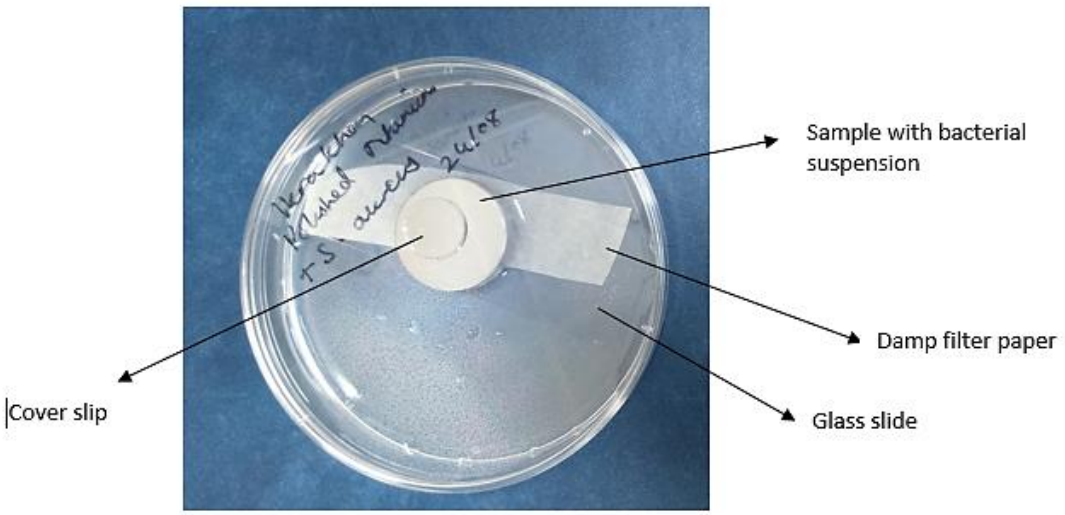

Figure 3.4.1b. Image illustrating how the petri dish was loaded.

Post incubation for 6 h, the samples were placed into sterile 50 ml falcon tubes which were pre-filled with 10 ml sterile PBS (phosphate-buffered saline). The falcon tubes with PBS and the samples were then vortex mixed for 20 s to transfer the bacterial cells from the sample surface to the PBS.

100 µl of the vortexed PBS with the cell suspensions were placed onto the TSA plates. Loops were used to spread the bacterial suspension evenly and the plates were then incubated overnight at 37 °C. The number of colonies found on each plate were counted and then averaged per each sample and bacteria.

A cell viability count was also undertaken in order to obtain the amount of cells in the original bacterial suspension (10^5 cells/ ml). This was conducted by placing 100 µl of the original bacterial suspension on a TSA plate and left to grow overnight in an incubator at a

temperature of 37 °C. This was used as the control number of cells. Percentage reductions were calculated using the equation:

$$\textbf{Eq 2. \% Bacterial reduction} = [C - C_0]/C] \times 100$$

C is the mean colony forming units of the control and C_0 is the mean colony forming units of the experimental samples, both after 6 h.

3.4.2 Anti-adhesion test

The effect of the treatment types was tested on *S. aureus* and *E. coli* to ascertain the attachment potential of the treatment types. As discussed previously, the attachment of bacteria onto a surface is the most crucial step in survival of bacteria and hence, this was tested. The anti-adhesion test was undertaken similarly to the antibacterial test discussed above in 3.4.1 however, the difference was the samples were not placed into solutions of PBS. Instead after 6 h of incubation, the samples with the bacterial suspension were immediately fixed using 20 ml of fixative which was made up using; 8 ml distilled water, 10 ml buffer and 2 ml glutaraldehyde. The purpose of the fixative was to prevent the bacterial colonies from moving so as to get a good SEM image of the cells. The fixative was then applied to the samples (covered the whole sample) for 10 minutes.

The samples were then dehydrated with differing concentrations of ethanol in sequential steps; 20 %, 30 %, 40 %, 50 %, 60 %, 70 %, 90 %, 95 % and 100 %. The ethanol solutions were added to the samples for 10 minutes each and 100 % ethanol was repeated. The vacuum in the SEM chamber can disrupt the cell wall of the bacteria thus, the samples were dehydrated with ethanol so that a good SEM image of the undamaged bacteria could

be formed. The 100% ethanol was then replaced with HDMS (hexamethyldisilazane) and the samples were then left in the fume cupboard overnight.

The samples were then sputter coated with gold for 2 minutes, using a deposition current of 25 mA which generated a coating thickness of 15 nm (K550x super coater, Emitech, UK). The samples were coated to dissipate electrical charge and heat so that clear images were generated. The samples were then imaged using the SEM that was mentioned above.

3.4.3 Cell viability testing

The potential cytocompatibility of the samples were measured using SAOS-2 human osteoblast-like cells to observe cell attachment and proliferation after 24 h. This was undertaken to assess whether the surface treatments will cause any negative effects to the osteoblast like cells, and in doing so the cytocompatibility of the surface treatments was evaluated. Additionally, only the attachment of the cells was tested on the surfaces to assess the attachment capability of the cells on the treated surfaces and whether the surface treatments would damage the structure of the cells. This basic attachment test was used as an indication of the cytocompatibility. Due to there being limited access to the labs, further tests such as MTT assay could not be undertaken. The original 5 sample types (P, PTO, MP, MPTO and TOMP) were used in this test as there was no access to the lab for the testing of the new samples.

3.4.3.1 Preparation

The initial step of the cell viability experiment was to sterilise the samples using a sonicator. The samples were sterilised for five minutes each in acetone, 70 % ethanol and distilled

water successively. The culture medium was then prepared: to make 45 ml of complete medium; 20 ml of McCoy's medium was used, 1 ml of HEPES (4-(2-hydroxyethyl)-1-piperazineethanesulfonic acid) buffer, 0.4 ml of Penicillin/Streptomycin and 4 ml of foetal calf serum (FCS) was used. Other than the HEPES buffer, all of the components were placed in a water bath at 37 °C for 15 minutes to thaw out.

SaOS-2 cells (osteoblast model cell) were cultured in the complete medium. Excess medium was pipetted away from the cells and 10 ml of trypsin was added to the cells to dissociate the cells adhering to the flask. The flask with the cells and trypsin were then placed in the incubator for one minute. After one minute the cells were observed under a standard microscope to view the shape of the cells (the cells were to be rounded rather than possessing a rod shape). If one minute was not sufficient, then the flask would be placed in the incubator again for another minute. This step continued until the preferred rounded cells were visible. The 10 ml trypsin was then pipetted away and fresh 10 ml trypsin was added to the flask with the cells which were then placed in the incubator again for one minute. After observation under the microscope, it was visible that the cells were not attached to the flask and were moving.

10 ml of the complete medium was then added to the cells with the trypsin. This was constantly pipetted away and added to the flask with the cells again (ten times) so as to mix the contents of the flask. The contents of the flask were then added into a BD falcon tube and was then centrifuged at 800 rpm for 6 minutes. After centrifugation a small pellet was visible at the bottom of the falcon tube. Subsequently, most of the liquid was pipetted away from the falcon tube so only a small amount remained with the pellet.

The side of the falcon tube was tapped gently to re-suspend the cells (pellet). 10 ml of fresh medium was then added to this falcon tube and this was pipetted away and added five times to mix the contents. A small amount was then taken away and added to a haemocytometer. This was undertaken to observe the number of cells grown without the presence of samples. The cells were counted using a standard light microscope and this number was used as the control.

The five different sample types were then placed into 6 well plates (34.8 mm diameter). A pipette was then used to add 4.5 ml of the cells plus the medium to the sample (cell density of 5×10^3 cells/mL) 4.5 ml was sufficient to cover the whole sample. The flask and the samples plus the cells were then placed into the incubator overnight.

3.4.3.2 Cell counting

After the overnight stay in the incubator, the cells were checked under the microscope to see if they were still viable. The medium was then removed and the samples were then washed with PBS three times. 20 ml of fixative was then made up using; 8 ml distilled water, 10 ml buffer and 2 ml glutaraldehyde. The purpose of the fixative was to prevent the cells from moving so as to get a good SEM image of the cells. The fixative was then applied to the samples (covered the whole sample) for 10 minutes.

The samples were then dehydrated with differing concentrations of ethanol as discussed above. The 100 % ethanol was then replaced with HDMS (hexamethyldisilazane) and the samples were then left in the fume cupboard overnight. The samples were then sputter coated with gold for 2 minutes and then imaged using the SEM (mentioned above) operating at 10 kV.

3.5 Tribological and Corrosion Response Measurements

3.5.1 Tribology testing

CoF (coefficient of friction) and wear resistance of the different samples were measured with a ball-on-plate TE79 multi-axis tribometer (Phoenix Tribology Ltd., UK) at room temperature under dry and lubricated conditions (Figure 3.5.1a). The dry tests were undertaken to determine the durability of the surface treatments under sliding conditions and the lubricated conditions were used to assess their suitability for medical applications. Lubricating conditions were chosen to replicate the environment of the body for medical applications. Ringer's solution was used to model human fluids such as synovial fluid and saliva (related to knee and dental implants, respectively). Linear reciprocating sliding tests were performed using hardened steel ball (~700 HV) and tungsten carbide (~1000 HV) counterparts of 8 mm diameter. The stroke length per cycle used was 6 mm and a total of 2000 cycles were used which resulted in a total sliding distance of 1200 mm. The distance of the lines was 6 mm per cycle and the reciprocating movements were executed with a speed of 2 mm/s for 2000 cycles. The load applied was 100 g (0.98 N). Figure 3.5.1b depicts the set-up of the wear tests. The samples were not cleaned after the lubricated tests to prevent the debris from being removed, to prevent damage to the wear tracks and so the wear tracks could be imaged as they were which is more reflective for medical implants.

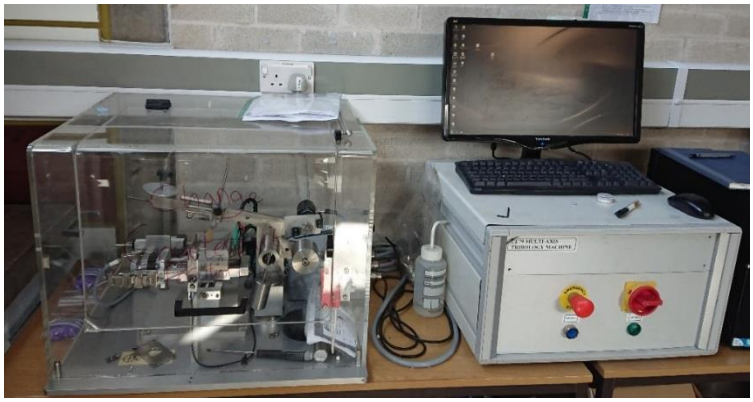

Figure 3.5.1a. Image of the ball-on-plate TE79 multi-axis tribometer

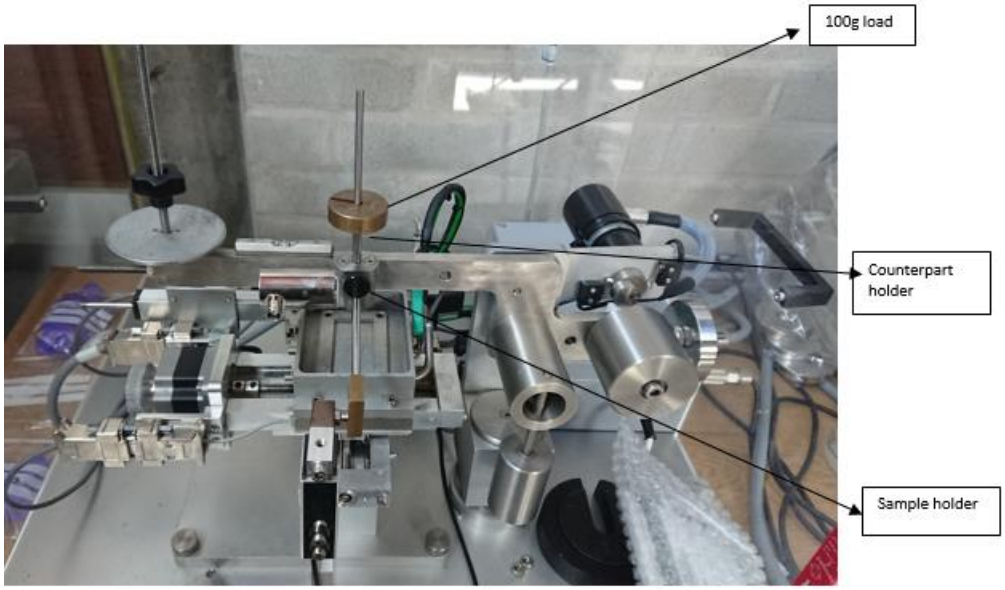

Figure 3.5.1b. Image depicting the set-up for the wear tests.

The load and counterparts were chosen after calculating the Hertzian contact stresses. The Hertzian contact stress is defined as the localised stress that occur when one curved surface and one flat surface come into contact and undergo minor deformation when under a specific load. Calculating the Hertzian contact stress is essential when undertaking wear tests in order to decide the suitability of the counterpart and load used in the test. The Hertzian contact stresses provide information on whether the counterpart or samples will undergo plastic deformation (when contacting) during the wear test under a specific load (89).

For the hardened steel counterpart (HS), the calculated maximum shear stress of the counterpart when in contact with the cp-Ti substrate under a load of 100 g was 128.9 MPa. Whereas the maximum shear stress of the cp-Ti substrate when in contact with the HS counterpart under a load of 100g was 124.7 MPa. The minimum yield strengths (stress at which material undergoes plastic deformation) of cp-Ti and hardened steel are 275 MPa and 540 MPa, respectively. The maximum shear stresses calculated using the Hertzian contact stresses for both cp-Ti and HS are lower than the aforementioned values and hence, it was concluded that the HS counterpart and the cp-Ti samples would not undergo plastic deformation when contacting under a load of 100 g. Hence, a hardened steel counterpart was a suitable choice for the wear tests.

The lubricated tests were undertaken in a similar fashion as the dry tests however, the lubricated tests were undertaken using Ringer's solution (Signa-Aldrich 4 x ¼ strength tablets in 1 L distilled water) which was used to replicate the bodily fluids in the body. A boundary using blue tack was formed on the circumference of the sample to prevent the liquid from escaping so it remained on the surface of the sample. 2 ml of Ringer's solution was added to the surface of the sample. However, once the test was completed it was noted that the hardened steel balls suffered some corrosion and began to rust due to the Ringer's solution. Thus, repeated tests under dry and lubricated tests were undertaken using a tungsten carbide (WC) counterpart (8 mm ball) which was proposed to be more resilient and corrosion resistant to the Ringer's solution.

However, the Hertzian contact stresses of the WC counterpart were calculated before the wear tests were undertaken in order to calculate whether the counterpart and

cp-Ti samples would undergo plastic deformation during the wear tests. The maximum shear stress of the WC counterpart under a load of 100 g when in contact with cp-Ti was calculated to be 164.4 MPa. The maximum shear stress of cp-Ti when in contact with WC under a load of 100 g was found to be 150.4 MPa. As previously mentioned, the minimum yield strength of cp-Ti is 275 MPa and the shear stress calculated was lower (164.4 MPa) than this value and hence, the cp-Ti samples would not undergo plastic deformation during the wear tests. The same could also be said for the WC counterpart as the minimum yield strength of WC is 330 MPa and the shear stress calculated was 150.4 MPa and thus the WC counterpart would also not deform plastically during the wear tests. Therefore, it was concluded that WC would be a suitable choice for the wear tests.

Once, the tests were completed the wear tracks on the samples were imaged using a JEOL 7000F Benchtop SEM, Japan at 15 kV in high vacuum mode with a working distance of 8 mm to assess the degree of wear that occurred on each sample type. Elemental analyses were also undertaken to measure any wear debris or removal of the surface from the counterpart onto the wear track. The wear tests could not be repeated due to limited access to the lab.

The counterparts were also imaged and analysed using the SEM, however, due to the curved nature of the balls the images were not clear as the balls kept charging. Hence, the counterparts were sputter coated with gold for 2 minutes, using a deposition current of 25 mA which generated a coating thickness of 15 nm (K550x super coater, Emitech, UK) to dissipate any charge and to achieve clearer images. Nonetheless, the resultant images were not of a good standard and hence, were not included in this study. Profilometer analysis was

undertaken on the resultant wear tracks. The data could not be produced and even after multiple attempts of optimisation, the wear depth could not be assessed and calculated.

3.5.2 Corrosion testing

The corrosion behaviour of untreated and CCT-treated surfaces was evaluated in an electrochemical cell (Figure 3.5.2) with a saturated calomel reference electrode (SCE) and a platinum counter electrode which were all attached with an Interface 1000 potentiostat (Gamry Instruments Inc., Warminster, PA, USA). The surface area of the sample (0.503 cm^2) was exposed to Ringer's solution at full strength. After open circuit potential (OCP) measurement for 3600 s, anodic potentiodynamic (PD) polarisation was carried out from −0.2 V to 1.2 V at a scan rate of 1 mV/s. Preferably, the test should have been undertaken at body temperature (37 °) to mimic the conditions in the body but the heating jacket of the equipment was faulty hence, the test was undertaken at room temperature. Once the corrosion behaviour was analysed, the samples were then imaged using a JEOL 7000F Benchtop SEM, Japan to view the corrosion damage on the samples. Due to limited access to the lab, the results could not be repeated.

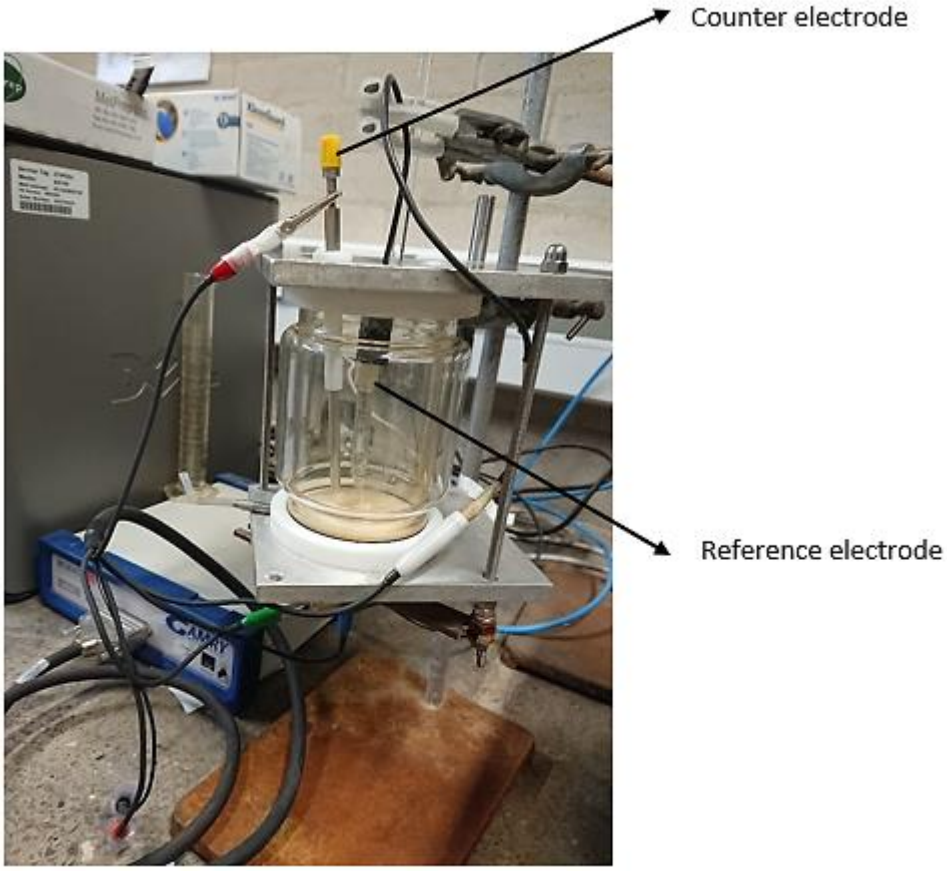

Figure 3.5.2. The electrochemical cell set-up for the corrosion tests.

3.6 Data Processing

The data achieved in this study was repeated three times and averaged. The averages of the data were then used as the main results. Standard deviations were calculated using Microsoft 2013 and expressed as error bars. Exceptions will be described later in the results.

Chapter 4

RESULTS

4.1 Surface Morphology

The typical surface appearance of laser micro patterned cp-Ti surface is exemplified in Figure 4.1 showing the rainbow colours as a result of the LIPSS formation.

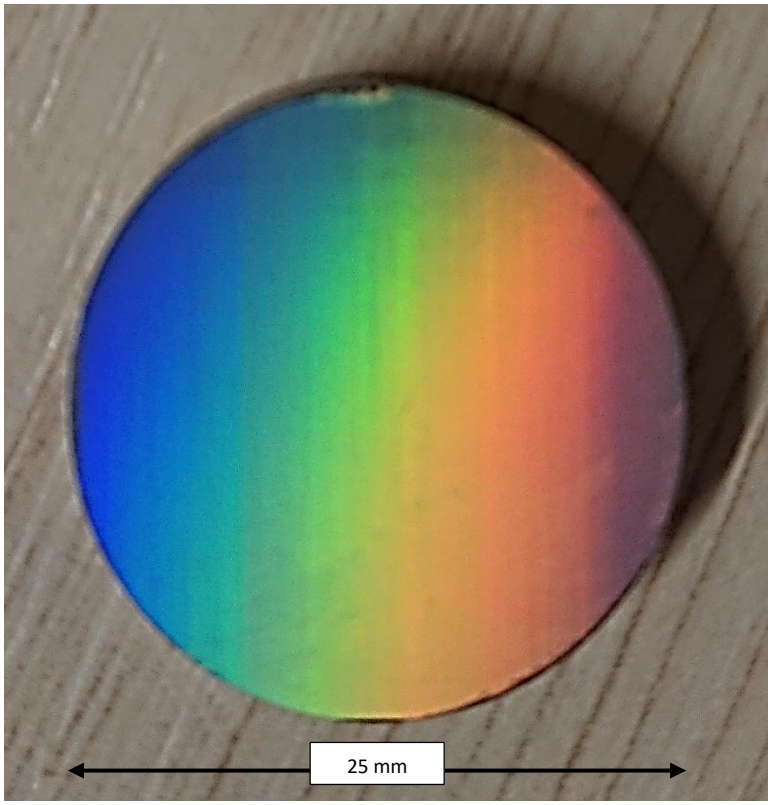

Figure 4.1. Image depicting the rainbow colours as a result of the LIPSS formation on the MP sample.

The rainbow colours on the patterned sample indicated that the spectral regions of the colours initially increased and then decreased with increasing spatial periods of the ripples induced by laser irradiation. Additionally, the elongation of the diffracted wavelengths led to the formation of a colour change from blue to red as seen in Figure 4.1.

4.1.1 SEM surface morphologies

The surfaces of all the samples were observed under SEM at X2000 magnification and a higher magnification of X5000. The representative SEM images for the first batch samples (P, PTO, MP, MPTO and TOMP) are present in Figures 4.1.1a, and b.

When looking at the SEM surface images, it could be seen that the untreated (P) sample was featureless under low magnification (Figure 4.1.1a) and a few minor polishing pits (under 1 µm) were observed under higher magnifications (Figure 4.1.1b). The CCT treated (PTO) sample was fairly uniform and when compared to the P sample, there seemed to be more texture which was due to the growth of the TiO_2 formed during the CCT.

The laser micro-patterned (MP) sample had the presence of patterns in the form of ripples. These ripples were approximately +/- 1 µm in size and had a periodicity (peak to valley distance) of +/- 300 nm or below (+/- 50 nm). The peak to peak distance between the ripples was +/- 1 µm. The patterns were uniform and covered the whole surface area of the sample.

The patterns formed were LSF LIPSS which are formed when the laser fluence is slightly larger than the material's ablation threshold. The orientation of the LIPSS was uniform indicating homogeneity in the LIPSS. There did not seem to be any issue of debris with the MP sample which indicated that there was minimal surface damage of the sample during the patterning process. There were also no signs of cracks or re-melting damage. Usually pulsed laser texturing involves the melting of the material from the surface to create fine structures. Femtosecond pulses offer a very short duration so that the energy cannot be transferred to the lattice. Hence, no significant heat diffusion could occur and instead the

energy delivered from the laser was built up at the surface. Thus, the surface of the material was not damaged.

When looking at the lower magnification images (Figure 4.1.1a) of the duplex (laser patterning followed by CCT) treated MPTO sample it could be seen that there was a presence of surface pattern or texture on the sample. They were in the form of long columns and were approximately +/- 5-10 µm in size. However, at a higher magnification (Figure 4.1.1b) the columns were present but the surface ripples which were seen in MP were not visible for MPTO. Particles, +/- 1 µm in size were visible and were probably oxide particles. The larger +/-5 µm columns were the oxide that had formed during CCT on the patterned sample. The oxide was not in a columnar fashion for the PTO sample which suggested that the presence of the LIPSS influenced the oxide formation so that it formed perpendicular to the LIPSS.

The formation of surface oxide layer during CCT seemed to damage the ripples in the sense that they were not as sharp or as visible as they were in MP. The MPTO sample did indeed have a presence of ripples on the surface but they were dampened by the oxide formation. The ripples however, were the same as the MP sample with the same size and periodicity although the appearance had altered slightly. It was not clear if the reduced sharpness of the ripples was due to the high heat of the CCT process or if it was due to a thick oxide layer formation which had dulled the appearance of the ripples in the SEM. Although, the ripples on this sample had changed, there did not seem to be any cracks or damage to the surface. There were some round oxide particles (+/- 1 µm) present on the surface which was similar to the PTO sample.

For the duplex (CCT followed by laser patterning) treated TOMP samples, SEM micrographs confirmed the presence of LIPSS. However, the LIPSS in TOMP were not as uniform when compared to MP and MPTO. There were some regions on the TOMP sample where the LIPSS stopped forming and then resumed at a later spot. At a higher magnification (Figure 4.1.1b) oxide columns were visible like the MPTO samples however, unlike MPTO the oxide on the TOMP sample had been damaged slightly. In this sample the LIPSS were formed after the CCT and during this process the laser with associated heat may have damaged the oxide that was formed. The ripples had formed but were not highly visible like the MPTO sample.

In Figure 4.1.1b the ripples on TOMP were present and again they were LIPSS. Unlike the MPTO sample, the TOMP sample had the presence of oxide particles and debris which was probably due to the ablation and back sputtering that occurred during the patterning process. The particles were less than +/- 1 μm in size and there did not seem to be any damage on the surface in the form of cracks or dents. The ripples were homogeneous and had the same orientation and size indicating the patterning process was successful.

The peak to peak distance of the ripples was +/- 1 μm and the peak to valley (periodicity) was 300 nm (+/-50 nm). The oxide columns were more visible in Figure 4.1.1b, the sides of the columns were ridged and possessed oxide particulates that seemed to be loosely attached to the oxide.

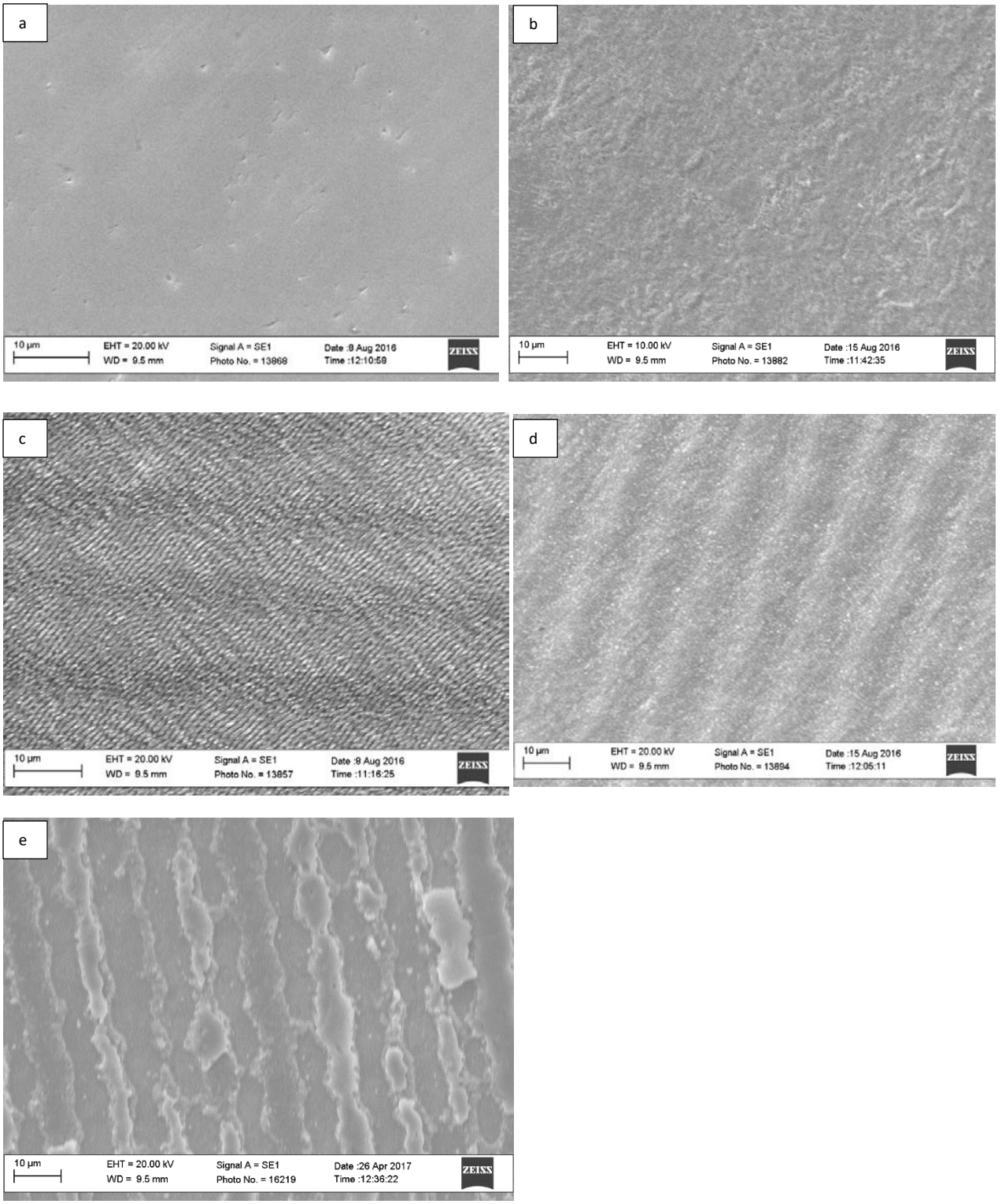

Figure 4.1.1a. SEM images taken of the five sample types; a: untreated (P), b: thermally oxidised (PTO), c: micro-patterned (MP), d: micro-patterned then thermally oxidised (MPTO) and e: thermally oxidised then micro-patterned (TOMP).

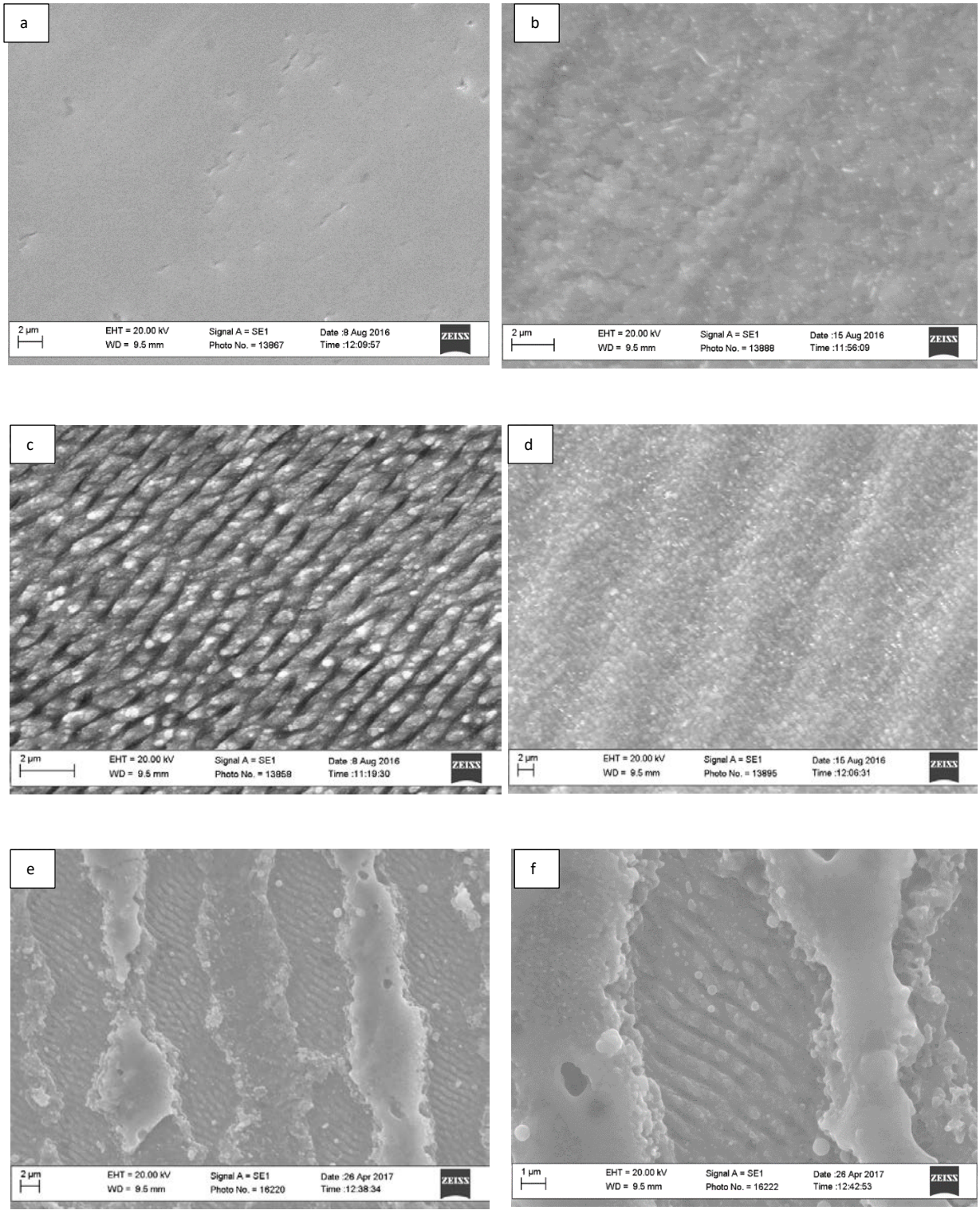

Figure 4.1.1b. SEM images taken of the five sample types; a: untreated (P), b: thermally oxidised (PTO), c: micro-patterned (MP), d: micro-patterned then thermally oxidised (MPTO), e: thermally oxidised then micro-patterned (TOMP) and f: TOMP taken at a higher magnification.

Second batch TOMP samples

Late into the project more TOMP samples were generated. However, due to the change in the laser machine and the operation, the previous TOMP samples could not be replicated even if the same nominal parameters were used. The patterning on the samples was not visible and the oxide “peeled off” (Figure 4.1.1c)

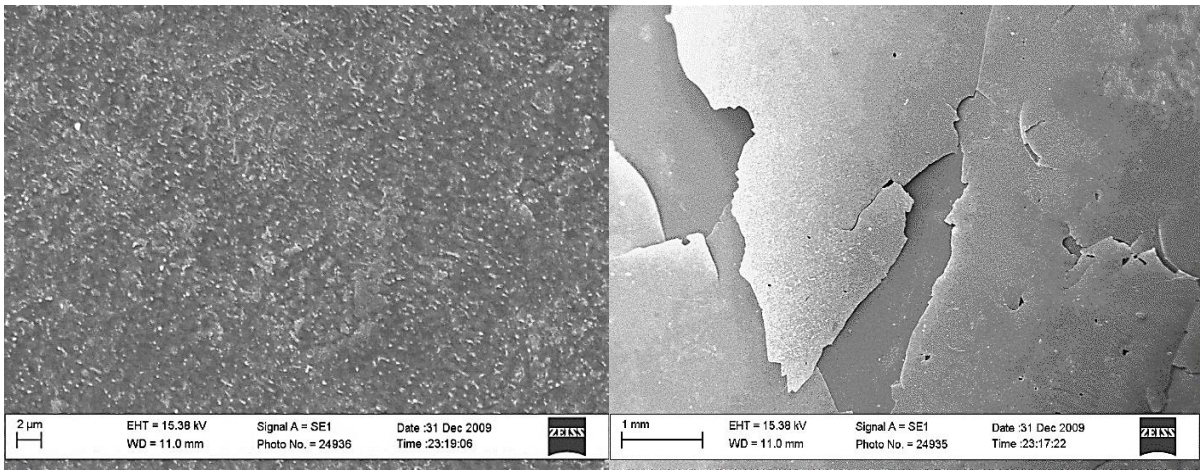

Figure 4.1.1c. SEM images depicting the TOMP samples where the surfaces were improper due to the destruction or alteration to the TiO_2. In the first image it can be seen that the LIPSS ripples have not formed and in the second image the oxide is peeling again with no ripple formation.

After many trial and error sessions involving different parameters a solution was found. The new samples had the same parameters except the laser power was altered to give two options. The first option was to have a sample with a laser power of 48 % which resulted in a higher quantity of the TiO_2 but with fewer LIPSS. The second option was to have a sample using a laser power of 58 % with an increased quantity of LIPSS but with more destruction of the oxide layer. There was interest in both sample types so a conclusion was made to test both sample types against bacteria and to test the tribology of both sample

types. This would help ascertain the effects of TiO_2 vs LIPSS and whether which treatment type was more antibacterial or wear resistant.

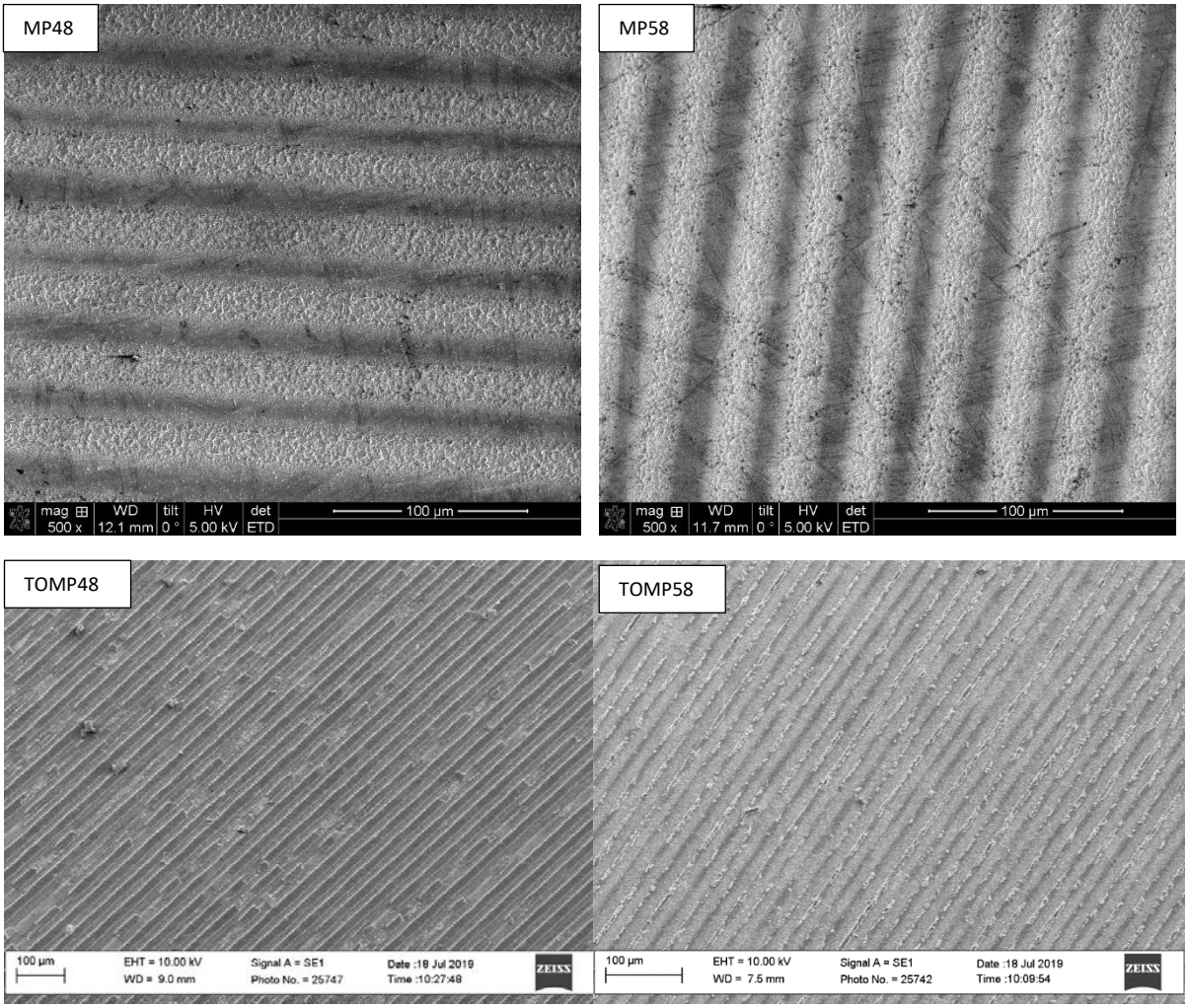

Figure 4.1.1d. New batch samples.

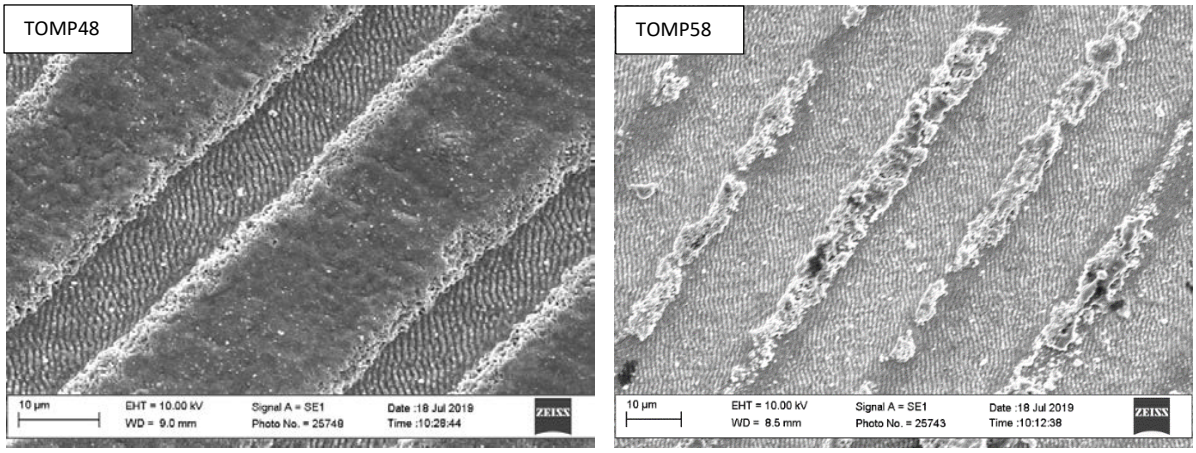

Medium magnification (X2000)

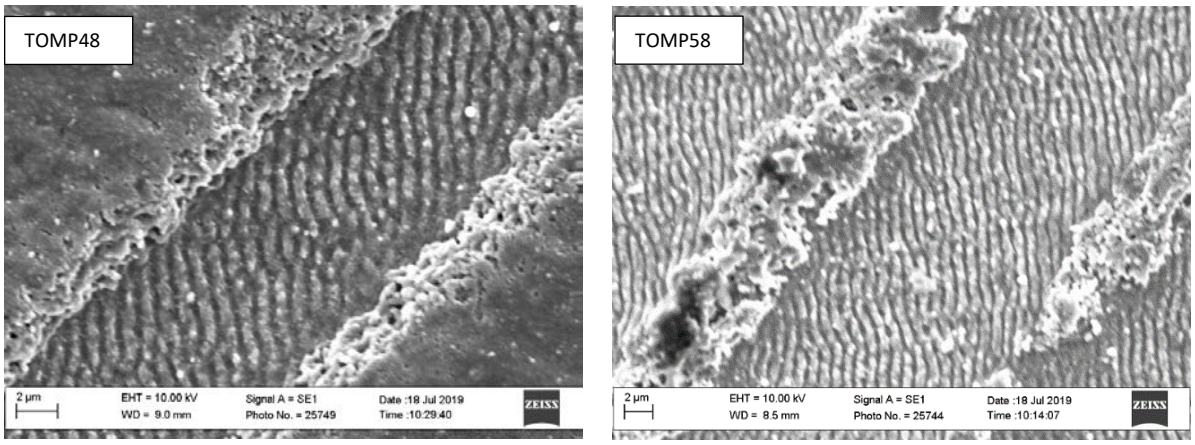

High magnification (X5000)

Figure 4.1.1e. SEM images taken of the samples at different magnifications. On the left in the TOMP48 samples it can be seen there is less TiO_2 destruction whereas in the TOMP58 samples (to the right) there is a higher number of LIPSS ripples but more oxide destruction.

In the TOMP48 sample (Figure 4.1.1d) the oxide columns were visible and again had suffered some damage like with the original TOMP sample. The oxide columns were not fully linear and broke off at some points. This was seen with the TOMP58 sample too but the difference between these samples was the oxide columnar width which was +/- 20 µm for TOMP48 and +/- 5 µm for TOMP58. This suggested that there was a higher concentration of TiO_2 on the TOMP48 than TOMP58. This indicated less oxide was destroyed on the TOMP48 when compared to TOMP58. The oxide columnar width for the original

TOMP sample was approximately +/- 6 µm and hence, the TOMP58 sample was similar to the original sample.

At X2000 magnification, the ripples were visible for both TOMP48 and TOMP58. The ripples formed were again LSF LIPSS and had a periodicity of +/- 300 nm and a ripple size of +/- 1 µm. There was a presence of oxide particulates on both samples but the TOMP58 sample had a higher amount due to increased damage of the oxide during the texturing process. This was again similar to the original TOMP sample however, TOMP58 had a higher oxide destruction and thus, more oxide debris.

At X5000 magnification, the oxide columns for both TOMP48 and TOMP58 were similar to the original TOMP sample for instance, the oxide columns on both these samples had rough edges. The difference with TOMP48 was that the oxide columns were linear and did not break in length unlike the TOMP58 sample. The TOMP58 sample had a higher presence of LIPSS and thus, there was more oxide destruction. The oxide particulates in TOMP48 were approximately +/- 0.3-0.5 µm and were rounded whereas, the oxide particles in TOMP58 were non-uniform in shape and larger (almost +/- 1 µm). These rougher oxide particles in TOMP58 may cause problems with wear resistance.

4.1.2 Surface chemical composition

The surface chemical compositions of the samples were probed using EDX to monitor the change in chemical composition with the surface treatments although it is known that the experimental errors for EDX measurement of such light elements as O is quite large.

The typical EDX charts are shown in Figure 4.1.2a and it can be seen that all the samples showed strong peaks of Ti. Other than the untreated P sample, all the other samples showed a clear peak for oxygen. Weak peaks of Al and C were also probed for some samples, which were most probably contamination as neither Al nor C existed in the bulk material or intentionally introduced during these surface treatments. Most probably, the aluminium on all the samples was due to the SEM sample holder and carbon was due to the contamination of the SEM chamber.

The results for Ti and O obtained from the EDX analysis are shown in Figure 4.1.2b. It can be seen that the untreated P sample had the highest weight percentage (wt%) of titanium as expected followed by the MP sample. The P sample had a 0 wt% oxygen which suggested that the naturally occurring oxide film that formed on titanium was too thin to be detected by EDX. The largest weight percentage of oxygen was detected on the MPTO sample as this sample had a thick oxide layer due to CCT. The micro-patterned MP sample also had +/- 8 wt% oxygen which was higher than the polished samples. This may be because the actual patterning of the samples was undertaken in the presence of oxygen and hence, the actual patterned surfaces were oxidised during the treatment. This could be visually seen as the patterned samples had an almost rainbow reflection (Figure 4.1) which suggested that the patterned surface was oxidised.

The MPTO sample had an oxygen wt% of +/- 41.8 which was marginally higher than that (+/- 40.9) of the PTO sample. This difference was negligible if the large measurement error for light elements is considered. The wt% of oxygen on TOMP was +/- 32.89 which was lower than MPTO and PTO but higher than MP as predicted. The oxide layer was formed before the LIPSS in the TOMP sample but the oxygen percentage detected was lower than the MPTO sample. This suggested that when LIPSS were formed on an already oxide treated sample, the laser removed some of the oxide present on the surface. The high power of the laser with associated heat and ablation may have removed some of the TiO_2 and hence, the oxygen detected was lower even though the patterning process itself causes some oxidation (seen in MP).

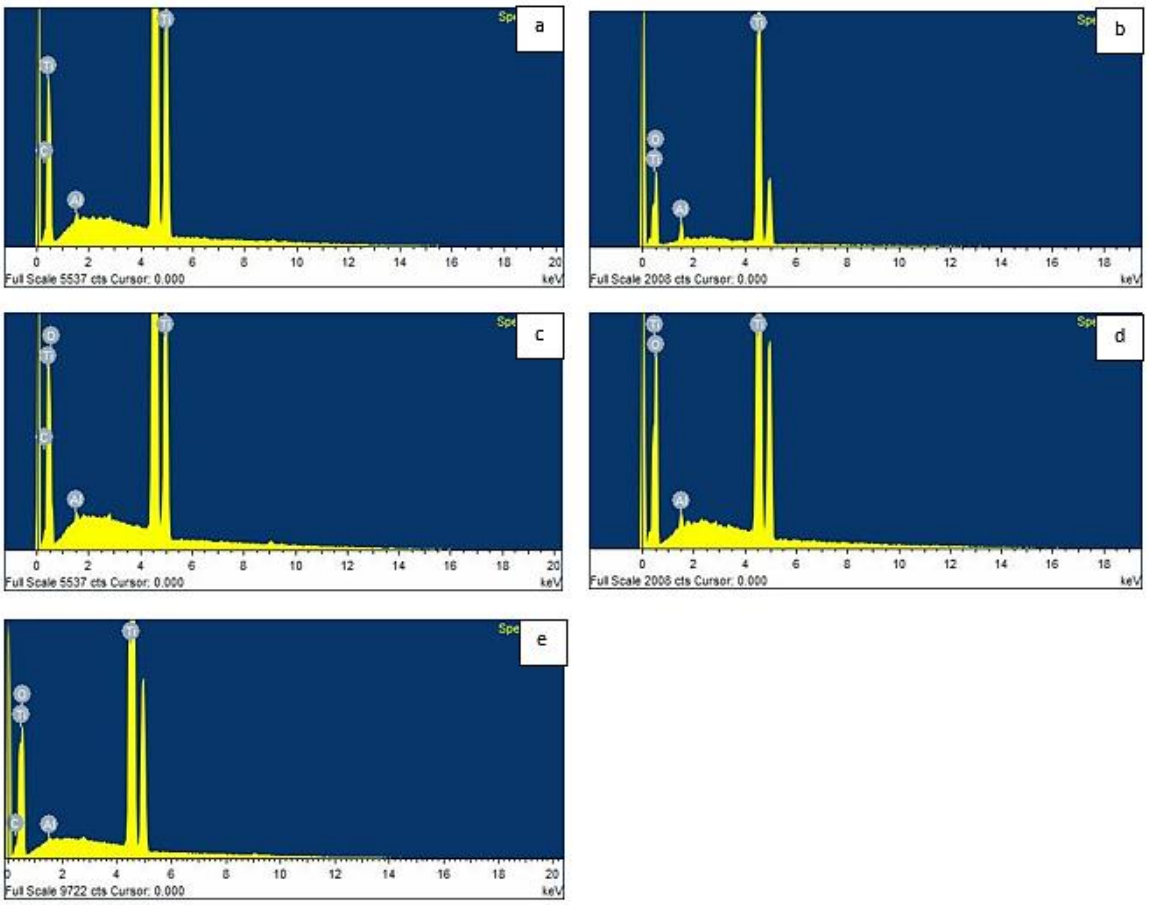

Figure 4.1.2a. EDX charts displaying the elemental peaks for each sample type. a: untreated (P), b: thermally oxidised (PTO), c: micro-patterned (MP), d: micro-patterned then thermally oxidised (MPTO), e: thermally oxidised then micro-patterned (TOMP)

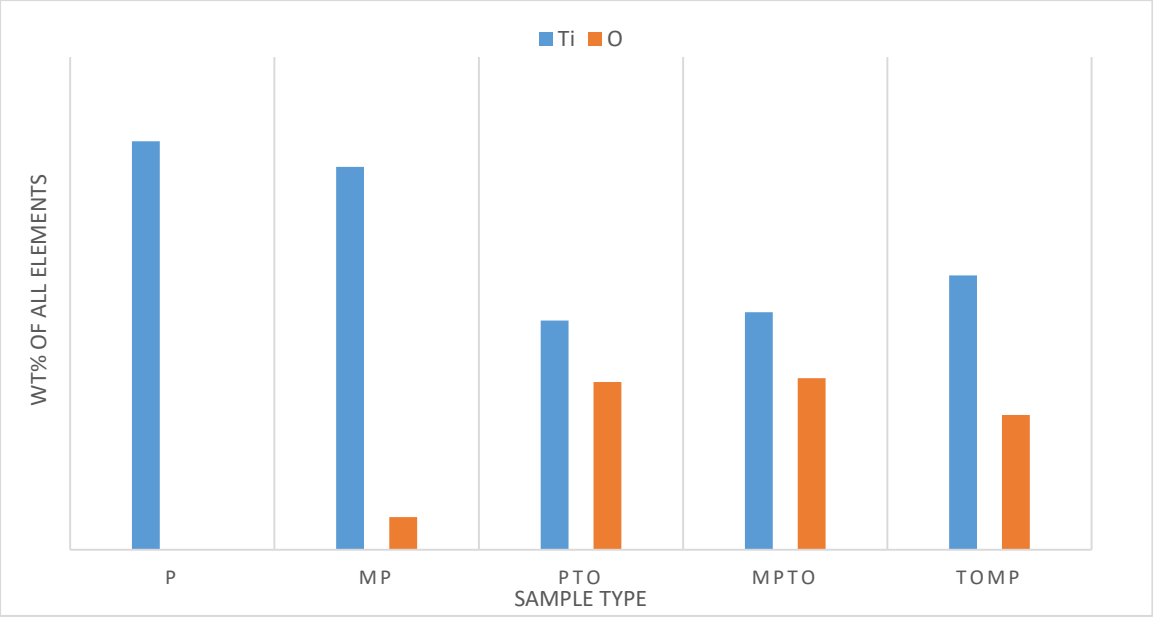

Figure 4.1.2b. EDX chart displaying the elemental analyses and average wt% of the elements present on the surface for each sample type

4.2 Phase structure and chemical bonding

4.2.1 Phase Constituents

The phases within the sample surfaces were identified using XRD and the results are summarised in Figures 4.2.1a for P, MPTO and PTO samples and in Figure 4.2.1b for TOMP and MP samples. As shown in Figure 4.2.1a, the XRD chart for the as-polished and micro-patterned cp-Ti consists of five peaks within the 2θ ranges from 20° to 70° which belongs to the alpha phase in the material.

It can be also seen from Figure 4.2.1a that all the peaks from the PTO and MPTO samples can be indexed to rutile phase with virtually no titanium peaks. This indicated that the titanium oxide film was thick and X-ray penetration could not occur as much as the substrate titanium peaks were not detected.

Figure 4.2.1b compares the XRD charts for MP and TOMP samples measured under the same conditions. The peaks for the micro-patterned MP sample were virtually the same as the peaks for the as-polished P sample. However, for the TOMP sample, in addition to the peaks from rutile as found for PTO and MPTO samples, peaks from alpha Ti as found for P and MP sample were also identified. This implied that after micro-patterning, some of the oxide layer generated by the CCT was removed and the peaks from the substrate cp-Ti were detectable by XRD. However, the intensity of the titanium peak was much higher for MP than TOMP which suggested there was still an oxide layer on the TOMP sample.

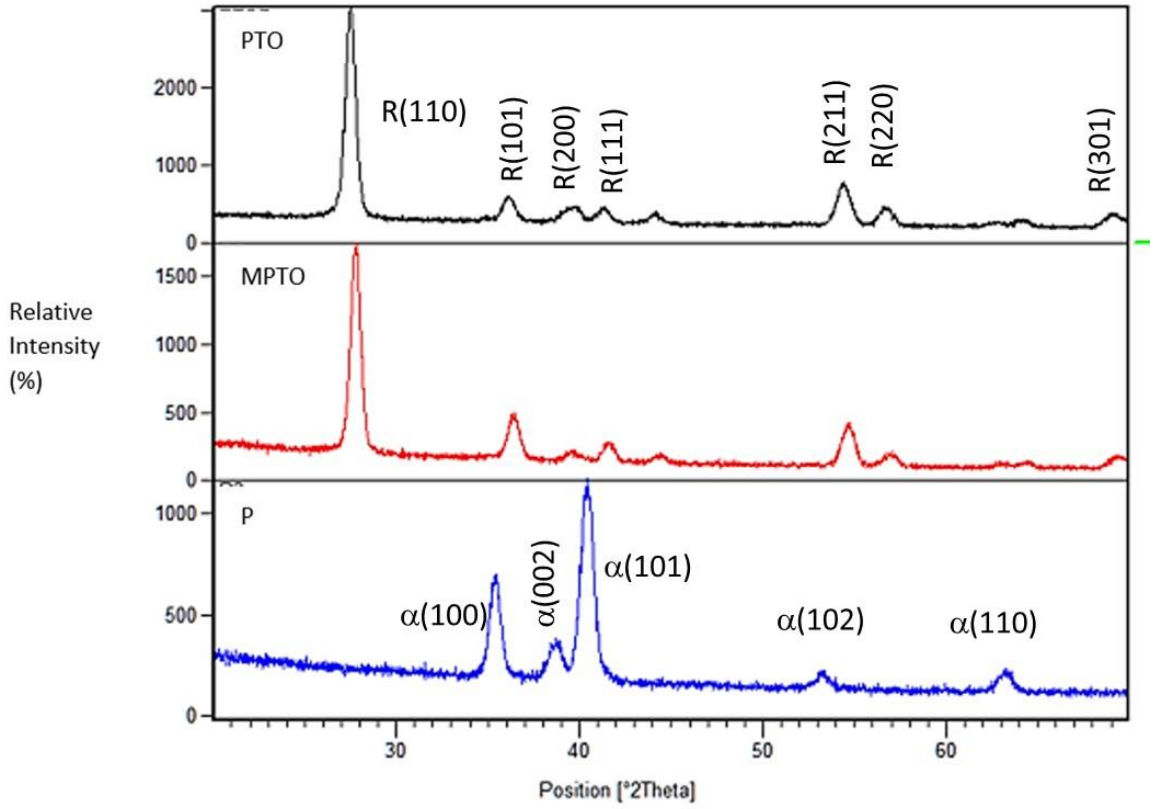

Figure 4.2.1a. XRD graph showing the different phases in the three sample types where the top is the PTO sample, middle is the MPTO sample and the bottom is the P sample.

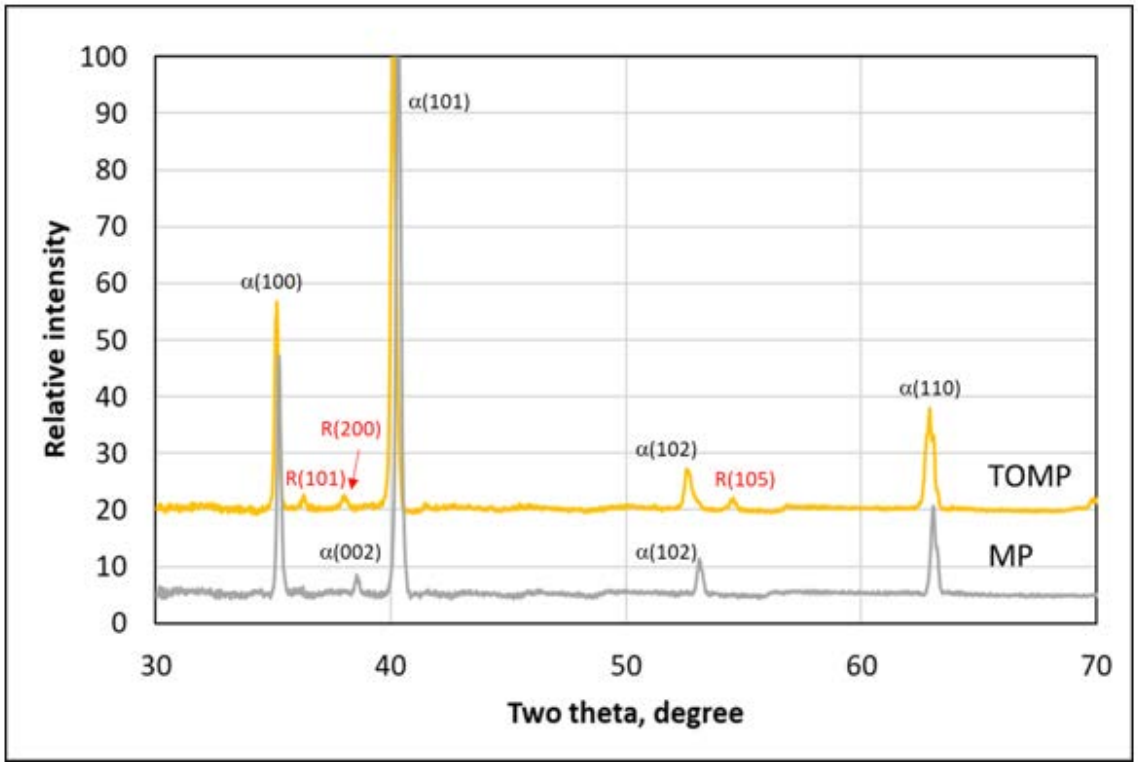

Figure 4.2.1b. XRD charts displaying the different phases for the MP and TOMP samples.

4.2.2 Chemical composition and bonding

XPS analysis was conducted on three selected samples, MP, TOMP and MPTO, to quantitatively measure their surface chemical compositions and bonding. The surface chemical composition of these three samples are summarised in Table 4.2.2a and XPS Ti peak fitting for sample MP, TOMP and MPTO are shown in Figures 4.2.2a to c. The surfaces of all three samples were covered with carbonaceous contamination.

For the MP sample, Ti was present mainly as TiO_2. A small concentration of metallic Ti was present due to the Ti substrate below the oxide. The detection of this small metallic Ti signal indicated that the oxide was just below +/- 10 nm thick. For the TOMP sample, the TiO_2 concentration was higher than in sample MP and the metallic peak was lower which indicated the TiO_2 thickness was greater than in sample MP but still just under +/- 10 nm in some areas. For sample MPTO, no peaks were detected of metallic Ti but the largest peak of TiO_2 was detected. The fact that only TiO_2 and no metallic Ti was detected on this surface indicated that the oxide in the case of this sample was thicker than +/- 10 nm.

As mentioned above, the surfaces of all three samples were initially covered with carbonaceous contamination. Therefore, in order to reduce or avoid the effect of the surface carbon contamination on the XPS analysis results, Ar ion etching of the surfaces was employed to remove this contamination before XPS probing. The quantitative results are summarised in Table 4.2.2b and the XPS peak fittings are displayed in Figures 4.2.2d to f. Carbon was not detected.

Table 4.2.2a. Atomic Concentration (%) of the elements plus Ti in the samples.

Sample	Atomic Concentration (%)			
	C	**O**	**Ti metal**	**TiO_2**
MP	41.9	40.4	0.7	13.1
TOMP	37.0	44.8	0.2	15.7
MPTO	30.9	47.9	-	16.9

Table 4.2.2b. Atomic Concentration (%) of the elements plus Ti in the samples after etching.

Sample	Atomic Concentration (%)		
	O	**Ti metal**	**TiO_2**
MP	48.3	7.9	8.8
TOMP	54.7	7.4	14.1
MPTO	62.8	-	17.6

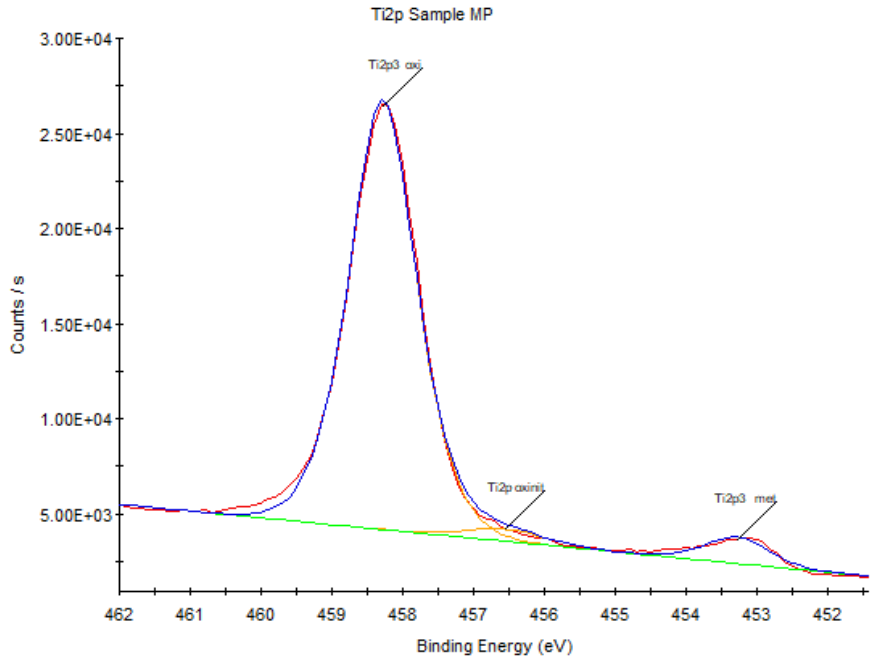

Figure 4.2.2a. XPS Ti peak fitting for Sample MP.

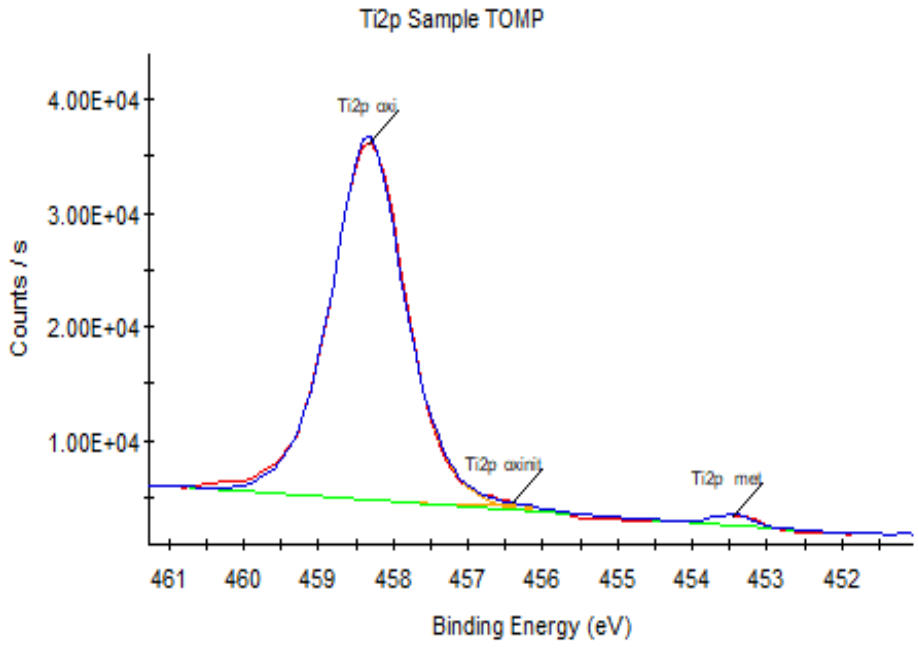

Figure 4.2.2b. XPS Ti peak fitting for Sample TOMP.

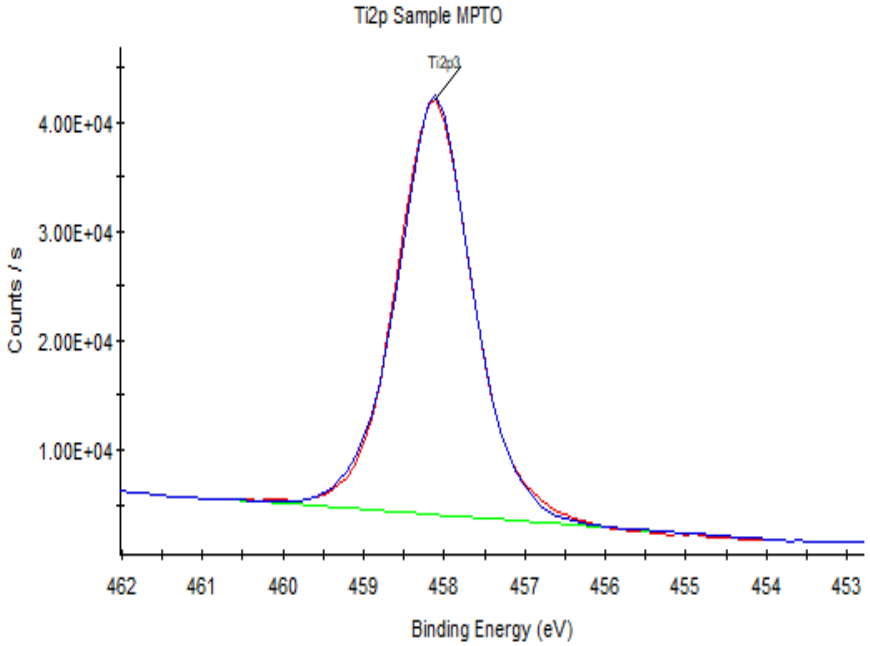

Figure 4.2.2c. XPS Ti peak fitting for Sample MPTO.

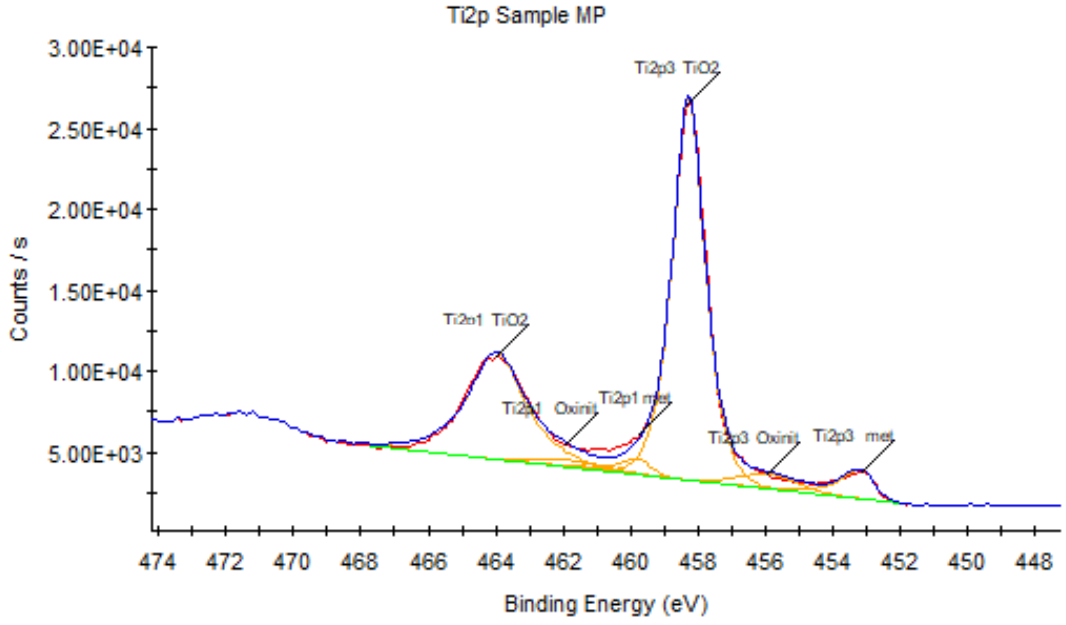

4.2.2d.XPS Ti peak fitting for Sample MP

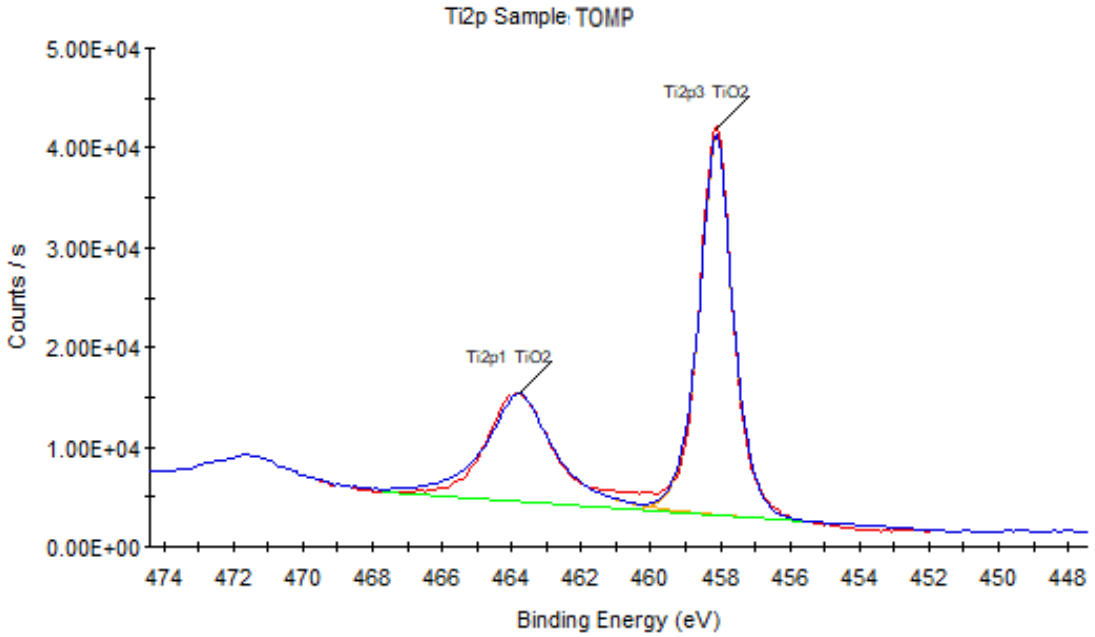

4.2.2e.XPS Ti peak fitting for Sample TOMP.

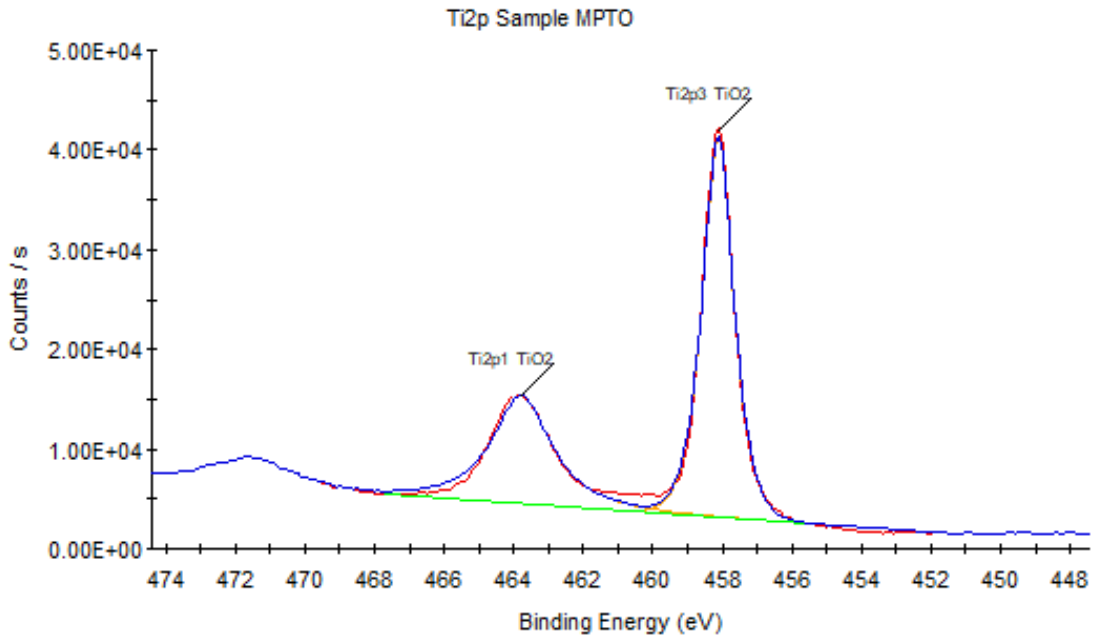

Figure 4.2.2f. XPS Ti peak fitting for Sample MPTO.

For the MP sample, TiO_2 was present plus Ti metal. The Ti peak was present due to the titanium substrate below the oxide. For the sample TOMP, TiO_2 again was present plus Ti metal which was present due to the Ti substrate below the oxide. The Ti metal detected in

TOMP was similar to MP but, the TiO_2 concentration was much larger. This indicated a thicker oxide. The MPTO sample had no Ti metal detected which indicated the oxide thickness was thicker than +/- 10 nm and although reduced chemically and in thickness by the Ar ion beam, no substrate material was detected. The fact that only Ti oxides and no metallic Ti was detected after removal of +/- 15 nm of the surface by ion etching, suggested that the oxide was significantly thicker than +/- 10 nm.

4.3 **Surface roughness**

4.3.1 2D analysis

When looking the SEM images in Section 4.1.1, it was suggested that the PTO sample looked rougher with more texture present on the surface when compared to P. This was confirmed by the roughness (Ra) results seen in Figure 4.3.1a. Ra represents the mean surface roughness over a length whereas Rt represents the distance between the highest peak and the lowest trough. The P sample had the lowest roughness (Ra) due to it being untreated and only mirror polished. The roughness of P was +/- 0.03 µm whereas the MP and PTO samples had roughness's of approximately +/- 0.07 µm and +/- 0.08 µm respectively. These results alone suggested that there was texture present on the surfaces which was confirmed by the SEM images. The CCT process caused a higher roughness than the MP sample and this probably was because the oxide film formed and covered the whole surface whereas, the MP sample had ripples and valleys and was thus, less densely covered. The valleys between the ripples may have led to lower Ra values.

The combined surface treatments on the samples caused large increases in surface roughness. The MPTO sample had a roughness of +/- 0.12 µm and the TOMP sample had a

roughness of +/- 0.14 µm. The MPTO sample may have had a lower surface roughness than TOMP because of the ripple rounding during CCT which was supported by the SEM image (Figure 4.1.1b). The reduced sharpness of the ripples and almost dampened patterning in MPTO caused by the high heat and ablation in CCT most likely caused a decrease in the surface roughness. This was also supported by the fact that although Ra of TOMP was only slightly larger than MPTO, the maximum peak to valley distance (Rt) is much larger for the former than for the latter.

The TOMP sample had the highest surface roughness in the first batch five samples (P, MP, PTO, MPTO and TOMP) which suggested that both surface treatments were produced successfully on the sample. The LIPSS ripples were sharp in TOMP and the oxide formed was also successful as supported by the EDX charts in Section 4.2. The oxide however, was destroyed slightly in this sample (Sections 4.1 and 4.2) but when looking at Figure 4.1.1b it was seen that the oxide columns that formed had rough edges which may have contributed to the increased roughness of TOMP.

The highest Ra value from all of the sample types was seen for TOMP48 (+/- 0.55 µm) which was closely followed by TOMP58 (+/- 0.55 µm). There was no significant difference between these values and hence, it can be said that roughness is not affected by changes in laser power as long as the samples and conditions remain the same. Nonetheless, these newer TOMP48 and TOMP58 samples had much higher Ra values when compared to the original TOMP produced in the first batch. The MP48 and MP58 samples had Ra values of +/- 0.15 µm and +/- 0.19 µm respectively. This implies that the presence of an oxide layer produced by CCT would have affected the patterning effect of laser.

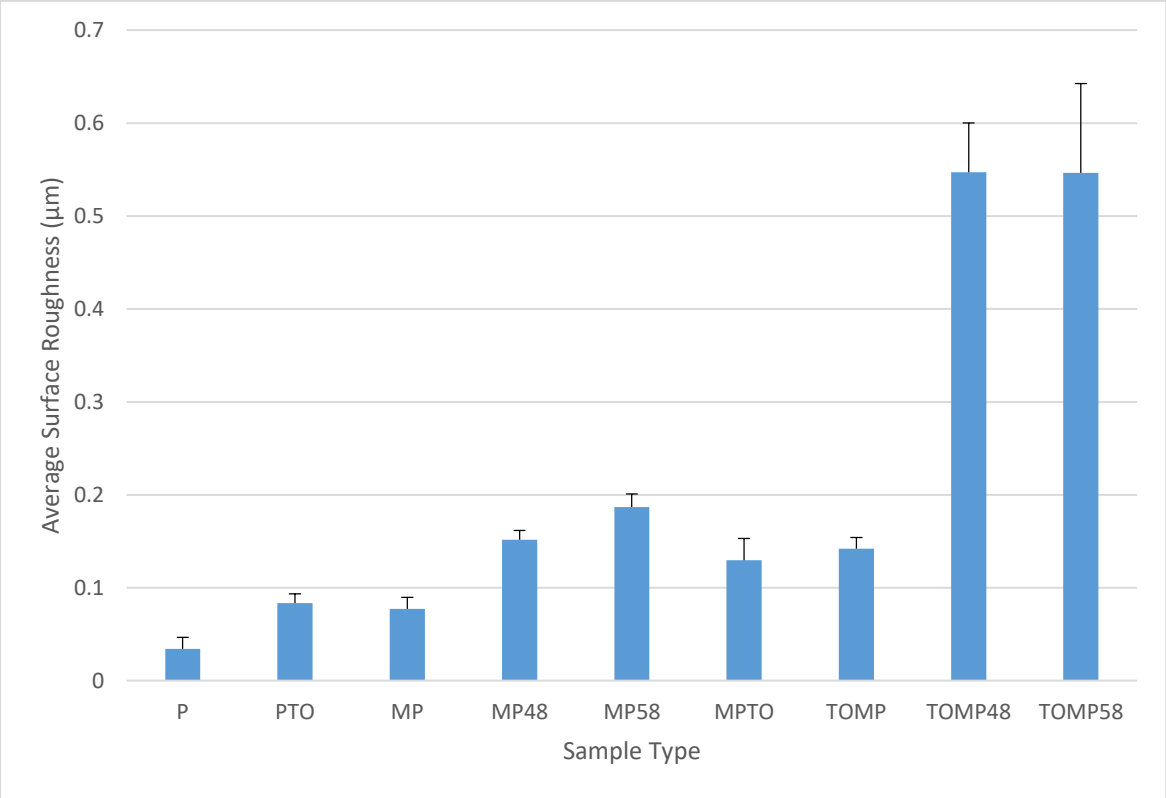

Figure 4.3.1a. A graphical representation of the mean surface roughness (Ra) of each sample type.

Rt represents the maximum peak-valley distance (Figure 4.3.1b) and was highest for TOMP58 (+/- 2.46 µm) and lowest for P (+/- 0.23 µm). The lowest Rt values out of the treated samples was for MP (+/- 0.57 µm) which suggested that the ripples were even and were not formed at a high height from the substrate. The samples with the combined treatments had high Rt values which suggested the oxide layer that formed on the samples was thick and the ripples formed were shallow when compared to the oxide which created a large distance between the oxide peak and the valley which was the LIPSS.

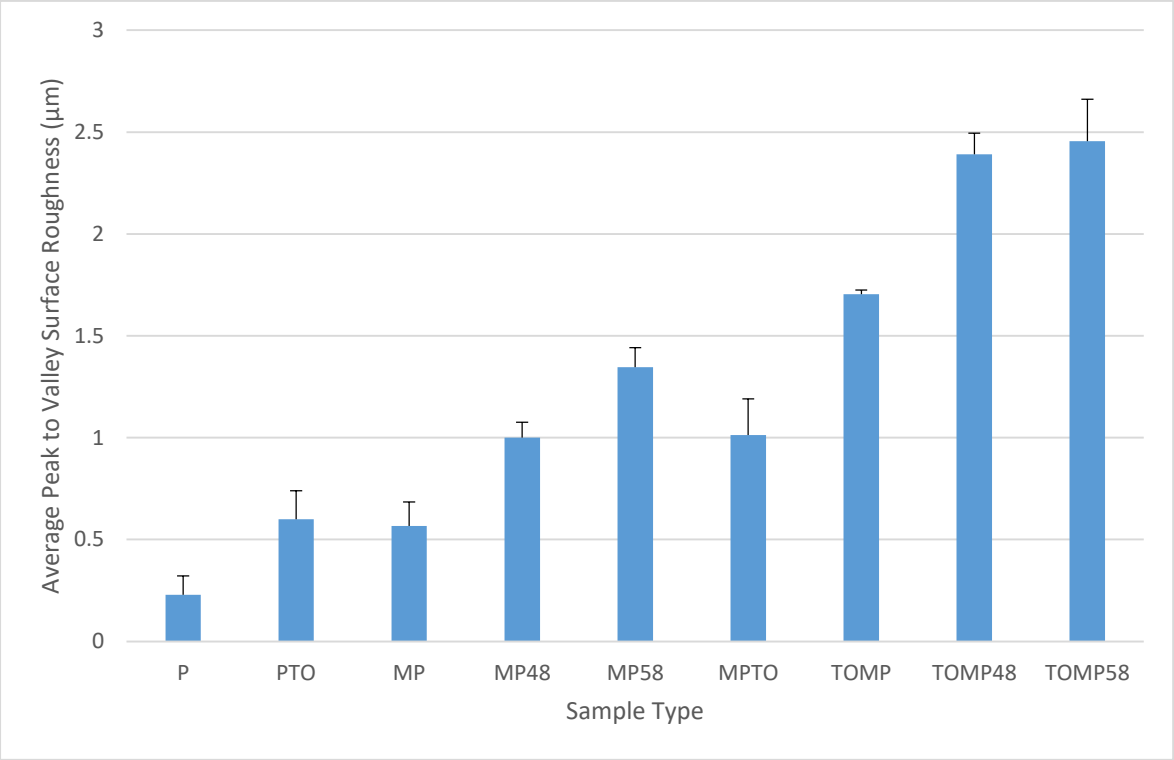

Figure 4.3.1b. A graphical representation of the mean distance between the highest peak and lowest trough (Rt) of each sample type.

4.3.2 3D surface topographical features

In addition to 2D surface roughness measurements, the 3D surface morphologies of all the samples from Batch 1 and Batch 2 and their 3D representation of the topographical features are shown Figures 4.3.2a-h. In general, the 3D analysis provided the same ranking trend as for 2D results as reported above. However, some special features are worth noting:

The MP sample surface looked smooth with very small values for Pa (+/- 0.084µm), Pq (+/- 0.103µm) and Pt (+/- 0.468µm). The surface became rougher after further CCT treatment (i.e. MPTO). Significant roughening was observed for the 2nd batch laser micro patterned MP48 and MP58 with the latter being significantly rough than the former.

The surface of PTO sample was significantly roughened by further laser micro patterning (i.e. TOMP) with the roughness values approaching that for MP58. The surface roughness values of the 2nd batch micro patterned TOMP48 and TOMP58 were similar, which were more than double (especially for Pq and Pt) that for TOMP.

Judging by the Pt values and the thickness of the oxide layer (approximately 2 microns, section 4.5), it could be deduced that at the valleys of TOMP sample, the oxide layer was almost totally removed (Pt= +/- 1.81 microns) and no oxide was left at the valleys of TOMP48 (Pt= +/- 3.95 microns) and TOMP58 (Pt= +/- 4.34 microns) samples.

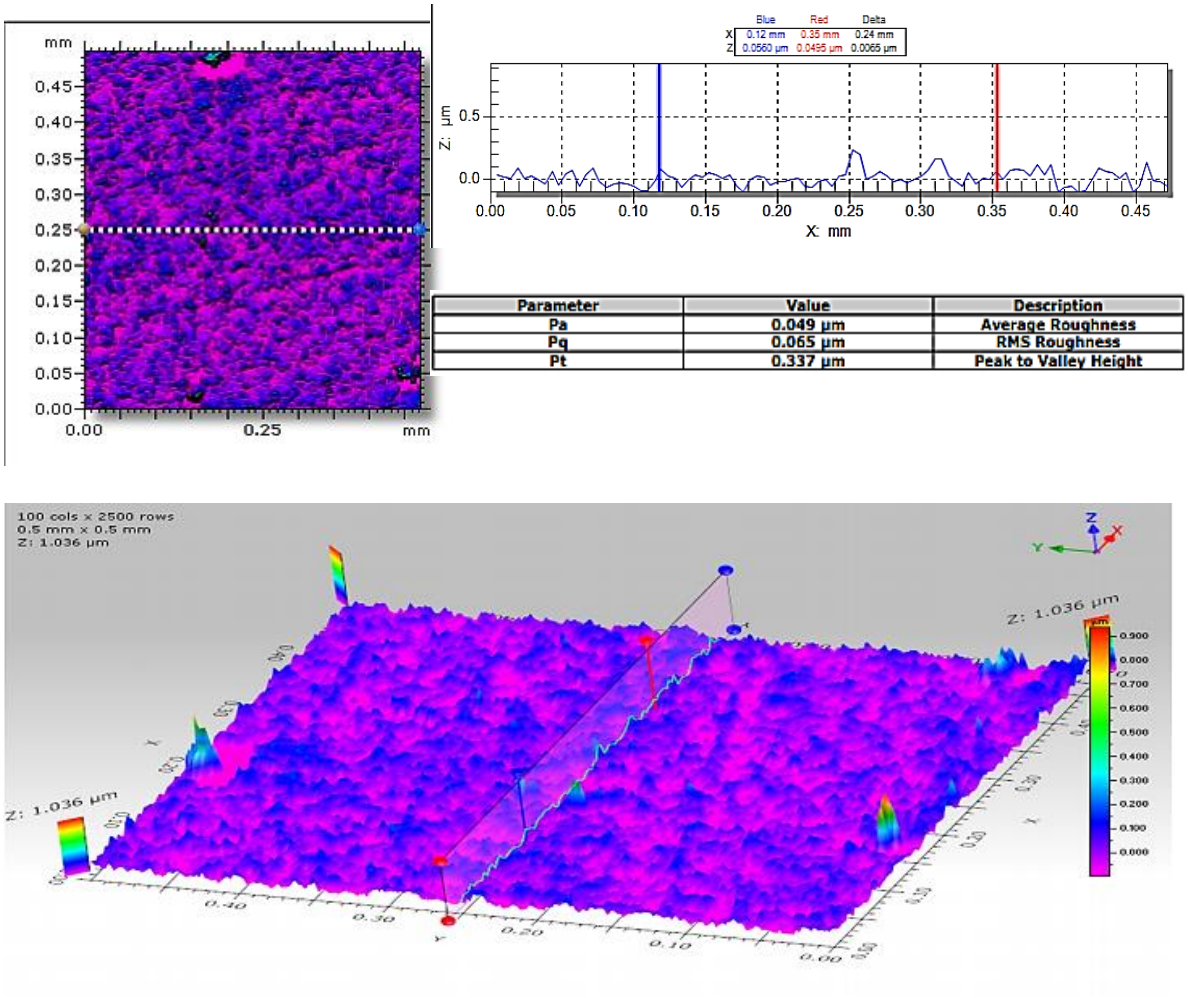

Figure 4.3.2a. 3D representation of the surface topographical features of the PTO sample.

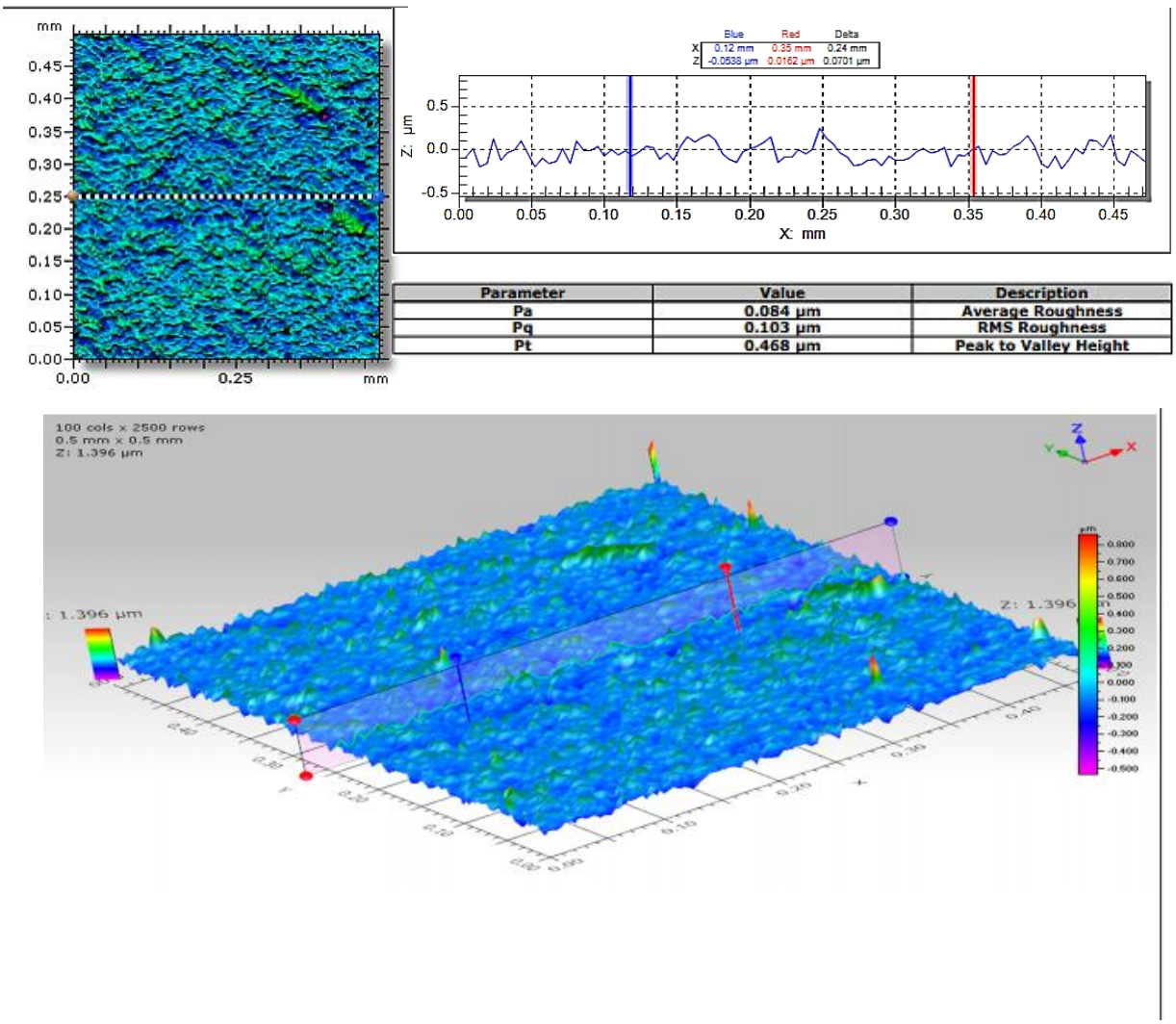

Figure 4.3.2b. 3D representation of the surface topographical features of the MP sample.

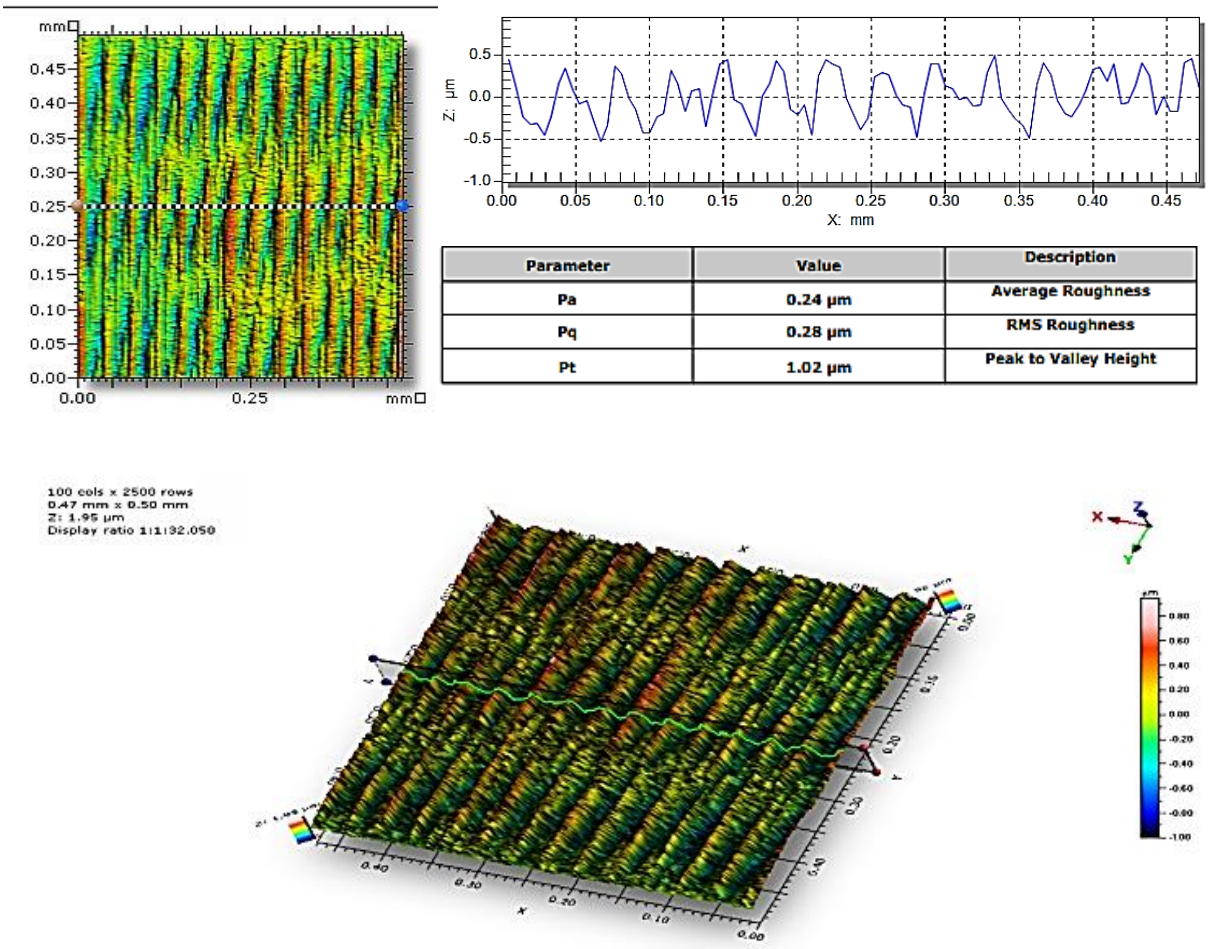

Parameter	Value	Description
Pa	0.24 µm	Average Roughness
Pq	0.28 µm	RMS Roughness
Pt	1.02 µm	Peak to Valley Height

Figure 4.3.2c. 3D representation of the surface topographical features of the MP48 sample.

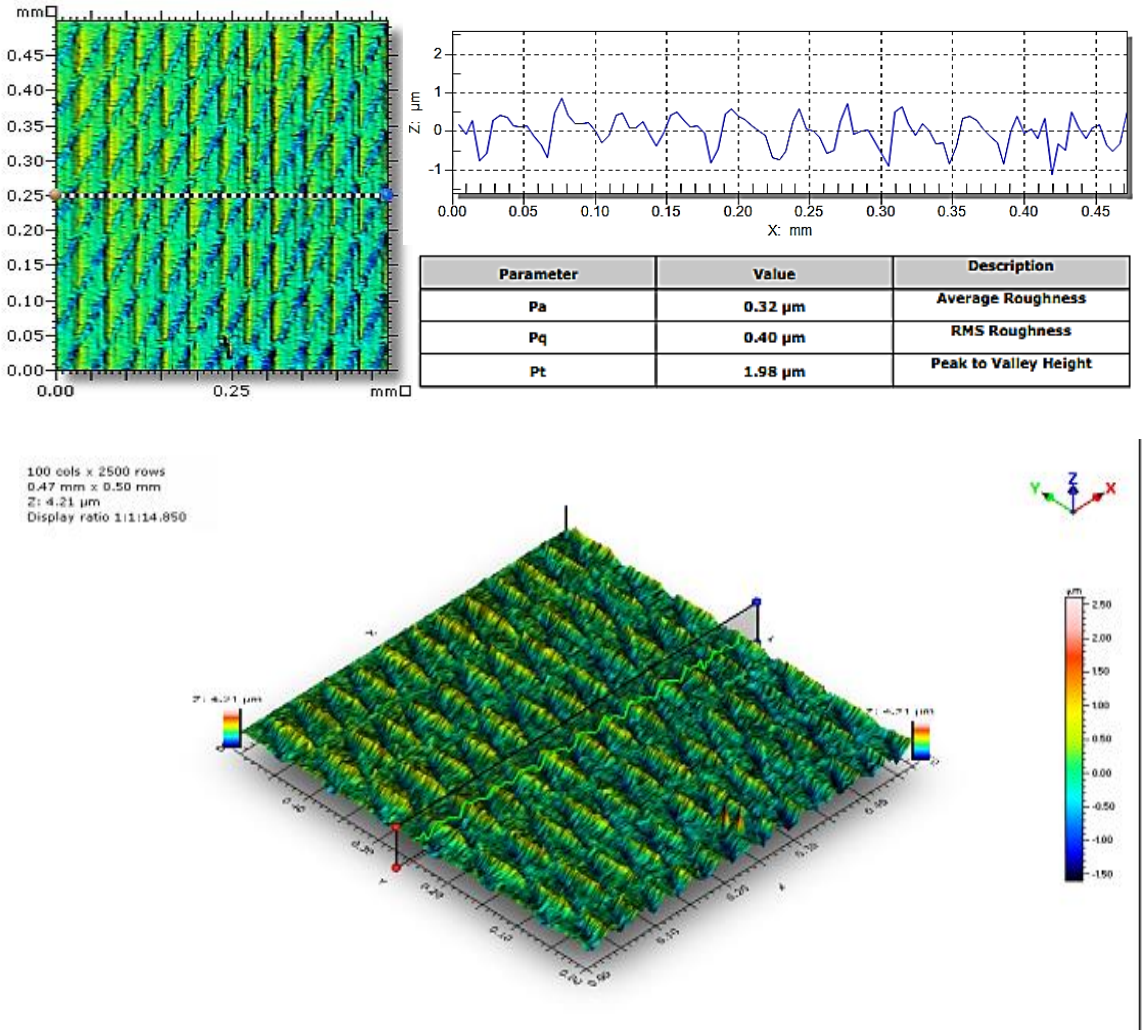

Parameter	Value	Description
Pa	0.32 µm	Average Roughness
Pq	0.40 µm	RMS Roughness
Pt	1.98 µm	Peak to Valley Height

Figure 4.3.2d. 3D representation of the surface topographical features of the MP58 sample.

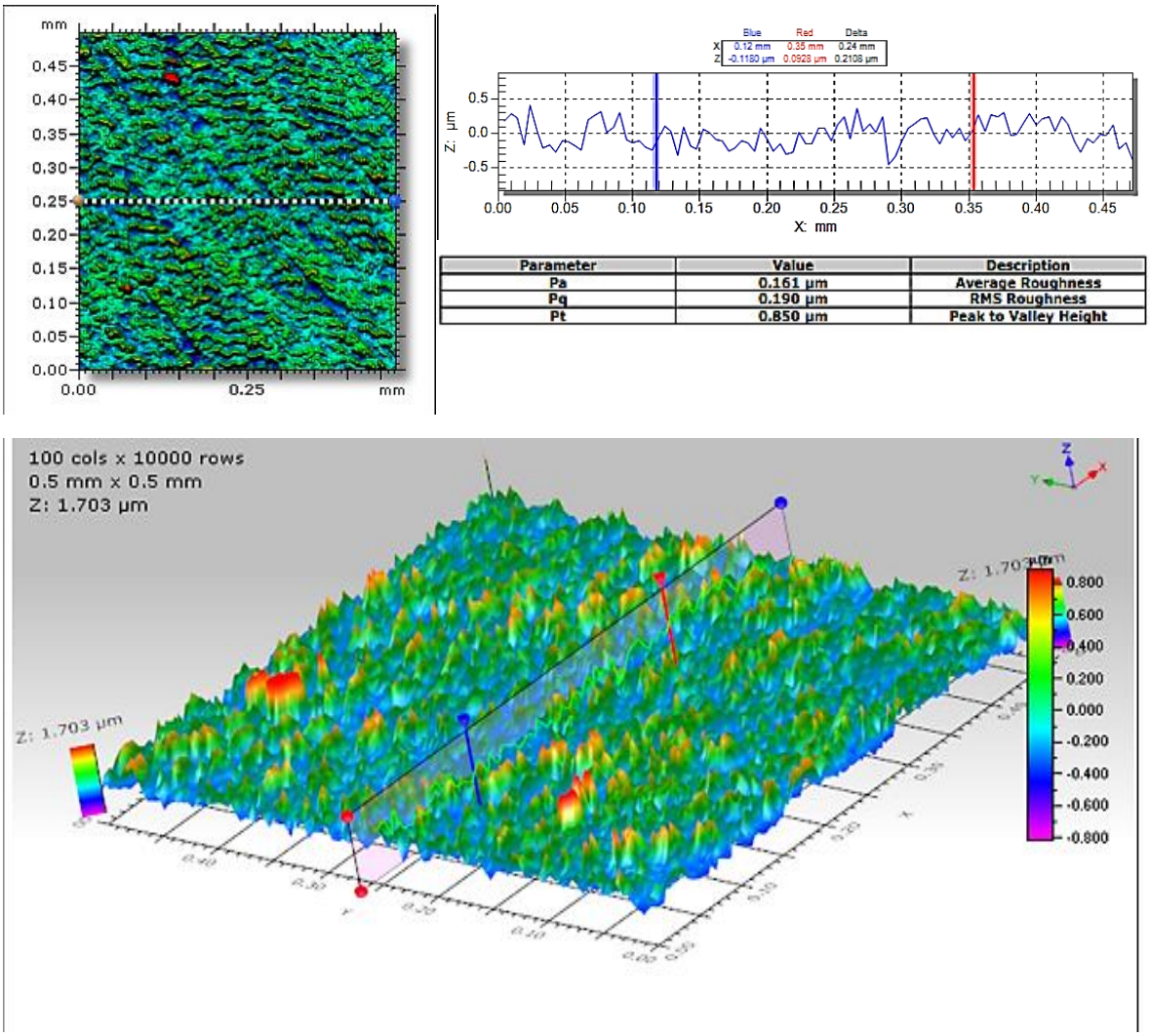

Parameter	Value	Description
Pa	0.161 µm	Average Roughness
Pq	0.190 µm	RMS Roughness
Pt	0.850 µm	Peak to Valley Height

Figure 4.3.2e. 3D representation of the surface topographical features of the MPTO sample.

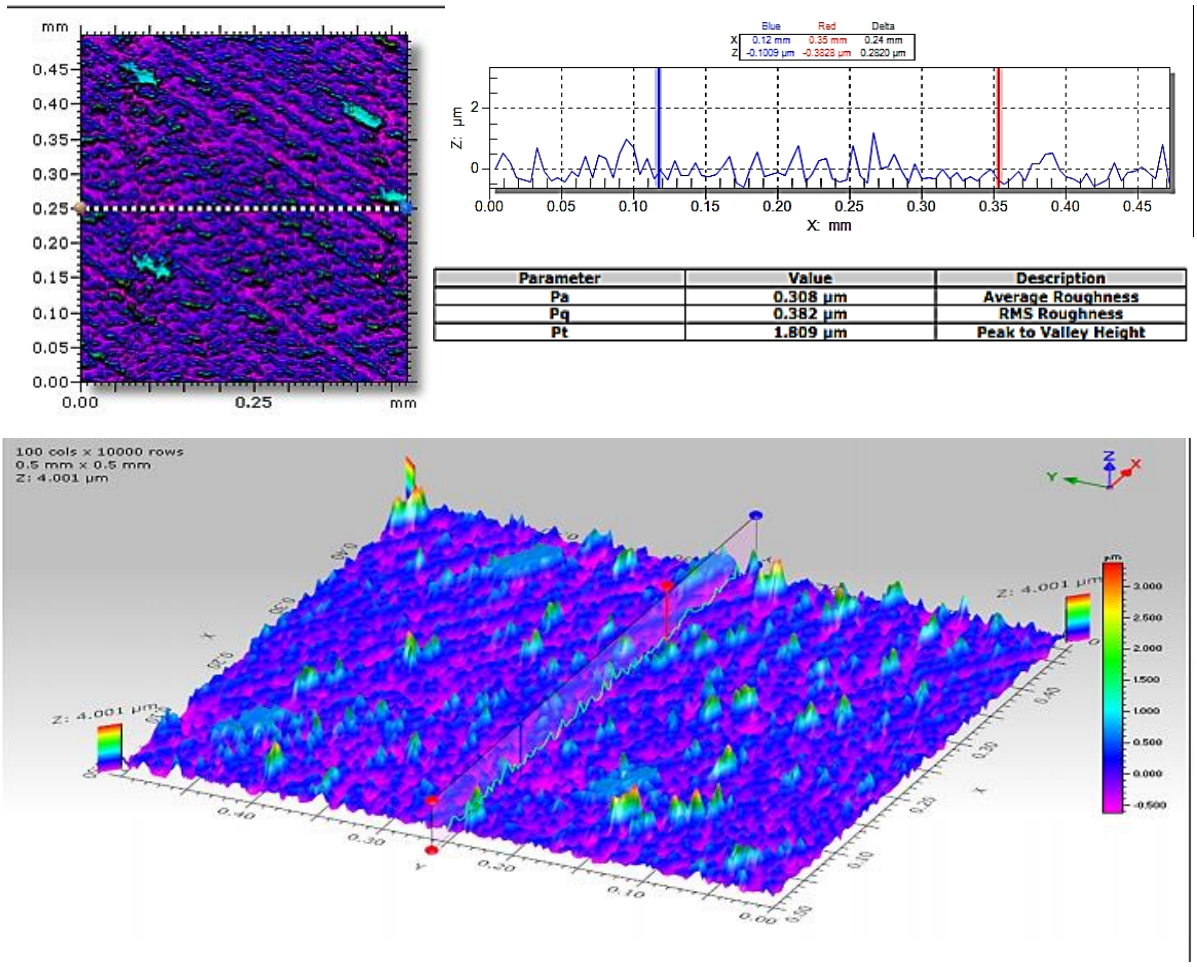

Figure 4.3.2f. 3D representation of the surface topographical features of the TOMP sample.

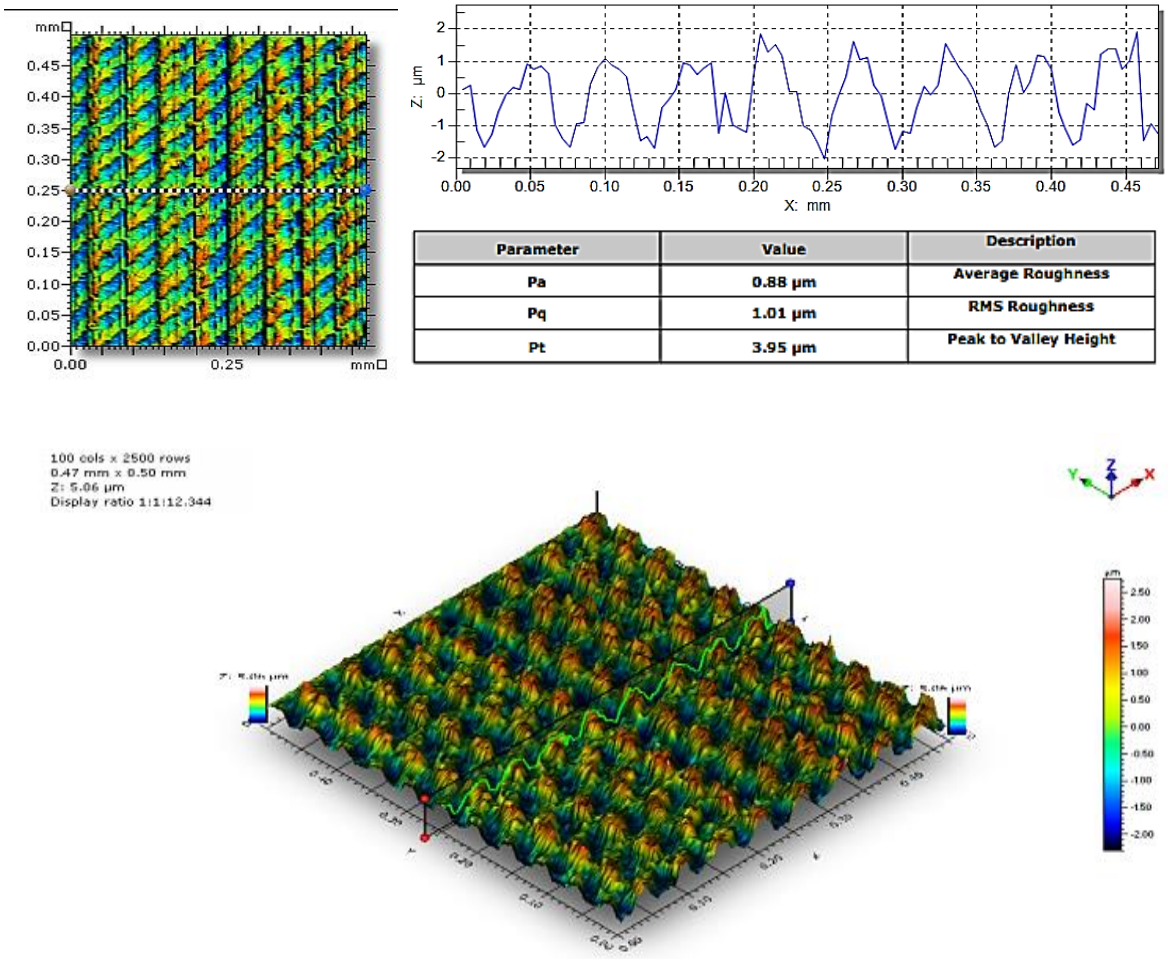

Parameter	Value	Description
Pa	0.88 µm	Average Roughness
Pq	1.01 µm	RMS Roughness
Pt	3.95 µm	Peak to Valley Height

Figure 4.3.2g. 3D representation of the surface topographical features of the TOMP48 sample.

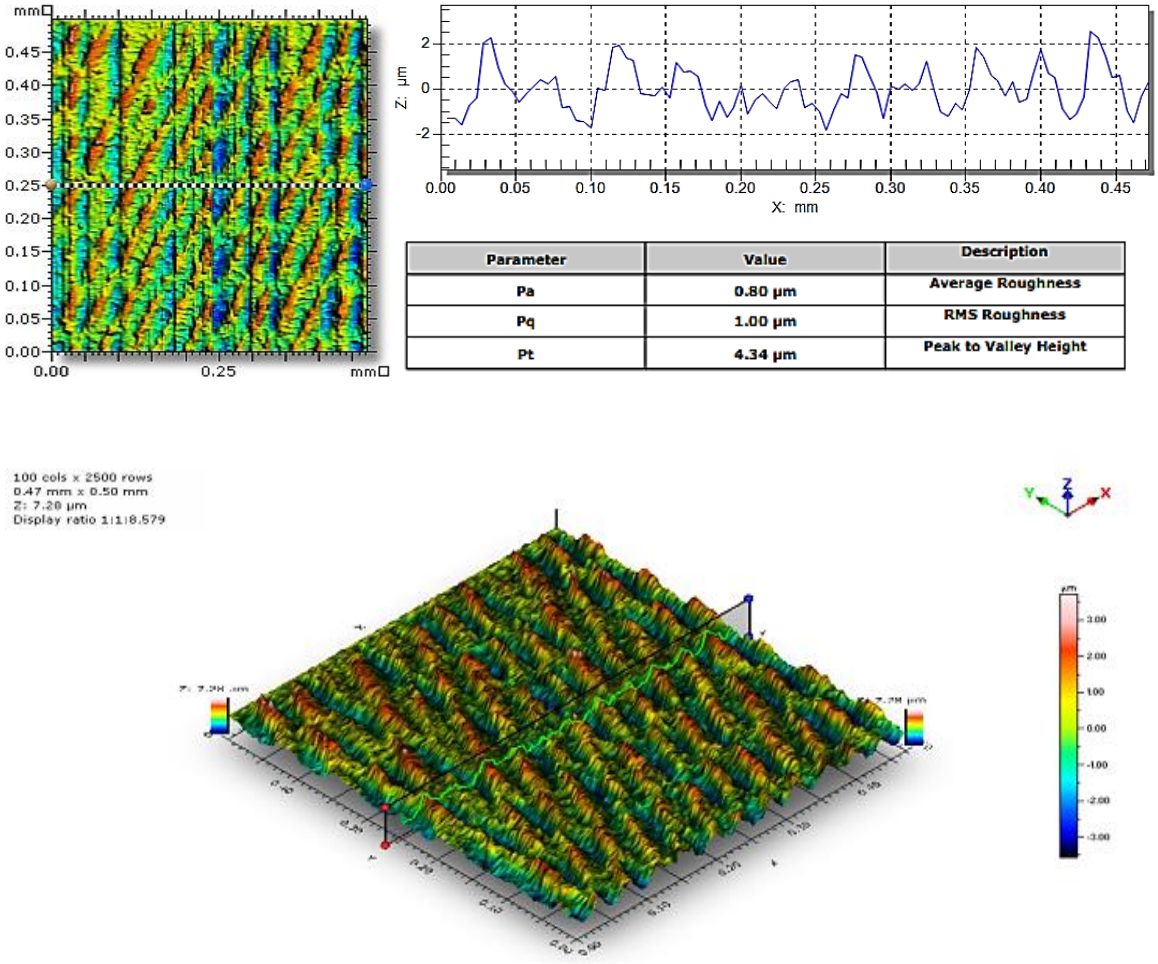

Parameter	Value	Description
Pa	0.80 µm	Average Roughness
Pq	1.00 µm	RMS Roughness
Pt	4.34 µm	Peak to Valley Height

Figure 4.3.2h. 3D representation of the surface topographical features of the TOMP58 sample.

4.4 Wettability

As shown in Figure 4.4.1a, the MPTO sample had the lowest water contact angle (WCA) at +/- 23.6° and the TOMP58 sample had the highest at +/- 131.3˚. This indicated that the MPTO sample was the most hydrophilic and the TOMP58 sample was the most hydrophobic. Surfaces with WCA's below 90° are viewed as hydrophilic whereas, surfaces with WCA's above 90° are seen as hydrophobic. Using this information it could be seen than the P, PTO and MPTO samples were all hydrophilic whereas MP48, MP58, TOMP48 and TOMP58 were all hydrophobic. The samples with LIPSS were all hydrophobic which indicated that the presence of the surface textures led to hydrophobic WCA'S. PTO was more hydrophilic (WCA of +/- 38.4°) than P which suggested the TiO_2 increased the wettability of the surface. MPTO surprisingly was more hydrophilic than the PTO sample even though the sample had LIPSS which led to the other samples being hydrophobic. MP58 had a lower WCA (+/- 117.7°) than MP48 (+/- 122.2°) whereas TOMP58 had a higher WCA than TOMP48 (+/- 128°).

Surface free energy (SFE) and the contact angle of a surface have an inverse relationship so that if the water contact angle is high, the SFE for that corresponding sample type will be low. The results of this investigation displayed this relationship. The SFE of the MPTO sample was the highest (+/- 65.5 mN/m) and the P sample had the lowest SFE (+/- 36.7 mN/m). There was so significant difference between the SFE results of the MP48 (+/- 51.4 mN/m) and MP58 (+/- 51.1 mN/m) samples which indicated different laser texturing parameters do not have a large effect on the SFE. There was a significant difference between the SFE results of TOMP48 (+/- 52.7 mN/m) and TOMP58 (+/- 54.4 mN/m) which may be due to the oxide destruction in TOMP58 rather than the LIPSS parameters.

Figure 4.1.1c displayed the water droplet formation on the sample types. The water droplet on MPTO spread the most followed by PTO which again confirmed the MPTO was the most hydrophilic as seen in Figure 4.4.1a. The spreading of the water droplets was the least for TOMP48 and TOMP58 and were similar. This again confirmed both these sample types were hydrophobic.

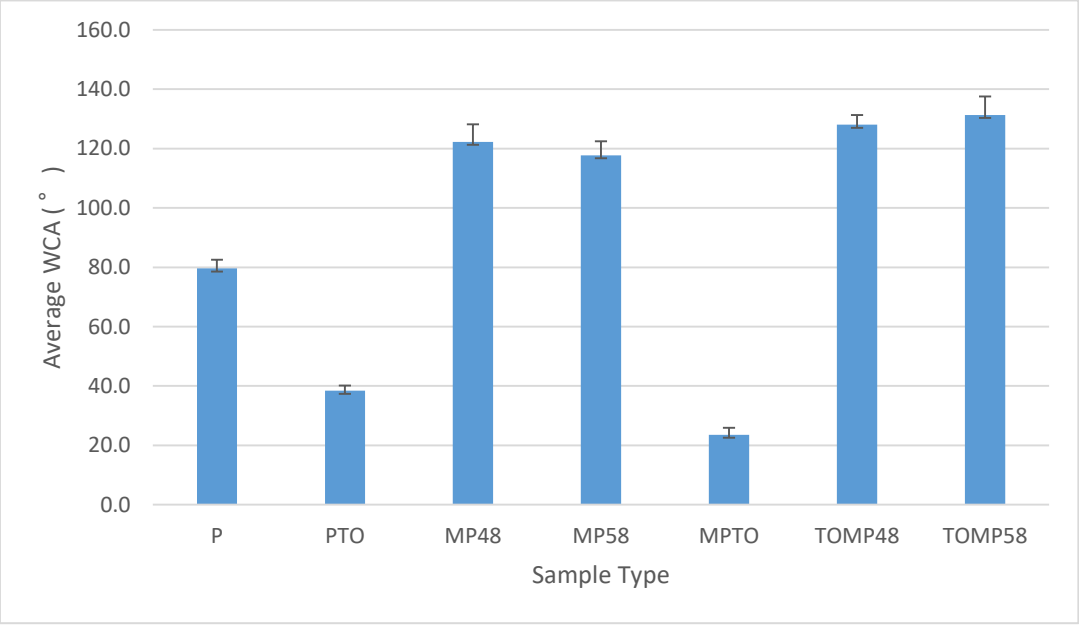

Figure 4.4.1a. A graphical representation of the mean water contact angles of each sample type.

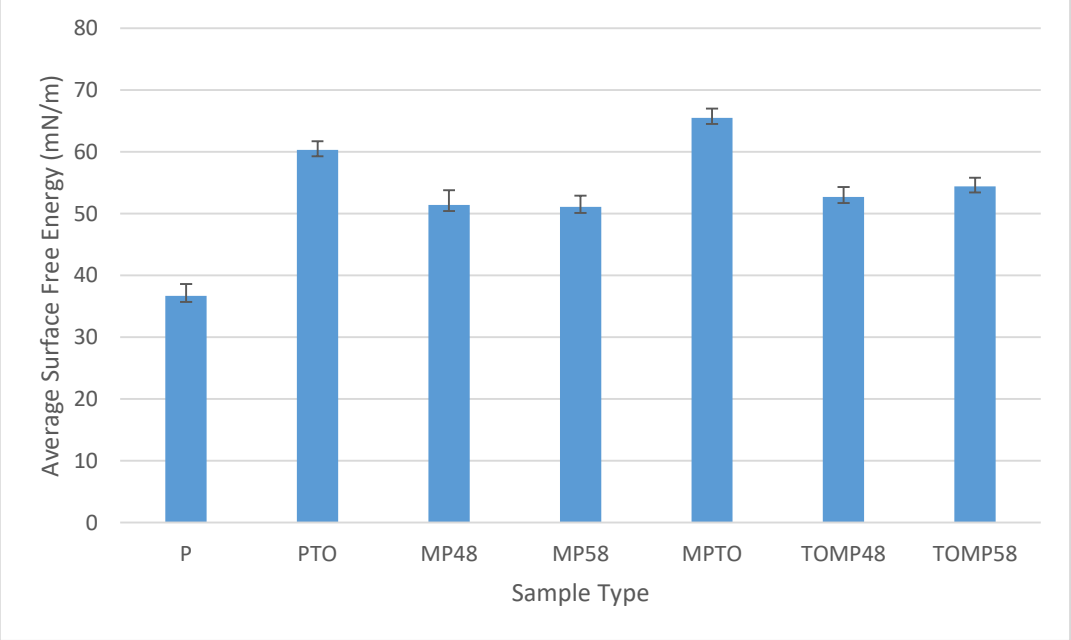

Figure 4.4.1b. A graphical representation of the mean SFE of each sample type.

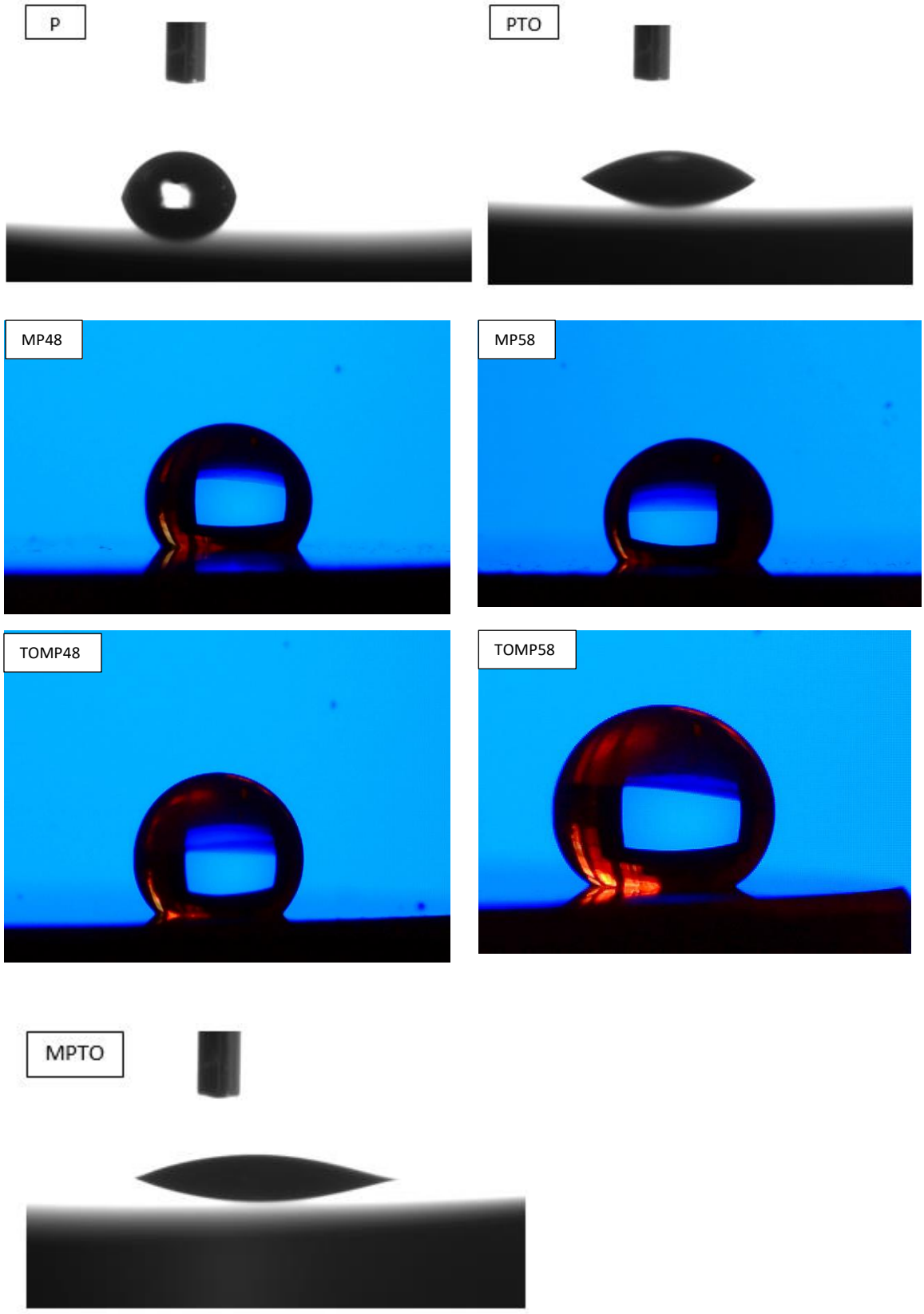

Figure 4.4.1c. The wetting profiles of each sample type using water.

4.5 Cross-sectional Microstructure

4.5.1 SEM

As shown in Figure 4.5.1a, the PTO sample had a clear TiO_2 layer and an ODZ (oxygen diffusion zone). The oxide was approximately +/- 2.5 µm thick and the ODZ was about +/- 10 µm thick. The ODZ was quite thick which indicated the TiO_2 layer would have good structural support. Also, the oxide was well bonded to the ODZ as there were no cracks, gaps or loosening of the treated surface layer from the substrate. This indicated the CCT process was successful.

For the MP48 and MP58 samples, there were a few minor dips that could be seen that are highlighted below. These dips correlate to the LIPSS and for MP48 the LIPSS depth was +/- 1.25 µm and for MP58 was +/- 2 µm. This suggested the higher 58 % power of the LIPSS laser penetrated the substrate further and hence, the greater depth. Cracks or other structural damage were not present and hence, the laser did not damage the samples.

For Figure 4.5.1b, there are 2 images that depict the MPTO sample. The second MPTO image showed a surface oxide layer on the top of the ODZ whereas, the first image only showed an ODZ without surface oxide layer. In the first image it could be seen that the oxide was not visible. This could be due to the way the samples were cut and the oxide may have been removed due to spallation. However, the ODZ was present which indicated CCT was successful. The ODZ was +/- 10 µm thick which was the same as the PTO sample. The LIPSS had a depth of +/- 1 µm which was smaller than the MP48 and MP58 samples. As seen in the SEM images (Figure 4.1.1b), the MPTO sample had LIPSS that were less visible due to

the CCT process which may have damaged the LIPSS. As a result, the LIPSS hay have lost their depth due to the resultant oxide that formed over the LIPSS.

In the second image for MPTO, the oxide was more visible which may be due to better preparation of the cross section. The oxide had a thickness of about +/- 2 µm which was slightly thinner that the oxide thickness of PTO (Figure 4.5.1a). This may be due to the cutting process. The ODZ of the MPTO sample was +/- 12 µm which was higher than the PTO sample. This suggested the presence of the LIPSS may have caused increased oxygen diffusion during the CCT process hence, the ODZ was slightly thicker. The LIPSS on this sample had a depth of +/- 1.2 µm which was similar to the MP48 sample. For the original TOMP sample, the oxide was clearly visible and possessed good bonding to the substrate. The ODZ was the thickest for this sample at +/- 14 µm. However, it was difficult to clearly show the LIPSS under a low magnification.

The cross section images (Figure 4.5.1c) suggested the TOMP48 and TOMP58 samples had damaged oxide layers that were poorly bonded to the substrate. This may be due to the improper preparation and cutting of the samples as the TOMP sample had a good oxide. The TOMP48 sample had an oxide thickness of +/- 1.2 µm and the TOMP58 sample had an oxide thickness of +/- 1.7 µm. The SEM images in Figure 4.1.1e suggested the TOMP58 sample had greater oxide damage yet the cross section images display the TOMP58 possessing thicker oxides. However, this may again be due to the improper cutting. The ODZ of TOMP58 was thicker when compared to TOMP48. TOMP58 had almost twice the depth of LIPSS (+/- 1.15 µm) when compared to TOMP48 (+/- 0.6 µm). This was similar to the MP58 sample which also had a greater LIPSS depth when compared to MP48.

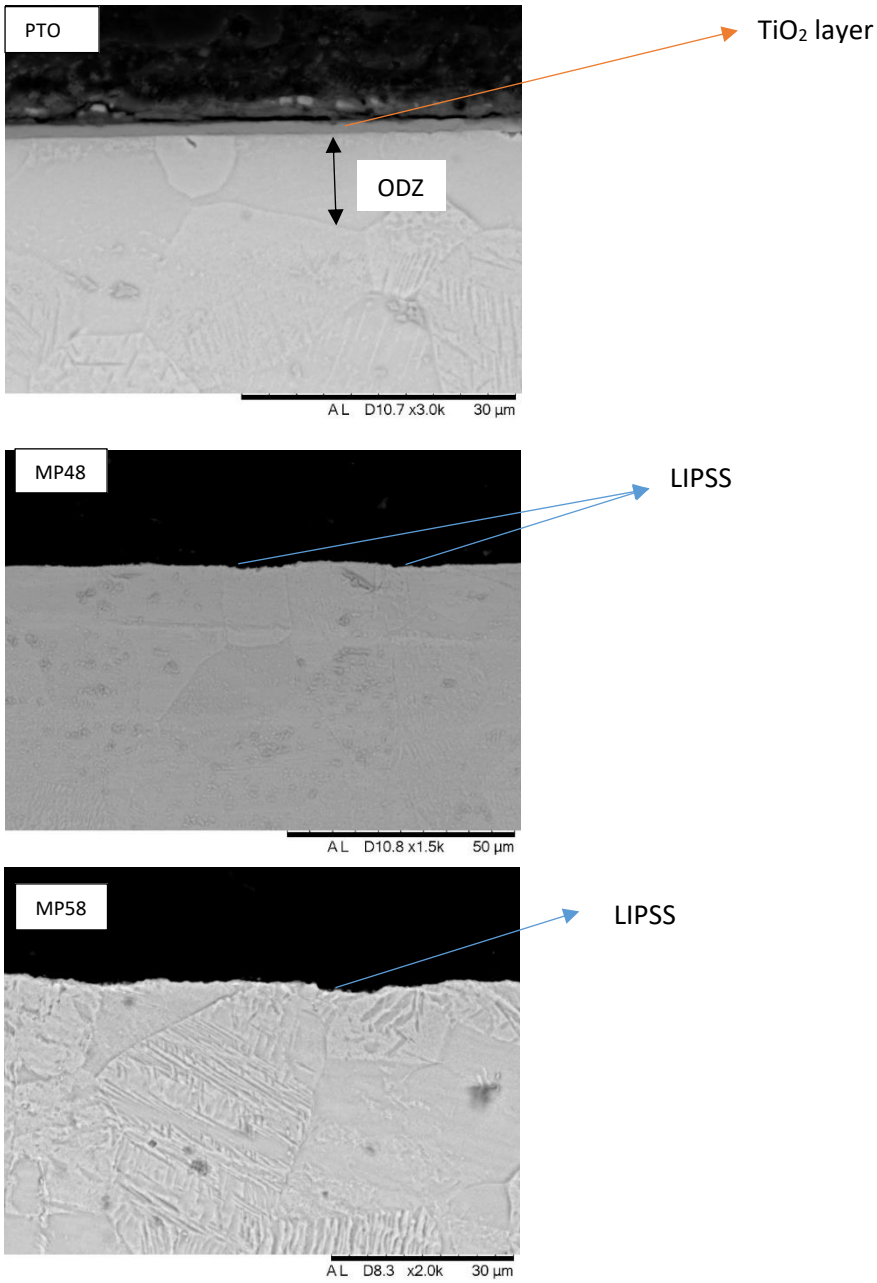

Figure 4.5.1a. SEM micrographs displaying the cross sections of the PTO, MP48 and MP58 samples after etching using Kroll's reagent.

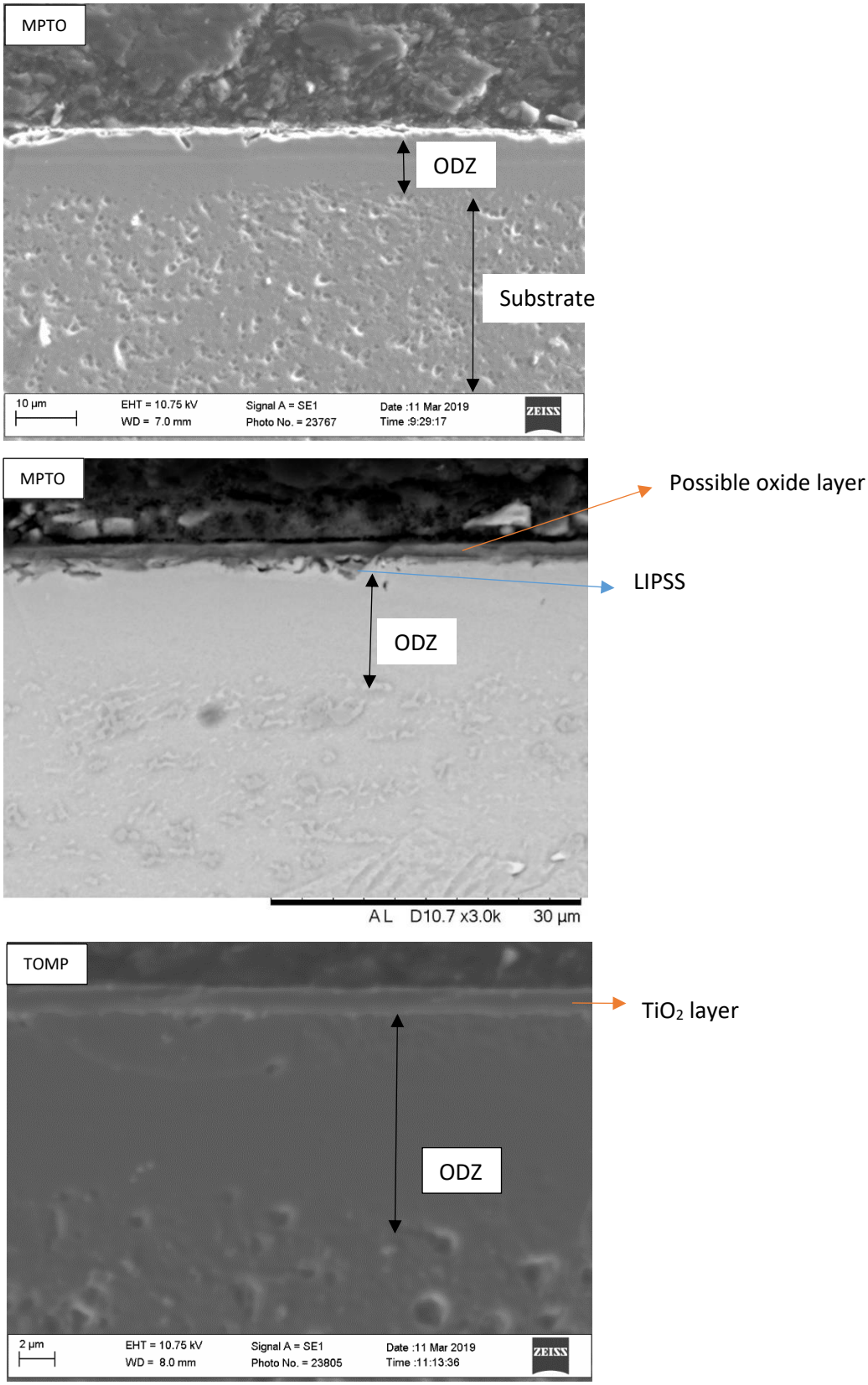

Figure 4.5.1b. SEM micrographs displaying the cross sections of the MPTO and TOMP samples after etching using Kroll's reagent.

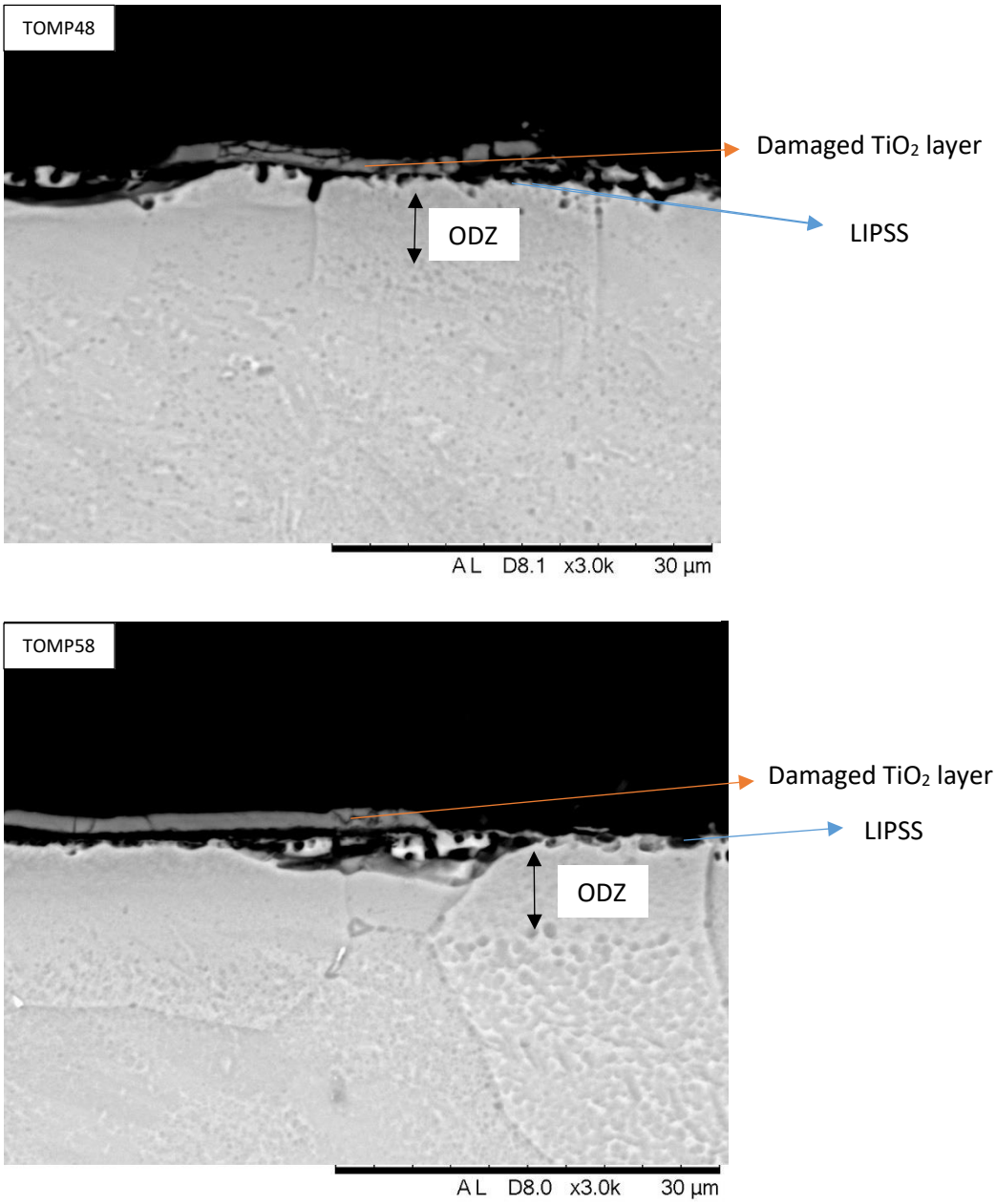

Figure 4.5.1c. SEM micrographs displaying the cross sections of the TOMP48 and TOMP58 samples after etching using Kroll's reagent.

4.5.2 Focused ion beam (FIB)

Figures 4.5.2a and 4.5.2b display the region of interest where the FIB analysis was undertaken and also the platinum coating, respectively. In Figure 4.5.2c it can be concluded than the LIPSS ripples did not form underneath the TiO_2 layer. During the patterning process, the laser caused the oxide layer to be destroyed and hence it was removed. The ripples completely stop forming (4.5.2c iii) and did not continue under the +/- 2 µm TiO_2 layer. The spacing between the ripples was +/- 0.3-0.7 µm and there were no gaps or cracks between the substrate and oxide layer. This indicated the bonding between the TiO_2 layer and the substrate was good. Figure 4.5.2d displays a higher magnification micrograph. In this image it was very clear that the ripples did not form under the oxide and stopped forming when approaching the TiO_2 layer.

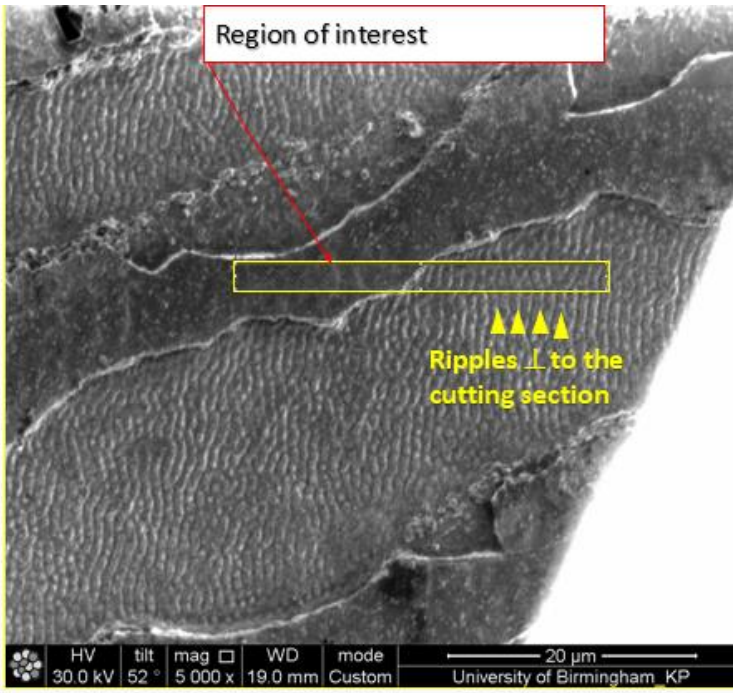

Figure 4.5.2a. Image displaying the region of interest which was cut perpendicular to the LIPSS ripples to view the cross section of the LIPSS.

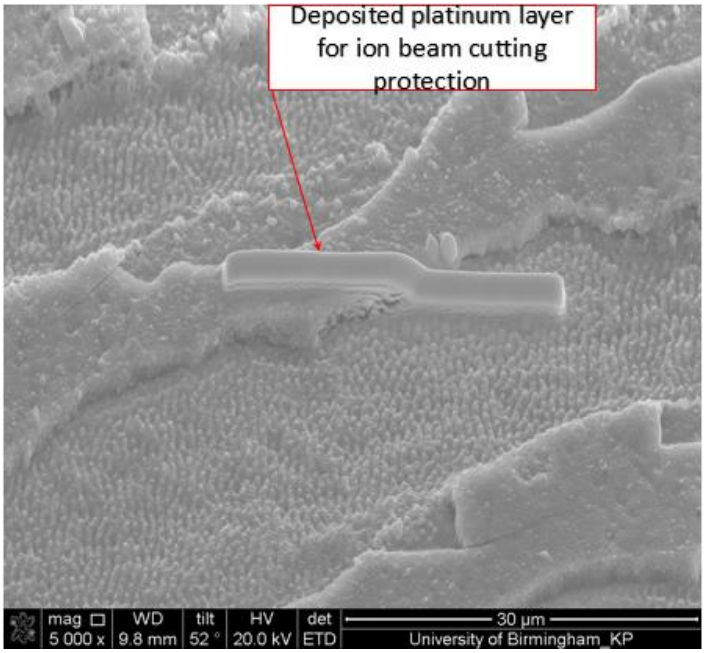

Figure 4.5.2b. Micrograph taken at 52° tilt which displays the platinum coating.

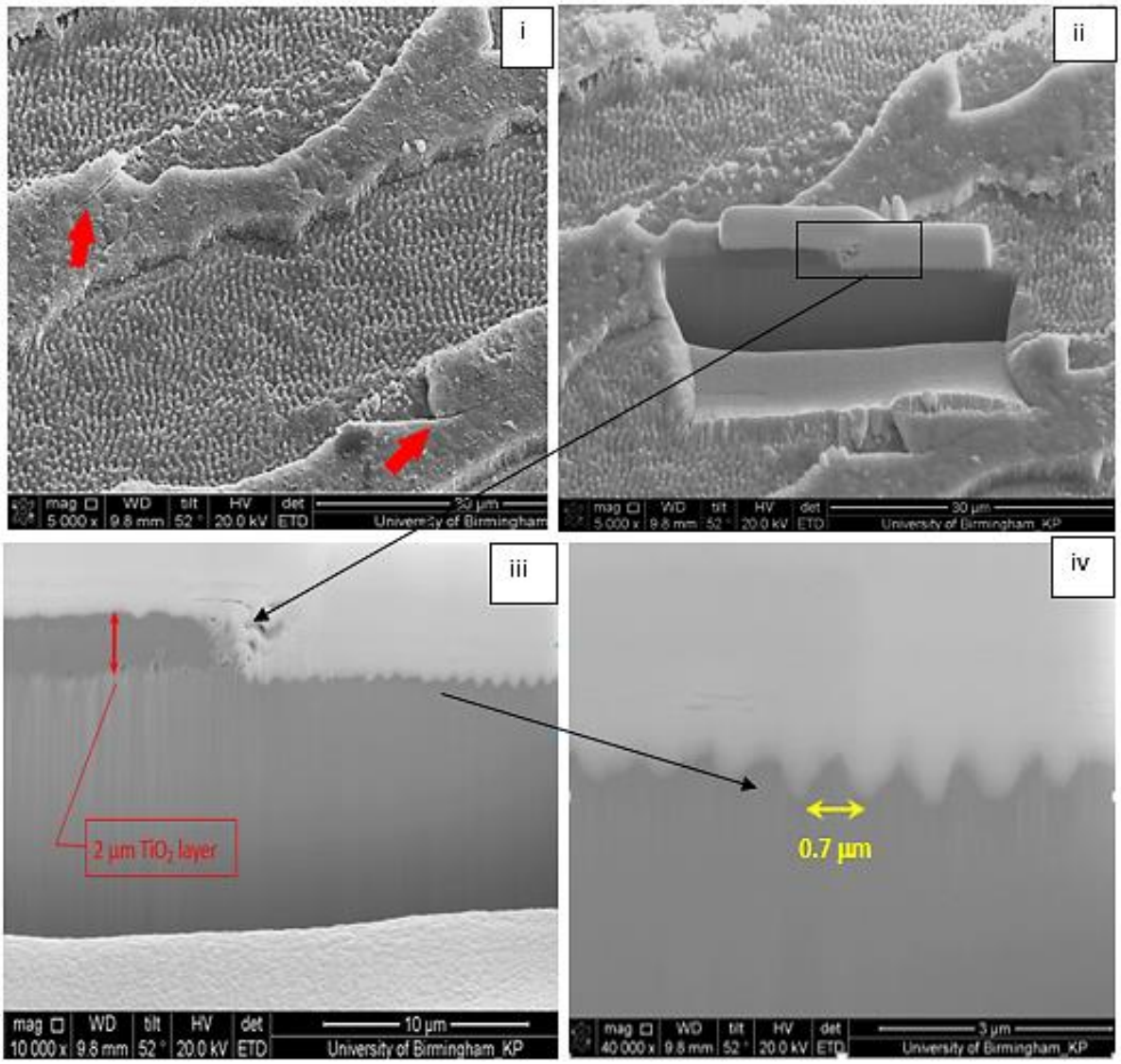

Figure 4.5.2c. i) ripples developed when the top TiO_2 layer was damaged by the laser beam as evidenced by the cracks (red arrows), ii) displays the cut section, iii) the +/- 2 µm TiO_2 is visible and d) higher magnification displaying the cross section of the individual ripples which have a spacing of +/- 0.7 µm.

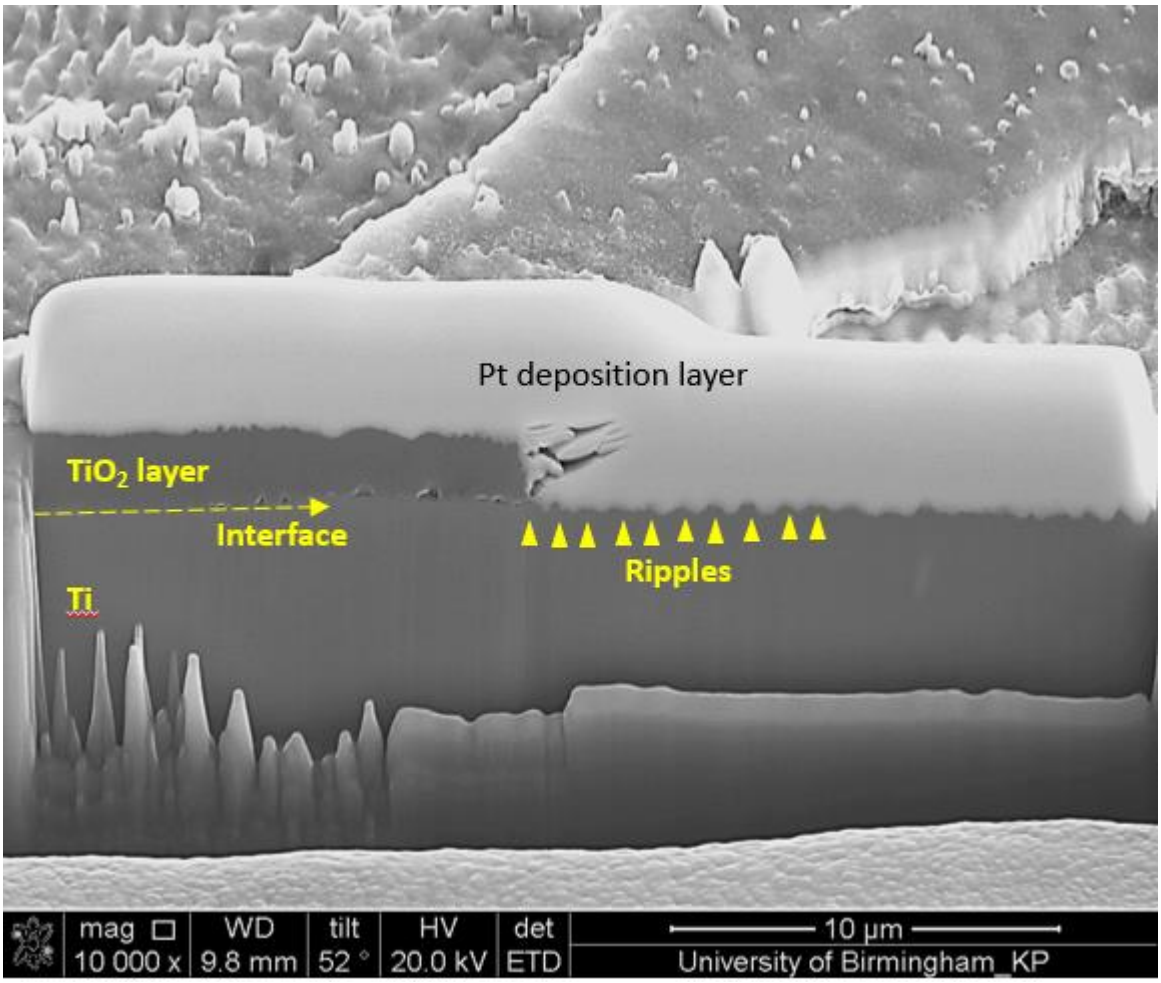

Figure 4.5.2d. Micrograph displays whole cross section of the region chosen. There are no ripples under the TiO_2 layer and hence, the ripples do not form under the TiO_2 layer.

4.6 Surface micro-hardness

The surface hardness of the first batch samples were measured and the results are depicted in Figure 4.6. It can be seen that PTO sample had the highest hardness (+/- 904.1 HV0.5) and the MP sample had the lowest (+/- 163.9 HV0.5). The MPTO sample had a lower micro-hardness (+/- 814.5 HV0.5) than the PTO sample and the MP sample had a lower micro-hardness than the P sample (+/- 188.7 HV0.5). This was most likely due to the patterning, which reduced the real contact areas under the indenter. This is also supported by the observation that the TOMP is not as hard as the PTO sample. Also, the TOMP sample had a lower micro-hardness (+/- 524.8 HV0.5) than the MPTO sample which was probably due to the sharper patterns and hard oxide layer destruction during the patterning process. In addition, the laser patterned surface was not fully dense with peaks and valleys, which thereby may have reduced the hardness of the samples.

The PTO sample had the highest hardness because the oxide evenly covered the whole surface area without possessing any valleys or dents on the surface and TiO_2 possesses a high hardness. On the other hand, the MP sample possessed patterns in the form of ripples with +/- 0.7 µm spacing between each ripple (Figure 4.5.2c). The spacing may have led to lower surface hardness values for the patterned samples. This suggested that the patterns alone on the sample would not be durable and hence, inappropriate for withstanding high loads. Nonetheless, when combined with CCT the micro-hardness increased which indicated that the oxide may increase the durability of the LIPSS. The MPTO sample had a higher hardness than the TOMP sample probably due to the thicker oxide and reduced sharpness of the patterns and hence, the reduced Rt values (as seen in Sections 4.1.1 and 4.3).

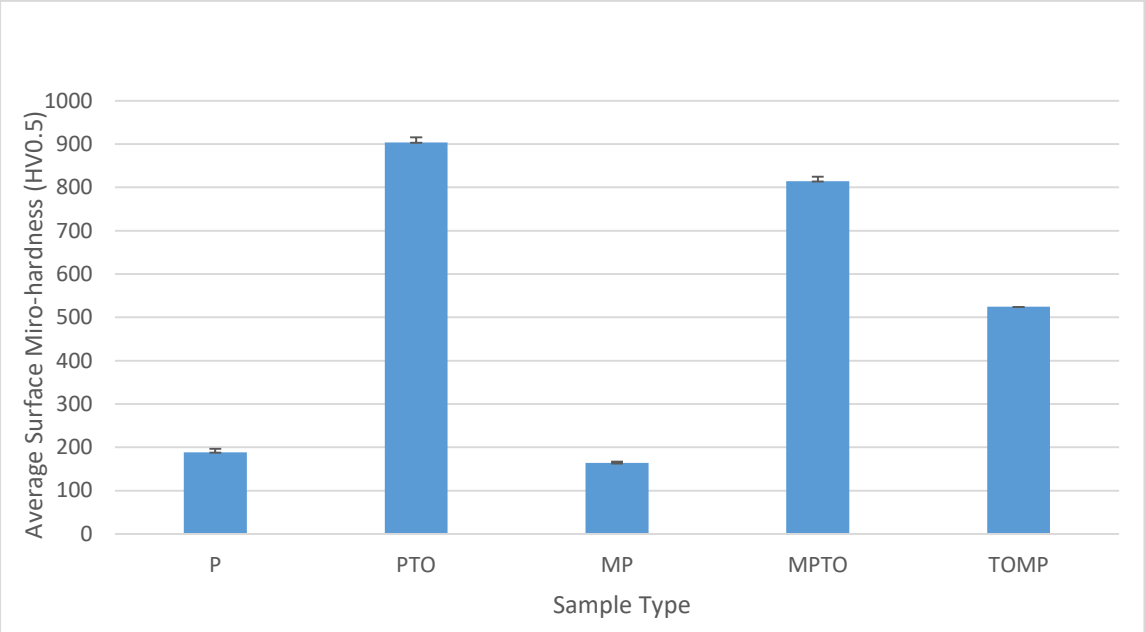

Figure 4.6. A graphical representation of the mean surface micro-hardness of each sample type.

4.7 Antibacterial Efficacy

4.7.1 Percentage reduction

The anti-bacterial efficacy of the surface engineered surfaces as well as untreated surfaces were evaluated. Table 4.7.1a and Figure 4.7.1a summarise the average number of *S. aureus* and *E. coli* colonies grown on these samples. It can be seen from Figure 4.7.1b that the P sample had the lowest percentage reduction meaning that a high number of colonies grew on the untreated sample. On the other hand, the TOMP sample had the largest percentage reduction so that the number of colonies grown on this sample type was the fewest. The results between the TOMP and the MPTO samples displayed a significant difference hence, indicating that patterning after thermally oxidising produced better results.

The effect of the micro-patterning and the titanium oxide formation on the colony growth was more visible with *S. aureus* than *E. coli*. Thus, it can be assumed for this study that micro-

patterning had a larger effect on Gram positive species. The LIPSS caused fewer colony growth probably due to the +/- 0.3-0.7 µm periodicity between the ripples which may have led to reduced contact area for the 1 µm bacteria and thus, reduced growth.

Nonetheless, in the case of the PTO sample, the increased presence of titanium oxide had a greater effect on the Gram negative *E. coli* than on the Gram positive *S. aureus.* Both treatment types (micro-patterning and CCT) caused a reduction in colony growth indicating that they can both be used to reduce the risk of infection in medical implants or instruments. Just the presence of titanium alone reduced the number of colonies but the presence of the surface treatments amplified the antibacterial effect (Figure 4.7.1c).

Table 4.7.1a. Average number of *E. coli* and *S. aureus* colonies grown per each sample type.

	Sample Type					
	Control	P	PTO	MP	MPTO	TOMP
Average number of *S. aureus* colonies per plate	7400	5891	4782	1829	2531	1648
Average number of *E. coli* colonies per plate	9483	7882	5810	3390	5335	3191

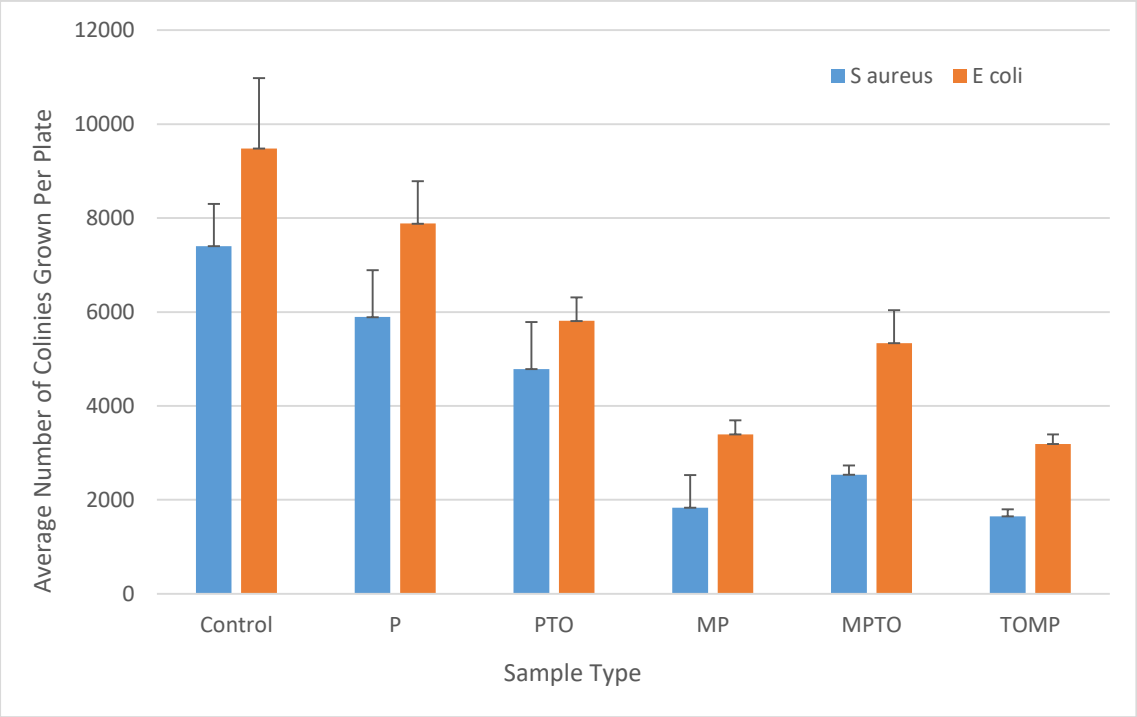

Figure 4.7.1a. Average number of *S. aureus* and *E. coli* colonies grown on all sample types.

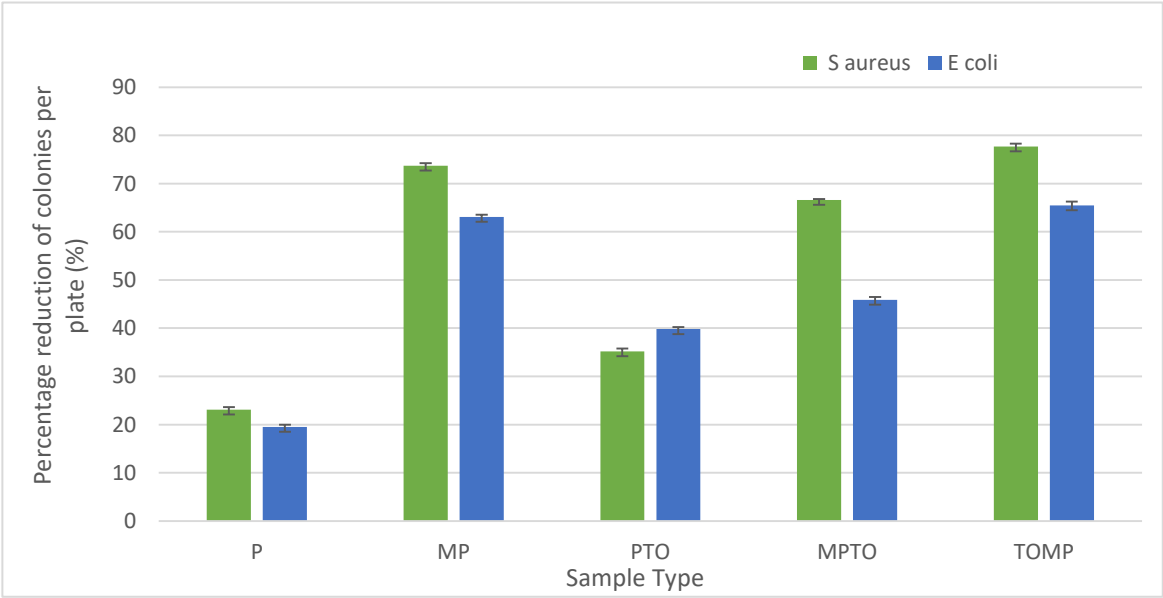

Figure 4.7.1b. Percentage reduction of the colonies grown per each sample type vs the control.

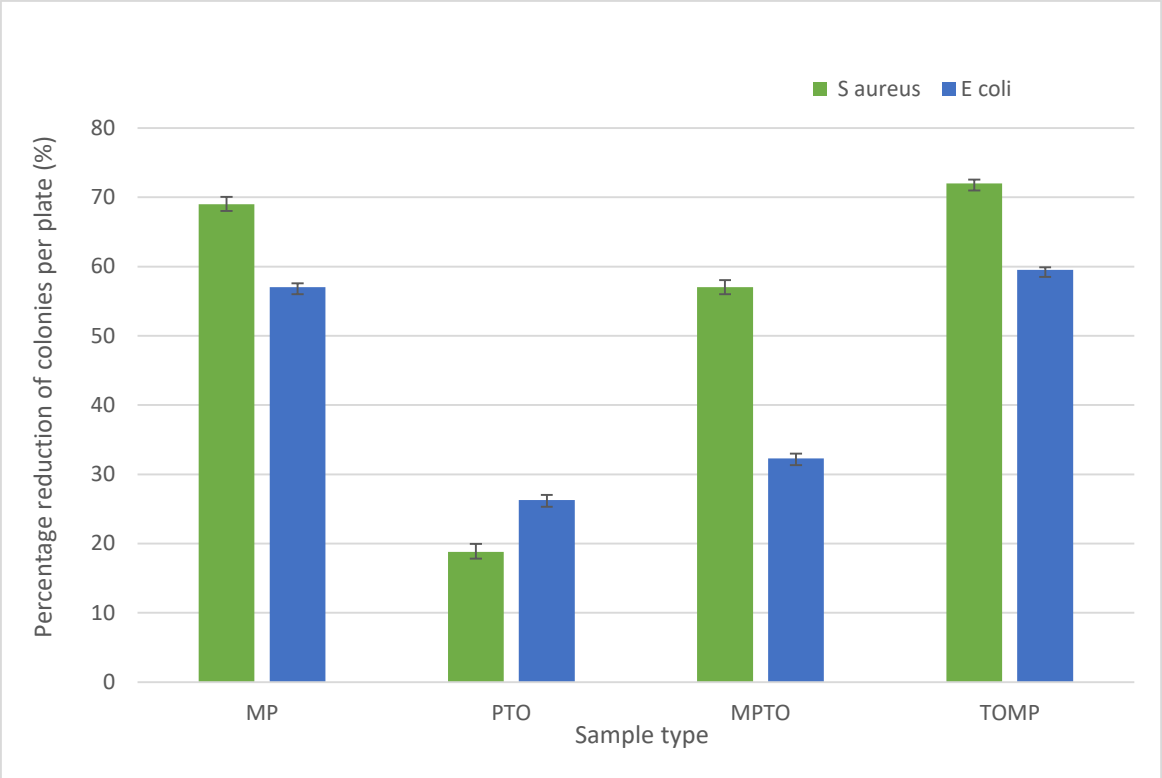

Figure 4.7.1c. Percentage reduction of the colonies grown per each treated sample type vs the untreated P sample.

4.7.2 Anti-adhesion

4.7.2.1 *S. aureus*

Anti-adhesion is another term for anti-biofouling and in this test bacterial suspensions were applied directly to the sample surfaces. It helped determine whether bacteria are able to survive on the sample's surfaces. Figure 4.7.2.1a displayed the number of *S. aureus* organisms present on the different sample types. The highest value was seen for PTO which had +/- 59 *S. aureus* organisms which was unexpected as it was proposed the P sample would have the highest count (as seen in the percentage reduction charts, Section 4.7.1). The MPTO sample had a higher *S. aureus* growth (+/- 25) than P (+/- 22). This suggested that the higher surface roughness may cause more *S. aureus* attachment. MP48 and TOMP48

both had the same value (+/- 7) which suggested that the presence of TiO_2 had little effect on the bacteria in the presence of LIPSS which was unlike the percentage reduction results. MP58 had the second lowest value (+/- 8) which again indicated the surface textures led to lower bacteria survival rates when compared with CCT. TOMP58 had +/- 15 *S. aureus* organisms which was higher than TOMP48, MP48 and MP58. There was no significance difference between the results of MP48, MP58 and TOMP48.

When observing the SEM images (Figure 4.7.2.1a) of the *S. aureus* anti-adhesion test, it was found that the *S. aureus* organisms survived the most on PTO and the least on TOMP48. The PTO sample had a higher surface roughness than MP and P (Section 4.3) and thus the higher surface roughness may have caused increased bacterial attachment and therefore, survival. The bacteria were cocci shaped as proposed and on the PTO sample attached in clusters. This suggested the PTO sample provided an adequate environment for *S. aureus* survival.

On the other hand, the *S. aureus* organisms had very low numbers on the MP48 and MP58 samples. Less than +/- 3 organisms were found on these samples which indicated the LIPSS possessed a high anti-biofouling potential. With the TOMP48 sample, the bacteria mainly survived on the oxide columns. Nonetheless, the TOMP58 had more oxide destruction yet displayed higher bacterial numbers. Regions where the oxide was destroyed had improper or no LIPSS formation. These non-textured regions were where the bacteria showed highest numbers on the TOMP58 sample.

The bacteria seemed to grow under or between the ripples on the TOMP58 sample and hence, BSD (back scattered electron) images (Figure 4.7.2.1d) were taken to help

visualise whether this occurred. On the TOMP48 sample in Figure 4.7.2.1d there was a region where the spacing between the ripples was almost +/- 0.5 µm wide which was the same size as the *S. aureus* organism. In this region (marked red) the bacteria managed to attach and hence, it suggested the spacing between the ripples should be smaller than the bacterial size for it to be most effective in killing the bacteria. The same was also visible for the TOMP58 sample.

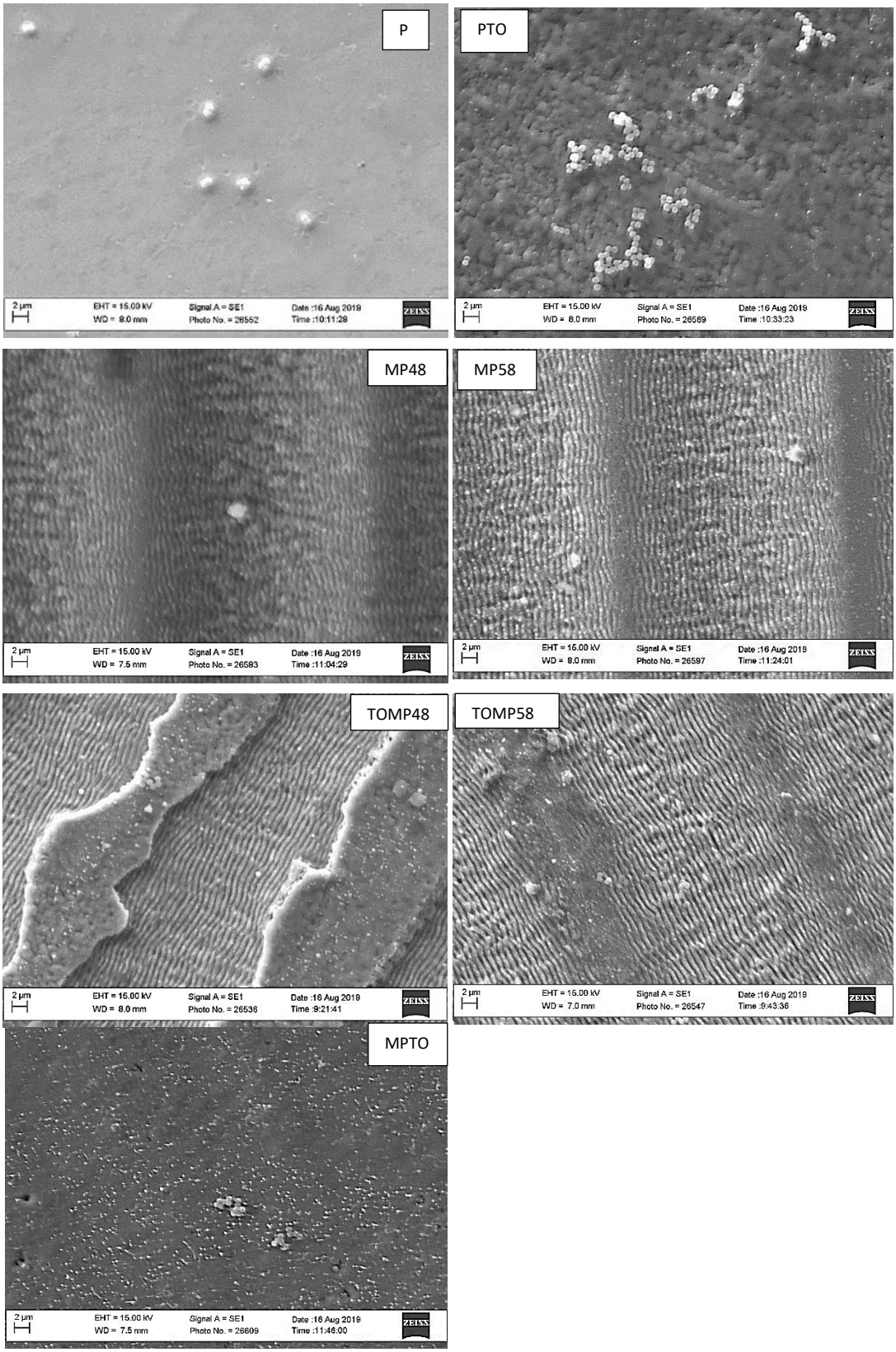

Figure 4.7.2.1a. SEM micrographs displaying the attachment of *S. aureus* organisms on each sample type.

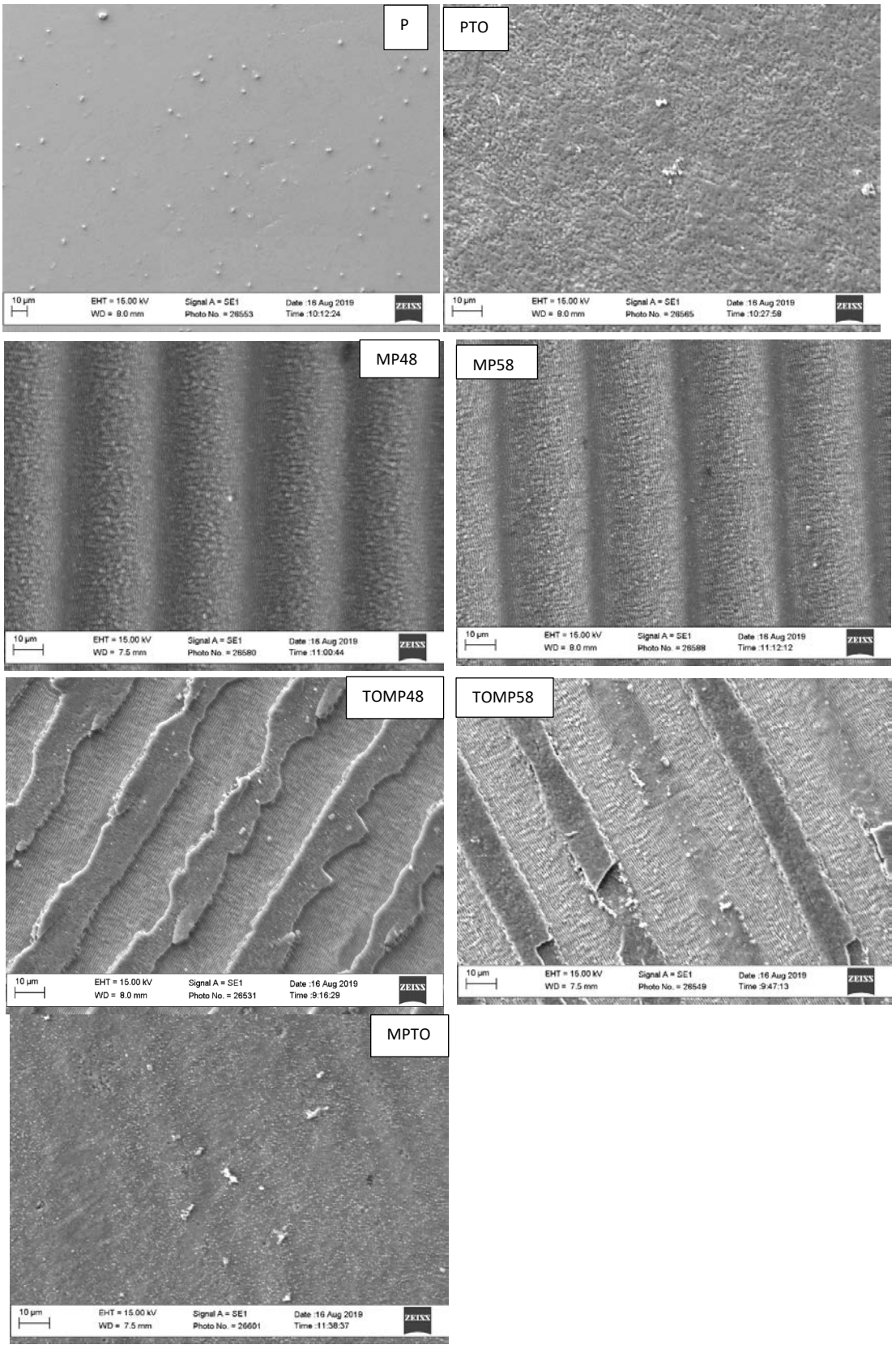

Figure 4.7.2.1b. SEM micrographs displaying the attachment of *S. aureus* organisms on each sample type.

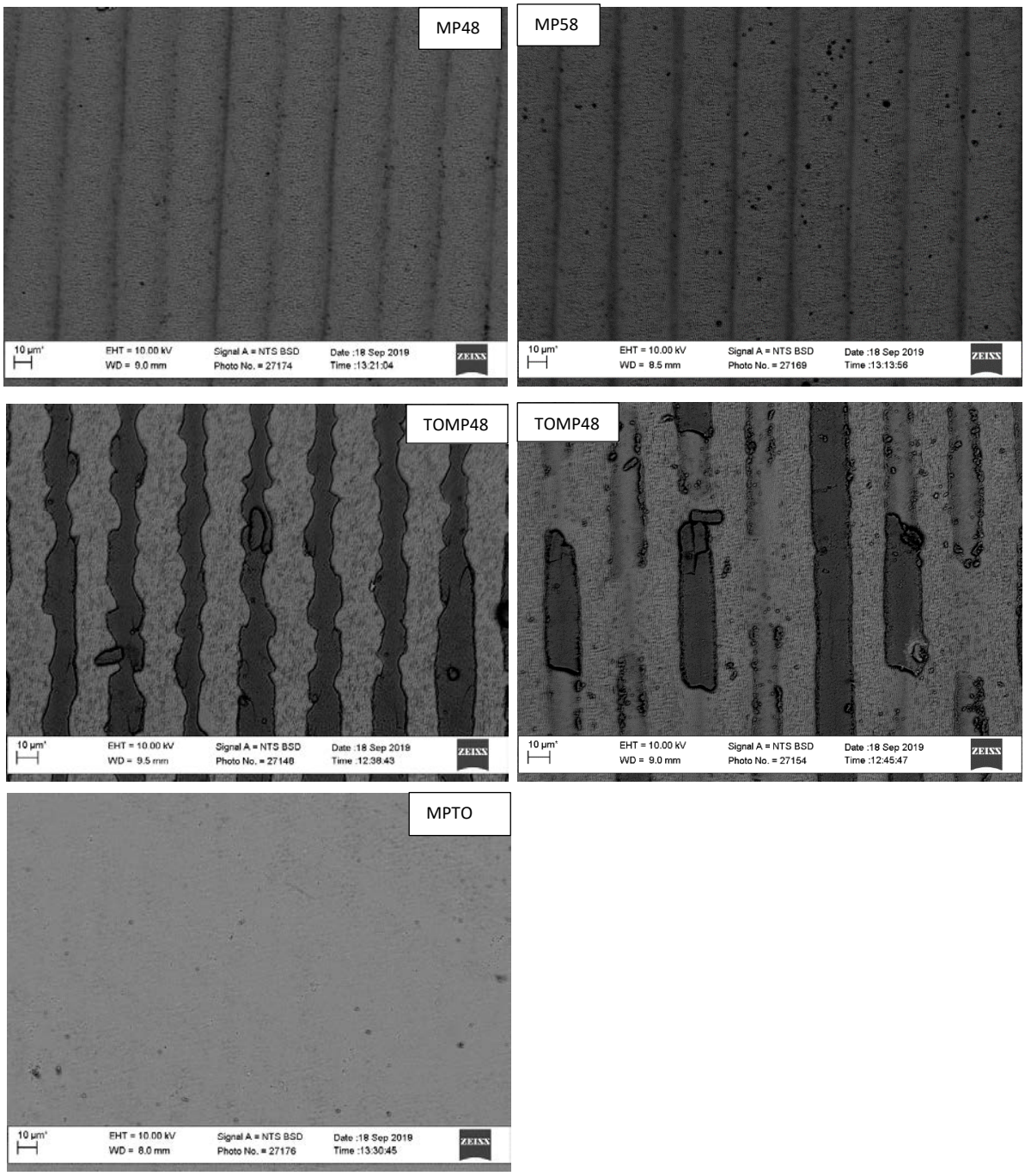

Figure 4.7.2.1c. Back-scattered micrographs displaying the attachment of *S. aureus* organisms on the treated sample types.

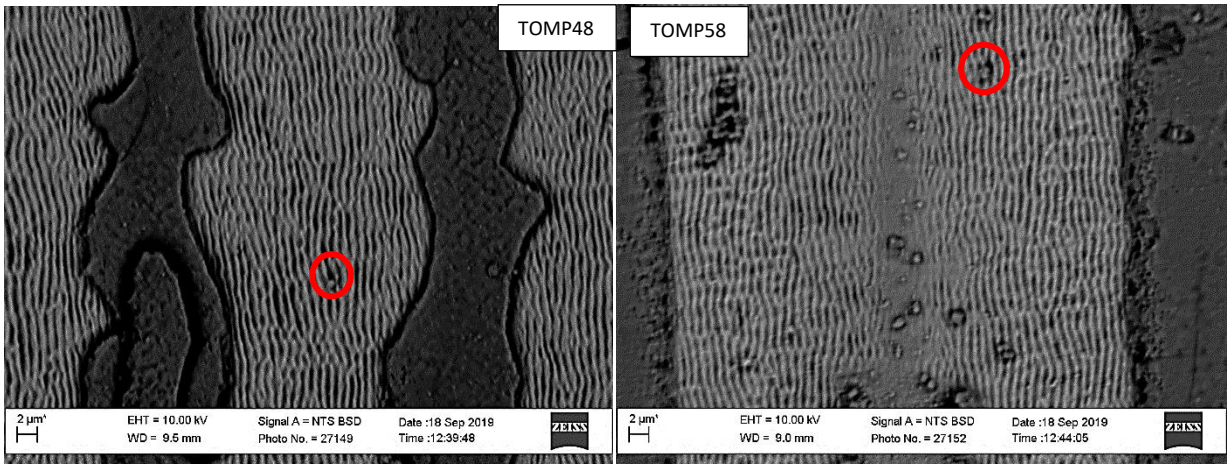

Figure 4.7.2.1d. Back-scattered micrographs displaying the attachment of *S. aureus* on the duplex treated sample types. The red circles indicate the areas where the bacteria have attached in the spacing between the ripples.

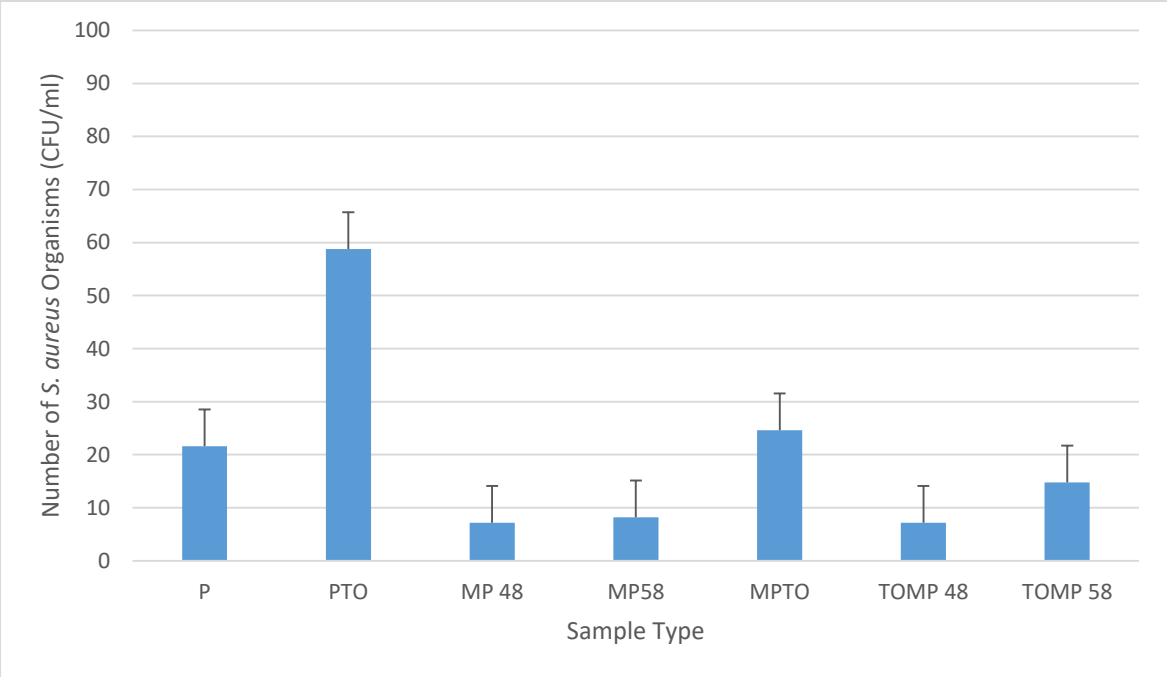

Figure 4.7.2.1e. Number of *S. aureus* bacterial organisms attached to the different sample types.

4.7.2.2 *E. coli*

As evidenced in Figure 4.7.2.2c, the highest *E. coli* value was seen for the P sample (+/- 250) and the lowest value was seen for the TOMP48 sample (+/- 63). TOMP58 had a higher *E. coli*

value (+/- 126) than MPTO (+/- 116) and MP48 (+/- 108). TOMP58 had higher oxide destruction and thus possessed regions where the LIPSS did not form fully. Similar to the results from *S. aureus*, these regions with improper patterning and no oxide may have caused higher bacterial adhesion as there was no anti-adhesion properties to these regions.

Nonetheless, *E. coli* being a Gram-negative bacterium is more difficult to destroy than *S. aureus* as it is more resilient hence, the results differ. The TOMP48 sample had the lowest value which suggested when the patterning is undertaken without damaging the oxide, the combined surface treatments caused less bacterial survival. The MP58 sample displayed an unexpected result of the second highest bacterial number.

When looking at the SEM images (Figure 4.7.2.2a) in it was seen that on the P sample, the *E. coli* organisms formed a thick, dense chain linking themselves together. This chain of bacteria suggested that the P sample provided an excellent environment for *E. coli* survival. This may have been the initial process of a biofilm formation. The PTO sample also provided a good environment for *E. coli* growth as it was visible the organisms formed a long chain (marked in red). The bacterial organisms on the MPTO sample grew and attached in clusters that were spaced out. The bacteria that attached on all the samples were rod-shaped which indicated healthy *E. coli* bacteria. When looking at the BSD images in Figure 4.7.2.2b, the MP58 sample had the most *E. coli* organisms present on the surface and TOMP48 had the fewest.

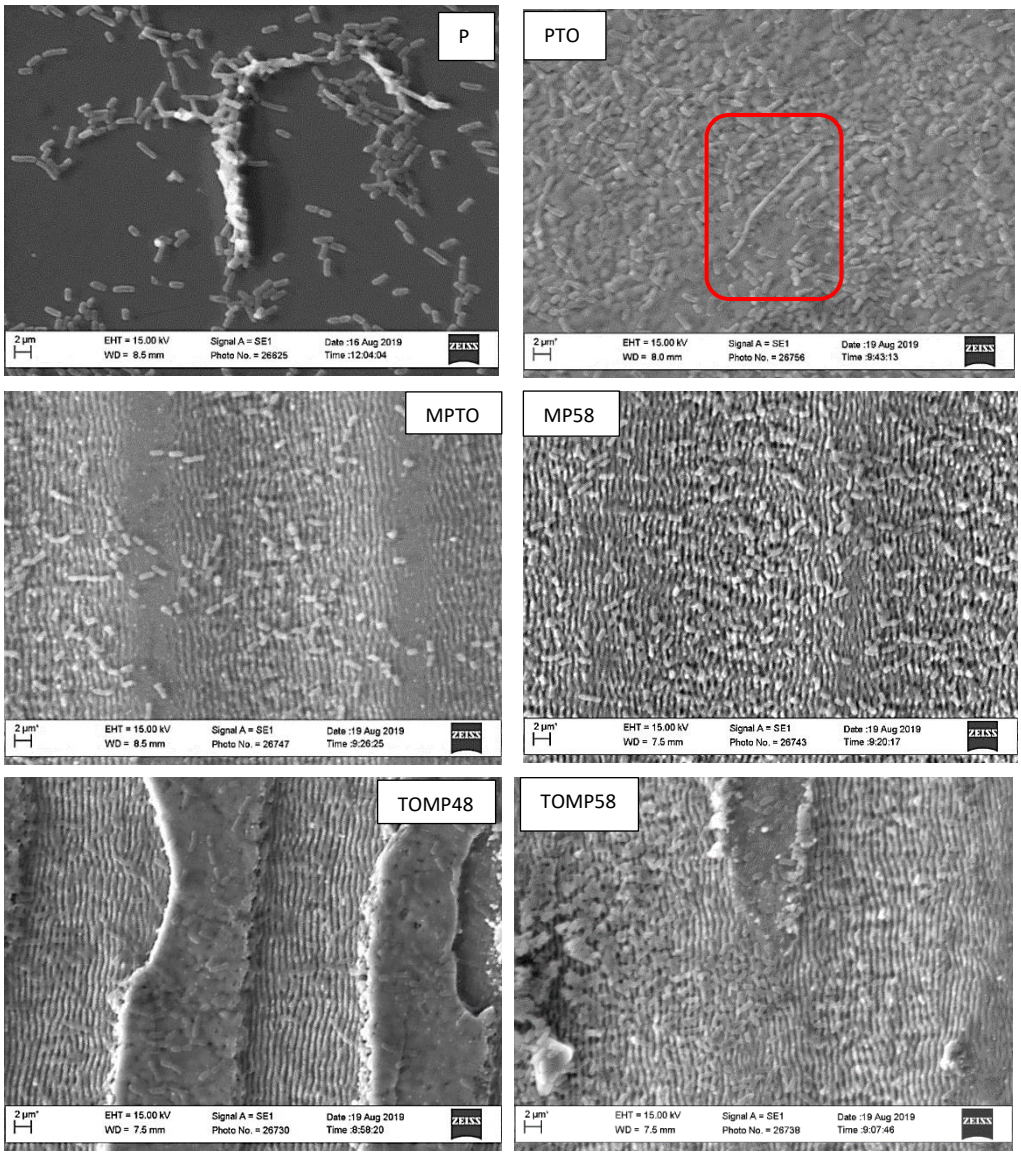

Figure 4.7.2.2a. SEM micrographs displaying the attachment of *E. coli* organisms on each sample type. The red mark on PTO displays the long chain of *E. coli* hat formed on the surface.

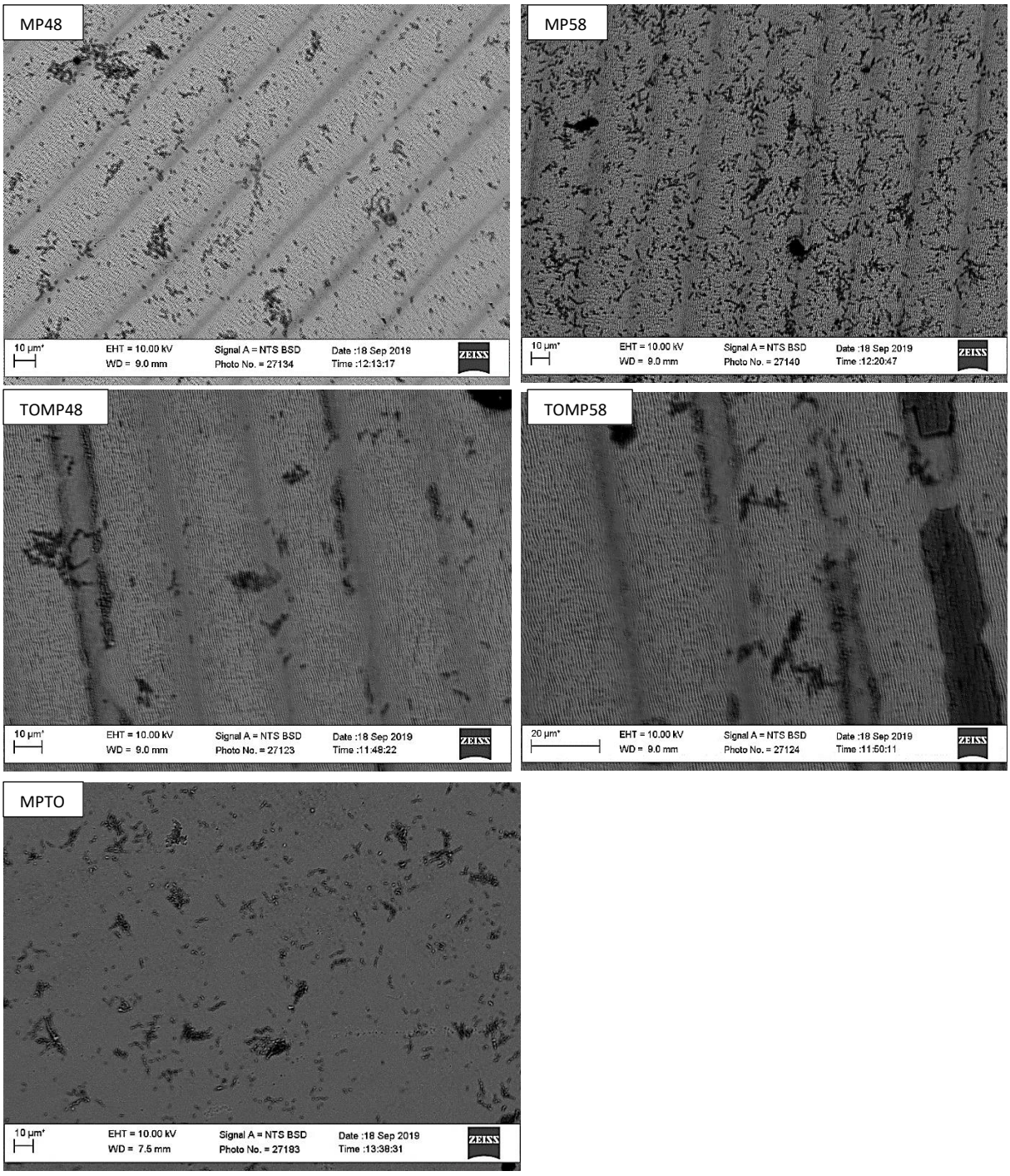

Figure 4.7.2.2b. Back-scattered micrographs displaying the attachment of *E. coli* organisms on the treated sample types.

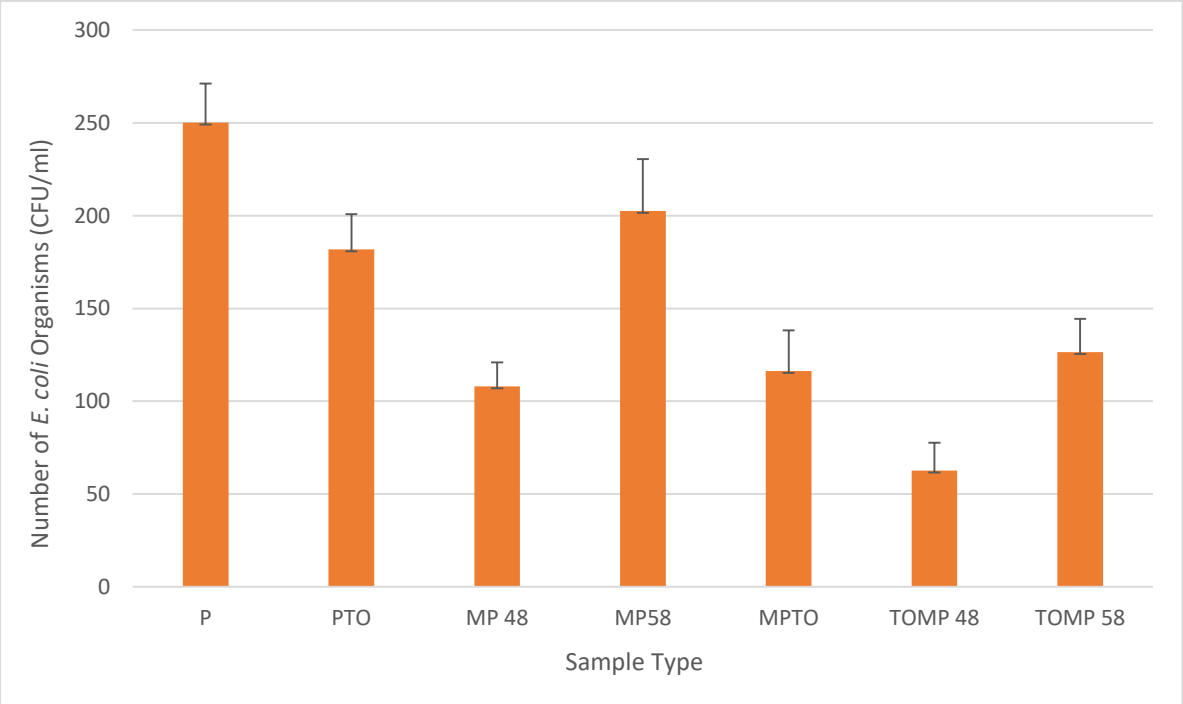

Figure 4.7.2.2c. Number of *E. coli* organisms attached to the different sample types.

4.8 **Cell viability**

The potential cytocompatibility of the samples was studied using SaOS-2 human osteoblast-like cells and the results are reported in this section. The SEM images (Figure 4.8a) helped visualise the attachment of the cells to the surface. In Figure 4.8a, the cells on the P sample had an elongated phenotype and with some of the cells, the cytoplasm and nucleus were clearly visible. The same was also seen on the PTO sample, however with this sample there was much larger cell growth and concentration. This indicated the TiO_2 helped stimulate the proliferation of the osteoblast like cells which was similar to the results seen with MPTO. The cells in both these sample types proliferated randomly and did not attach in a particular pattern or orientation.

On the other hand in the MP and TOMP samples, the osteoblast like cells proliferated parallel to the laser ripples and grew along the patterns. The number of cells

were fewer on these samples when compared with PTO which suggested that the LIPSS did not stimulate the cell proliferation as much as the oxide. Although in Figure 4.8d there was no significant difference in cell growth numbers between the MPTO and TOMP sample, the SEM micrographs displayed a slightly higher cell count on the TOMP surface than MPTO. On the MPTO sample, the cells grew randomly as with P and PTO which further suggested the oxide present on MPTO reduced the effect of the LIPSS and hence, the SaOS-2 cells behaved in a similar fashion to as they were on the PTO sample. The cells on TOMP also seemed larger in size when compared to MP and also some of the cells had visible cytoplasms and nuclei.

In Figures 4.8b and 4.8c at a higher magnification, the cellular features were visible. The cells on the P sample had a size ranging between +/- 20 µm and +/- 50 µm. The larger cells had a highly visible cytoplasm which suggested healthy cells. Some of the cells on the PTO sample were larger and were ranging between +/- 20 µm and +/- 80 µm. They were less circular in shape which suggested that these cells on PTO were not as healthy as they were on P as the circularity of a cell is a measure used to determine cell health (90).

The cells on TOMP and MPTO developed cell structures referred to as filopodia. The filopodia of the cells caused them to attach to one another and to the oxide columns on the sample surface. The filopodia also attached to some of the 1 µm ripples which helped anchor the cells onto the sample surface. This suggested the cells were able to withstand the surface textures and also supported each other to aid cell proliferation and growth. In Figure 4.8c, the cells on PTO also developed filopodia; however, the filopodia were thinner and smaller on this sample. Nonetheless, the cell filopodia on PTO attached to the rougher

oxide features on the sample surface as they did on TOMP. This suggested the TiO_2 layer helped to support the attachment of the cells. The LIPSS also did not cause a negative effect in the growth and attachment of the cells.

As summarised in Figure 4.8d, the PTO sample had the largest number of cells (+/- 158) and the control (haemocytometer) had the lowest (+/- 10). The control had the fewest cells due to the limited attachment properties of the haemocytometer when compared to the titanium samples. Hence, the presence of all the sample types caused an increase in cell number when compared to the control. When comparing P to MP it can be seen that the presence of the pattern actually caused a decrease in cell proliferation (+/- 71 and +/- 58 respectively) but nonetheless, the cell count was higher than the cell count for the control thus, indicating that the pattern initiated some cell proliferation.

A significant difference was not seen between the MPTO and TOMP (+/- 108 and +/- 106 respectively) samples which suggested that in terms of cell proliferation patterning before or patterning after thermally oxidising (i.e. CCT) a sample had little effect. Lower cell proliferation for the patterned samples may be due to increases in surface roughness as literature has suggested that higher surface roughness may cause lower proliferation rates (91). In addition, a higher proliferation for the thermally oxidised samples (when compared to P and MP) may be due to the thicker oxide layer present on MPTO which may aid the growth and proliferation of cells.

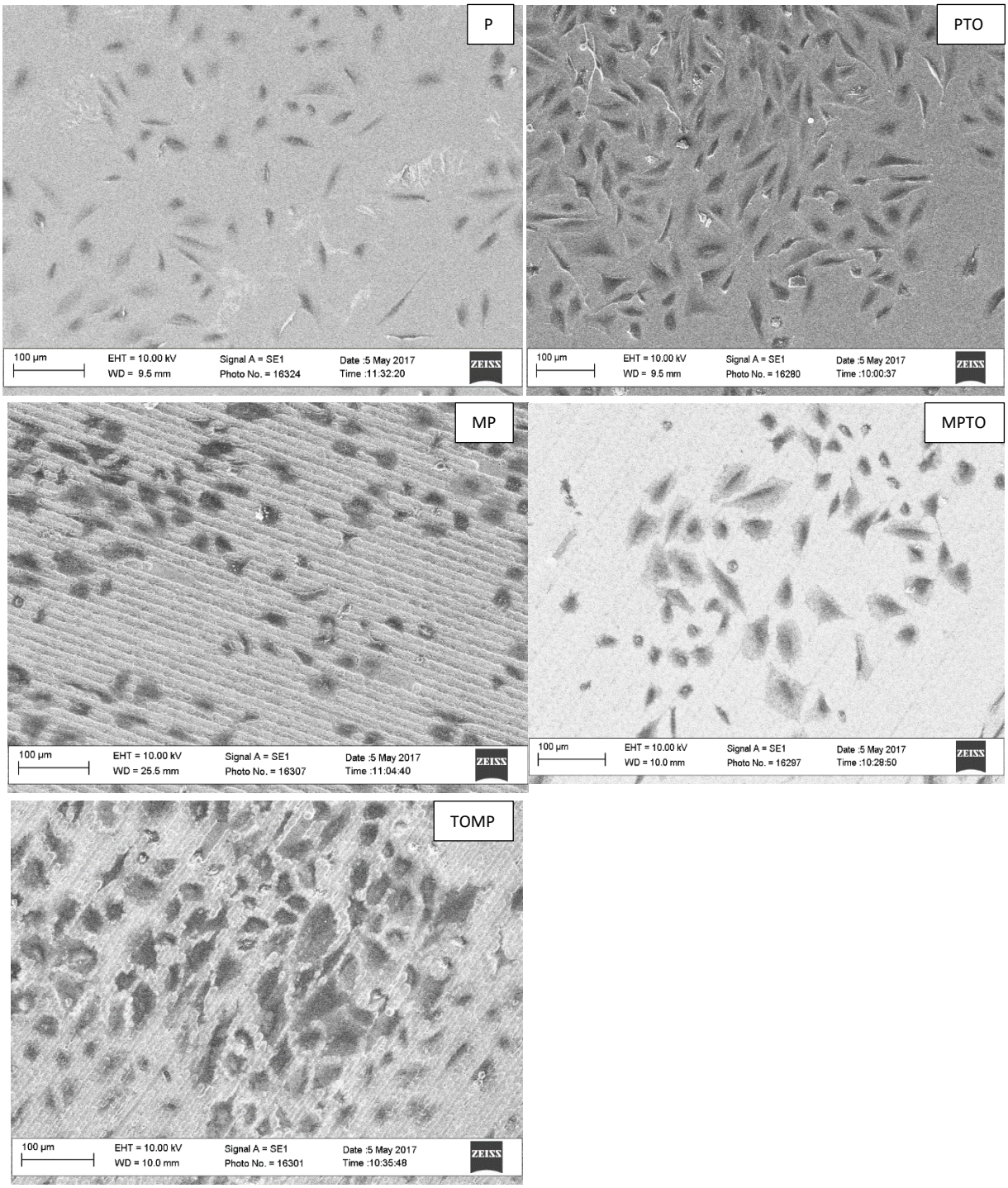

Figure 4.8a. SEM micrographs displaying the growth and morphology of the SaOS-2 cells on each sample type.

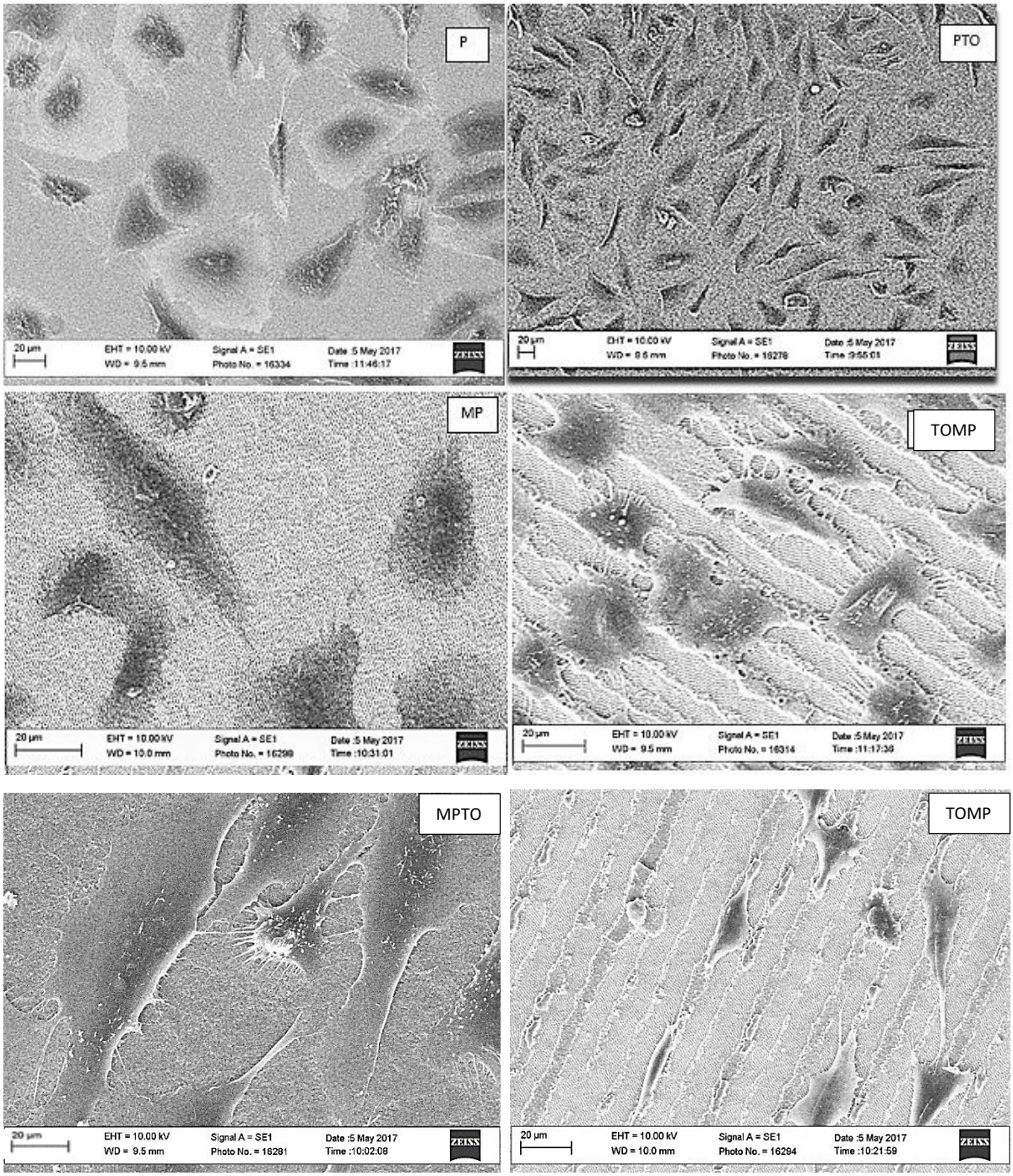

Figure 4.8b. SEM micrographs displaying the growth and morphology of the SaOS-2 cells on each sample type.

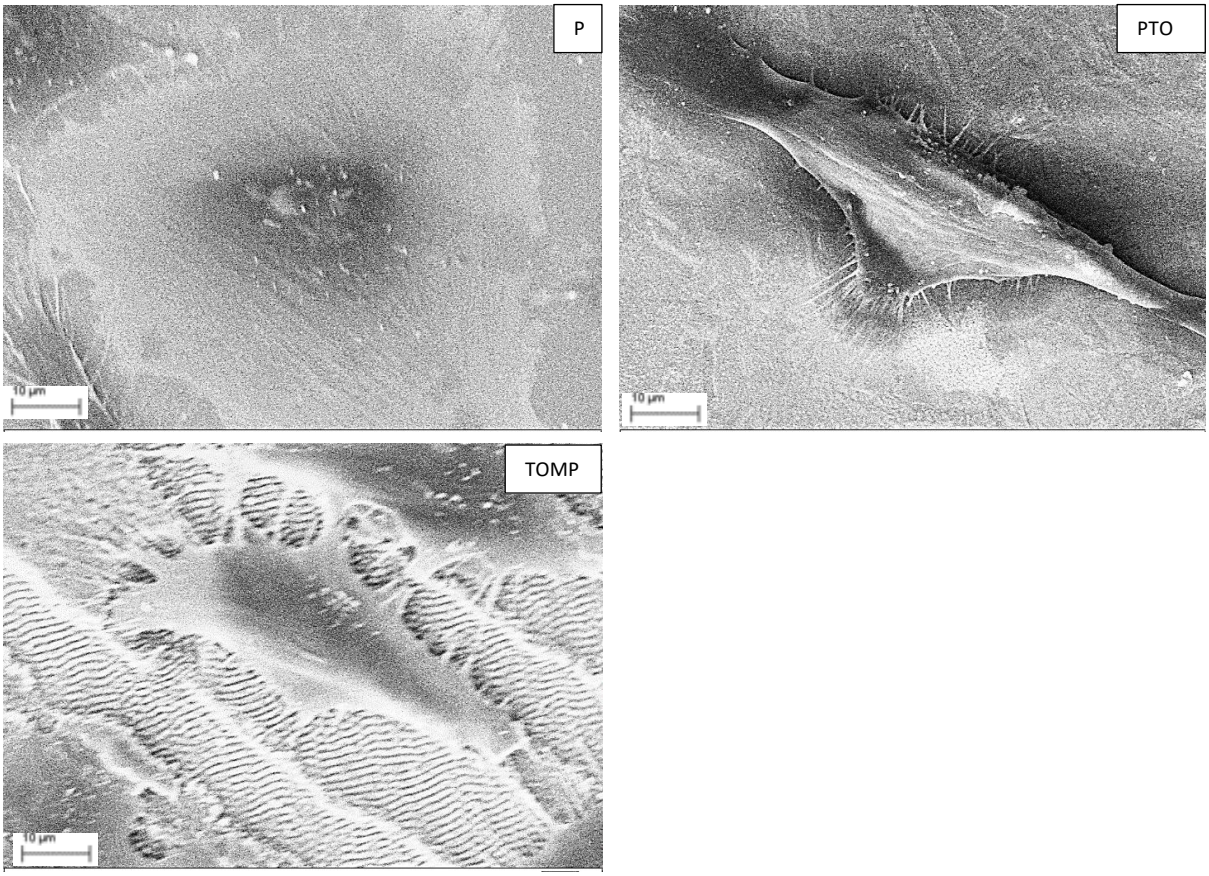

Figure 4.8c. SEM micrographs displaying the growth and morphology of the SaOS-2 cells on P, PTO and TOMP.

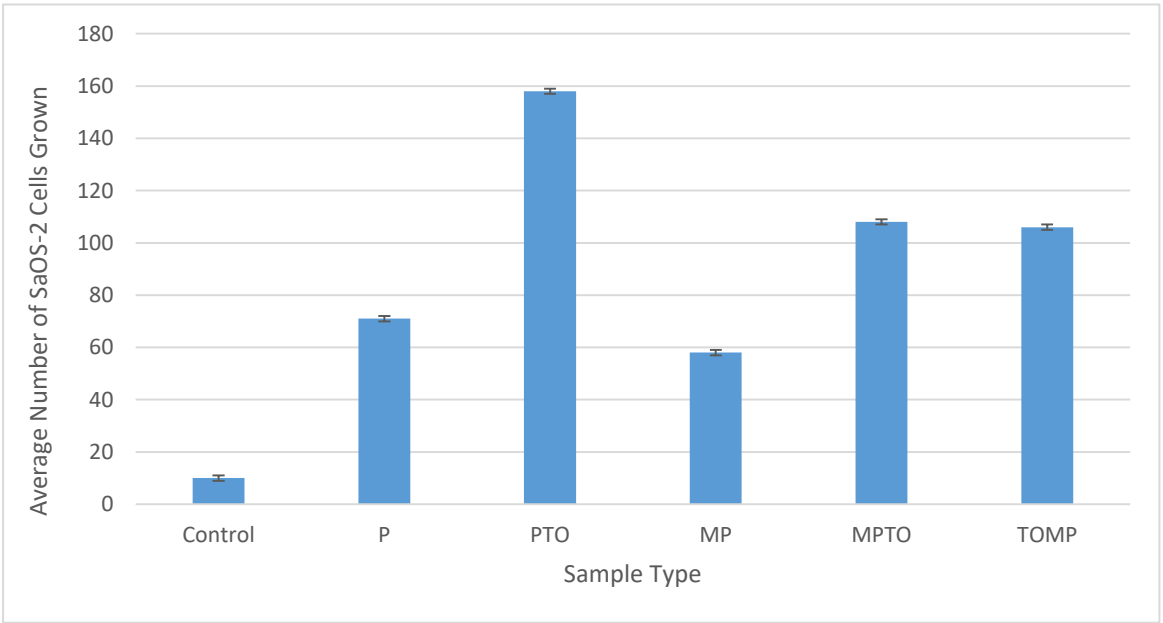

Figure 4.8d. Average number of SaOS-2 cells grown per sample type vs the control (haemocytometer).

4.9 **Tribological and Corrosion results**

4.9.1 Friction and Wear

The tribological behaviour of the samples were studied in air (dry) and in Ringer's solution (lubricated). When comparing the results between the patterned samples, the lowest value was seen for MPTO (+/- 0.087) which was the overall second lowest value. MP48 had a higher CoF (+/- 0.151) than MP58 (+/- 0.121). However, these values were lower than PTO. TOMP48 had a higher oxide concentration than TOMP58 but displayed a lower friction coefficient. When the LIPSS are undertaken before CCT as with MPTO, the friction coefficient decreased which indicated that LIPSS have the potential in reducing CoF. Nonetheless, the MP48 and MP58 samples had higher friction coefficients than the P sample. There was no significant difference between the values of TOMP58 and PTO.

The wear tests under lubrication produced results that displayed a different pattern to the dry tests. Under lubrication the friction coefficients of all the samples decreased and were under +/- 0.080. The MPTO sample displayed the highest friction coefficient (+/- 0.079) while all other samples showed very close CoF values if the experimental errors are considered.

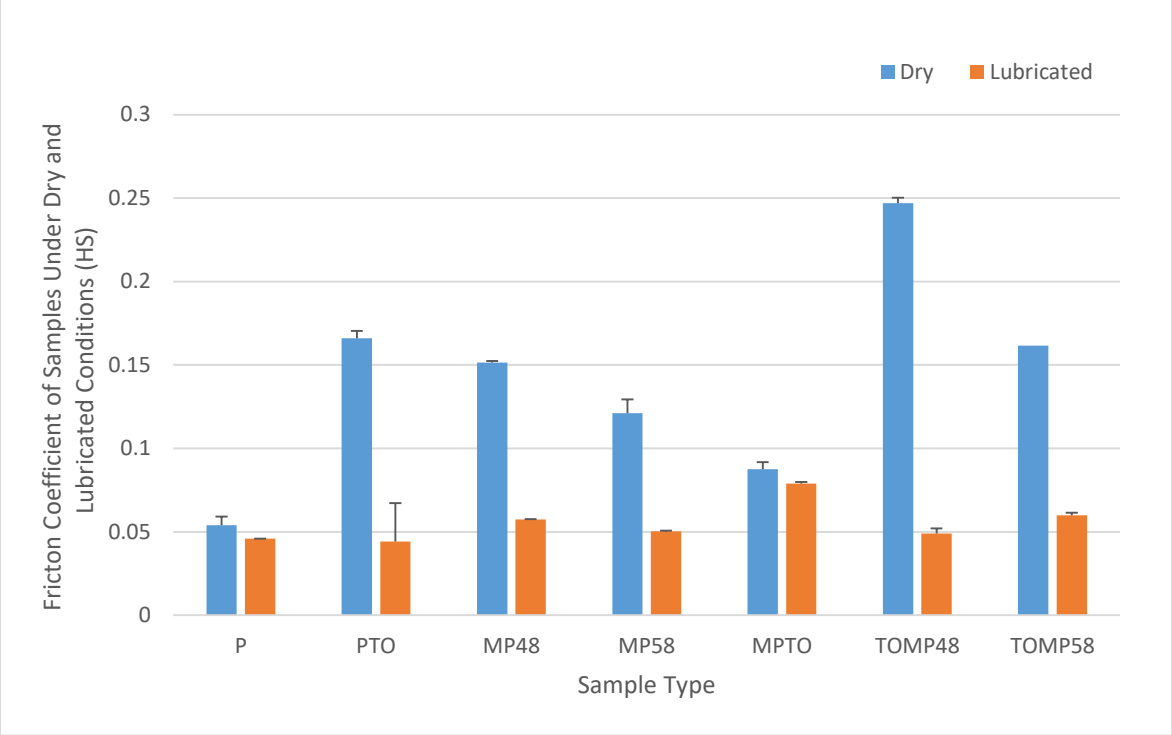

Figure 4.9.1a. Figure displaying the mean friction coefficients of all the samples types under dry and lubricating conditions using a load of 0.98N and a hardened steel counterpart.

The CoF results using a hardened steel (HS) counterpart were complicated and thus further tests using a WC counterpart were undertaken. A WC counterpart was used as the HS counterpart corroded with the Ringer's solution and hence, a harder counterpart was used to investigate the type of wear that occurred (for instance, whether it was adhesive or abrasive wear). For the dry tests using a WC counterpart (Figure 4.9.1b), the MP58 sample had the lowest friction coefficient at +/- 0.3 and the TOMP58 had the highest at 0.5. TOMP48 had the second lowest friction coefficient at +/- 0.4. On the other hand, for the lubricated tests the TOMP58 had the lowest coefficient of friction at +/- 0.17. The value under lubrication decreased nearly three-fold. Whereas. The MP58 sample had the highest friction coefficient under lubrication (+/- 0.4) and actually increased when compared to the dry wear results. This was unexpected as it was hoped the friction coefficient would decease

under lubrication. Nevertheless, the rest of the samples had lower coefficients of friction under lubricated conditions which was expected. The TOMP48 sample had the second lowest friction coefficient at +/- 0.22 under lubrication using Ringer's solution. This value was very good and suggested both the TOMP48 and TOMP58 samples possessed good wear resistances under lubrication and hence, would perform better in the body when compared to the solely LIPSS treated samples.

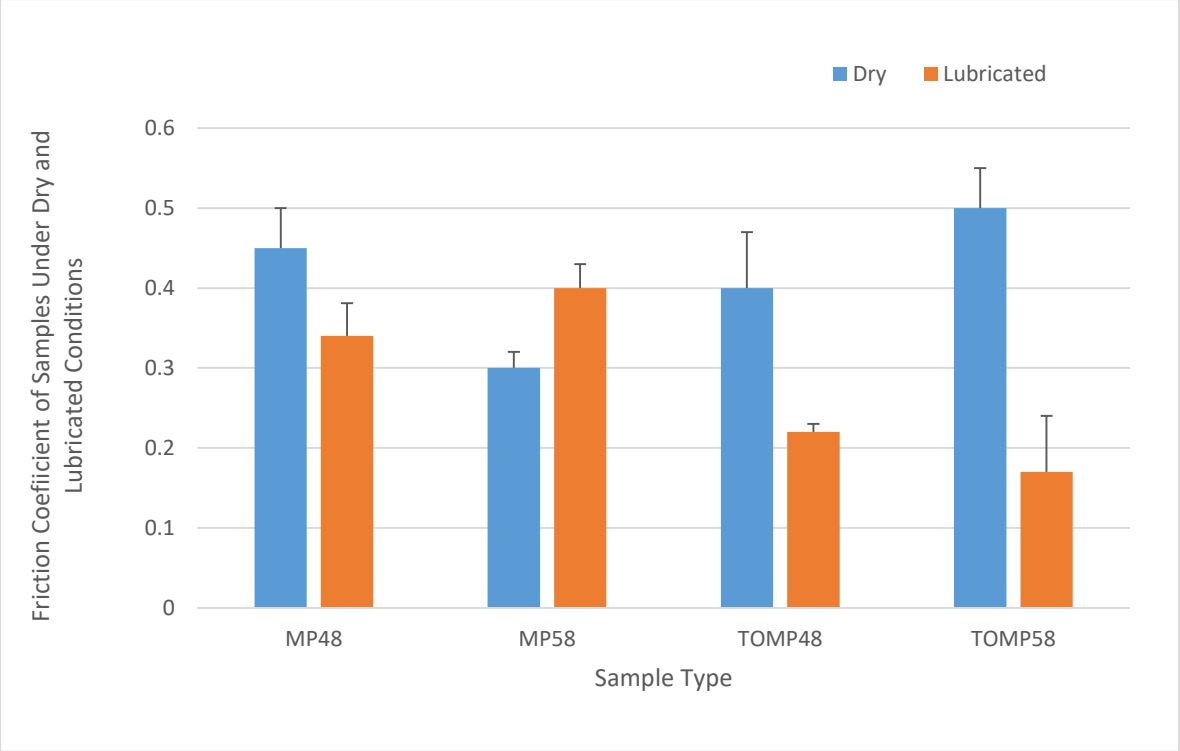

Figure 4.9.1b. Figure displaying the average friction coefficients of the treated samples types under dry and lubricating conditions using a load of 0.98N and a tungsten carbide counterpart.

4.9.1.1 SEM analysis of wear tracks

Hardened steel (HS) counterpart

Dry wear tests

After the wear tests, the wear tracks formed were carefully examined under SEM. As shown in Figure 4.9.1.1a the wear tracks are clearly visible for all the sample types with no surface oxide layers (P, MP48 and MP58) under dry conditions using a HS counterpart. These wear tracks displayed similar wear features with severe plastic deformation and parallel grooves. This indicated that severe adhesive wear and abrasive wear occurred to the cp-Ti surface whether it was polished (P) or laser micro-patterned (MP48 & MP58). The wear track formed on the polished P sample was slightly narrower (+/- 400 μm) than that formed on the micro-patterned MP48 & MP58 (+/- 450 μm); however, more severe adhesive wear occurred to the former than to the latter.

In contrast, the PTO sample had a much smoother wear track as compared with P, MP48 & MP58 samples which suggested the wear was less in PTO. Some debris was also visible and EDX analysis of the wear track revealed a high level of Fe (see Section 4.9.1.2). Most probably, such debris came from the steel counterpart. The wear track formed on MPTO sample was wider and rougher than that formed on the PTO but the original patterns were still visible. This implied that the wear of the MPTO sample was very mild but more than the PTO sample.

It is of great interest to note that the wear track on the TOMP48 was barely visible which suggested there was hardly any measurable wear caused by the hardened steel counterpart. There were no grooves present but the oxide columns were damaged slightly as they seemed flattened. As revealed in Section 4.3, the oxide columns were at a height on

TOMP48 and may have helped to protect the surface from the wear by the counterpart. A similar mechanism may have also led to the mild wear of TOMP58. However, it seemed that more wear occurred to TOMP58 than to TOMP48 because the former had less retained oxide than the latter (see Section 4.3).

Figure 4.9.1.1b provided more detailed information on the wear features. The wear track on P showed clear severe adhesive wear features with severe plastic deformation, adhesion craters and some deep and wide grooves were present on the wear track. The wear morphologies of MP48 and MP58 were almost the same as or similar to that for the P sample with similar severe adhesive wear.

The oxide columns were clearly visible from Figure 4.9.1.1b for TOMP48 with mild wear to the oxide columns as their edges became rounded; more wear was observed to the oxide columns on TOMP58 as most of them were partially or wholly removed. However, as evidenced in Figure 4.9.1.1c, the overall wear of the surface of these two samples was very low because the wear tracks on samples TOMP48 and TOMP58 had visible LIPSS ripples. This again indicated the oxide layer protected the LIPSS from wear damage.

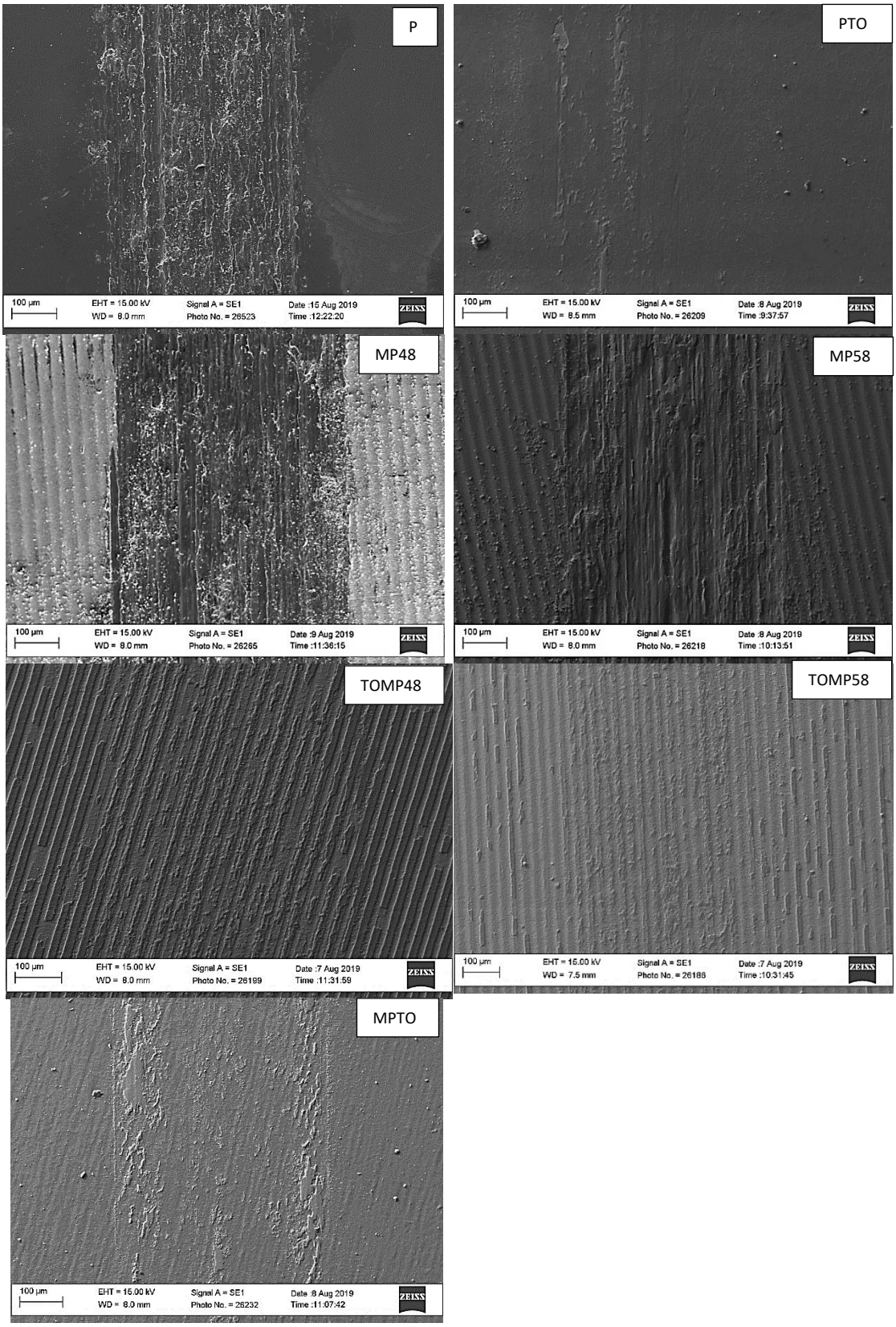

4.9.1.1a. SEM micrographs displaying the middle of the wear tracks formed during the dry wear tests using a hardened steel counterpart.

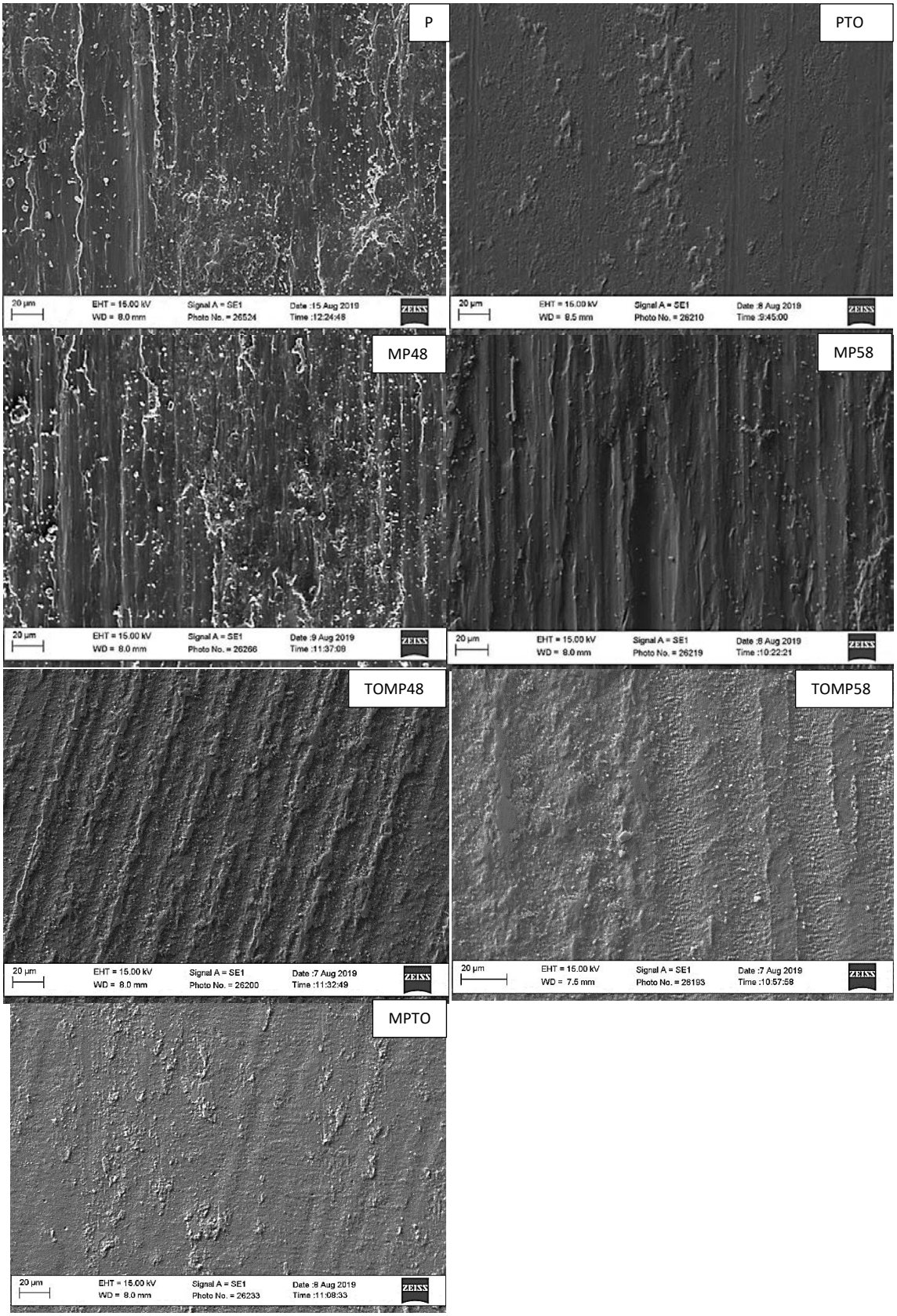

4.9.1.1b. SEM micrographs depicting the middle of the wear tracks formed during the dry wear tests using a hardened steel counterpart.

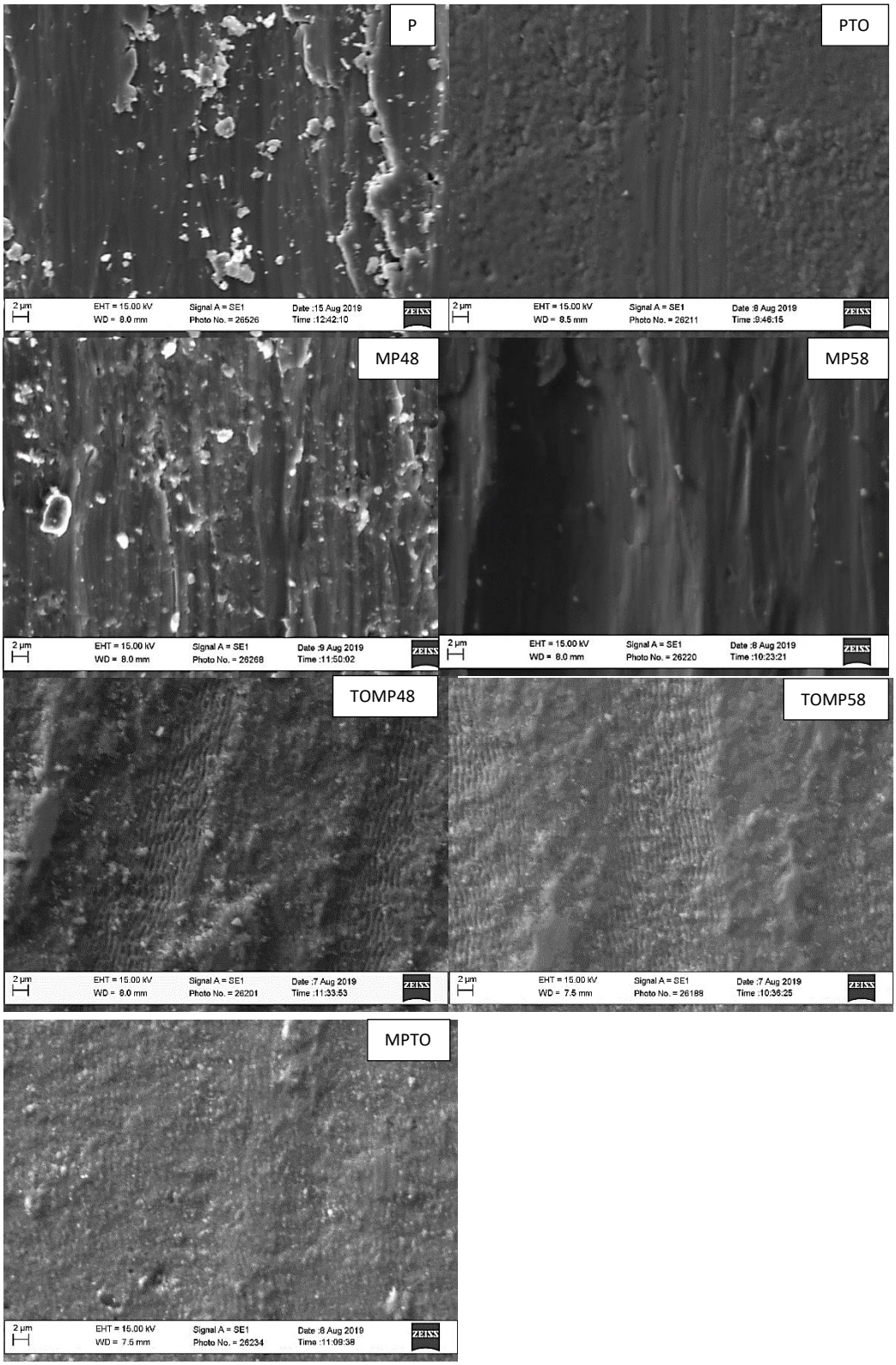

4.9.1.1c. SEM micrographs depicting the middle of the wear tracks formed during the dry wear tests using a hardened steel counterpart.

Lubricated Wear Tests

The SEM micrographs of the wear tracks formed under lubrication using a HS counterpart are shown in Figures 4.9.1.1d- f. It can be seen from Figure 4.9.1.1d that the wear tracks formed in Ringer's solution (lubrication) were smaller than formed in air (dry) showing the lubrication effect of Ringer's solution; however, the wear mode and the wear ranking of these samples under lubrication were similar to that for dry tested surfaces.

As shown in Figures 4.9.1.1d, the wear track of P was +/- 400 µm wide and displayed severe adhesive wear features. This indicates that Ringer's solution lubrication had very limited, if any, anti-wear effect. In contrast, the PTO wear track was much smaller in width (+/- 60-100 µm) and was covered with some flat wear debris-like particles, which suggested very mild wear. The wear track on MP58 was about +/- 300 µm wide and displayed very large and deep ploughing grooves which indicated adhesive wear. There were large +/- 10 µm particles which could be from the Ringer's solution deposit. MP48 had a wider wear track (+/- 500 µm) but the sliding wear grooves were less than on MP58.

TOMP48 possessed a wear track that was narrower (+/- 300 µm) and the oxide columns were visible. Hardly any wear damage occurred on this sample which suggested TOMP48 had higher wear resistances than the other samples. TOMP58 also displayed a wear track that was barely visible due to limited wear damage. This wear track however, was wider (+/- 450 µm) and had some oxide removed and wear debris which indicated more damage than TOMP48. MPTO sample also had a wear track that was difficult to view due to the limited damage. This wear track was +/- 400 µm wide and suffered some oxide removal and damage. Scratches were present on the MPTO wear track that were almost +/- 200 µm long and the wear debris was present.

Observation under higher magnifications provided further wear track details (Figures 4.9.1.1e & f). Especially, it can be seen that the PTO sample wear track was covered by a flat layer with crack networks and as the samples were imaged as they were after the test, this layer may be due to the Ringer's precipitates on the sample. As evidenced in Figure 4.9.1.1e, TOMP48 still possessed the oxide columns but some damages were observed along their edges. This indicated mild wear damage to the sample surface. The MPTO sample possessed the most wear debris particles but neither clear adhesive craters nor abrasive grooves could be observed.

Under a high magnification (Figure 4.9.1.1f), the wear track of TOMP58 had visible ripples which was similar to the results under dry conditions. Nonetheless, a large degree of +/- 2 μm wear debris particles were found on this sample. The TOMP48 wear track was covered in the crystallised Ringer's solution (samples were not cleaned after the wear test to achieve results that are more representative of medical implants). It is believed that the LIPSS should be protected by the oxide columns although it was difficult to see whether the LIPSS were present after the wear test due to the deposited particles.

Clearly, the LIPSS were not visible on the MP48 and MP58 which was similar to the results from the dry wear tests. They were however, visible on MPTO, TOMP48 and TOMP58 which indicated that when CCT and LIPSS were combined, the presence of the oxide protected the LIPSS from the sliding wear, which will be discussed further in Chapter 5.

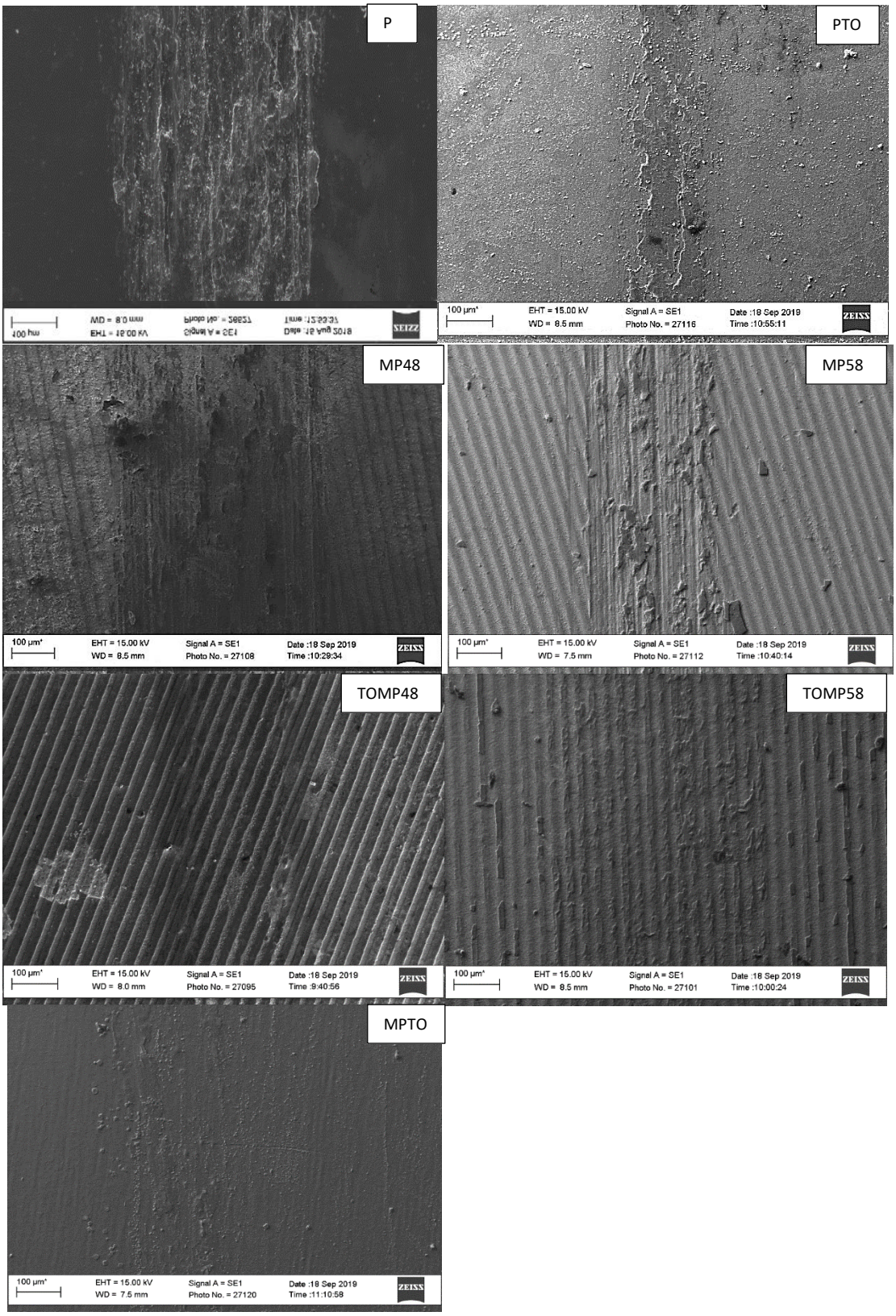

4.9.1.1d. SEM micrographs displaying the middle of the wear tracks formed during the lubricated wear tests (Ringer's solution) using a hardened steel counterpart.

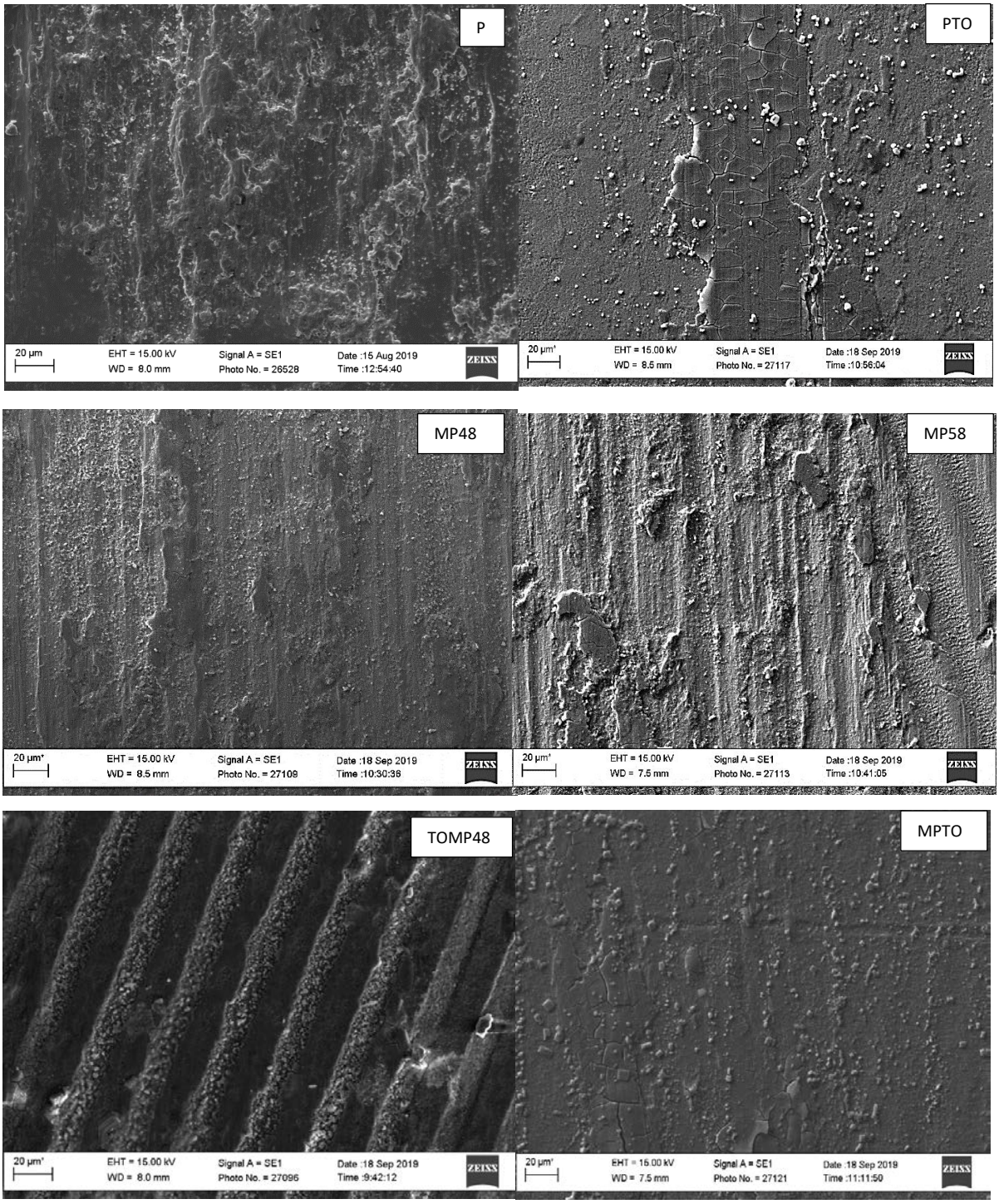

4.9.1.1e. SEM micrographs displaying the middle of the wear tracks formed during the lubricated wear tests (Ringer's solution) using a hardened steel counterpart.

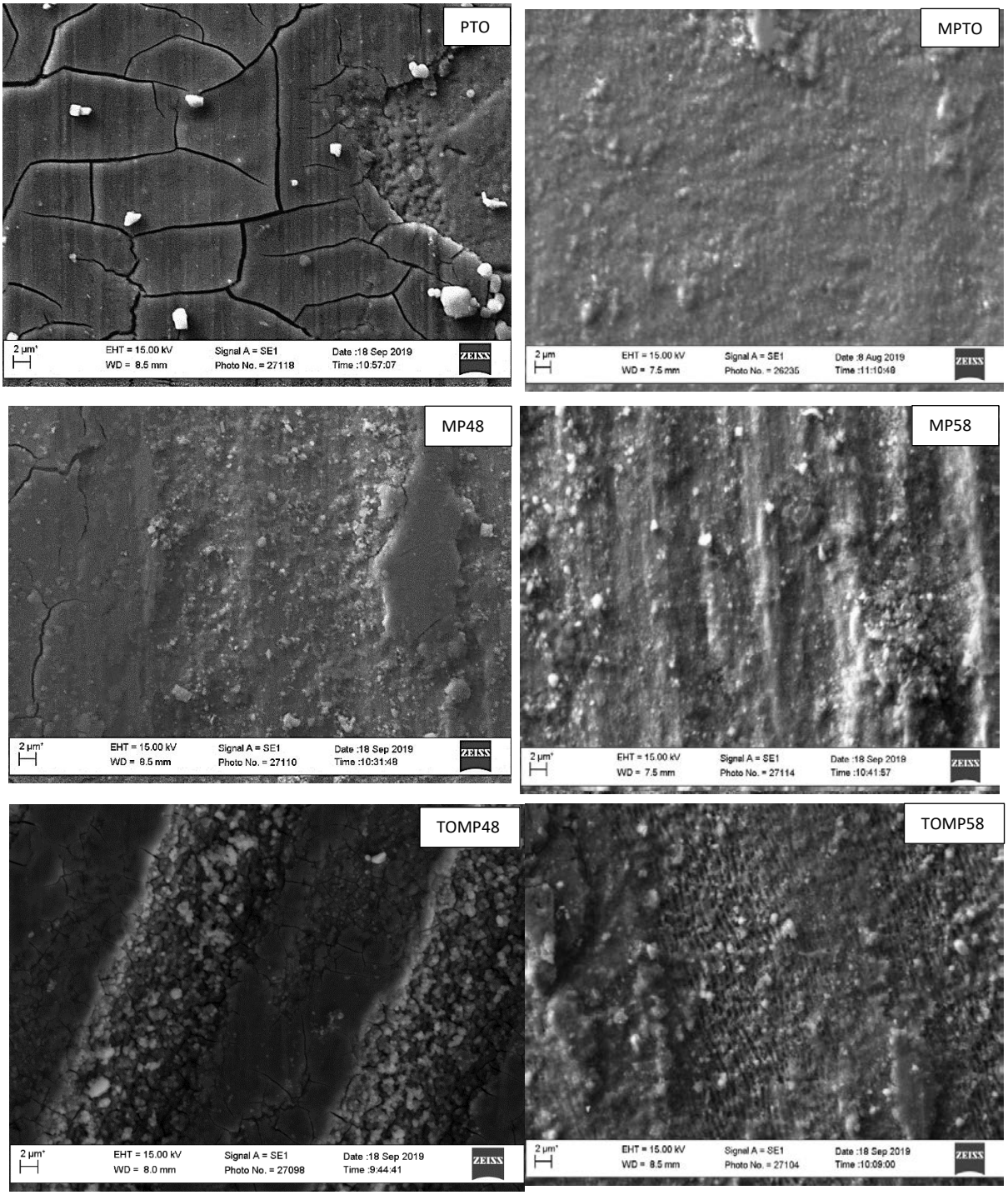

4.9.1.1f. SEM micrographs displaying the middle of the wear tracks formed during the lubricated wear tests (Ringer's solution) using a hardened steel counterpart.

Tungsten carbide (WC) counterpart

Dry wear tests

The wear tracks formed by WC counterpart were also examined under SEM and the results are given in Figures 4.9.1.1g-l. When looking at SEM images of the dry wear track using a tungsten carbide counterpart (Figure 4.9.1.1g), the MP48 and MP58 samples suffered the most damage during the sliding wear. The MP48 and MP58 samples both had wear tracks with widths of +/- 500 µm, no LIPSS columns were left and the wear tracks had features that suggested severe adhesive wear had taken place. For instance, ploughing grooves were present on the wear track surface, and there were also some regions that appeared darker, which indicated material removal and build-up.

The duplex treated samples had much smaller wear tracks. The wear track on TOMP48 was not clear and it was difficult to identify the edges. This suggested hardly any wear damage occurred on this sample type. The wear track on TOMP58 was not too dissimilar to the wear track on TOMP48. Likewise, the wear track was faint but it was more evident when compared to TOMP48 which indicated more wear damage had occurred on this sample. The oxide columns seemed flatter which indicated some surface damage.

Under higher magnifications (Figures 4.9.1.1h-i), the MP48 sample had many debris particles ranging in size up to +/- 10 µm. The particles were ragged and the wear track possessed regions where material had built up. This again was indicative of adhesive wear. There was less debris present on the MP58 sample but there were also some regions where material had been removed. For the TOMP48 sample, the wear debris collected in the spaces between the oxide columns. The oxide columns were also flattened and slightly

damaged. However, there was no presence of grooves or material transfer on both of the duplex treated samples which indicated less wear damage had occurred.

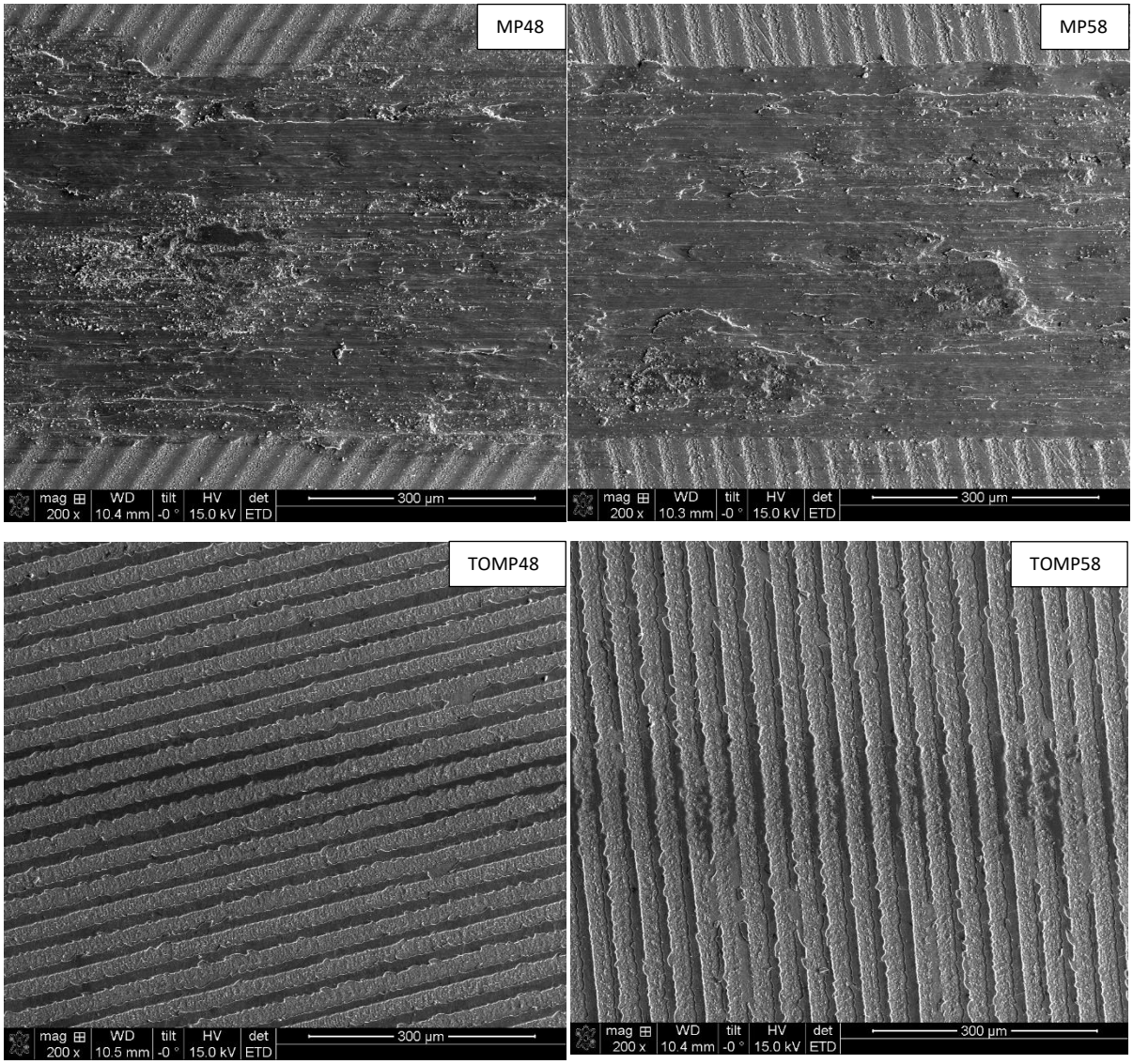

4.9.1.1g. SEM micrographs displaying the middle of the wear tracks formed during the dry wear tests using a tungsten carbide counterpart.

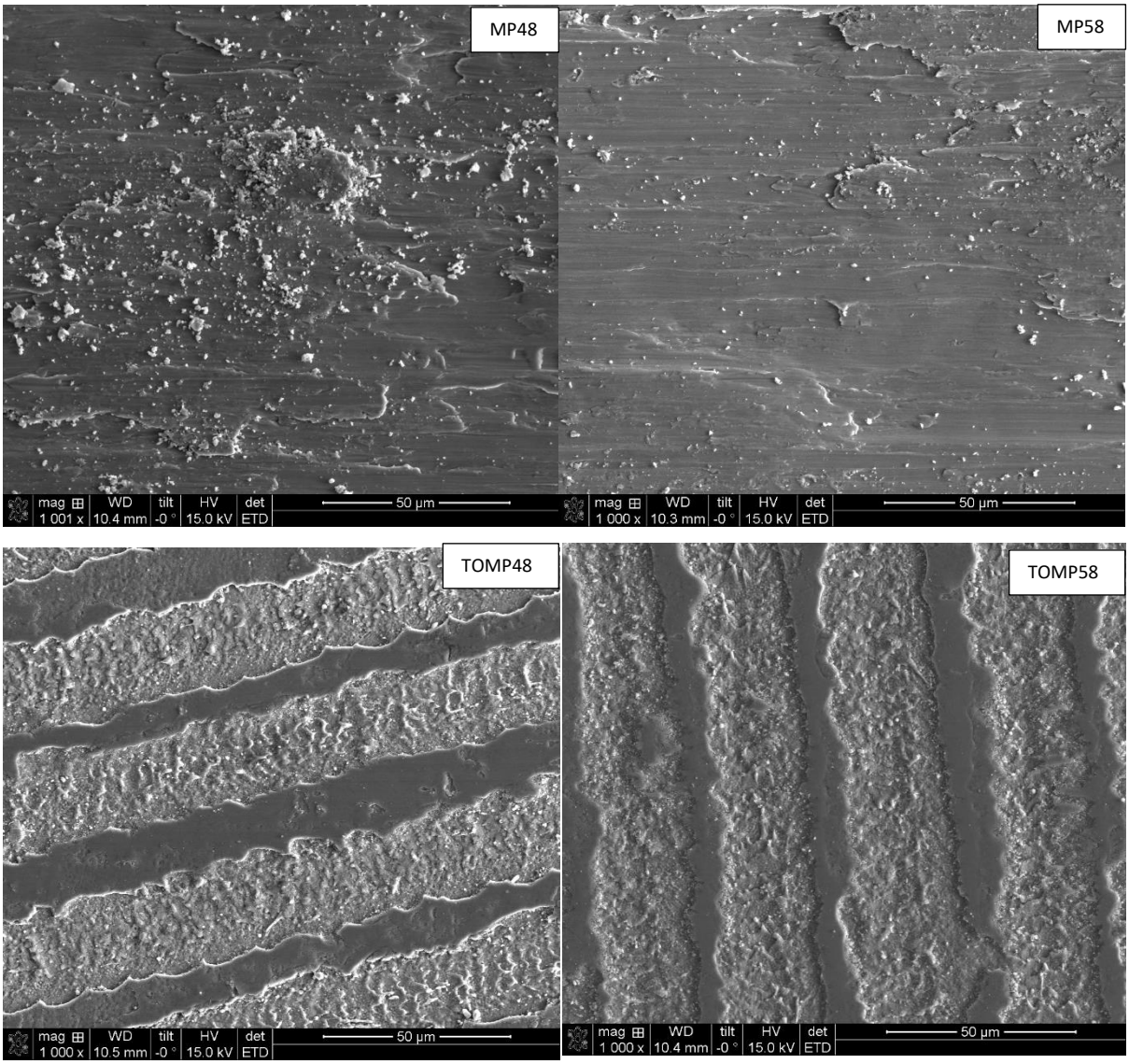

4.9.1.1h. SEM micrographs displaying the middle of the wear tracks formed during the dry wear tests using a tungsten carbide counterpart.

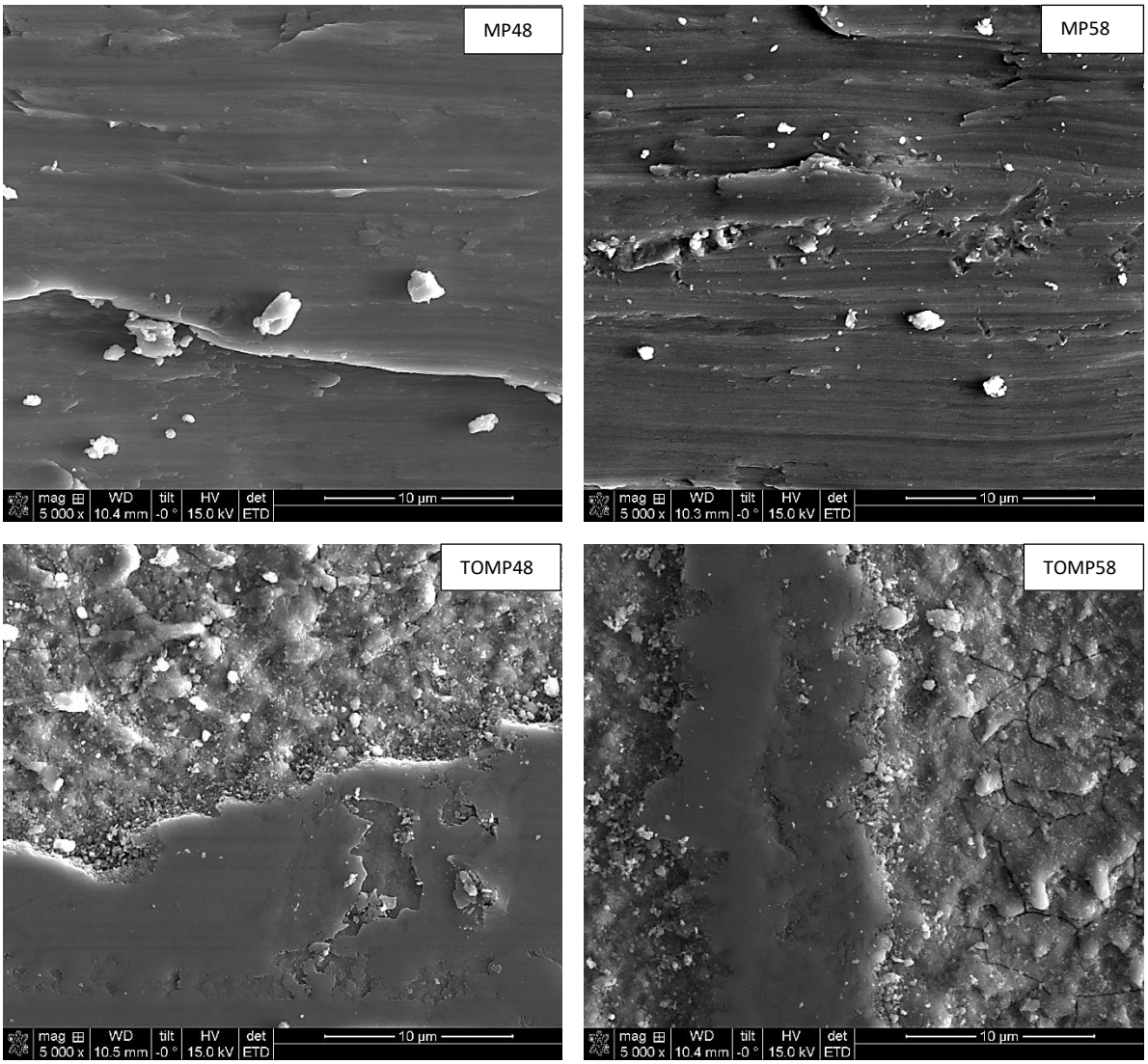

4.9.1.1i. SEM micrographs displaying the middle of the wear tracks formed during the dry wear tests using a tungsten carbide counterpart.

Lubricated Wear Tests

For the lubricated wear tracks, (Figure 4.9.1.1j), the MP48 sample had a wear track that was +/- 150 µm wide and there were some grooves present on the wear track which suggested wear damage had taken place. The MP58 sample had a much larger wear track (+/- 300 µm) and also regions on the wear track that displayed deformation and material removal. Hence, adhesive wear had taken place. There were also cracks within the wear track on the MP58 sample. It is also noted that these cracks extended from the wear track to the adjacent areas. The duplex treated samples had very small wear tracks (+/- 50 µm) in comparison and thus, the TOMP48 and TOMP58 samples had higher wear resistances. This was also evident in the friction coefficient chart seen in Figure 4.9.1b.

In Figure 4.9.1.1k (high magnification), there were many wear debris particles present in the MP48 and MP58 samples. Material transfer had also taken place which was displayed in the darker regions on the wear tracks. For the TOMP48 and TOMP58 samples, the 1 µm LIPSS ripples were visible after sliding wear had taken place. The ripples were slightly flattened and damaged but, they were still clearly visible. The oxide columns suffered greater wear damage than the LIPSS ripples. The oxide columns may have protected the ripples as the counterpart came into contact with the oxide rather than the ripples and thus, the oxide was damaged at a larger extent than the LIPSS. This is supported by the observation under even higher magnification as shown in Figure 4.9.1.1l. The ripples were more visible due to the higher magnification, and the oxide column suffered damage at the edges which led to the formation of wear debris. There was also a crack present on the oxide column which again supported the theory of the oxide suffering greater wear damage due to the small contact area. This inadvertently, protected the LIPSS ripples from

suffering wear damage. These results were good as they displayed by combining CCT with LIPSS, the hard oxide layer could potentially protect and increase the durability of LIPSS.

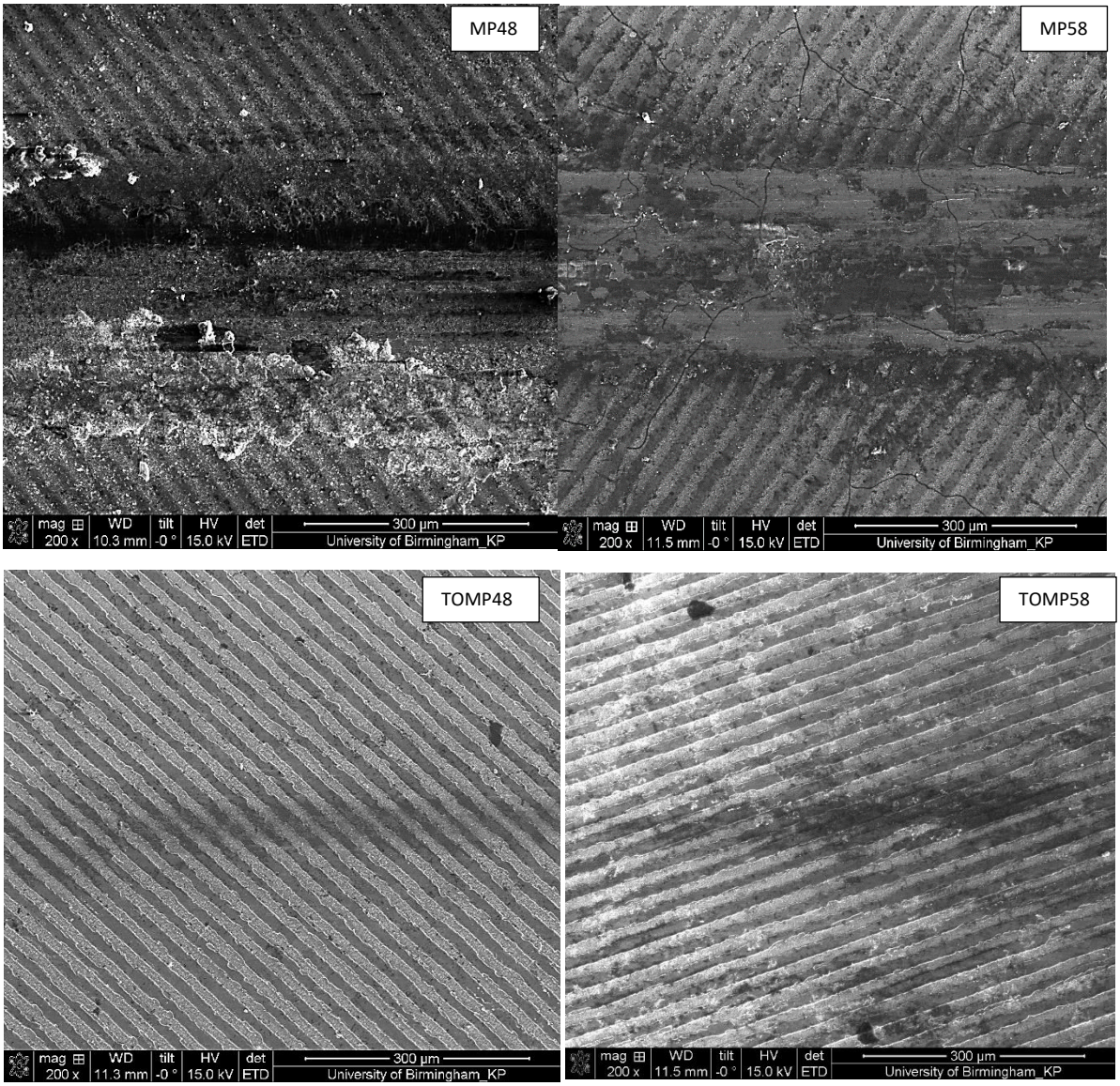

4.9.1.1j. SEM micrographs displaying the middle of the wear tracks formed in Ringer's solution) using a tungsten carbide counterpart.

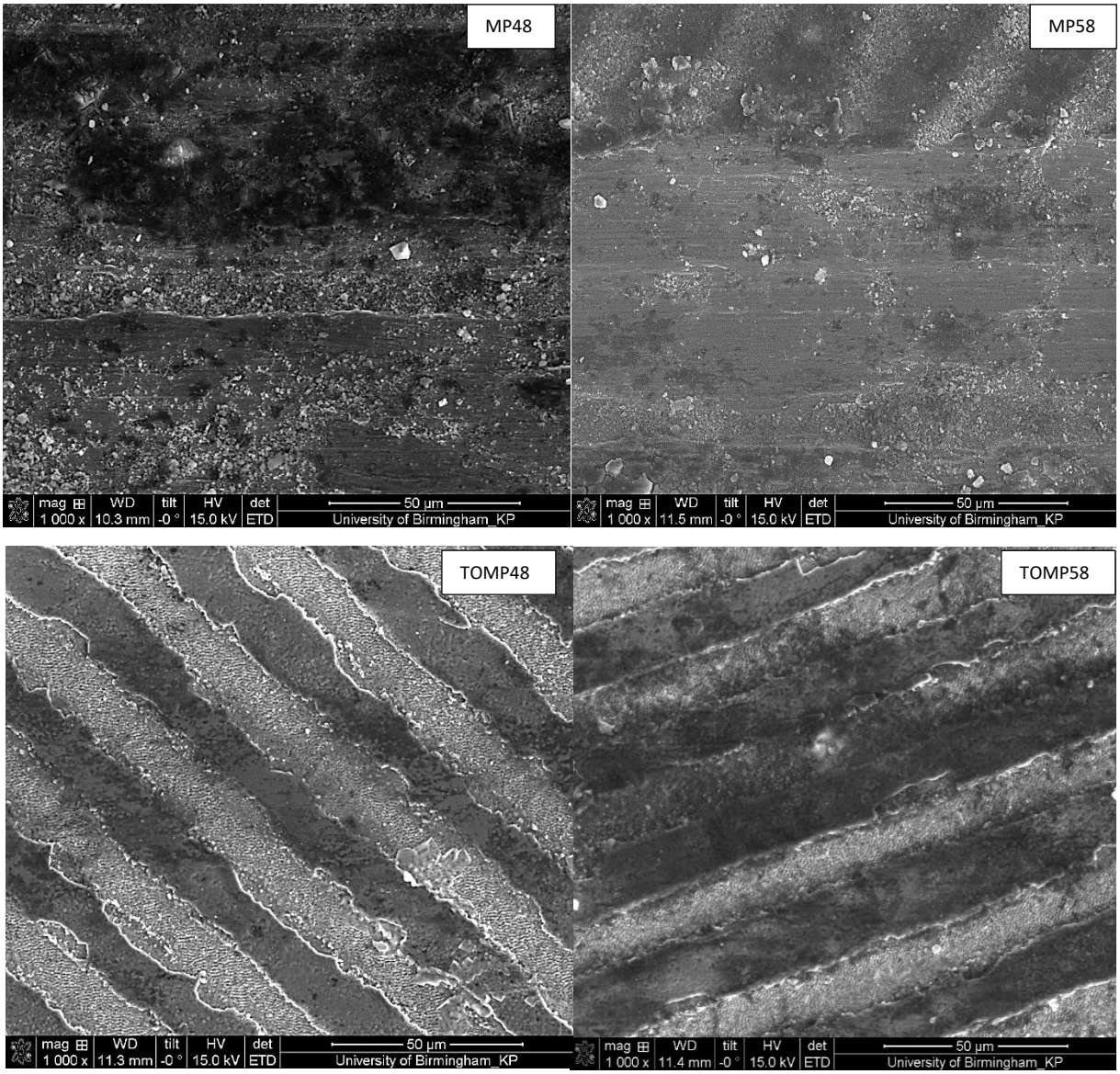

4.9.1.1k. SEM micrographs displaying the middle of the wear tracks formed in Ringer's solution) using a tungsten carbide counterpart.

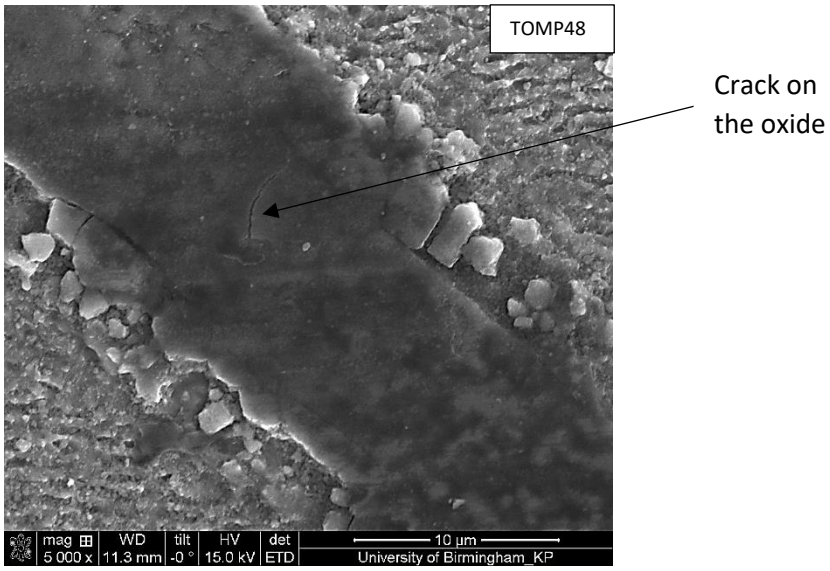

4.9.1.1l. SEM micrographs displaying the middle of the wear track of the TOMP48 sample formed in Ringer's solution using a tungsten carbide counterpart.

4.9.1.2 EDX Analyses of wear tracks formed by HS counterpart

As reported above, granular wear debris and/or wear debris-like layers were observed in the wear tracks after wear tests. Hence, in order to provide insight information on the source of such debris, EDX analysis was carried out and the results are summarised in Figure 4.9.1.2a and Figure 4.9.1.2b for dry and lubricated wear respectively.

When looking at the EDX analyses for the dry wear tracks in Figure 4.9.1.2a, although all of the sample types except MP58 had Fe present, significant amount of Fe was identified from all the samples with surface oxide layers formed by CCT (i.e. PTO, TOMP48 and TOMP58) due to material removal and transfer from the hardened steel counterparts. This indicated that, the steel counterpart underwent abrasive wear by the hard and thick surface oxide layers.

The EDX analyses results for the lubricated wear tracks are depicted in Figure 4.9.1.2b. In addition to Fe, many other elements were detected for these samples due to the presence of Ringer's solution deposits as evidenced by the presence of Ca, P and Na.

This supports the discussion on the presence of the flat wear debris-like layers formed on some samples after lubricated wear tests.

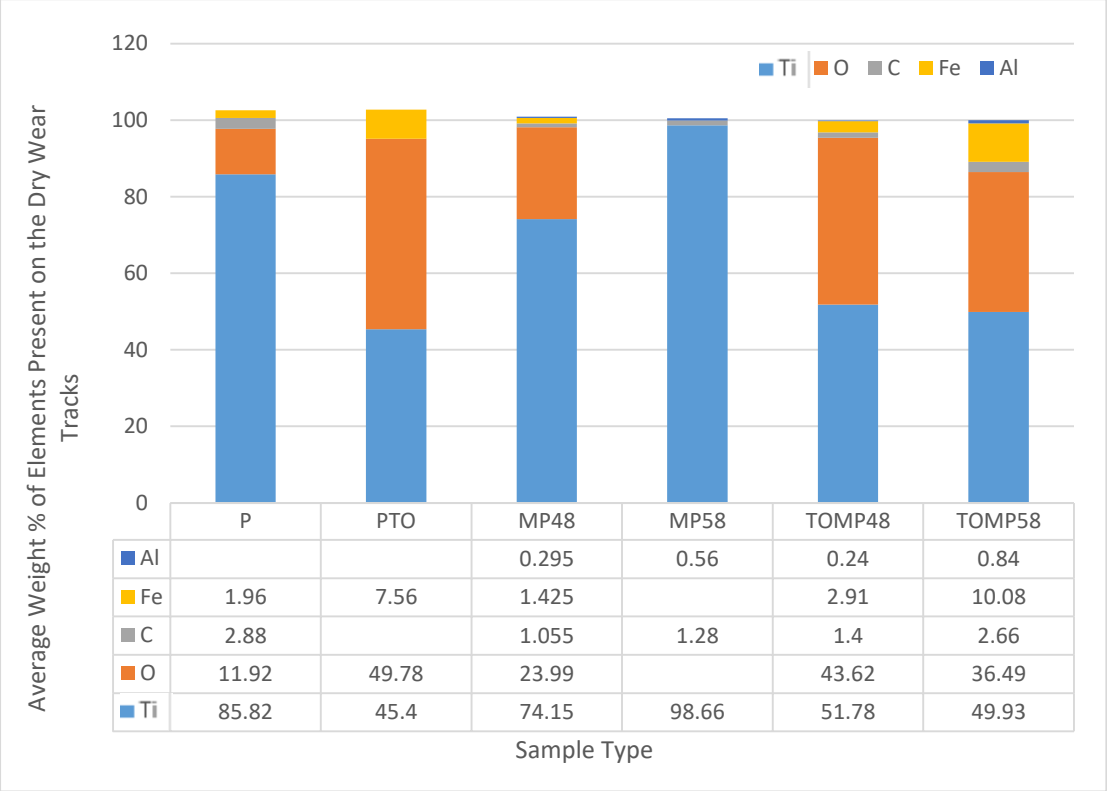

	P	PTO	MP48	MP58	TOMP48	TOMP58
Al			0.295	0.56	0.24	0.84
Fe	1.96	7.56	1.425		2.91	10.08
C	2.88		1.055	1.28	1.4	2.66
O	11.92	49.78	23.99		43.62	36.49
Ti	85.82	45.4	74.15	98.66	51.78	49.93

Figure 4.9.1.2a. Figure displaying the average weight percent of elements present on the middle of the dry wear tracks using a HS counterpart for all sample types.

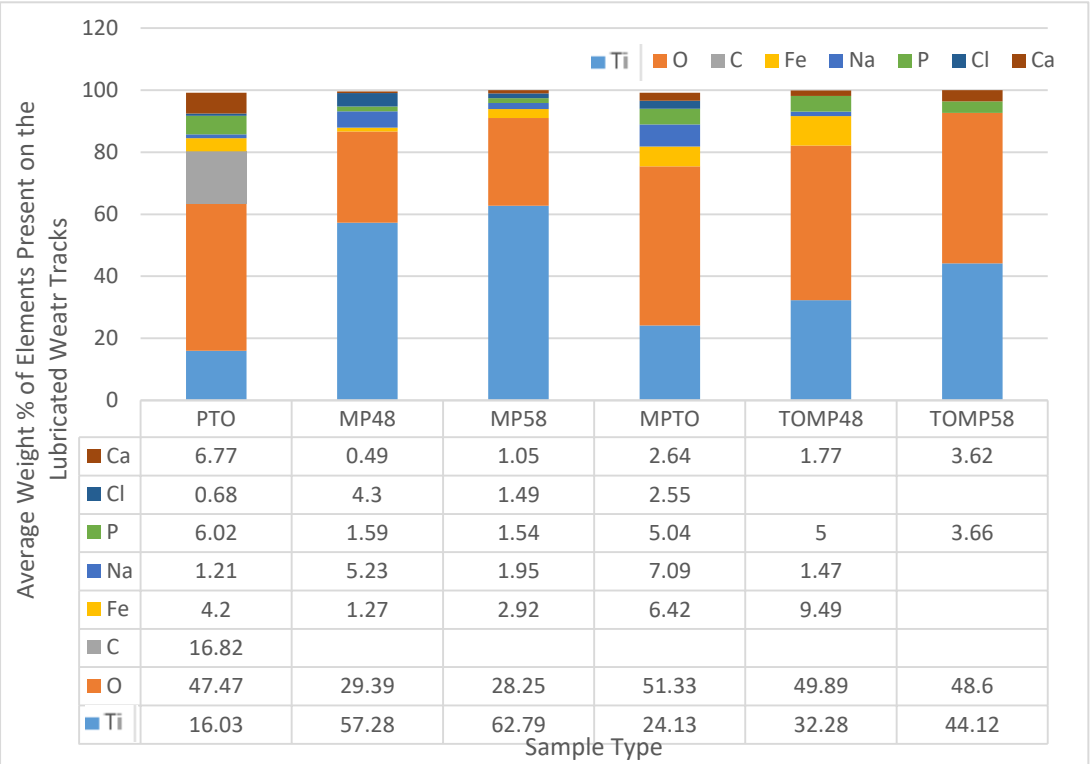

	PTO	MP48	MP58	MPTO	TOMP48	TOMP58
Ca	6.77	0.49	1.05	2.64	1.77	3.62
Cl	0.68	4.3	1.49	2.55		
P	6.02	1.59	1.54	5.04	5	3.66
Na	1.21	5.23	1.95	7.09	1.47	
Fe	4.2	1.27	2.92	6.42	9.49	
C	16.82					
O	47.47	29.39	28.25	51.33	49.89	48.6
Ti	16.03	57.28	62.79	24.13	32.28	44.12

Figure 4.9.1.2b. Figure displaying the average weight percent of elements present on the middle of the lubricated wear tracks using a HS counterpart for all sample types.

4.9.2 Corrosion behaviour

4.9.2.1 Potentiodynamic polarisation curves

The corrosion behaviour of all the sample types were investigated by potentiodynamic polarisation in Ringer's solution. Due to limited access to the labs, the results could not be repeated. The representative polarisation curves are shown in Figure 4.9.2.1. The corrosion charts for each sample type are displayed in separate charts because when combined, the results overlapped and were difficult to analyse. It can be seen that the corrosion potential of the as-polished P sample was about +/- -350 mV vs SCE and the current density was about +/- 10 $\mu A/cm^2$. The current density is defined as the amount of charge per unit time that flows through a unit area of a chosen cross section (92). Metastable pitting may have occurred as evidenced by the small fluctuations on the polarisation curves.

After CCT, the PTO sample showed an increased corrosion potential of about +/- -250 mV vs SCE but the current density increased gradually from +/- 10 to 100 $\mu A/cm^2$. This means that the CCT may have delayed the corrosion of P but could have possibly increased the current density. Micro-patterned MP48 and MP58 showed further increased corrosion potential to +/- 10 and +/- -100 mV vs SCE respectively and slightly reduced corrosion current density about +/- 7-8 $\mu A/cm^2$. However, it is noted that the corrosion current density of MP58 increased rapidly towards the end of the test above 1V vs SCE. The corrosion potential of the micro-patterning of CCT treated samples (i.e. TOMP48 and TOMP58) increased (to +/- -200 mV vs SCE for TOMP48) or decreased (to +/- -350 mV vs SCE for TOMP58) when compared to the corrosion potential of PTO (+/- -250 mV vs SCE). However, the corrosion current density was reduced.

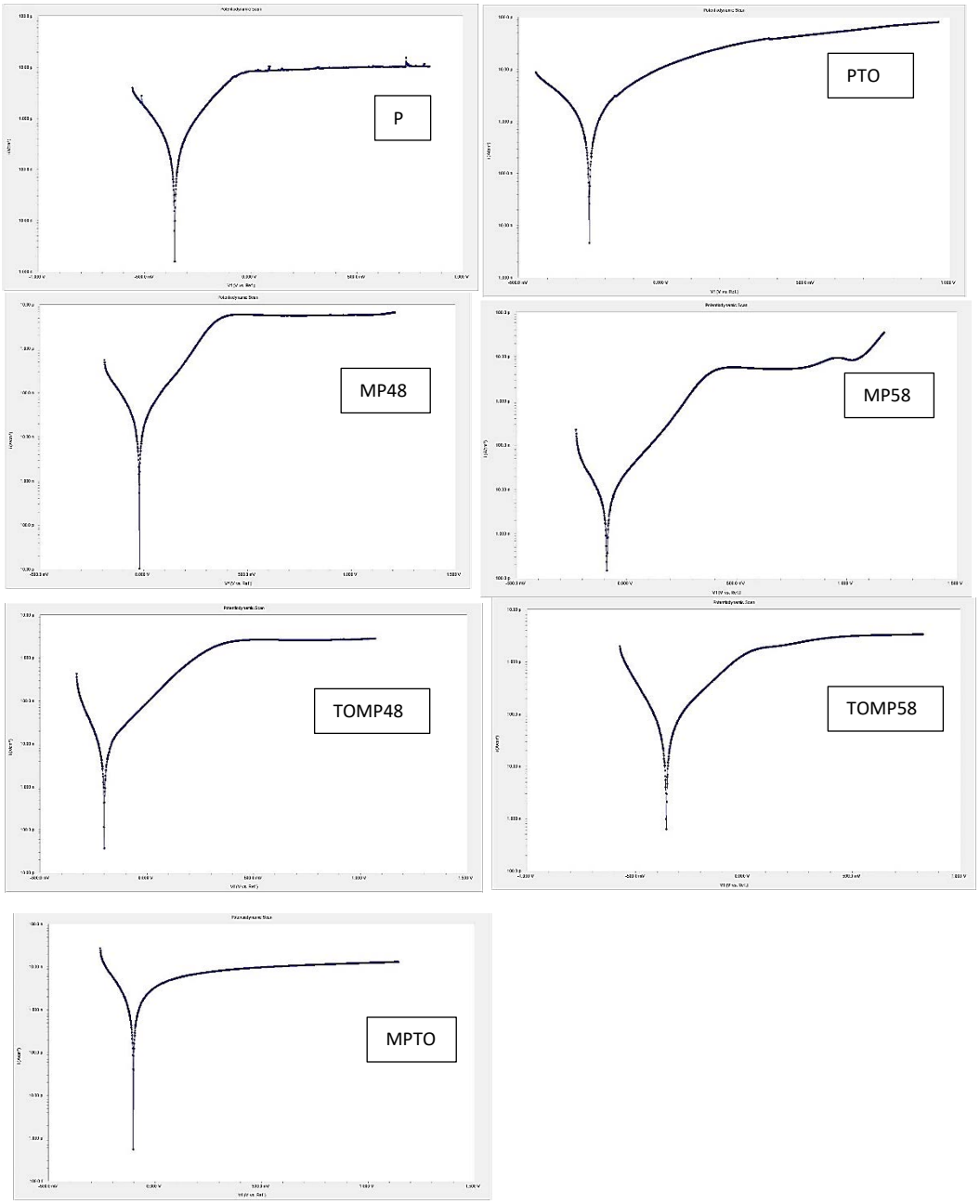

Figure 4.9.2.1. Potentiodynamic polarisation curves of the sample types.

4.9.2.2 Corrosion charts

Based on the potentiodynamic polarisation curves, the corrosion potentials of these tested samples are summarised in Figure 4.9.2.2b; the corrosion rate was calculated and the results are depicted in Figure 4.9.2.2a.

As expected, the untreated sample (P) had the highest corrosion rate followed by the PTO sample. The introduction of TiO_2 via CCT may have caused the corrosion rate to decrease by over half, when compared to the P sample. LIPSS however, may have led to the corrosion rates for MP48 to decrease by +/- 93.2 % and for MP58 to decrease by +/-96.7 %. This was a huge decrease in corrosion rate which indicated the LIPSS ripples could possibly increase the corrosion resistance more when compared to TiO_2. There was no significant difference between the MP58 and TOMP48 corrosion rates. Both these samples led to decreases in corrosion rates by +/-96.5 %. The MPTO sample had the lowest corrosion rate and thus, the highest corrosion resistance. The corrosion rate decreased by +/-98.9 %.

In the potentiodynamic charts in Figure 4.9.2.1, the P sample passivated at 0V (V vs SCE) with a current density of $+/-10x10^{-6}$ A/cm^2. The current density remained steady largely with very small metastable peaks along an anodic passivation which ended at +/-820 mV. The potential in the human body is +/-600-900 mV, and the passive current of P falls in this range. This suggested the untreated sample could be susceptible to corrosion in the body. The PTO sample passivated quickly at +/-200 mV with a passivation current of $+/-2x10^{-6}$ A/cm^2. The passivation current increased to$+/- 80x10^{-6}$ A/cm^2 along a polarisation that reached to 1V. The lower initial passivation current of the PTO sample and the higher anodic polarisation, suggested this sample had a better corrosion resistance than P and perhaps

would not be susceptible to corrosion in the body as the polarisation is larger than the potential value in the body.

The MP48 sample passivated at 350 mV (vs SCE) with a current density of +/-7x10^{-6}A/cm^2. The MP58 sample passivated at +/-400 mV (vs SCE) with a passive current density of 5x10^{-6} A/cm^2. The current density decreased to 4x10^{-6} A/cm^2 and then increased again to its original value. The current density had a sharp increase to +/-50x10^{-6} A/cm^2. The anodic polarisation finished at +/-1.2V (vs SCE).

The TOMP48 sample passivated at +/-350 mV (vs SCE) with a current density of +/-2x10^{-6}A/cm^2. The current density was lower than the MP48 and MP58 sample which indicated better corrosion resistance however, the corrosion rate was higher for TOMP48. The passive current density remained steady for the whole anodic polarisation which ended at +/-1.1V (vs SCE). The TOMP58 sample passivated at 0V (vs SCE) with a current density of +/-1.5x10^{-6} A/cm^2 which increased slightly to +/-2x10^{-6} A/cm^2. The anodic polarisation ended at +/-850 mV (vs SCE) which falls in the range of the potential in the body (+/-600-900 mV). This suggested the TOMP58 sample may be susceptible to corrosion in the body.

The lowest current density was seen for the MPTO sample at +/-0.003x10^{-6} A/cm^2. The MPTO sample also had the lowest corrosion rate. The MPTO sample had an instant passivation at 0V and the current density increased slightly to +/-0.01x10^{-6} A/cm^2. The anodic polarisation was completed at +/-1.2V which is larger than the potential in the body hence, the MPTO sample may not be prone to corrosion if applied in the body.

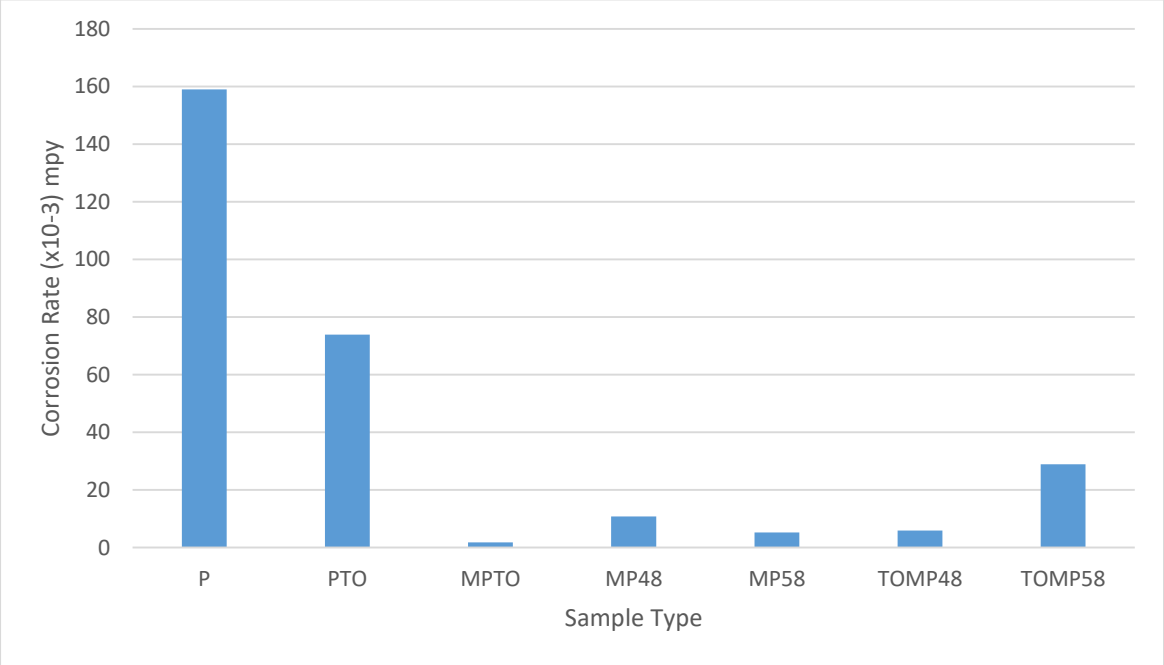

Figure 4.9.2.2a. Corrosion rate of the sample types, error bars are absent as the results could not be repeated.

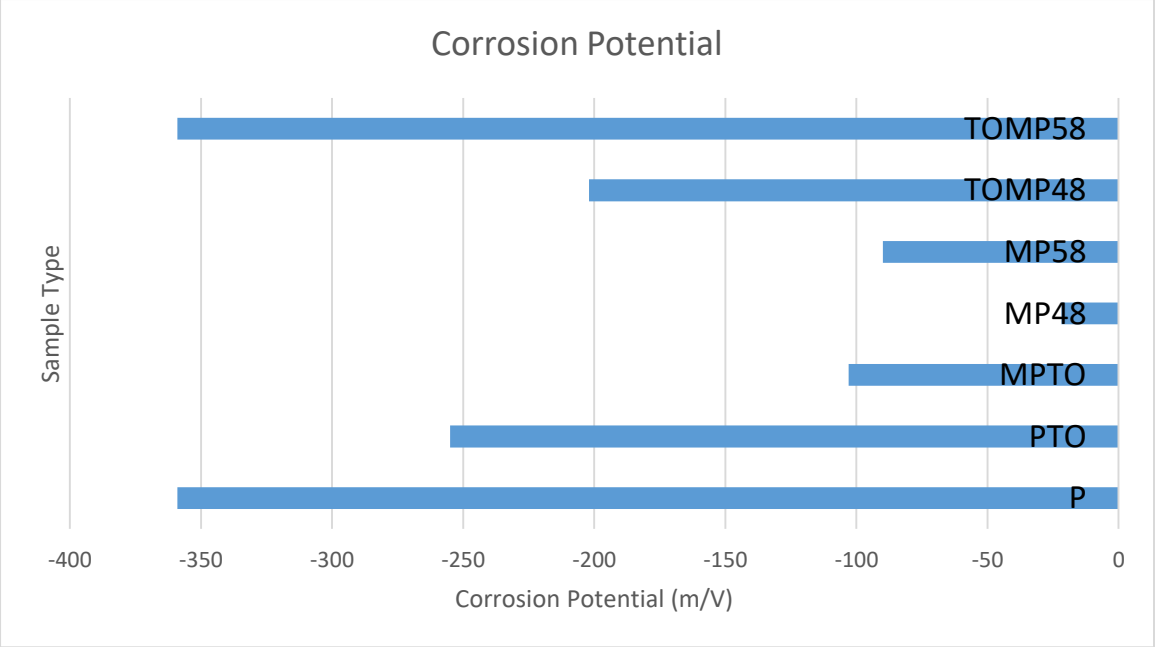

Figure 4.9.2.2b. Corrosion potential of the sample types, error bars are absent as the results could not be repeated.

4.9.2.3 SEM micrograph of corroded areas

The treated samples after corrosion displayed no obvious features of corrosive damage. This is in line with the potentiodynamic polarisation curves showing no pitting corrosion for these samples. Therefore, the corrosion of these samples would be mild general corrosion without localised corrosion.

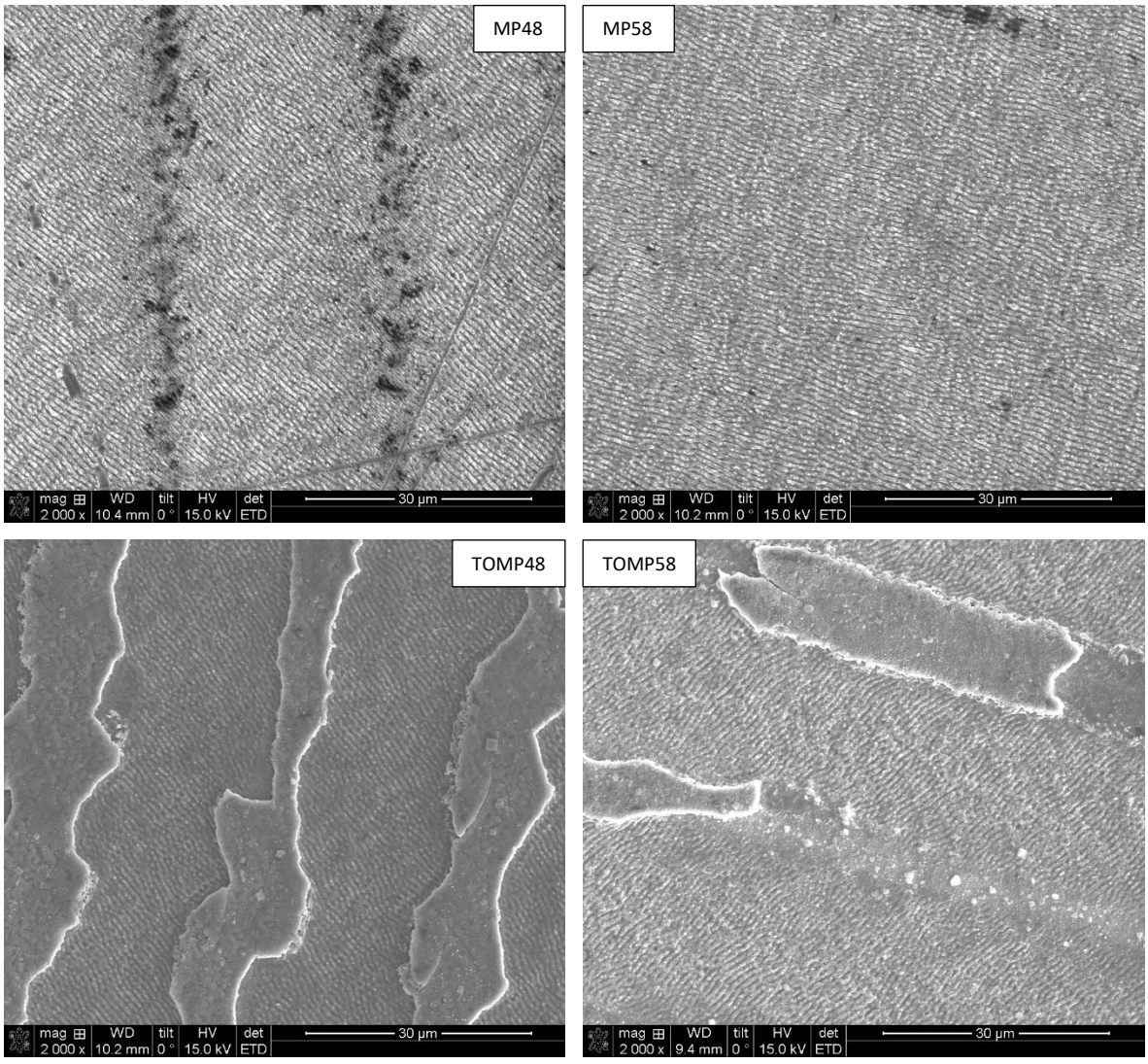

Figure 4.9.2.3. SEM images displaying the samples after the corrosion tests.

Chapter 5

DISCUSSION

5.1 The Antibacterial Effect of Engineered Surfaces

As discussed in Chapter 2, the adhesion of bacteria on surfaces is dependent on many factors such as wettability, surface free energy, surface roughness, the chemical composition of a surface and most importantly, the surface topography (75).

5.1.1 The effect of surface roughness on bacteria

For the percentage reduction antibacterial results in Table 4.7.1a, the highest value for *S. aureus* growth (when comparing cp-Ti samples) was seen for the P sample followed by PTO with the lowest value for TOMP. Similar results were also seen for *E. coli* although the numbers were greater for *E. coli* which indicated that *E. coli* was more resistant to the cp-Ti surfaces. These results could be related to the Ra values as it was seen that the P sample followed by the PTO had the lowest surface roughness and the highest bacterial growth. Previous studies have illustrated the importance of surface roughness in relation to antibacterial efficacy. Surface roughness has a greater effect on bacterial behaviour than wettability in *in vitro* settings (93). Figures 5.1.1a and 5.1.1b depict the correlation between Ra and *S. aureus* and *E. coli* attachment, respectively.

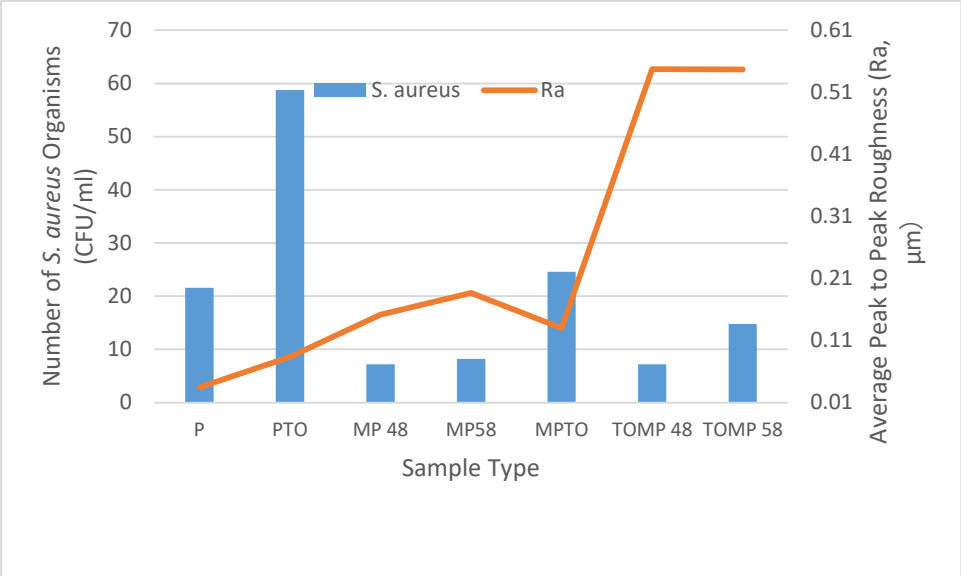

Figure 5.1.1a. The correlation between the number of *S. aureus* organisms and the Ra values of each samples type are depicted.

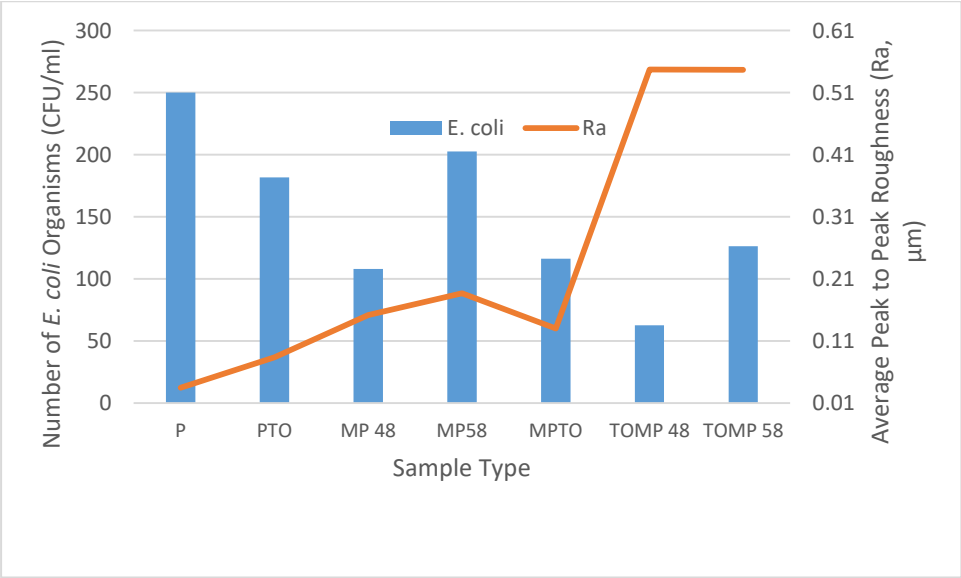

Figure 5.1.1b. The correlation between the number of *E. coli* organisms and the Ra values of each samples type are depicted.

Zitelli et al found bacteria avoid surfaces with small pits and grooves, ridges and protrusions (94). This may have been the case for this study. For instance, when looking at the Rt values for the 1st batch samples (used in the percentage reduction test) in Figure

4.3.1, The P sample had the lowest Rt value which meant it had the lowest peak to valley height. On the other hand, TOMP had the highest Rt value which suggested it possessed textures at a higher height than the other samples and thus, possessed protrusions which may have reduced the bacteria to sample surface contact area. This relationship between Rt and bacterial attachment are depicted in Figures 5.1.1c and 5.1.1d. Furthermore, it has also been found how surface features larger than the size of the bacteria have little effect on reducing bacterial colonisation as the bacteria to surface area contact is not limited (94). As the surface features were smaller in this study than the bacteria, they may have caused less surface contact and thus, less bacterial adhesion.

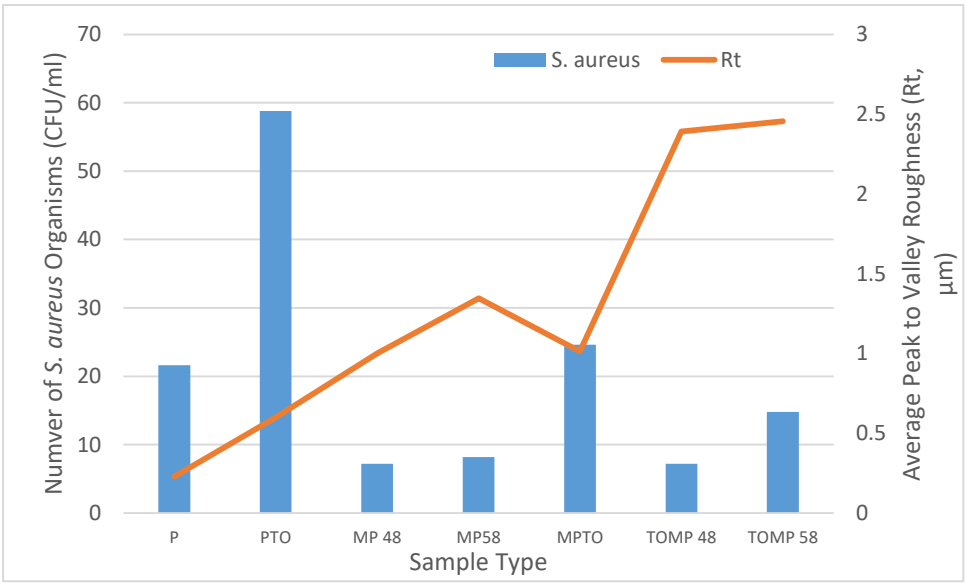

Figure 5.1.1c. The correlation between the number of *S. aureus* organisms and the Rt values of each samples type are depicted.

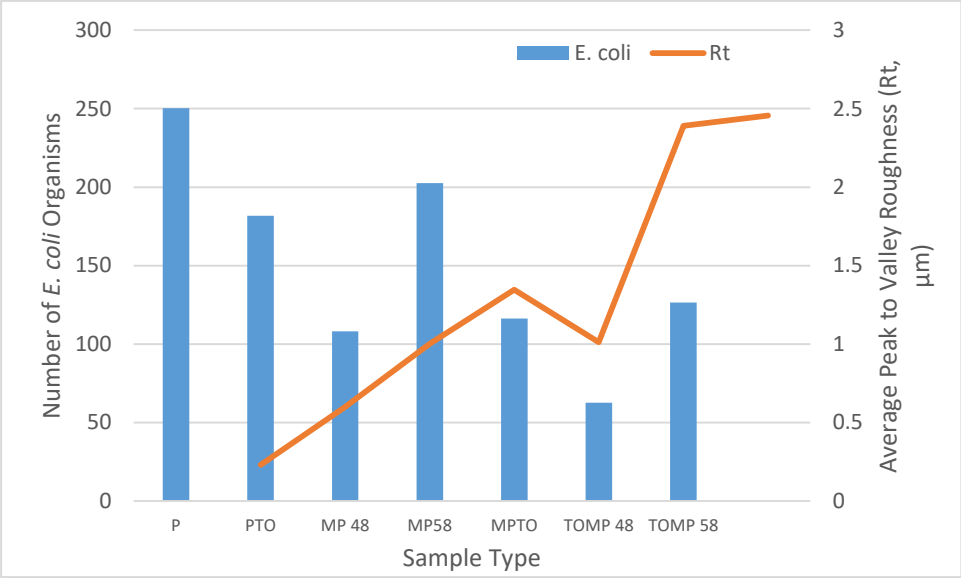

Figure 5.1.1d. The correlation between the number of *E. coli* organisms and the Rt values of each samples type are depicted.

As discussed previously in Chapter 2, the most important stage of bacterial colonisation is the initial contact with the surface, and if this contact area is reduced or obstructed the bacteria cannot attach and colonise the sample surface (34). As the LIPSS treated samples had periodicities of approximately 300 nm (smaller than 1 µm bacteria), the contact area was reduced for the bacteria and hence, the bacteria could not attach to their full potential.

Other studies have also illustrated the effect of surface roughness in relation to bacterial colonisation. Low Ra values can have an effect on reducing the bacterial adhesion; however, the largest effect can be seen when the Ra value is similar or smaller in size than the bacteria (94). *S. aureus* is typically 0.5-1.5 µm in diameter and *E. coli* is typically 1-2 µm long. Keeping this in mind, the Ra values for all the sample types in this study were smaller than the size of the bacteria used in this study and hence, all the sample types displayed some antibacterial potential when compared to the control (agar dish). Previous studies

have documented how smoother surfaces have led to increases in the growth and attachment numbers of *S. aureus* when compared to rougher surfaces (95). This was seen in this study as the smoother P and PTO samples had greater bacterial growth in comparison to the rougher TOMP and MP samples however, this may also have been due to the latter samples possessing LIPSS ripples.

Previous reports have also been documented regarding the antibacterial effect of laser treated surfaces with specific surface roughness. Ra values below 0.3 µm (smaller than bacteria) on surfaces with dense laser treated surface features were found to have hindered the bacteria to contact the surface and thus, the bacterial colonisation was decreased (75). This may have occurred in this study as the Ra values for TOMP were +/-0.14 µm and TOMP possessed 1 µm ripples with +/-300 nm periodicities. The presence of the ripples may have reduced the contact area for the bacteria to appropriate colonise. On the other hand, although the P sample possessed a Ra value of +/-0.3 µm, there were no surface features on the sample that could prevent the bacterial contact and hence, the bacterial growth was higher on P. This suggests surface topography such as the presence of LIPSS and the spacing between the ripples has a greater antibacterial effect than surface roughness as the antibacterial effect of surface roughness has many conflicting results. Hence, the presence of surface features are more important than surface roughness.

There are many contradicting reports on the effect of surface roughness in relation to bacterial behaviour. There are two arguments; the first argument explains how higher Ra values lead to increased bacterial colonisation due to increases in available contact areas and binding sites. The second argument explains how increasing the surface roughness in

the nanometre range may decrease the bacterial colonisation due to the larger microscale bacteria's inability to attach to the smaller nanometre surface features (96). The second argument is most applicable to this study, as the higher Ra values led to fewer bacterial numbers and also, the presence of the 300 nm spacing between the LIPSS ripples may have reduced the contact area for the bacteria and thus, reduced the colonisation.

5.1.2 The effect of WCA and SFE on bacteria

In Figure 4.4.1a the wettability results are displayed. MPTO sample had the lowest WCA and thus, was the most hydrophilic. P, PTO and MPTO samples were all hydrophilic as they possessed WCAs lower than 90˚. The samples with LIPSS possessed WCA'S above 90˚ and hence, these samples were hydrophobic. The highest WCA was seen for TOMP58 followed by TOMP48 and hence, these samples were the most hydrophobic. For the SFE results, the highest SFE was observed for MPTO and the lowest was for P. The samples with thicker oxides formed by CCT (PTO, MPTO, TOMP48 and TOMP58) all had higher surface energies when compared to the samples without CCT. The SFE values for as-patterned MP48 and MP58 are also lower than for as-polished P but lower than for TOMP48 and TOMP58. This is probably related to the oxide film formed during laser patterning in air (see Section 4.1).

The number of *S. aureus* organisms that attached to the samples was seen in Figure 4.7.2.1b. The lowest *S. aureus* organism count was seen for MP48 and TOMP48 as there was no significant difference between the results. The second lowest value was seen on the TOMP58 samples whereas, the highest *S. aureus* count was observed on PTO followed by MPTO. This suggested the samples with TiO_2 (PTO and MPTO) had higher bacterial counts when compared to samples with sharp LIPSS (MP48, MP58 & TOMP48) and this may be due

to their hydrophilic nature. For improved visualisation, the relationship between WCA and *S. aureus* and *E. coli* growth are depicted in Figures 5.1.2a and 5.1.2b, respectively.

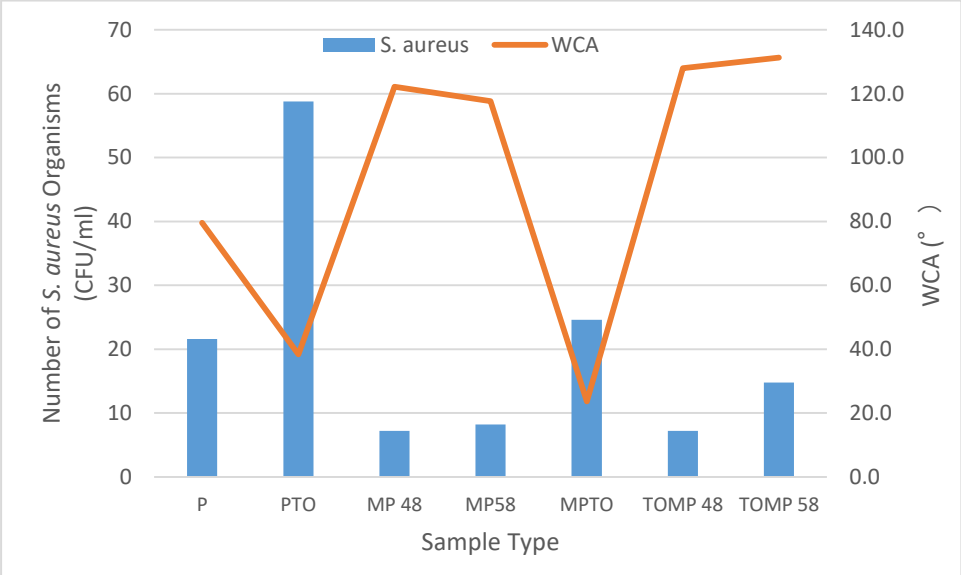

Figure 5.1.2a. The correlation between the water contact angle of the samples types and the number of attached *S. aureus* organisms is demonstrated.

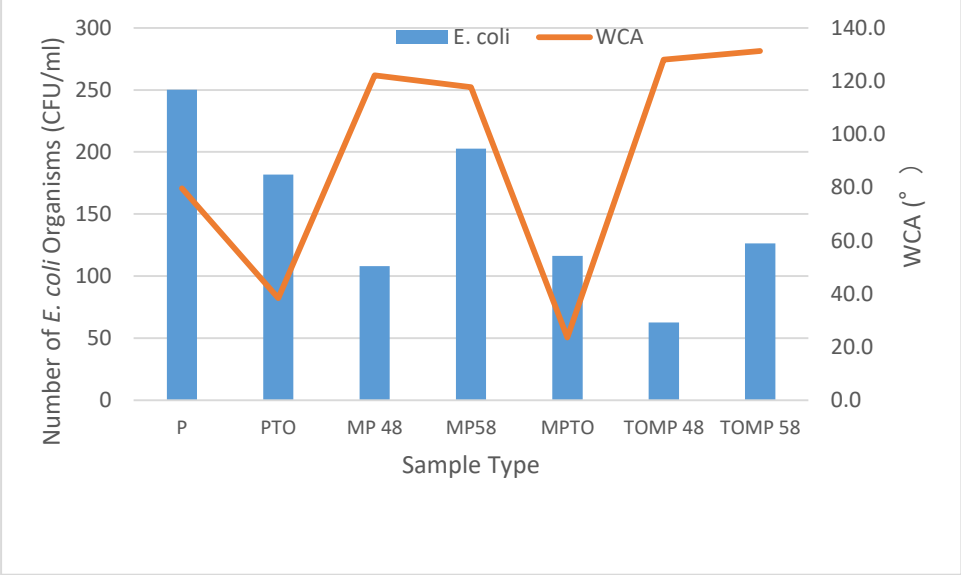

Figure 5.1.2b. The correlation between the water contact angle of the samples types and the number of attached *E. coli* organisms is demonstrated.

For *E. coli* (Figure 4.7.2.2c), the organisms that attached on the samples were much higher than *S. aureus* and this may be due to their more persistent nature owing to their

Gram-negative structure. The highest value was seen for the P sample followed by the MP58 sample. The lowest numbers were seen on the TOMP48 sample followed by MP48. This suggested that the LIPSS that were formed using 48 % power were the most effective in inhibiting the attachment of *E. coli*. When the LIPSS however combined with CCT, the *E. coli* numbers reduced by almost half which indicated that the two treatments types together provide the most antibacterial effect.

Bacteria are negatively charged and the surface of Ti is also negatively charged and this may contribute to the antibacterial results. When Ti is placed in a pH neutral aqueous environment, small negative charges form on the surface due to the presence of the TiO_2 layer. When the negatively charged bacteria approach this negative surface, there are small electrostatic repulsion forces which can affect the attachment of bacteria to the surfaces (95). This may be the reason why the P sample displayed antibacterial efficacy when compared to the control (agar plate).

In general, there have been some theories related to the hydrophilic/hydrophobic nature and bacteria. It has been found that hydrophobic bacteria preferably attach to hydrophobic surfaces and hydrophilic bacteria prefer hydrophilic surfaces. *S. aureu*s and *E. coli* are both generally referred to as hydrophobic bacteria so they would prefer to attach to hydrophobic surfaces (93,95). However, this was not the case for *S. aureus* as the PTO and MPTO samples were hydrophilic yet they had high *S. aureus* counts. For *E. coli* P, PTO and MP58 had high numbers and these sample types were hydrophilic and hydrophobic respectively. This indicated that, the surface features rather than the surface wettability may have had a greater effect on the attachment of bacteria. Previous studies have also

illustrated the greater importance of surface topography when compared to surface wettability (95). Other studies have also reported insignificant differences between the attachment of *S. sanguinis* on hydrophilic and hydrophobic surfaces and attributed the bacterial attachment to surface topography and composition (93).

Previously, reports have been made in regards to the hydrophilic nature of laser treated samples causing increases in *S. aureus* attachment (75). These results are similar to the results in this study as the hydrophilic PTO, MPTO and P samples all had greater *S. aureus* attachment when compared to the hydrophobic samples. Hydrophobic surfaces can limit the adhesion of bacteria due to the entrapment of air. A layer of air can form between the surface and the liquid containing the bacteria. This layer of air can limit the movement and adhesion of bacteria and hence, the colonisation is reduced (97). This may explain the results in this study as the hydrophobic samples had less bacterial attachment and greater percentage reductions.

Furthermore, bacteria can be classified as colloidal particles. When bacteria approach a surface, they begin to adhere to the surface via electrostatic interactions between the cell wall of the bacteria and the surface. The initial factor that can affect this adhesion is the SFE which is affected by the interfacial energy of the microbe and the surface tension of the suspension medium. With hydrophilic surfaces, the forces between the cells and the sample surface are stronger and hence, hydrophilic surfaces are easily colonised by bacteria when compared to hydrophobic. However, using SFE as a measure to deduce antibacterial behaviour is not completely valid as SFE *in vitro* is different to *in vivo*. For instance, with dental implants post implantation, saliva covers the dental implant and

this saliva with its associated enzymes and proteins alters the SFE of the implant. Thus, the antibacterial effect may differ. Hence, factors such as surface topography and roughness are better measures when deducing antibacterial behaviours (98).

5.1.3 The effect of surface texture on antibacterial efficacy

Ti and its alloys possess the ability to absorb calcium and proteins that help enable the process of osseointegration. However, this ability can also promote bacterial adhesion and hence, the need for antibacterial surfaces is high. In nature antibacterial surfaces exist that possess high aspect ratio topographies. For example, the wings of a dragonfly possess topographies that have disrupted the membranes of bacteria eventually leading to bacterial death. This phenomenon has caused interest in the manufacture of chemical or physical surface features with antibacterial abilities (96). As mentioned previously, the surface topography is the most important factor in altering the antibacterial efficacy of surfaces (95). Studies have also demonstrated the importance of surface topography and morphology. For instance, investigations using samples with the same surface roughness yet different morphologies displayed different bacterial colonisation rates between the samples. They attributed the changes in antibacterial efficacy to the surface morphology of the samples (93).

In Section 4.7.2.1, the SEM images for the *S. aureus* attachment on the samples were observed (Figures 4.7.2.1a and 4.7.2.1b). The MP48 and MP58 samples had very few organisms attached to the samples which indicated that the LIPSS had a high anti-biofouling capability. The TOMP48 sample had a higher number of attached *S. aureus* organisms which attached to the areas of the sample that had oxide present with no ripples. The TOMP58

had more oxide destruction yet displayed higher bacterial numbers. Regions where the oxide was destroyed had improper or no LIPSS formation. These non-textured regions were where the bacteria showed highest numbers on the TOMP58 sample (Figure 4.7.2.1b).

In addition, on the TOMP48 sample in Figure 4.7.2.1d there was a region where the spacing between the ripples was almost +/- 0.5 µm wide which was the same size as the *S. aureus* organism. In this region the bacteria managed to attach and hence, this suggested that the spacing between the ripples should be smaller than the bacterial size for it to be most effective in killing the bacteria. Hence, the optimal spacing between the ripples to prevent *S. aureus* attachment should be below 0.3 µm (below 0.5 µm). The same was also visible for the TOMP58 sample.

The presence of the 1 µm ripples with the 300 nm spacing may have reduced *S. aureus* adhesion capability due to limited surface area for it to adhere to. As, previously mentioned the most important stage of bacterial colonisation is the initial contact of the bacteria with the surface. With the LIPSS treated samples, the contact area for *S. aureus* is reduced due to the protrusions and spacing between the LIPSS that is smaller than the size of the bacteria. This inhibited the bacteria from attaching to the surface and hence, bacterial colonisation could not occur. This is further supported by the SEM images of the MPTO sample. The MPTO sample had the 1 µm ripples which were damaged due to the CCT process. As the ripples were covered by a thick hydrophilic TiO_2, the bacteria had a better surface area to attach to and thus, more *S. aureus* attached on the MPTO sample (Fig. 4.7.2.1a).

This has also been reported in previous studies as discussed in Chapter 2. It has been documented that when nano-pillars are formed using LIPSS, the *S. aureus* colonisation is inhibited as the bacteria cannot penetrate into the spacing and depressions between the pillars in order to produce a stable bond to the surface. When this occurs, the *S. aureus* organisms are only able to attach to the peaks of the pillars and are unable to attach to the substrate material. As a result, the surface area for bacterial contact is reduced which leads to a weaker adhesion bond and thus, the bacteria are removed (75). Figure 5.1.3a below helps demonstrate this. This may have occurred in this study as the *S. aureus* organisms attached to the oxide columns that provided greater contact area but were unable to attach to the ripples in the MP48 and MP58 samples (Figure 4.7.2.1a).

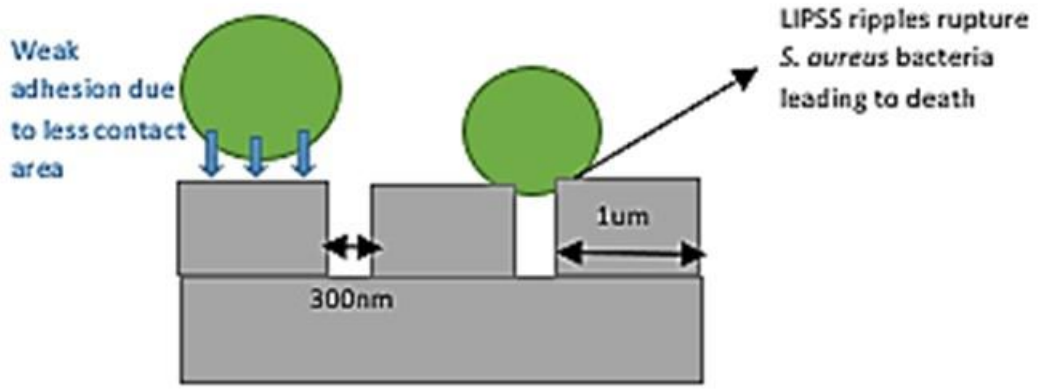

Figure 5.1.3a. Illustration of the limited contact area between the *S. aureus* organisms and the LIPSS treated surfaces.

Surfaces with sub-micron topographies have shown to display antibacterial properties. Bacteria in general are 1-2 µm in size and with Gram positive bacteria (like *S. aureus*), if surfaces have surface textures with periodicities or spacing's less than 1.5 µm,

there have been reports of reduced bacterial attachment. Sub-micron protrusions have displayed the ability to rupture bacterial organisms leading to their death (72). This may have occurred in this study and hence, the reduced number of *S. aureus* organisms on the LIPSS treated samples. Several studies have demonstrated the anti-biofouling capability of LIPSS. Using a femtosecond laser, ripples and nano-pillars were formed on the surface of stainless steel. The bacterial reduction on these samples were reduced by 50-80 % (72). This was also seen in this study as the percentage reduction for the MP and TOMP samples (Figure 4.7.1b) was over +/-70 % for *S. aureus* and over +/- 60 % for *E. coli*. Similarly, other studies have also demonstrated LIPSS treated Ti surfaces to reduce the adhesion and biofilm formation of *S. aureus* (75).

As has been shown in Figure 4.7.2.2c, for *E. coli*, the TOMP58 had higher oxide destruction and thus possessed regions where the LIPSS did not form fully. Similar to the results from *S. aureus*, these regions with improper patterning and no oxide may have caused higher bacterial adhesion as there was no anti-adhesion properties to these regions. *E. coli* being a Gram negative bacteria is more difficult to destroy than *S. aureus* as it is more resilient. The TOMP48 sample had the lowest value which suggested when the patterning is undertaken without damaging the oxide, the combined surface treatments caused less bacterial survival.

On the P sample, the *E. coli* organisms formed a thick, dense chain linking themselves together (Figure 4.7.2.2a). This chain of bacteria suggested that the P sample provided an excellent environment for *E. coli* survival. This may have been the initial process of a biofilm formation. The PTO sample also provided a good environment for *E. coli* growth

as it was visible the organisms formed a long chain (marked in red in Figure 4.7.2.2a). The bacterial organisms on the MPTO sample grew and attached in clusters that were spaced out. The bacteria that attached on all the samples were rod-shaped which indicated healthy *E. coli* bacteria. When looking at the back-scattered (BSD) images in Figure 4.7.2.2b, the MP58 sample had the most *E. coli* organisms present on the surface and TOMP48 had the fewest.

As *E. coli* is a large rod-shaped bacterium it was able to attach to the LIPSS ripples as it possessed greater points of contact and cannot be ruptured easily by the ripples due to its thick cell wall as demonstrated in Figure 5.1.3b. In a previous study it was found that *S. aureus* organisms attach in cervices that were able to hold the bacteria (99). This may have been the case with the results in this study as with the TOMP48 sample (Figure 4.7.2.1d) there was a region on the sample that had a spacing of 0.5 µm and the *S. aureus* managed to attach to that area as it was the same size as the bacteria.

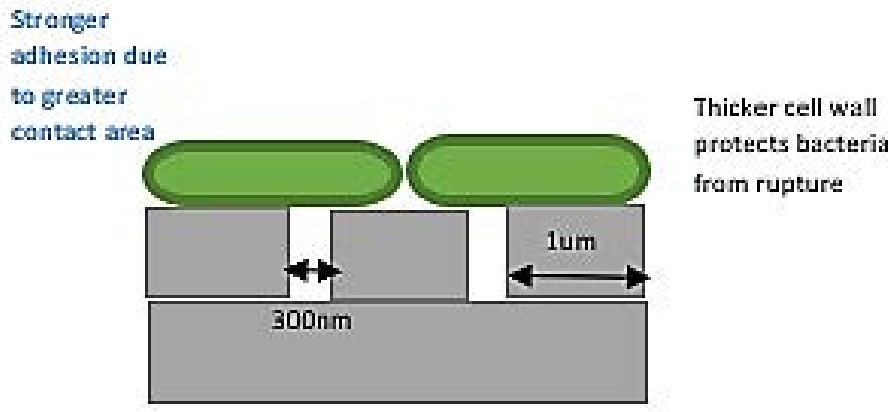

Figure 5.1.3b. Illustration of the contact area between the *E. coli* organisms and the LIPSS treated surfaces.

In a previous study it was found that *E. coli* organisms lay across the grooves in the direction of the surface textures. They attributed this to the size of the bacteria. For instance, the surface grooves were smaller in size than the *E. coli* organisms and hence, the *E. coli* were able to lay across the grooves without being affected by the grooves (99). This also occurred in this study. The *E. coli* organisms were able to attach to the MP48 and MP58 samples and lay across the 1 μm ripples. The number of attached organisms were decreased in the laser treated samples when compared to the P and PTO, but there were many more attached bacteria when compared to *S. aureus*. This may be due to their cell wall protecting them from rupture by the ripples and also, due to their larger size.

It has been documented how surface morphology has a larger effect on *E. coli* adhesion than surface wettability. Whereas for *S. aureus*, the surface roughness and wettability alongside the morphology all affect the adhesion. LIPSS in the form of pillars with many peaks can strongly reduce the ability of *E. coli* to adhere to the surface. Polished surfaces however, increase the adhesion of *E. coli* (100). This was seen for the samples in this study.

The P sample which was mirror polished had the largest number of *E. coli* organisms attached that formed a chain between themselves which indicated the surface provided excellent conditions for *E. coli* colonisation. The number of organisms was also high on the PTO sample which may be due to the small heights of the peaks as seen in Section 4.3.2. The MP48 sample had much higher peaks than PTO and MP58 and it also had fewer *E. coli* organisms attached. Similarly, the TOMP48 sample had the highest peaks and also the lowest number of *E. coli* organisms. This suggests that the presence of peaks created via

LIPSS does have the highest effect on reducing the attachment of *E. coli* organisms. On the other hand, it has been stated how surface roughness and wettability have a large effect on *S. aureus* attachment (100). This may have been true for this study as the MPTO, PTO and P samples were all hydrophilic and these samples had the most *S. aureus* organisms attached.

Other studies have also demonstrated the ability of LIPSS in causing percentage reductions of 56 % for *E. coli*. The LIPSS in that study were similar in size to *E. coli* which is also similar to this study. Percentage reductions of over 60 % for *E. coli* were observed for the LIPSS treated samples in this study and the ripples were also similar in size to the size of *E. coli*.

Previous research has documented how bacteria prefer to attach to the grooves or spacing between LIPSS rather than attaching directly to the LIPSS textures. Bacteria have shown to attach in clusters in order to protect one another from shear stresses and forces. By doing so, the clusters become larger than the individual ripples and thus, the bacteria are protected from rupture by the ripples (101). These results match the results from this study as the *E. coli* organisms formed chains and clusters on the P, PTO and MPTO samples.

An interesting point to mention is occasionally bacteria attach on a surface after being ruptured and hence, are dead. The dead bacteria however, remain attached to the surface and therefore, in this study it was difficult to distinguish whether the bacteria were dead or alive on the surfaces without the use of fluorescence imaging. Dead bacteria can wrap or encase themselves around surface textures like ripples. They have previously been recorded on LIPSS treated surfaces (101). This may have been the case for the results in TOMP48 and TOMP58. Some of the *E. coli* on these surfaces attached under and around the

1 µm ripples. This *E. coli* may be dead but as it was not tested further it cannot be confirmed.

Another reason for a reduction in bacterial numbers on the LIPSS treated surfaces may be due to the reduced contact area as mentioned previously. When bacteria approach and adhere to a textured surface, due to the limited contact area on the surface the bacteria stretch themselves in order to increase the contact points. As they stretch, they damage their membrane which can lead to death (101). This may have occurred hence, the increased percentage reduction for the LIPSS treated samples.

It was hypothesised that the antibacterial effect would be greater for *E. coli* than *S. aureus* due to the larger bacteria size. Previous research has discussed how larger bacteria cannot accommodate the smaller grooves on textured surfaces and hence, less *E. coli* attach to the surface (97). However, this was not the case as the larger *E. coli* were able to lie across the ripples. Also, being a Gram-negative bacterium, *E. coli* has shown to adhere to Ti more than *S. aureus*. This is because Gram-negative bacteria release endotoxins that strengthen and aid their adhesion to implants (102). This may be another reason why there were higher *E. coli* numbers on the samples in this study than *S. aureus.*

5.1.4 The effect of TiO_2 on antibacterial efficacy

The chemical composition of a surface also has an effect on the antibacterial efficacy of a sample. For instance, a TiO_2 layer has shown to possess an antibacterial effect thus, leading to the reduction in *S. aureus* attachment. LIPSS is carried out in air and as a result, the oxide thickens during the process. This thicker oxide has led to reduced bacterial adhesion in previous studies (75). This has occurred in this investigation for example, when looking at

the EDX results in Figure 4.1.2a, the MP sample has a higher concentration of oxygen when compared to P which suggests oxidation has occurred.

However, when looking at the antibacterial results in Section 4.7, the MPTO sample which has a thicker oxide has more bacterial colonies on the sample when compared to MP which has a lower oxide concentration. Also, when looking at the XPS data after etching (Table 4.2.2.b), the MPTO sample has more TiO_2 than the TOMP sample yet, the TOMP sample is more antibacterial. This suggests, the topography and presence of LIPSS has a greater effect on bacteria rather than the oxide thickness.

There has been research that has reported the antibacterial effect of oxide nanoparticles (34) and the photoactivation of anatase heavy TiO_2 films to produce an antibacterial effect using UV light. However, recently it was found that rutile has a higher photoactivation capability as well as a higher antimicrobial effect against *E. coli.* The mechanism behind this antibacterial activity has been attributed to the production of radicals and reactive oxygen intermediates as well as hydrogen peroxide. These radicals can be absorbed by microbes and can damage the DNA of the bacteria leading to death (83).

However, the use of fluorescent light (normal room light) can also initiate this mechanism although, it not yet understood how. It has been agreed that the photoactivation by normal room light is affected by the grain size and surface area of the samples. Rutile-based oxide films were able to reduce the adhesion of a cocci bacteria by 50% when compared to an anatase based oxide (83). The oxide formed in this investigation was also rutile based when looking at the XRD data in Section 4.2.1. The presence of rutile may have increased the antibacterial effect on the samples in this investigation as the PTO

samples were more antibacterial than the polished P sample. However, in this study the surface features had the greatest antibacterial effect.

5.2 Cytocompatibility Effect

The good cytocompatibility of titanium is due to the ability of the native oxide film to react with water ions and cellular proteins. When forming surface textures or features on the surface of titanium, one must ensure the features do not hinder the human cell behaviour. When developing these surface features, it is hoped that they will be bioactive and most importantly, cytocompatible. The host tissues response to implants is dependent on the chemical and physical features of the implant surface. For instance, the surface topography affects the ability of host cells to attach, and the oxide thickness and composition can affect the antibacterial or tribological properties of the implant (96).

5.2.1 Effect of surface roughness on SaOS-2 cell viability

Surface composition and morphology have a high effect on the success of an implant. Orthopaedic implants must have a surface that can enable or initiate osseointegration or osteogenic differentiation to occur. Surface energy, roughness and substrate composition can have a direct or indirect influence on the behaviour (proliferation, growth and differentiation) of osteoblasts and can thus, affect the integration of implants into bone (103).

Ideally, dental implants should display a certain topographical micro-roughness without affecting the hydrophilic nature of the implant's surface. The surface roughness of an implant can be in the micrometre (1-100 μm) or nanometre (1-100 nm) range. As discussed in Chapter 2, it has been reported how surface roughness in these ranges can

influence the bone response by positively affecting the cell attachment due to increases in surface area. Nano sized proteins can infiltrate nanometre textures on an implants surface and in doing so, can enhance cellular behaviours like differentiation and proliferation (103).

Previous studies have reported how smooth implant surfaces have led to improved cell proliferation and rough topographies have led to osteoblast differentiation. Osteoblast differentiation is better as it would lead to bone formation and thus, implant integration. Autophagic osteoblast processes can be mechanically stimulated by osteoblast contact with rougher topographies consequently, leading to cell differentiation. Rougher surfaces with nanoscale features may also have the ability to increase the secretion of proteins and osteogenic markers such as osteopontin and osteocalcin. The release of these markers can hasten the bone-implant contact and bone formation. The rougher surfaces have shown to possess the ability to initiate osteoblast maturation which is an essential step in osseointegration (103).

As previously mentioned, the surface energy, topography and chemistry all have an effect on cell behaviour. To help understand the results, initially the relationship between the roughness of the samples and cells will be analysed followed by the wettability, topography and TiO_2 effect. As reported in Section 4.3 and discussed in Section 5.1.1, the P sample had the lowest Ra and Rt values followed by the MP sample and TOMP possessed the highest Ra and Rt values in the 1st batch samples.

As reported in Section 4.8, in the cp-Ti sample group the P sample had the second lowest SaOS-2 cell count and the lowest roughness (+/-0.03 µm). The highest cell count was seen on the PTO sample which had a roughness of +/-0.08 µm. The MP sample had a similar

roughness) to PTO yet it had the lowest cell count. The TOMP sample had the highest roughness but its cell count was less than MPTO and PTO.

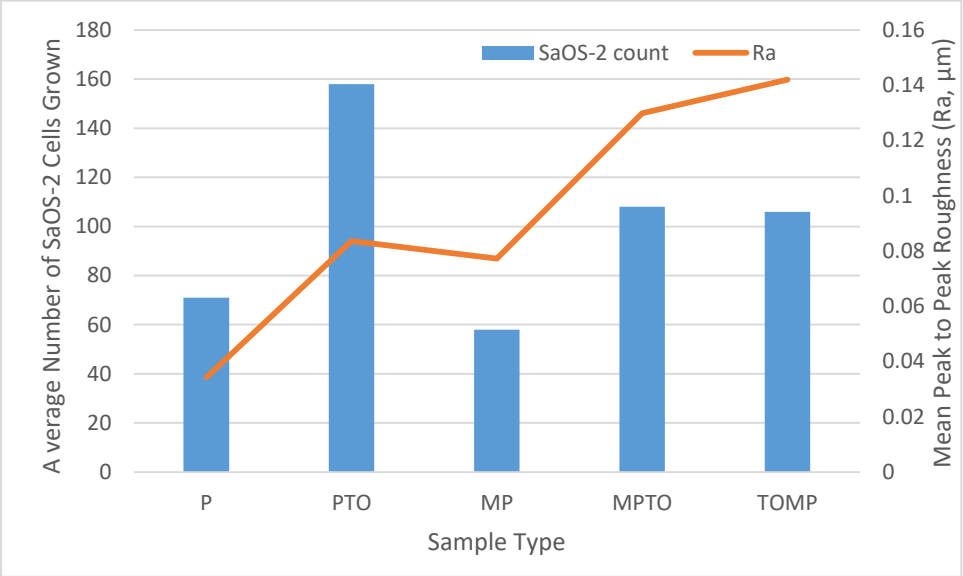

Figure 5.2.1. Chart displaying the relationship between the mean surface roughness (Ra) and the number of SaOS-2 cells attached.

Clearly, there is no close relationship between surface roughness and SaOS-2 cell attachment (Figure 5.2.1) as the MPTO and TOMP samples had differing Ra values yet the SaOS-2 cell count was almost the same. The samples with CCT led to higher cell numbers whereas the LIPSS led to lower cell attachments. This may be due to the chemistry of TiO_2, the wettability of the samples surfaces or surface topography of the LIPSS. Previous studies have reported for optimum osseointegration to occur, surface roughness should be in the range of 550-880 nm (95). The roughness of MP and PTO both fall into this range but MP had the lowest cell count. This suggests that the attachment of osteoblast like cells is not affected by roughness to a large degree and rather the topography or chemistry of the surface has a larger effect.

These results contradicted the results from Cordeiro and Barao (103) as they stated that osteoblasts prefer smoother surfaces for attachment. Nonetheless, they also stated how rougher surfaces lead to lower cell numbers but better cell differentiation which may have been the case in this study (103). For instance, when looking at the SEM images (Figures 4.8a and 4.8b), the P sample had rounded SaOS-2 cells which indicated less spreading of the cell and thus, less cell to sample surface contact. Whereas, the MP and TOMP samples had cells which were longer (when compared to the cells on P) and the cells had developed filopodia. This indicated that the cells maintained a strong contact to the sample surface and spread more. These results would be better for orthopaedic implants as it suggests that the cells had improved contact with the sample surface on the textured surfaces and thus, potentially would lead to better cell responses such as bone formation (103).

Similar findings to this study were found by Sista et al (104). They reported that when changing the roughness of a Ti-6Al-4V alloy between 0.25-0.87 µm, the higher roughness led to better cell behaviours. Protein adsorption increased on the rougher surfaces when compared to the smoother surfaces which led to the conclusion that for long term orthopaedic implants, rougher surfaces lead to better cell behaviours (104).

In a previous study undertaken by Wu et al. the roughness had a large effect on osteoblast cells. The smoother surfaces led to lower osteoblast attachment rates and the shape of the osteoblasts were rounded which was similar to the results from this investigation (P sample was smoother and had round osteoblasts seen in Figure 4.8b). They found that on smooth surfaces, the focal adhesion points of the individual osteoblast cells

membrane can spread and contact the sample surface uniformly which leads to the rounder shape. The highest number of osteoblasts was seen on their plasma sprayed Ti samples and lowest on polished. This is similar to the results of this study; however, P had the second lowest cell count behind MP (Figure 4.8d). Wu et al. discussed how the osteoblasts preferred rougher surfaces as the texture increased the adhesion bond to the sample surface which protected the cells from shear forces (94). They also reported how rougher surfaces may have better results *in vivo* as rougher surfaces lead to osteoblast differentiation, increased ALP activity and mineralisation of the extracellular matrix. They suggested that rougher surfaces help modulate the bone response and thus, can have an effect on implant integration. These findings were similar to the findings of Cordeiro and Barao (103).

On the other hand, Jager et al. found that the roughness of metallic surfaces does not have a large effect on the initial adhesion rates and proliferation of osteoblast cells (105). These findings are similar to the results from this study for instance, the PTO and MP sample had similar roughness yet the cell count was very different and larger on PTO. This suggests that, roughness may have some part to play in cell attachment but other factors such as surface chemistry, hydrophobicity and surface features need to be considered. The cell viability results of the current study were established after 24 h of incubation and hence, the cells numbers were less. If the incubation period was longer, similar results to the above studies may have been found. However, for now it can be concluded that surface roughness may have contributed but is not the only affecting factor for cell attachment.

5.2.2 Effect of surface wettability and SFE on SaOS-2 cell viability

As reported in Section 4.4 (Figure 4.4.1a), MPTO sample had the lowest WCA and thus, was the most hydrophilic. P, PTO and MPTO samples were all hydrophilic whilst samples with LIPSS were hydrophobic. To interpret the relationship between WCA, SFE and cell viability, TOMP58 and MP58 will be used to discuss the cell results in place of TOMP and MP respectively because MP58 and TOMP58 were more similar to the 1st batch MP and TOMP samples than MP48 and TOMP48. PTO had the second lowest WCA and the most SaOS-2 cells. MPTO was hydrophilic and TOMP was hydrophobic; however, the osteoblast like cell attachment was similar between these two samples and had no significant difference. This suggested that WCA did not have a major effect on the cell attachment rates which is similar to the roughness results. The lowest cell count was seen on MP and this sample was hydrophobic. The LIPSS textures led to the samples becoming hydrophobic and it was these samples that displayed lower cell attachment numbers when compared to the CCT samples.

It has been previously reported how cp-Ti samples with a submicron roughness (<1 µm) and high hydrophilicity display better osteoblast attachment and proliferation (103). This is similar to the findings of this study as PTO sample had the highest cell count and had a roughness of 0.08 µm which is submicron and was hydrophilic. Similarly, studies have reported WCA and wettability do have an effect on osteoblast attachment rates. It was reported how increasing the surface wettability and decreasing the WCA of metallic implants enhanced the adhesion of fibrin and thus, increased cell attachment (96).

In general, implant surfaces that are hydrophilic are preferred over hydrophobic surfaces *in vivo* due to better implant integration observed with hydrophilic implants. Better

interaction with the host environment was seen for hydrophilic implants due to the higher wetting potential which allowed for human serum and fluids to come fully into contact with implant surfaces. Hydrophobic surfaces can potentially lead to the isolation of the implant via thrombosis due to improper integration of the implant (67). Ivanova et al. have also reported how higher wettability lead to better cell attachment. They found that the greater the hydrophilicity, the greater the interaction between liquids and thus, cells to the implant (95). This was similar to the findings of this study as PTO, P and MPTO samples were all hydrophilic and had high cell counts. Likewise, previous studies have revealed that hydrophilic surfaces display better cell attachment and colonisation numbers due to the fast and strong attractive forces between the hydrophilic surface and the cells (98). There may be some concern for the LIPSS treated samples to be rejected by the body due to their high hydrophobicity.

On the other hand, it was reported that a hydrophilic laser ablated Ti sample with surface features of 300 nm displayed very low osteoblast attachment numbers on its surface. It was concluded that WCA had little effect on osteoblast attachment. Rather the surface topography and features had the greatest effect on cellular behaviour (67). This may have been the case with the results from this study, as TOMP was highly hydrophobic and MPTO was hydrophilic yet, there was no significant difference between the SaOS-2 cell numbers grown on these samples. It has been stated that surface roughness plays a larger role in cell attachment than wettability and surface free energy. *In vitro* studies do not display the many factors an implant encounters in the human body. The SFE of samples *in vitro* differs to the SFE *in vivo* due to the presence of fluids and proteins in the body. Hence,

SFE results are not entirely valid as SFE is very sensitive to the environment and other factors such as surface or host chemistry.

5.2.3 Effect of surface topography and LIPSS on SaOS-2 cell viability

In the MP and TOMP samples, the osteoblast like cells proliferated parallel to the laser ripples and grew along the patterns. Although in Figure 4.8c there was no significant difference in cell growth between the MPTO and TOMP sample, the SEM micrographs displayed a slightly higher cell concentration on the TOMP surface than on the MPTO surface. On the MPTO sample, the cells grew randomly as with P and PTO which further suggested that the oxide present on MPTO reduced the effect of the LIPSS and hence, the SaOS-2 cells behaved in a similar fashion to as they were on the PTO sample.

The cells on the P sample had a size ranging between +/-20 µm and +/-50 µm. The larger cells had a highly visible cytoplasm which suggested healthy cells. Some of the cells on the PTO sample were larger ranging between +/-20 µm and +/-80 µm. The cells on the treated samples were less circular in shape when compared to the cells on P. This suggested less cell spreading and weaker adhesion.

The cells on TOMP and MPTO developed cell structures referred to as filopodia. The filopodia of the cells caused them to attach to one another and to the oxide columns on the sample surface. The filopodia also attached to some of the 1 µm ripples which helped anchor the cells onto the sample surface. This suggested that the cells had weaker attachment when compared to P hence, the requirement for filopodia to support the cell attachment. On the other hand, it can also be said that the development of filopodia may enhance the resistance of the cells to shear stresses if inserted in the body. Overall, the cells

were able to withstand the surface textures and also supported each other to aid cell proliferation and growth.

As evidenced in Figure 4.8c, the cells on PTO also developed filopodia; however, the filopodia were thinner and smaller on this sample. This suggested that the necessity of filopodia was decreased due to overall improved cell attachment to the sample (in comparison to the textured samples). The cell filopodia on PTO attached to the rougher oxide features on the sample surface as they did on TOMP. This implied that the TiO_2 layer helped to support the attachment of the cells via changes in surface roughness. The LIPSS also did not cause a negative effect in the growth and attachment of the cells and did not induce cell death.

There have been previous reports discussing the potential of femtosecond surface textures on Ti and its alloys. The main positives of LIPSS is their self-organisation, scale and anisotropy. Previous investigations have illustrated the ability of LIPSS (micrometre or nanometre topography) in behaving similar to the extracellular matrix of bone. LIPSS can also affect the attachment and behaviour of osteoblasts. Although, there have been positive reports of LIPSS on bone related cells, other reports have discussed how LIPSS in the nanometre range are not as effective and do not improve the long-term bone-implant stability or integration. LIPSS in the micrometre range have provided strong osseointegration and thus, it has been suggested a combination of LIPSS in the micrometre and nanometre range would provide the best results for implant integration (48). The samples in this study fit the requirement as the textured samples have both nanometre

topographies due to the 300 nm spacing between the LIPSS ripples and micrometre topographies due to the 1 µm ripples.

The presence of focal adhesion sites on a cell are dependent on the surface topography. Polished surfaces have been found to cause lower focal adhesion sites on cells when compared to laser treated surfaces (48) which was also seen in this study as the cells on the P sample did not possess filopodia unlike the cells on the duplex treated samples. Filopodia behave like sensory tools that probe the environment for any changes in surface topography or chemistry and thus, aid the motion and behaviour of cells. The presence of filopodia on cells indicate lower cell adhesion rates. When cells are unable to form strong attachment bonds to a surface, they develop anchoring sites such as filopodia to increase and aid adhesion. Laser induced surface textures that protrude with heights greater than 70 nm have shown to decrease focal adhesion and thus, increase the formation of filopodia (106). These results match the results in this study. For instance, the LIPSS treated samples had surface features with heights in the micrometre range which may have reduced the contact area between the cells and surface and hence, the attachment and focal adhesion decreased which led to the formation of filopodia.

Mature osteoblasts have been found to join together to form a layered film over the top of surface textures. The presence of surface features can affect the behaviour of osteoblasts by causing them to grow in a pattern and align alongside the grooves in a specific direction (96). This was seen on the MP and TOMP samples as the cells attached in a parallel direction to the oxide columns. However, on the rest of the samples the SaOS-2 cells attached randomly which suggested, the presence of LIPSS led to ordering of the cells and hence,

LIPSS possess the ability to affect the behaviour of SaOS-2 cells. This phenomenon is referred to as contact guidance and has been seen in laser textured samples with SaOS-2 cells (67,101).

Other studies have also demonstrated how LIPSS do not negatively affect the growth of osteoblasts. LIPSS have shown to encourage cell spreading and thus, cell maturation. This suggests that LIPSS can potentially be used for bone related applications as they do not cause cytotoxic effects to bone cells (67). Although some reports state lower cell circularity is an indication of poor cell health (48), other reports have documented the reverse. For instance, it was found that laser treated samples led to reduced circularity of cells and hence, better spreading. This increase in cell spreading has been linked to less cell apoptosis and death and thus, is a good indication of cell health. Filopodia was also present on the cells that attached to the laser treated samples with the filopodia attaching directly to the laser features (67,101). Similar results were also seen for this study. When looking at the cell SEM images in Section 4.8, it was seen that the treated samples had better cell spreading and the cells on TOMP (Figure 4.8c) had filopodia that anchored the cells to the 1 µm ripples. This suggests that when LIPSS and CCT are combined cell health is improved and thus, the surface treatments are cytocompatible.

5.2.4 Effect of CCT on SaOS-2 cell viability

When LIPSS is undertaken in air, the introduction of laser textures is accompanied by an increase in the oxide thickness and composition which has shown to affect cell behaviour. Thicker oxide films have shown to cause improvements in cytocompatibility (107). In this study, the PTO sample had the highest SaOS-2 cell number followed by the MPTO and

TOMP samples. All of these samples had high TiO_2 peaks (Figures 4.2.1a and 4.2.1b) which suggested the presence of TiO_2 increases SaOS-2 cell attachment and growth. The porous and crystalline nature of TiO_2 aids the adsorption of substances and proteins that enable matrix mineralisation and bone formation (107).

Reports have documented that oxide thicknesses above 600 nm have led to increases in cell attachment. Researchers have also reported the porosity of thick oxides lead to better cell behaviour and attachment (108). This may have been the case for this study as the PTO sample had a thick oxide layer and had the most SaOS-2 attachment. It has also been shown, the formation of TiO_2 has led to increases in cell spreading and extension and hence, a larger degree of cell growth. This was due to the increased porosity of the TiO_2 that led to increased fibronectin adsorption (96). It is likely that the increases in cell attachment of the TO treated samples are probably due to the changes in surface topography, wettability and surface roughness (as discussed above) rather than the surface chemistry alone. Hence, it is difficult to ascertain whether the TiO_2 film alone caused increases in cell attachment.

5.3 Wear Behaviour

It has been revealed that novel surface treatments by combining CCT with laser micro-patterning can effectively increase the anti-bacterial efficacy of cp-Ti without reducing and indeed enhancing SaOS-2 cell growth. However, the durability of such promising biological effects is determined by the wear resistance of the patterned surfaces. Hence, as reported in Section 4.9, the wear behaviour of the novel engineered surfaces has been investigated in

air (dry) and in Ringer's solution (lubricated or corrosion-wear) sliding against both hardened steel (HS) and tungsten-carbide (WC) ball counterparts.

5.3.1 Wear of cp-Ti

As has been reported in Section 4.9.1.1, the as-polished P sample (as expected), showed very severe wear under both dry wear (Figures 4.9.1.1a-c) and under Ringer's solution lubricated corrosion wear conditions (Figures 4.9.1.1d-f). This is evidenced by severe deformation, large adhesion craters and deep grooves. Ringer's solution lubrication did not reduce the extent of adhesive wear (Figure 4.9.1.1a vs Figure 4.9.1.1d) indicating that lubrication by Ringer's solution was not effective in reducing wear although it slightly reduced the coefficient of friction (CoF) as shown in Figure 4.9.1a. The severe adhesive wear of cp-Ti observed in this study is in good agreement with the findings by other researchers. The poor wear behaviour of Ti and its alloys is related to their low hardness, high ductility, atomic structure, crystal structure and high reactivities, which lead to strong adhesion, severe adhesive wear and a strong tendency for scuffing (77).

5.3.2 Effect of micro-patterning

It was reported that when compared with untreated samples, textured samples displayed improvements in friction coefficients and wear rates (109). However, the tribological tests in this research have revealed that micro-patterning actually increased CoF (MP48 and MP58 in Figure 4.9.1c) of cp-Ti under both dry and lubricated conditions. In addition, micro-patterning marginally reduced the wear of cp-Ti under lubricated conditions (Figure 4.9.1.1d) but hardly any improvement could be seen under dry condition. This is supported by the fact that the wear tracks of the micro-patterned MP48 and MP58 are still

characterised by the typical adhesive wear features (Figure 4.9.1a) after the dry wear test. Ringer's solution lubrication to some extent reduced the adhesive wear but the wear tracks were still characterised by typical adhesive wear features.

The above results are seemingly contradicted by the findings reported in (109). However, it should be pointed out that in the previous research the improvements of wear resistance due to LIPSS only occurred when the loads were lower. This is because as reported in Chapter 4, a very thin oxide film was formed when laser micro-patterning was carried out in air. In principle, this very thin oxide film could protect the Ti substrate from direct contact with hardened steel. However, the hardness of cp-Ti (<200 HV0.5) is very low (Figure 4.6.1) and the thin oxide film would be quickly cracked and removed without necessary mechanical support from the soft substrate. Hence, the protection of the oxide films produced during laser patterning could provide limited, if any, protection to the substrate at the beginning of the test if the tested load is very low. This is supported by the fact that the micro-patterning induced surface oxide films provided a certain degree of protection when tested in lubricated conditions. Clearly, the micro-patterned cp-Ti surfaces were not able to withstand high loads and contact stresses thus, leading to poor durability.

5.3.3 Effect of CCT

It has previously been reported how the presence of TiO_2 formed via thermal oxidation can improve wear resistances (77,80) . On samples treated via thermal oxidation, the wear tracks that formed had less wear damage and adhesive wear features were not present. They attributed the improved wear resistances due to the formation of a hard TiO_2 that was supported by a hard interface oxide layer and an ODZ under the newly formed oxide (81).

This may have occurred in this study as the PTO sample had the smallest wear track and the least wear damage under both dry and lubricated conditions. As evidenced in Figures 4.9.1.1 a-c, the wear track formed during the dry wear test was very narrow with some wear debris and mild abrasion scratches; some flat wear-debris-like layers were formed on the wear track formed in lubricated wear (Figures 4.9.1.1 d-f). EDX analysis has revealed that the wear tracks formed by the hardened steel ball in dry conditions were covered by the material transferred from the ball (Figure 4.9.1.2a) or covered by the deposition layer when tested in Ringer's solution (Figure 4.9.1.2a).

Other studies have also displayed similar results. Thermally oxidised Ti has shown to cause improvements in wear resistances especially if the oxide is based on rutile. The wear rates were reduced by 2 orders of magnitude and this was due to the formation of the tough, strongly adhered rutile oxide. Adhesive wear is dependent on the metallurgical compatibility between the surfaces and the deformation. When a CCT treated Ti comes into contact with steel, the occurrence of adhesive wear is limited as the TiO_2 that forms during CCT behaves like a ceramic (77). This leads to metal-ceramic contact (82) and thus, the metallurgical compatibility is lowered between steel and oxide when compared to steel to untreated Ti and hence, adhesive wear is limited. It has also been reported how a rutile-based oxide has a considerably lower modulus to hardness ratio when compared to untreated Ti. This reduction can lead to elastic deformation which can reduce the adhesive wear rate (77) and can also improve the load-bearing capacity (109). The TiO_2 layer has also shown to have reduced shear strength which leads to lower friction coefficients and lower wear rates (61).

5.3.4 Wear of duplex treated samples

As reported in Chapter 4, the introduction of the TiO_2 via CCT as the first or pre-treatment in the TOMP48 and TOMP58 samples led to significant improved wear resistance of the laser-induced micro-patterns. As evidenced in Figure 4.9.1.1a, the wear tracks formed on TOMP48 had hardly any damage whereas, while the MP48 wear track had features of severe adhesive wear such as material removal and ploughing grooves. The pre-formed TiO_2 layer protected the LIPSS ripples from being damaged in TOMP48 and TOMP58. This indicated that CCT leads to improved wear resistances and increases the durability of the LIPSS. Such significantly increased wear resistance has also been achieved when sliding against a very hard WC ball under both dry and lubricated conditions. From the results of this study it can be concluded that the LIPSS formed on CCT treated cp-Ti possess high wear resistance and hence good durability.

5.4 Effect of LIPSS and CCT on Corrosion Resistance

5.4.1 Corrosion behaviour of Ti

Electrochemical corrosion occurs on nearly all metallic surfaces. Corrosion is not ideal if it were to occur on an implant as it can reduce the structural integrity of an implant and cause the release of toxic particulates. Corrosion of orthopaedic implants is dependent on surface structure, the presence of an oxide, mechanical features such as stress, the pH of the solution and the degree of movement or the presence of contact forces in the environment. The most important of all of these factors is the presence of an oxide. A surface oxide can behave like a kinetic barrier to corrosion. This barrier can physically decrease the rate at which corrosion occurs. Passivation is the phenomenon where a metal-oxide is formed

during the process of corrosion to prevent or limit the corrosive effects. Passivation helps prevent the transfer of metal ions from the metal to the solution and thus, decreases the rate at which corrosion occurs. These passivation films however, must be dense and possess strong bonds to the surface of the metal in order for them to be successful in limiting corrosion (56).

Ti in general displays good corrosion resistances due to the formation of a stable passive TiO_2 layer. This stable passive TiO_2 offers stability to the surface and protects it from corrosion by physiological fluids. It also reduces the release of metal or oxygen ions which also contributes in lowering the corrosion potential. All of these factors lead to Ti being referred to as a cytocompatible metal with high cytocompatibility. However, if the integrity of the TiO_2 layer is disturbed, the corrosion resistance of Ti is reduced. Mechanical wear or the presence of metabolites produced by microorganisms like bacteria can reduce the integrity of this TiO_2 layer and thus, reduce its corrosion resistance (103).

Looking at the results in Section 4.9.2, the P sample had the highest corrosion rate followed by the PTO sample. The introduction of TiO_2 via CCT led to the corrosion rate decreasing by over half, when compared to the P sample. LIPSS however, led to the corrosion rates for MP48 to decrease by +/-93.2 % and for MP58 to decrease by +/-96.7 %. This was a huge decrease in corrosion rate which indicated the LIPSS ripples increase corrosion resistance more than TiO_2. There was no significant difference between the MP58 and TOMP48 corrosion rates. Both these samples led to decreases in corrosion rates by +/-96.5 %. The MPTO sample had the lowest corrosion rate and thus, the highest corrosion resistance. The corrosion rate decreased by +/-98.9 % and may be due to the increased

wettability and the thick oxide layer (MPTO sample had the highest wettability). TOMP58 had the third highest corrosion rate which may be due to the low wettability or higher surface roughness's.

5.4.2 Effect of LIPSS on corrosion resistance

The introduction of LIPSS to the samples caused the samples to be hydrophobic. Wettability and surface roughness have been reported to have an effect on corrosion resistance (110,111). Rough hydrophobic surfaces have been shown to cause large effects on the corrosion potential of a material. For the untreated samples, the corrosion occurred on all of the sample surface without any preference for direction. Whereas, when hydrophobic LIPSS treated samples were tested for corrosion the hydrophobic nature of the sample in combination with the LIPSS valleys inhibited the corrosion pathway. The corrosive fluid could not move along the hydrophobic LIPSS valleys and this led to the reduction in corrosion rate (112). This may have occurred in this study as the hydrophobic LIPSS treated samples displayed lower corrosion rates than the hydrophilic P sample. Nonetheless, the MPTO and PTO samples were hydrophilic yet they had low corrosion rates. Hence, their corrosion behaviour is most probably also related to their surface oxide layer formed by CCT.

5.4.3 Effect of CCT on corrosion resistance

Previous reports have been made regarding the effect of CCT on corrosion resistance. CCT leads to the formation of a dense, inert and amorphous oxide that behaves as a ceramic. This ceramic behaviour of the TiO_2 has shown to significantly improve the corrosion resistance of the TO treated samples when compared to untreated Ti (82). Similarly, a rutile

based TiO_2 was shown to be very passive and hence, reduced the effects of corrosion. Even when high voltages were applied to CCT treated Ti-6Al-4V, the rutile-based oxide protected the surface from corrosive blister formation and the corrosion rate was decreased (113).

Other researches have also noted how CCT treated TiN samples displayed improved corrosion resistances in Ringer's solution. The formed TiO_2 was chemically inert in neutral and acidic solutions and thus, it protected the Ti surface from corrosion. Also, if the TiO_2 that forms is free of any defects such as scratches and it is dense and adheres strongly to the substrate, the corrosion is decreased considerably (80). These above reasons may explain why the PTO and MPTO samples displayed better corrosion resistances than the untreated sample.

Looking back at the SEM results in Section 4.1.1, whilst the MPTO sample had a thick oxide that covered all of the sample, the oxide on the TOMP58 sample was mostly destructed during the laser process. The destruction of the oxide and the introduction of pores in the TOMP58 sample may have possibly led to it having a higher corrosion potential than MPTO. When a defective oxide forms on the surface, many diffusion paths are also created that allow the migration of oxygen and metal ions. This migration cannot be controlled (113) and may be the reason why TOMP58 had a higher corrosion potential than the MPTO and TOMP48 samples.

Corrosion resistance of a sample is dependent on the chemical stability and defect free surface structure. Minor defects or scratches may increase the corrosion behaviour of the samples and the failure of oxidised samples. Aggressive ions can travel towards the oxide metal interface penetrating it leading to the detachment of the oxide from the

substrate. The detachment of the oxide can lead to the formation of wear debris and can thus, cause inflammatory responses in the body (114,115).

Researchers have demonstrated the better corrosion potential of rutile-based oxides when compared to anatase-based oxides. Anatase was prone to attack from corrosive fluids and dissolved in reducing acids. Whereas, rutile was inert and resistant to corrosion. In this study, XRD results revealed that the oxide formed is based on rutile (Section 4.2.1). Similarly, cp-Ti treated with CCT offered better corrosion resistances owing to its dense, thick oxide. The uniformity of the oxide covering the whole surface and its compact nature protected the surface from corrosion (116). This may explain why the PTO and MPTO samples displayed good corrosion resistances as they possessed uniform rutile-based oxide layers that had good bonding to the substrate.

Chapter 6

CONCLUSIONS AND FUTURE WORK

Surface Patterning

1. Femtosecond pulsed laser micro-patterning was applied to polished cp-Ti and ceramic conversion treated (CCT) cp-Ti to form laser induced periodic surface structure (LIPSS) with a depth of about +/- 1 μm and a spacing of approximately 300 nm.
2. Removal of surface oxide layer was observed for CCT pre-treated cp-Ti surfaces. Using the laser power at 48 % removed some of the oxide on TOMP48; however, when the laser power was increased to 58% the oxide on TOMP58 was mostly removed mainly due to laser ablation.
3. Post-CCT, the laser micro-patterned cp-Ti partially destroyed the LIPSS produced by the femtosecond pulsed laser due to the formation of surface oxide layer, although the rounded ripples were still visible.
4. The surface hardness of cp-Ti (+/- 188.7 HV0.5) was significantly increased by the CCT induced surface rutile oxide layer and the formation of oxygen diffusion zones (+/- 904.1 HV0.5). The presence of LIPSS reduced the surface micro-hardness of the polished P and the CCT treated TOMP surfaces.
5. The untreated sample was hydrophilic and CCT increased the hydrophilicity further. The highest hydrophilicity was seen for the MPTO sample which was fully covered by a TiO_2 layer induced by the CCT. The presence of LIPSS caused the samples to be

hydrophobic and the TOMP58 sample was the most hydrophobic even with the presence of TiO_2.

Biological Response

6. The LIPSS had the greatest effect on the antibacterial response due to the small size and the limited contact area for the bacteria to attach to. The highest percentage reduction for both bacteria was seen for the TOMP sample followed by the MP sample (+/- 65-75 % for both sample types). This suggested that when combining the two surface treatments, the antibacterial resistance is the most optimum.
7. For the anti-adhesion test the most anti-biofouling surface was the TOMP48 sample followed by MP48. This suggested that when the laser is at a 48 % power the LIPSS that form provide the highest antibacterial resistance and also due to the limited oxide destruction in TOMP48, the sample had an even higher resistance to bacterial attachment. The TiO_2 caused higher bacterial attachment than the LIPSS which may be due to the hydrophilic nature and the lower surface roughness and protrusions.
8. The TiO_2 provided the highest SaOS-2 cell viabilities which indicated that the CCT treatment was cytocompatible. The LIPSS however, reduced the number of SaOS-2 cells when compared to the untreated sample. However, when combined with TiO_2 the numbers increased. This suggested when the surface treatments are combined they are cytoompatible, non-toxic and also possess high antibacterial resistances.

Tribological and Corrosion Response

9. Untreated cp-Ti under a 100 g load with a hardened steel counterpart revealed severe adhesive and abrasive wear in both air and Ringer's solution characterised as severe plastic deformation, large adhesion craters and deep ploughing grooves due to the low hardness and strong adhesion tendency of cp-Ti.
10. The wear resistance of untreated and laser micro-patterned cp-Ti can potentially be effectively improved by CCT due to the increase of surface hardness and formation of a surface rutile oxide layer supported by an oxygen diffusion hardened subsurface.
11. Under the test conditions used in the study, laser micro-patterned cp-Ti revealed very poor tribological responses and the LIPSS were fully destroyed by the wear of a hardened steel counterpart even under lubricated conditions. This has demonstrated that the durability of the LIPSS formed on cp-Ti is very low.
12. The durability of LIPSS on cp-Ti can be effectively improved by the novel duplex treatment combining laser micro-patterning with pre-CCT under dry (unlubricated) and Ringer's solution lubricated conditions sliding against both hardened steel and very hard WC counterpart balls.
13. All the surface treated samples potentially had lower corrosion rates and higher corrosion potentials (except for TOMP58) as compared with untreated cp-Ti when electrochemically tested in Ringer's solution.

To summarise, the novel duplex surface system developed from the research by combining CCT treatment with laser micro-patterning has provided the best antibacterial results, good cytocompatibility, high corrosion and wear resistances and hence, possibly long durability. This study has demonstrated that when combined, CCT and LIPSS have the potential to be applied in medical implants in order to improve the infection and wear resistance whilst also maintaining the good corrosion resistance of cp-Ti without causing any toxicity issues.

Future work

- For the future work it would be good to test the effect of size of the LIPSS and its periodicity on antibacterial efficacy and cytocompatibility in order to optimise the laser patterning process.
- The use of larger anaerobic bacteria such as Actinomyces naeslundii or small Mycoplasma (0.3 μm size) to determine if larger bacteria are affected by the ripples to a higher extent when compared to smaller bacteria.
- To assess the antibacterial effect of the samples for a longer duration. Currently, the incubation period was 6 hours however it would be interesting to analyse the antibacterial effect over 24 hours or more to assess whether the LIPSS or CCT remained antibacterial over a longer period of time.
- Measure the antibacterial effect of the treatment types after wear testing to determine whether the antibacterial effect remains after wear damage.
- Undertake fatigue tests of the treated samples for further investigation to evaluate the longevity of the treatment types for other orthopaedic and high load-bearing applications.

BIBLIOGRAPHY

1. Aniołek K, Kupka M, Barylski A, Dercz G. Mechanical and tribological properties of oxide layers obtained on titanium in the thermal oxidation process. Appl Surf Sci. 2015.
2. Cunha A, Elie AM, Plawinski L, Serro AP, Botelho Do Rego AM, Almeida A, et al. Femtosecond laser surface texturing of titanium as a method to reduce the adhesion of Staphylococcus aureus and biofilm formation. Appl Surf Sci. 2016.
3. Bonse J, Höhm S, Koter R, Hartelt M, Spaltmann D, Pentzien S, et al. Tribological performance of sub-100-nm femtosecond laser-induced periodic surface structures on titanium. Appl Surf Sci. 2016; 374:190–6.
4. Albayrak Ç, Hacisalihoğlu I, Yenal vangölü S, Alsaran A. Tribocorrosion behavior of duplex treated pure titanium in Simulated Body Fluid. Wear. 2013.
5. Zhang Z. Switchable and Responsive Surfaces and Materials for Biomedical Applications. Switchable and Responsive Surfaces and Materials for Biomedical Applications. 2015.
6. Fang F, Aabith S, Homer-Vanniasinkam S, Tiwari MK. High-resolution 3D printing for healthcare underpinned by small-scale fluidics. In: 3D Printing in Medicine. 2017.
7. Kose N, Ayse Kose A. Application of Nanomaterials in Prevention of Bone and Joint Infections. In: Nanotechnology in Diagnosis, Treatment and Prophylaxis of Infectious Diseases. 2015.
8. Helmus MN, Gibbons DF, Cebon D. Biocompatibility: Meeting a Key Functional Requirement of Next-Generation Medical Devices. Toxicol Pathol. 2008.
9. Sidambe AT. Biocompatibility of advanced manufactured titanium implants-A review. Materials. 2014.
10. Mändl S, Rauschenbach B. Improving the biocompatibility of medical implants with plasma immersion ion implantation. Surf Coatings Technol. 2002; 156(1–3):276–83.
11. Holzapfel BM, Reichert JC, Schantz JT, Gbureck U, Rackwitz L, Nöth U, et al. How smart do biomaterials need to be? A translational science and clinical point of view. Advanced Drug Delivery Reviews. 2013.
12. Teo AJT, Mishra A, Park I, Kim YJ, Park WT, Yoon YJ. Polymeric Biomaterials for Medical Implants and Devices. ACS Biomater Sci Eng. 2016; 2(4):454–72.
13. Pandolfino JE, Richter JE, Ours T, Guardino JM, Chapman J, Kahrilas PJ. Ambulatory esophageal pH monitoring using a wireless system. Am J Gastroenterol. 2003.

14. Chang JHC, Liu Y, Tai YC. Long term glass-encapsulated packaging for implant electronics. In: Proceedings of the IEEE International Conference on Micro Electro Mechanical Systems (MEMS). 2014.
15. Kamachi Mudali U, Sridhar TM, Baldev RAJ. Corrosion of bio implants. Sadhana - Acad Proc Eng Sci. 2003.
16. Thomas P, Weik T, Roider G, Summer B, Thomsen M. Influence of surface coating on metal ion release: Evaluation in patients with metal allergy. Orthopedics. 2016.
17. Niinomi M. Mechanical biocompatibilities of titanium alloys for biomedical applications. Journal of the Mechanical Behaviour of Biomedical Materials. 2008.
18. Harris P, Normand V, Norton IT. GELATIN. Encyclopaedia of Food Sciences and Nutrition. 2003.
19. Bailey R. Tribocorrosion response of surface-modified Ti in a 0.9% NaCl solution. Lubricants. 2018; 6(4).
20. Obadele BA, Andrews A, Olubambi PA, Mathew MT, Pityana S. Tribocorrosion behaviour of laser cladded biomedical grade titanium alloy. Mater Corros. 2015; 66(10):1133–9.
21. Biswas A, Li L, Maity TK, Chatterjee UK, Mordike BL, Manna I, et al. Laser surface treatment of Ti-6Al-4V for bio-implant application. Lasers Eng. 2007;17 (1–2):59–73.
22. Charles C. Modelling microstructure evolution of weld deposited Ti--6Al--4V. 2008: 76.
23. Wanhill R, Barter S. Fatigue of Beta Processed and Beta Heat-treated Titanium Alloys. Fatique Beta Process Beta Heat-treated Titan Alloy. 2012.
24. Geetha M, Singh AK, Asokamani R, Gogia AK. Ti based biomaterials, the ultimate choice for orthopaedic implants - A review. Progress in Materials Science. 2009.
25. Titanium alloys for aerospace structures and engines. Introduction to Aerospace Materials. 2012.
26. Talha M, Behera CK, Sinha OP. A review on nickel-free nitrogen containing austenitic stainless steels for biomedical applications. Materials Science and Engineering C. 2013
27. Albrektsson T, Johansson C. Osteoinduction, osteoconduction and osseointegration. Eur Spine J. 2001.
28. Johansson CB, Wennerberg A, Albrektsson T. Quantitative comparison of screw-shaped commercially pure titanium and zirconium implants in rabbit tibia. J Mater Sci Mater Med. 1994.

29. Palmquist A, Lindberg F, Emanuelsson L, Brånemark R, Engqvist H, Thomsen P. Morphological studies on machined implants of commercially pure titanium and titanium alloy (Ti6Al4V) in the rabbit. J Biomed Mater Res - Part B Appl Biomater. 2009.
30. Kumar S, Narayanan TSNS, Raman SGS, Seshadri SK. Thermal oxidation of CP-Ti: Evaluation of characteristics and corrosion resistance as a function of treatment time. Mater Sci Eng C. 2009.
31. Busscher HJ, Van Der Mei HC, Subbiahdoss G, Jutte PC, Van Den Dungen JJAM, Zaat SAJ, et al. Biomaterial-associated infection: Locating the finish line in the race for the surface. Science Translational Medicine. 2012.
32. Bodelón OG, Clemente C, Alobera MA, Aguado-Henche S, Escudero ML, Alonso MCG. Osseointegration of TI6Al4V dental implants modified by thermal oxidation in osteoporotic rabbits. Int J Implant Dent. 2016.
33. Parithimarkalaignan S, Padmanabhan T V. Osseointegration: An update. Journal of Indian Prosthodontist Society. 2013.
34. Ferraris S, Spriano S. Antibacterial titanium surfaces for medical implants. Materials Science and Engineering C. 2016.
35. Gristina AG, Dobbins JJ, Giammara B, Lewis JC, Devries WC. Biomaterial-Centered Sepsis and the Total Artificial Heart: Microbial Adhesion vs Tissue Integration. JAMA J Am Med Assoc. 1988.
36. Hori K, Matsumoto S. Bacterial adhesion: From mechanism to control. Biochemical Engineering Journal. 2010.
37. Arciola CR, Campoccia D, Speziale P, Montanaro L, Costerton JW. Biofilm formation in Staphylococcus implant infections. A review of molecular mechanisms and implications for biofilm-resistant materials. Biomaterials [Internet]. 2012; 33(26):5967–82
38. Pirrone M, Pinciroli R, Berra L. Microbiome, biofilms, and pneumonia in the ICU. Current Opinion in Infectious Diseases. 2016.
39. Hou S, Gu H, Smith C, Ren D. Microtopographic patterns affect escherichia coli biofilm formation on poly(dimethylsiloxane) surfaces. Langmuir. 2011.
40. Panawala L. Difference Between Gram Positive and Gram Negative Bacteria. Pediaa. 2017;
41. Cenciarelli O. Use of Non-Pathogenic Biological Agents as Biological Warfare Simulants for the Development of a Stand-Off Detection System. J Microb Biochem Technol. 2014.
42. Liu X, Chu PK, Ding C. Surface nano-functionalization of biomaterials. In: Materials Science and Engineering R: Reports. 2010.

43. Uhm SH, Song DH, Kwon JS, Lee SB, Han JG, Kim KM, et al. E-beam fabrication of antibacterial silver nanoparticles on diameter-controlled TiO2 nanotubes for bio-implants. Surf Coatings Technol 2013; 228: 360–6.
44. Hu H, Zhang W, Qiao Y, Jiang X, Liu X, Ding C. Antibacterial activity and increased bone marrow stem cell functions of Zn-incorporated TiO 2 coatings on titanium. Acta Biomater. 2012; 8(2):904–15.
45. Lorenzetti M, Dogša I, Stošicki T, Stopar D, Kalin M, Kobe S, et al. The influence of surface modification on bacterial adhesion to titanium-based substrates. ACS Appl Mater Interfaces. 2015; 7(3):1644–51.
46. Marx DE, Barillo DJ. Silver in medicine: The basic science. Burns [Internet]. 2014; 40:S9–18.
47. Grandcolas M, Ye J, Hanagata N. Combination of photocatalytic and antibacterial effects of silver oxide loaded on titania nanotubes. Mater Lett. 2011; 65(2):236–9.
48. Chen X, Li Y, Hodgson PD, Wen C. In vitro behavior of human osteoblast-like cells (SaOS2) cultured on surface modified titanium and titanium-zirconium alloy. Mater Sci Eng C 2011; 31(7):1545–52.
49. Salou L, Hoornaert A, Louarn G, Layrolle P. Enhanced osseointegration of titanium implants with nanostructured surfaces: An experimental study in rabbits. Acta Biomater. 2015; 11(1):494–502.
50. Yoshihara C, Ueno T, Chen P, Tsutsumi Y, Hanawa T, Wakabayashi N. Inverse response of osteoblasts and fibroblasts to growth on carbon-deposited titanium surfaces. J Biomed Mater Res - Part B Appl Biomater. 2018; 106(5):1869–77.
51. Postiglione L, Di Domenico G, Ramaglia L, Montagnani S, Salzano S, Di Meglio F, et al. Behavior of SaOS-2 cells cultured on different titanium surfaces. J Dent Res. 2003; 82(9):692–6.
52. Czekanska EM, Stoddart MJ, Richards RG, Hayes JS. In search of an osteoblast cell model for in vitro research. Eur Cells Mater. 2012; 24:1–17.
53. Asri RIM, Harun WSW, Samykano M, Lah NAC, Ghani SAC, Tarlochan F, et al. Corrosion and surface modification on biocompatible metals: A review. Materials Science and Engineering C. 2017.
54. Kumar S, Narayanan TSNS, Ganesh Sundara Raman S, Seshadri SK. Surface modification of CP-Ti to improve the fretting-corrosion resistance: Thermal oxidation vs. anodizing. Mater Sci Eng C. 2010.
55. Garbacz H, Motyka M. Tribology. In: Nanocrystalline Titanium. 2018.

56. Hallab NJ, Jacobs JJ. Orthopedic Applications. In: Biomaterials Science: An Introduction to Materials: Third Edition. 2013.
57. Damm P, Dymke J, Ackermann R, Bender A, Graichen F, Haider A, et al. Friction in total hip joint prostheses measured in vivo during walking. PLoS One. 2013.
58. Hung KY, Lo SC, Shih CS, Yang YC, Feng HP, Lin YC. Titanium surface modified by hydroxyapatite coating for dental implants. Surf Coatings Technol. 2013.
59. Harun WSW, Asri RIM, Alias J, Zulkifli FH, Kadirgama K, Ghani SAC, et al. A comprehensive review of hydroxyapatite-based coatings adhesion on metallic biomaterials. Ceramics International. 2018.
60. Nishimoto A, Nii H, Narita R, Akamatsu K. Simultaneous duplex process of TiN coating and nitriding by active screen plasma nitriding. Surf Coatings Technol. 2013.
61. El-Hossary FM, Negm NZ, Abd El-Rahman AM, Raaif M, Seleem AA, Abd El-Moula AA. Tribo-mechanical and electrochemical properties of plasma nitriding titanium. Surf Coatings Technol. 2015.
62. Zhang Z, Li X, Almandoz E, Fuentes GG, Dong H. Sliding friction and wear behaviour of Titanium-Zirconium-Molybdenum (TZM) alloy against Al2O3 and Si3N4 balls under several environments and temperatures. Tribol Int. 2017; 110.
63. Zwahr C, Günther D, Brinkmann T, Gulow N, Oswald S, Grosse Holthaus M, et al. Laser Surface Pattering of Titanium for Improving the Biological Performance of Dental Implants. Adv Healthc Mater. 2017.
64. You A, Be MAY, In I. Femtosecond laser-induced periodic surface structures. 2012.
65. Jwad T, Penchev P, Nasrollahi V, Dimov S. Laser induced ripples' gratings with angular periodicity for fabrication of diffraction holograms. Appl Surf Sci. 2018; 453:449–56.
66. Höhm S, Herzlieb M, Rosenfeld A, Krüger J, Bonse J. Dynamics of the formation of laser-induced periodic surface structures (LIPSS) upon femtosecond two-color double-pulse irradiation of metals, semiconductors, and dielectrics. Appl Surf Sci [Internet]. 2016; 374:331–8.
67. Lee BEJ, Exir H, Weck A, Grandfield K. Characterization and evaluation of femtosecond laser-induced sub-micron periodic structures generated on titanium to improve osseointegration of implants. Appl Surf Sci. 2018; 441:1034–42.
68. Hikage H, Nosaka N, Matsuo S. High-spatial-frequency periodic surface structures on steel substrate induced by subnanosecond laser pulses. Appl Phys Express. 2017.

69. Bonse J, Hohm S, Kirner S V., Rosenfeld A, Kruger J. Laser-Induced Periodic Surface Structures-A Scientific Evergreen. IEEE J Sel Top Quantum Electron. 2017; 23(3).
70. Müller FA, Kunz C, Gräf S. Bio-inspired functional surfaces based on laser-induced periodic surface structures. Materials (Basel). 2016; 9(6).
71. Nouri A, Wen C. Introduction to surface coating and modification for metallic biomaterials. In: Surface Coating and Modification of Metallic Biomaterials. 2015.
72. Siddiquie RY, Gaddam A, Agrawal A, Dimov SS, Joshi SS. Anti-Biofouling Properties of Femtosecond Laser-Induced Submicron Topographies on Elastomeric Surfaces. Langmuir. 2020.
73. Epperlein N, Menzel F, Schwibbert K, Koter R, Bonse J, Sameith J, et al. Influence of femtosecond laser produced nanostructures on biofilm growth on steel. Appl Surf Sci. 2017; 418:420–4.
74. Orazi L, Pogorielov M, Deineka V, Husak E, Korniienko V, Mishchenko O, et al. Osteoblast cell response to LIPSS-modified Ti-implants. In: Key Engineering Materials. 2019.
75. Cunha A, Oliveira V, Vilar R. Ultrafast laser surface texturing of titanium alloys [Internet]. Laser Surface Modification of Biomaterials: Techniques and Applications. Elsevier Ltd; 2016. 301–322.
76. Van der Poel SH, Mezera M, Römer G willem RBE, de Vries EG, Matthews DTA. Fabricating laser-induced periodic surface structures on medical grade cobalt-chrome-molybdenum: Tribological, wetting and leaching properties. Lubricants. 2019.
77. Dong H, Bell T. Enhanced wear resistance of titanium surfaces by a new thermal oxidation treatment. Wear. 2000.
78. Aniołek K, Kupka M, Barylski A. Sliding wear resistance of oxide layers formed on a titanium surface during thermal oxidation. Wear. 2016; 356–357:23–9.
79. Lin N, Xie R, Zou J, Qin J, Wang Y, Yuan S, et al. Surface damage mitigation of titanium and its alloys via thermal oxidation: A brief review. Reviews on Advanced Materials Science. 2019.
80. Li X, Dong H. Ceramic conversion treatment of titanium-based materials. In: Surface Engineering of Light Alloys: Aluminium, Magnesium and Titanium Alloys. 2010.
81. Redmore E, Li X, Dong H. Tribological performance of surface engineered low-cost beta titanium alloy. Wear [Internet]. 2019; 426–427.
82. Sawyer V, Tao X, Dong H, Dashtbozorg B, Li X, Sammons R, et al. Improving the tribological properties and biocompatibility of Zr-based bulk metallic glass for potential biomedical applications. Materials (Basel). 2020.

83. Dong H, Mukinay T, Li M, Hood R, Soo SL, Cockshott S, et al. Improving tribological and anti-bacterial properties of titanium external fixation pins through surface ceramic conversion. J Mater Sci Mater Med [Internet]. 2017; 28(1):1.
84. Faustini M, Marmiroli B, Malfatti L, Louis B, Krins N, Falcaro P, et al. Direct nano-in-micropatterning of TiO2 thin layers and TiO 2/Pt nanoelectrode arrays by deep X-ray lithography. J Mater Chem. 2011.
85. Elias CN, Lima JHC, Valiev R, Meyers MA. Biomedical applications of titanium and its alloys. JOM. 2008.
86. Jwad T, Penchev P, Nasrollahi V, Dimov S. Laser induced ripples' gratings with angular periodicity for fabrication of diffraction holograms. Appl Surf Sci. 2018.
87. Suzuki K, Iijima K, Sakamoto K, Saihi M, Yamashita H. A review of hop resistance in beer spoilage lactic acid bacteria. Journal of the Institute of Brewing. 2006.
88. Sanders ER. Aseptic laboratory techniques: Plating methods. J Vis Exp. 2012.
89. Kong F, Huang W, Jiang Y, Wang W, Zhao X. A vibration model of ball bearings with a localized defect based on the hertzian contact stress distribution. Shock Vib. 2018.
90. Zheng S, Bawazir M, Dhall A, Kim HE, He L, Heo J, et al. Implication of Surface Properties, Bacterial Motility, and Hydrodynamic Conditions on Bacterial Surface Sensing and Their Initial Adhesion. Frontiers in Bioengineering and Biotechnology, 2021.
91. Hart ML, Lauer JC, Selig M, Hanak M, Walters B, Rolauffs B. Shaping the cell and the future: Recent advancements in biophysical aspects relevant to regenerative medicine. Journal of Functional Morphology and Kinesiology. 2018.
92. Walker J, Halliday D, Resnick R. Fundamentals of Physics. Halliday and Resnick 10ed. Wiley. 2014
93. Wassmann T, Kreis S, Behr M, Buergers R. The influence of surface texture and wettability on initial bacterial adhesion on titanium and zirconium oxide dental implants. Int J Implant Dent. 2017.
94. Wu Y, Zitelli JP, TenHuisen KS, Yu X, Libera MR. Differential response of Staphylococci and osteoblasts to varying titanium surface roughness. Biomaterials. 2011,
95. Truong VK, Lapovok R, Estrin YS, Rundell S, Wang JY, Fluke CJ, et al. The influence of nano-scale surface roughness on bacterial adhesion to ultrafine-grained titanium. Biomaterials. 2010; 31(13):3674–83.

96. Damiati L, Eales MG, Nobbs AH, Su B, Tsimbouri PM, Salmeron-Sanchez M, et al. Impact of surface topography and coating on osteogenesis and bacterial attachment on titanium implants. J Tissue Eng. 2018.
97. Pan Q, Cao Y, Xue W, Zhu D, Liu W. Picosecond Laser-Textured Stainless Steel Superhydrophobic Surface with an Antibacterial Adhesion Property. Langmuir. 2019.
98. Rimondini L, Fare S, Carrassi A, Brambilla E, Brossa F, Consonni C. Early bacterial colonization of titanium oral implant: The effect of wettability and surface roughness. In: Transactions of the Annual Meeting of the Society for Biomaterials in conjunction with the International Biomaterials Symposium. 1996.
99. Santhosh Kumar S, Hiremath SS, Ramachandran B, Muthuvijayan V. Effect of Surface Finish on Wettability and Bacterial Adhesion of Micromachined Biomaterials. Biotribology. 2019.
100. Lutey AHA, Gemini L, Romoli L, Lazzini G, Fuso F, Faucon M, et al. Towards laser-textured antibacterial surfaces. Sci Rep. 2018; 1;8(1).
101. Luo X, Yao S, Zhang H, Cai M, Liu W, Pan R, et al. Biocompatible nano-ripples structured surfaces induced by femtosecond laser to rebel bacterial colonization and biofilm formation. Opt Laser Technol. 2020.
102. Al-Radha ASD, Dymock D, Younes C, O'Sullivan D. Surface properties of titanium and zirconia dental implant materials and their effect on bacterial adhesion. J Dent. 2012.
103. Cordeiro JM, Barão VAR. Is there scientific evidence favoring the substitution of commercially pure titanium with titanium alloys for the manufacture of dental implants? Materials Science and Engineering C. 2017.
104. Sista S, Wen C, Hodgson PD, Pande G. The influence of surface energy of titanium-zirconium alloy on osteoblast cell functions in vitro. J Biomed Mater Res - Part A. 2011.
105. Biggs MJP, Richards RG, Dalby MJ. Nanotopographical modification: A regulator of cellular function through focal adhesions. Nanomedicine: Nanotechnology, Biology, and Medicine. 2010
106. Jäger M, Zilkens C, Zanger K, Krauspe R. Significance of nano- and microtopography for cell-surface interactions in orthopaedic implants. Journal of Biomedicine and Biotechnology. 2007.
107. Cunha A, Zouani OF, Plawinski L, Botelho Do Rego AM, Almeida A, Vilar R, et al. Human mesenchymal stem cell behavior on femtosecond laser-textured Ti-6Al-4V surfaces. Nanomedicine. 2015.

108. Sul YT, Johansson CB, Kang Y, Jeon DG, Albrektsson T. Bone reactions to oxidized titanium implants with electrochemical anion sulphuric acid and phosphoric acid incorporation. Clin Implant Dent Relat Res. 2002.

109. Lin N, Li D, Zou J, Xie R, Wang Z, Tang B. Surface texture-based surface treatments on Ti6Al4V titanium alloys for tribological and biological applications: A mini review. Materials. 2018.

110. Chi G, Yi D, Liu H. Effect of roughness on electrochemical and pitting corrosion of Ti-6Al-4V alloy in 12 wt.% HCl solution at 35»°C. J Mater Res Technol. 2020.

111. Amadeh A, Heshmati-Manesh S, Labbe JC, Laimeche A, Quintard P. Wettability and corrosion of TiN, TiN-BN and TiN-A1N by liquid steel. J Eur Ceram Soc. 2001.

112. Yusuf Y, Ghazali MJ, Otsuka Y, Ohnuma K, Morakul S, Nakamura S, et al. Antibacterial properties of laser surface-textured TiO2/ZnO ceramic coatings. Ceram Int. 2020.

113. Dearnley PA, Dahm KL, Çimenoğlu H. The corrosion-wear behaviour of thermally oxidised CP-Ti and Ti-6Al-4V. Wear. 2004.

114. Mathew MT, Wimmer MA. Tribocorrosion in artificial joints: In vitro testing and clinical implications. In: Bio-Tribocorrosion in Biomaterials and Medical Implants. 2013.

115. Bailey R, Sun Y. Corrosion and Tribocorrosion Performance of Thermally Oxidized Commercially Pure Titanium in a 0.9% NaCl Solution. J Mater Eng Perform. 2015; 24(4):1669–78.

116. Jamesh M, Kumar S, Sankara Narayanan TSN. Effect of thermal oxidation on corrosion resistance of commercially pure titanium in acid medium. J Mater Eng Perform. 2012.